Application of stable isotope analyses to examine patterns of water uptake, water use strategies and water-use-efficiency of contrasting ecosystems in Australia

Rizwana Rumman

November 2016

A thesis submitted in fulfilment of the requirements for the degree of Doctor of Philosophy in School of Life Sciences at the University of Technology Sydney.

Certificate of Authorship

I certify that the work presented in this thesis has not previously been submitted for a degree, nor has it been submitted as part of requirements for a degree except as fully acknowledged within the text.

I also certify that the thesis has been written by me. Any help that I have received in my research work and the preparation of the thesis itself has been acknowledged. In addition, I certify that all information sources and literature used are indicated in the thesis.

This research is supported by an Australian Government Reserach Training Program Scholarship.

Signature of Student: _____

Date:

Acknowledgement

I dedicate this work to my parents, Kishwar Sultana and Abu Abdullah, for always being the source of support and inspiration in my life.

This research is supported by an Australian Government Research Training Program (RTP) Scholarship.

I wish to express my most sincere gratitude to the government and people of Bangladesh for the financial support throughout my academic life. I would like to thank Bangladesh University of Engineering and Technology (BUET), The School of Life Sciences at the University of Technology Sydney (UTS), the Graduate Research School, UTS and The National Centre for Groundwater Research and Training (NCGRT) for financial support. Additionally, I would like to thank the Terrestrial Ecology Research Network (TERN) for giving me the opportunity to be a part of an amazing project.

It is a pleasure to thank my generous and encouraging supervisor, Prof Derek Eamus, for seeing potential in me and for being a constant help and support whilst encouraging me to work in my own way. Thanks Derek, a lot, for opening me the doors of nature and for your invaluable guidance throughout this journey!

I would like to thank Dr Brad Murray for his insightful comments and patience through my endless emails and queries. My sincere thanks also go to Dr James Cleverly who helped me with his valuable insights and data collection and to Dr Charles Price of University of Western Australia for his helpful guidance and support.

This work would not have been possible without the support of the members of the Terrestrial Ecohydrology Research Group. I am especially thankful to Ralph Faux for being the pathfinder in the red and vast Australian deserts whenever I needed to collect some more samples and for providing me with technical advice and assistance. Thanks to Nicole, Sepideh, Randoll, Tomek, Nadia, Tonantzin, Rachael and John for sharing your stories with me!

I thank Mahboob, my husband, for sharing these PhD years with me, for his willingness to transform hard times into mellow ones and for not giving up on me. I thank my beautiful daughter who encouraged me to push myself even further in ways I did not think was possible.

I thank my brother and his family for being there whenever I needed. Thanks to my wonderful family and friends back in Bangladesh and across the world, the endless fun and pleasure of being with whom has always been a source of solace.

Publications

A portion of the work presented in this thesis has directly contributed to the following papers:

Cleverly, J., Eamus, D., Van Gorsel, E., Chen, C., **Rumman, R**., Luo, Q., Coupe, N.R., Li, L., Kljun, N. and Faux, R., 2016. Productivity and evapotranspiration of two contrasting semiarid ecosystems following the 2011 global carbon land sink anomaly. *Agricultural and Forest Meteorology*, 220: 151-159.

Zolfaghar, S., Villalobos-Vega, R., Cleverly, J., Zeppel, M., **Rumman, R**. and Eamus, D., 2014. The influence of depth-to-groundwater on structure and productivity of Eucalyptus woodlands. *Australian Journal of Botany*, 62(5): 428-437.

Data gathered as part of, but which do not directly contribute to this thesis, have contributed to the following publications:

Cleverly, J., Eamus, D., Coupe, N. R., Chen, C., Maes, W., Li, L., Faux, R., Santini, N. S., **Rumman, R**., Yu, Q. & Huete, A. (2016). Soil moisture controls on phenology and productivity in a semi-arid critical zone. *Science of the Total Environment*, 568:1227-1237

Santini, N. S., Cleverly, J., Faux, R., Lestrange, C., **Rumman, R**., & Eamus, D., 2016. Xylem traits and water-use-efficiency of woody species co-occurring in the Ti Tree Basin arid zone. *Trees*, 30(1), 295-303.

Apgaua, D. M., Ishida, F. Y., Tng, D. Y., Laidlaw, M. J., Santos, R. M., **Rumman, R.**, Eamus, D., Holtum, J. A. M. & Laurance, S. G. (2015). Functional traits and water transport strategies in lowland tropical rainforest trees. *PloS one*, 10(6): e0130799.

Table of Contents

List of Figures

List of Tables

Abbreviations, acronyms & symbols

‰	Parts per thousand
α	significance level
ε	evaporative index (ratio of actual evapotranspiration to precipitation)
Φ	dryness index (ratio of potential evapotranspiration to precipitation)
λ	Pagel's parameter for phylogenetic signal
^{13}C	carbon isotope with an atomic weight of 13
^{2}H	hydrogen isotope with an atomic weight of 2
^{18}O	oxygen isotope with an atomic weight of 18
a	diffusional fractionation
A	CO_2 assimilation rate
A400.a	Net assimilation at [CO_2] 400 ppm (μmol CO_2 m^{-2} s^{-1})
Adj r^2	adjusted regression co-efficient
AMU	Alice Mulga (SuperSite)
ANOVA	analysis of variance
b	carboxylation fractionation
C_a	atmospheric concentration (mole fraction) of CO_2
C_i	intercellular concentration (mole fraction) of CO_2
C_i400	Intercellular [CO_2] with CO_2 reference at 400 ppm (μmol CO_2 mol^{-1})
C_i/C_a	Intercellular [CO_2] : ambient [CO_2]
CM	Calperum Mallee (SuperSite)
CP	Cumberland Plain (SuperSite)
CT	FNQ - Cape Tribulation node (SuperSite)
δ^2H	ratio of ^2H to ^1H (‰)
$\delta^{13}C$	ratio of ^{13}C to ^{12}C (‰)
$\delta^{13}C_a$	$\delta^{13}C$ of CO_2 in air
$\delta^{13}C_p$	$\delta^{13}C$ of CO_2 in plant
$\delta^{18}O$	ratio of ^{18}O to ^{16}O (‰)
$\Delta^{13}C$	discrimination against ^{13}C
DTGW	depth-to-groundwater
E400.a	Transpiration rate at [CO_2] 400 ppm (mmol CO_2 m^{-2} s^{-1})
ET_a	actual evapotranspiration
ET_p	potential evapotranspiration
F	variance ratio
FMA	fresh mass per unit area (g m^{-2})

FNQ	Far North Queensland (SuperSite)
GDE	groundwater dependent ecosystems
GISP	Greenland Ice Sheet Precipitation
GLS	generalized least square
GMWL	global meteoric water line
GNIP	Global Network of Isotopes in Precipitation
g_s400	Stomatal conductance at [CO_2] 400 ppm (mmol H_2O m^{-2} s^{-1})
GWW	Great Western Woodlands (SuperSite)
HRT	high rainfall tropical savanna (biome)
IAEA	International Atomic Energy Agency
K	Blomberg's parameter for phylogenetic signal
LDMC	ratio of leaf dry to leaf fresh mass
LF	Litchfield Savanna (SuperSite)
LMA	leaf mass per unit area (g m^{-2})
LMWL	local meteoric water line
$LeafN_{area}$	Total leaf [N], (area basis) (mg m^{-2})
$LeafN_{mass}$	Total leaf [N] (mg g^{-1})
$LeafP_{area}$	Total leaf [P], (area basis) (mg m^{-2})
$LeafP_{mass}$	Total leaf [P] (mg g^{-1})
LR	likelihood ratio
LTR	lowland wet tropical rainforest (biome)
MAP	mean annual precipitation (mm)
MI	moisture index (unitless)
NIST	National Institute of Standards and Technology
NRETAS	Department of Natural Resources, Environment, the Arts and Sport, Northern Territory Government
PCA	principal component analysis
PCM	phylogenetic comparative methods
PC1	first principal component
PC2	second principal component
pGLS	phylogenetic generalized least square
PIC	phylogenetic independent contrast
PNUE	photosynthetic nitrogen use efficiency (μmol CO_2 s^{-1} g^{-1} N)
PPUE	photosynthetic phosphorus use efficiency (μmol CO_2 s^{-1} g^{-1} P)
R	language and environment for statistical computing and graphics
RC	FNQ - Robson Creek node (SuperSite)
RatioNP	ratio of total leaf [N] : [P]
r^2	regression co-efficient
R_{sample}	ratio of heavy to light isotopes in a sample
$R_{standard}$	ratio of heavy to light isotopes in a standard
SCA	Sydney Catchment Authority
SE	one standard error of the mean
SLA	specific leaf area (m^2 g^{-1})
SLAP-2	Standard Light Antarctic Precipitation 2
SIMM	stable isotope mixing model

STS	semi-arid tropical savanna (biome)
SW	semi-arid woodland (biome)
TEF	trophic enrichment factor
TERN	Terrestrial Ecosystem Research Network
TW	temperate woodland (biome)
TWF	temperate wet forest
UTR	upland wet tropical rainforest (biome)
VSMOW-2	Vienna Standard Mean Ocean Water 2
vpdL400	vapour pressure deficit based on leaf temperature (KPa)
WR	Warra Tall Eucalypt (SuperSite)
WUE_i	intrinsic water-use-efficiency (µmol/mol)
WUE_{inst}	instantaneous water-use-efficiency (µmol/mol)
ZPE	zero point energy (cal mol^{-1})

Abstract

Spatial differences and temporal variation in the availability of water accessible by plants have significant influences on a range of plant functions, including photosynthesis, transpiration, growth and yield. Coexisting plant species often adopt contrasting water use strategies to reduce inter-species competition for water and to cope with seasonal and/or geographical differences in water availability. The work described in this thesis aimed to analyse the variations in sources of water uptake by vegetation as well as contrasting water use strategies across spatial and temporal scales in a range of sites across Australia. In particular, it employs stable hydrogen, oxygen and carbon isotopes to investigate variations in sources of water uptake by vegetation and discrimination against carbon-13 and water-use-efficiency at a range of spatial scales (from 10s of metres to thousands of kilometres) across a range of sites located along gradients of water availability. The generality of the trends found within smaller spatial scales in contrasting mesic and semi-arid ecosystems across water availability gradients are compared with trends obtained from different sites at a continental scale across a climate gradient (with mean annual precipitation ranging from 255 mm to 2140 mm).

At smaller spatial scales, analyses were performed along two naturally occurring depth-to-groundwater gradients in contrasting mesic and arid ecosystems. Results from stable deuterium and ^{18}O analysis revealed that, even in the mesic site that received >1000 mm rainfall for two consecutive years prior to sampling, increased water availability (via access to groundwater) still exerted some influence on sources of water uptake by dominant vegetation. However, stable isotope analysis more consistently and reliably identified access to groundwater by deep-rooted vegetation in the semi-arid sites that receives rainfall < 350 mm year^{-1}. A key result identified in this research was that discrimination against stable ^{13}C isotopes ($\Delta^{13}C$) and leaf intrinsic water-use-efficiency (WUE_i) calculated from ^{13}C at the leaf-level accurately identified water availability, specifically, groundwater use and spatial and/or seasonal patterns of groundwater use especially in water-limited regions. Consistent with the results of (branch water) deuterium and ^{18}O analysis, discrimination against ^{13}C

and WUE_i (leaf-level) did not vary significantly with depth-to-groundwater in shallower rooted (*Acacia*) species but showed significant trends up to a threshold value of depth-to-groundwater of 13.9 m in the deep-rooted (*Eucalyptus* and *Corymbia*) species, indicating possible access to groundwater.

A strong positive correlation of bulk-leaf $\Delta^{13}C$ (strong negative correlation with WUE_i) of the dominant overstorey species with MAP and moisture index was observed during both dry- and wet-season across an eight-fold increase in mean annual precipitation (MAP) along a continental-scale climate gradient. Up to 3.7‰ and 4.5‰ differences among biomes during the dry- and wet-season respectively were observed in $\Delta^{13}C$. Among 19 other climate parameters in addition to MAP that were considered in the multiple regression analyses, isothermality as a secondary predictor during the wet-season was the only model with notable explanatory power. Among the gas-exchange traits, $\Delta^{13}C$ and WUE_i was tightly associated with C_i/C_a ratio and stomatal conductance and this explained the strong response of $\Delta^{13}C$ to MAP during both seasons. During the dry-season, $\Delta^{13}C$ and WUE_i were more strongly regulated by stomatal conductance than photosynthetic capacity. In contrast, during the wet-season when canopy photosynthesis is the most active under favourable conditions of water availability, photosynthetic capacity was found to have a stronger relationship with $\Delta^{13}C$ than stomatal conductance at a continental scale. Leaf mass per unit area (LMA) among the leaf structural traits, showed a strong negative correlation with $\Delta^{13}C$ suggesting that these two structural (LMA) and functional ($\Delta^{13}C$) leaf-traits are possibly linked through the effects of low (soil) water availability on decreasing C_i.

In 55 dominant overstorey species distributed widely across the country and experiencing distinctly different climates and ecosystem structures and compositions, a pattern of similarity was identified in terms of species mean values of $\Delta^{13}C$ among closely related species. Phylogenetic analysis suggests that more closely related species were found under a given set of climate conditions across the gradient at a large spatial scale in Australia. Cross-species relationships of $\Delta^{13}C/WUE_i$ and climate variables/leaf-traits were generally quite robust and well supported after taking their genealogical relationships into account. Combining phylogenetic and trait-based information supported the hypothesis that climate variables, in particular variables related to precipitation, influenced the evolution of discriminatory traits of leaves of the dominant species at the scale of this present analysis by reducing discrimination against ^{13}C with decreasing water availability and with increasing temperature.

Chapter 1 General Introduction

Introduction

Australia is well known as the driest of all permanently inhabited continents. The majority of Australia's land area is classified as semi-arid (O'Grady *et al.*, 2006b) with a mean annual precipitation of about 350-450 mm, considerably lower than the mean annual precipitation of South America (1800 mm), Europe (820 mm), North America (800 mm), Africa (750 mm) and Asia (650 mm). The annual amount of precipitation, however, varies considerably across Australia: some regions receive very low levels of precipitation: < 250 mm yr^{-1}, other regions receive very large quantities: 1500-3000 mm yr^{-1} (Eamus *et al.*, 2006b). This variability, coupled with variation in mean summer and winter temperatures, results in Australia's landscape having distinctly different climate zones (Hughes, 2003). Furthermore, precipitation in Australia is highly variable between years, more variable than any other continent in the world (Eamus *et al.*, 2006b). Thus much of the Australian vegetation has evolved a range of strategies to cope with periods of water surplus followed by extended periods of severe water-stress.

Owing to it being the driest of all continents in terms of precipitation, Australian vegetation can, in some locations, be heavily reliant on groundwater[1]. Groundwater is often the only reliably available source of water in arid (MAP < 250 mm yr^{-1} in the south or 350 mm yr^{-1} in the north (Eamus *et al.*, 2006b)) and semi-arid (larger MAP yr^{-1} than arid regions but it still too low and unreliable for crop-growth) regions of the continent. About 20% of the total water used to support human activities in Australia comes directly from groundwater reserves via bores sunk into aquifers (Eamus *et al.*, 2006b). Annual evaporation also frequently exceeds annual rainfall across most of the continent, particularly in arid and semi-arid regions (Warner, 2004). As a result, a significant fraction

[1] Groundwater is defined as the saturated zone of the regolith and its associated capillary fringe (Eamus *et al.,* 2006b).

of the ecology, industry and population of Australia are highly dependent on groundwater resources.

Many structural and functional attributes of vegetation change in a predictable manner in parallel to change in availability of water – from precipitation and/or other sources – in Australia. Structural traits, for example, plant density, degree of canopy closure, leaf area index and other traits are determined very much by water availability (Eamus *et al.*, 2006b; Schulze *et al.*, 1998a; Williams and Ehleringer, 1996). In a range of sites across Australia, tree water use increased significantly with increased MAP for a range of species (Schulze *et al.*, 1998a). The availability of water accessible by plants has a major impact on a range of plant functions such as photosynthesis, transpiration, growth and yield, which makes it one of the key concepts in Ecohydrology. During photosynthesis, plants open their stomata for gas-exchange and as a consequence a considerable amount of water is lost via transpiration which also contributes to nutrient uptake and leaf cooling (Couvreur *et al.*, 2014). Transpiration by plants at the leaf-level also generates water potential gradients that induce xylem water flow via roots in the soil. Consequently, a reliable stock of water is of extreme importance to sustain essential plant functions.

For over a century ecologists have been interested in how vegetation maintains the balance between carbon gain and water loss, especially in response to seasonal and/or geographical changes in moisture availability. A very useful concept developed in pioneering studies for a better understanding of the interactions between water and carbon fluxes in evaluating plant physiological responses is that of "water-use-efficiency", defined broadly as the ratio of photosynthesis to transpiration (Briggs and Shantz, 1913a; Briggs and Shantz, 1913b; Stanhill, 1986). A relatively new technology adopted by ecologists and plant biologists in investigating plant water sources and/or carbon-water relations, i.e. water-use-efficiency, is incorporating measurements of the stable isotope composition of leaves, sapwood and xylem water (Michener and Lajtha, 2008). Isotopic compositions of elements at their natural abundance level can be used as an effective tool to examine a number of processes, such as, to identify sources (e.g., pollutants to a stream), infer processes (e.g., heterotrophic nitrification), estimate rates (e.g., soil C turnover), determine proportional inputs (e.g., percent contribution of a particular source of food in a diet), or to confirm, reject, or constrain models derived from the use of other techniques (Michener and Lajtha, 2008). Based on a strong theoretical framework and the empirical database developed for the use of isotopes to study plant carbon and water relations, isotope analysis has become almost a

standard tool for plant-physiologists, ecologists, and eco-hydrologists over the last couple of decades (Saugier *et al.*, 2012).

This thesis aims to increase our understanding of the differentiation of source of water-uptake by dominant vegetation across a range of sites in Australia characterized by varying degrees of water availability. My research also sought to examine the variation in plant carbon-water relations in response to water availability. I principally used the stable isotope approach, specifically, deuterium and ^{18}O to trace sources of water-uptake by vegetation and ^{13}C at the leaf/stem-wood level to couple water availability and water-use-efficiency based on a robust mechanistic understanding of their relationships. In this introductory chapter, I provide an overview of the current understanding of using stable isotopes in tracing plant water sources and biochemical basis of carbon isotope fractionation to investigate carbon-water relations before identifying the knowledge gaps this study addressed.

Stable isotopes

Definition and terminology

Isotopes are atoms with the same number of protons and electrons but differing numbers of neutrons, thereby having different atomic masses (Michener and Lajtha, 2008). The mass number is noted as the superscript number on the left of the element's designation. For example, the most common isotope of carbon is $^{12}_{6}C$, where 12 (superscript) is the atomic mass, i.e., the sum of neutrons and protons, and 6 (subscript) is the atomic number (number of protons or number of electrons). The number of neutrons can be determined by difference of these two numbers such as, another stable isotope of carbon, $^{13}_{6}C$, has 6 electrons and protons and 7 neutrons. "Stable" isotopes are further characterized as being energetically stable and thus do not decay into any other nuclide once they are formed (Unkovich *et al.*, 2013) although may themselves be produced from the decay of radioactive isotopes (Kendall and McDonnell, 2012). In contrast to stable isotopes, radioactive isotopes decay spontaneously and emit α or β particles in order to become stable isotopes themselves, for example, ^{14}C β -decays to its stable form ^{14}N (Kendall and Caldwell, 1998).

Most elements of biological interests have two or more stable isotopes, although one isotope among them is usually overwhelmingly abundant (see **Table 1.1**) and one or two of

relatively minor abundance (Kendall and Caldwell, 1998). Low abundance of usually heavier isotopes provides opportunities to use enriched sources of the isotopes as "tracers" in biochemical, biological and environmental studies (Unkovich *et al.*, 2013). **Table 1.1** lists the average terrestrial abundances of the isotopes of the most common elements generally used in ecological studies.

Table 1.1: Percent abundance in terrestrial environments of the principal stable isotopes commonly used in ecological research (from Michener and Lajtha, 2008).

Element	Isotope	Mass (amu*)	Abundance (%)
Hydrogen	^{1}H	1.007825	99.985
	^{2}H	2.014102	0.015
Carbon	^{12}C	12.00	98.89
	^{13}C	13.003355	1.11
Nitrogen	^{14}N	14.003074	99.63
	^{15}N	15.000109	0.37
Oxygen	^{16}O	15.994915	99.759
	^{17}O	16.999131	0.037
	^{18}O	17.999159	0.204
Sulphur	^{32}S	31.972072	95.00
	^{33}S	32.971459	0.76
	^{34}S	33.967868	4.22
	^{36}S	35.967079	0.014

* amu = atomic mass unit.

The isotopic differences between various components of the biosphere (e.g., seawater, minerals or leaves) are exceedingly small, therefore isotopic composition is reported relative to an arbitrary but internationally accepted standard and expressed in parts per thousand (‰) deviation from that standard by:

$$\delta = \left(\frac{R_{sample}}{R_{standard}} - 1\right) X\ 1000 \quad [‰]$$

Here, R denotes the ratio of the heavy to light (or rare to abundant) isotope (e.g., $^{13}C/^{12}C$) in atomic percent. R_{sample} and $R_{standard}$ are the heavy to light ratios in sample and standard, respectively. A positive δ-value indicates that the isotopic ratio of the heavy to light isotope in the sample is higher than that of the standard, i.e., the sample contains more of the heavier (rare) isotopic species compared to the standard; whereas, a negative δ-value expresses the opposite, i.e., the sample contains less of the heavier isotopic species compared to the standard (Kendall and McDonnell, 2012).

International standards in isotope analysis

The isotopic compositions of materials analysed are usually reported relative to an arbitrary but internationally accepted, reference standard. The δ-value of all internationally accepted reference standards is by definition 0‰. A list of standards for the isotopes used in this present study (^{2}H, ^{18}O and ^{13}C) are listed in **Table 1.2**. Owing to the international standards being too expensive for daily use for a large number of samples, each laboratory generally has one or more internal working standards. These standards are chosen based on the type of analysis being performed and usually are unique to a particular analytical laboratory. A common practice is to analyse the samples at the same time as a reference standard or with internal laboratory standards that has been calibrated relative to the international standard (Kendall and McDonnell, 2012). Reference standards in small quantities are available for calibration purposes from the National Institute of Standards and Technology (NIST) in the USA (Web site: http://www.nist.gov/), or the International Atomic Energy Agency (IAEA) in Vienna (Web site: http://www.iaea.or.at/).

Table 1.2: Internationally accepted reference standards used in the present study and their abundance ratio (modified from Unkovich *et al.*, 2013).

Isotope	The ratio measures	International Reference Standard	Abundance Ratio of Reference Standards
^{2}H	$^{2}H/^{1}H$	Vienna Standard Mean Ocean Water (V-SMOW)	1.5575×10^{-4}
^{13}C	$^{13}C/^{12}C$	V-Pee Dee Belemnite (V-PDB)	1.1237×10^{-2}
^{18}O	$^{18}O/^{16}O$	Vienna Standard Mean Ocean Water (V-SMOW)	2.0052×10^{-3}

Fundamental isotope behaviour

There are two fundamental characteristics of isotopes and their compounds in terms of reactivity:

a) The chemical behaviour of two isotopes is qualitatively similar because the number of electrons and protons of two isotopes of an element is exactly the same
b) The physical and chemical behaviour of two isotopes is quantitatively different.

The difference in the *physical* behaviour of two isotope arises from the difference in their number of neutrons. Differences in the number of neutrons determines the atomic mass of an element, which determines the vibrational energy of the nucleus, thus differences in mass lead to differences in both reaction rate and bond strength (Michener and Lajtha, 2008). This differential reaction rate and bond strength results in differential representation in reactants and products which is primarily why isotope exists in different proportions with different δ-values in each pool (Unkovich *et al.*, 2013). The largest differences between two isotopes occurs among the lightest elements where the percent change in mass is the largest (Michener and Lajtha, 2008). For example, a ^{2}H atom has twice the mass of a ^{1}H atom (**Table 1.1**), whereas the extra neutron in ^{33}S leads to only a 3% heavier mass than ^{32}S; thus, behavioural differences between ^{1}H and ^{2}H is significantly larger than between those of ^{33}S and ^{32}S. Such mass-dependant differences in isotopes are manifested in the isotope "fractionation" effect, which is described below.

Isotopic fractionation

Isotopic fractionation is defined as, "the partitioning of isotopes between two substances (e.g., reactant *versus* product), of two phase of the same substance (e.g., liquid *versus* vapour) with different isotope ratios (δ-values)" (Dawson and Brooks, 2001). Fractionation is caused because of the differences in velocity and bond strength among isotopes. Molecules with heavy isotopes are more stable (because they have a higher dissociation energy) than molecules with lighter isotopes and therefore, isotopic fractionations between molecules can be explained by differences in their zero point energies[2] (ZPE). Molecules composed of different isotopic species will have different vibrational motions and consequently,

[2]At a temperature of absolute zero, a vibrating element or molecule, composed of a unique mixture of protons/neutrons and/or isotopes will have a certain zero-point energy content which lies above the minimum potential energy level of that molecule (Unkovich *et al.,* 2013).

different ZPE content despite having the same chemical formula. For example in hydrogen, there is about a 2 kcal/mole difference in ZPE associated with the breaking of the H-H bond of lighter isotopes compared to the ^{2}H-^{2}H bond of heavier isotopes resulting in an easier dissociation of H-H bond compared to ^{2}H-^{2}H bond (Kendall and McDonnell, 2012). Differential breaking of bonds of heavier and lighter isotope results in differences in chemical reactions which ultimately results in fractionation.

Following are the two main types of phenomena that create mass-dependent isotopic fractionations: isotope exchange reactions and kinetic processes.

Isotopic exchange reactions: equilibrium fractionation

Isotope-exchange reactions/equilibrium fractionation involves the redistribution of isotopes of an element among various species or compounds (Kendall and McDonnell, 2012). In theory, the reactants and products remain in close contact in a closed, well-mixed system such that backwards reactions can occur and chemical equilibrium can be attained. The forward and backward rate of reactions of any isotope is the same but the ratios of different isotopes are different in each compound or phase of a substance (e.g. liquid water and water vapour) at any particular moment/temperature (Unkovich *et al.*, 2013). Among different phases of the same compound or different (isotopic) species of the same element, the denser the material, the more it tends to be enriched in the heavier isotope (Kendall and McDonnell, 2012). For example, for the various phases of water at equilibrium, the ^{18}O (larger $\delta^{18}O$) in the species will occur in the following order: solid> liquid > vapour. As for a reaction involving C and H_2O at equilibrium, ^{18}O and ^{13}C will occur in the following order: $CO_2 < HCO_3^- < CO_3^{2-}$.

Kinetic fractionation

Unlike equilibrium fractionation, kinetic fractionation is a unidirectional and irreversible process (non-identical rates of forward and backward reaction) due to the reverse reaction being inhibited or not occurring, for example, evaporation in an open system when water vapour moves away from the liquid water pool (Michener and Lajtha, 2008). Unkovich *et al.*, (2013) outlined two processes that lead to kinetic fractionation of isotopes:

a) By differences in *diffusional flux* of the molecules impinging on a surface where they are absorbed (determined by Graham's law of diffusion), and,

b) By differences in the *rates of diffusion* of molecules through a substance (air, water etc.) by mass transfer (determined by Fick's law).

As discussed earlier, the lighter isotopes have bonds that are easier to break compared to equivalent bonds of heavier isotopes. Hence, the light isotopes react faster and become concentrated in the products, causing the residual reactants to become enriched in the heavy isotopes. In contrast, reversible equilibrium reactions can produce both heavier and lighter products than the original reactants.

Kinetic fractionation, like equilibrium fractionation, is also mass dependent. The difference in physical or chemical properties of elements arising from differences in their atomic mass (β) can be quantified from the kinetic energy $K.E. = ½\ mv^2$, where m = mass and v = velocity. For CO_2 of two species, e.g. $^{12}C^{16}O_2$ and $^{13}C^{16}O_2$ having a mass of 44 and 45 respectively,

$$\beta = \frac{v\ of\ the\ heavier\ element}{v\ of\ the\ lighter\ element} = \sqrt{\left(\frac{45}{44}\right)} = 1.01129$$

Therefore, regardless of temperature, the velocity of $^{12}C^{16}O_2$ is 1.01% greater than that of $^{13}C^{16}O_2$ and this difference in velocity causes different isotopic ratios in the reactants and in the products. When such a process is enzyme mediated, the enzyme can "discriminate" against one species over another thereby resulting in isotopic fractionation. This will be further discussed in the following sections.

Application of stable water isotopes in plant ecology

Low abundance of heavier isotopes enables us to use enriched sources of the isotopes as "tracers" and can assist in the solution of hydro-geochemical and biological processes. The following section highlights the application of stable water isotopes specifically in plant ecology.

The isotopic composition of plants was first investigated in the early 1960s. These studies revealed that water extracted from leaves is considerably enriched due to evaporative

enrichment during transpiration and also varies daily depending on humidity gradients, transpiration rate and the isotopic composition of atmospheric water (Gonfiantini *et al.*, 1965). However, researchers primarily concentrating on leaf-water isotopic signals also observed that, unlike leaf water, there was no fractionation of hydrogen and oxygen isotopes during water uptake through roots from the analysis of xylem sap (Gonfiantini *et al.*, 1965; Wershaw *et al.*, 1966). Consequently, water in plant branches (xylem) carries the same isotopic signal as the source water – until it reaches the sites of evaporation, generally in the leaves (**Figure 1.1**). Since the isotopic compositions of the "pools" of water used by plants are easily distinguishable (Dawson *et al.*, 2002), xylem sap analysis can be a very reliable tool for determining plant water sources by comparing the isotopic composition of the xylem sap with that of possible sources (Saugier *et al.*, 2012). This method of tracing source water uptake can be particularly useful, especially when the various water sources are sufficiently distinct in their isotopic composition, e.g., surface water *versus* groundwater *versus* rain water.

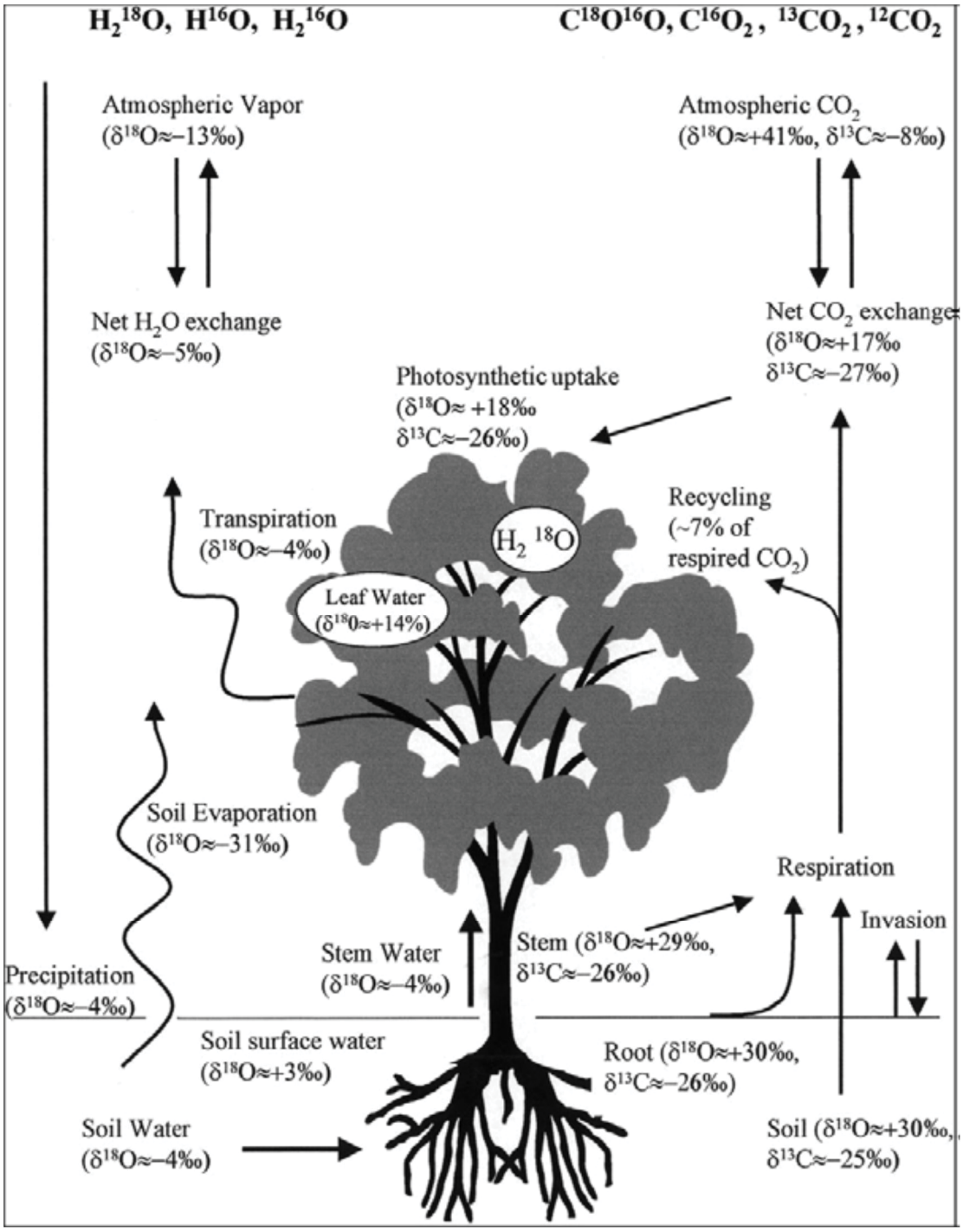

Figure 1.1: Isotopic compositions and fractionations of major components of carbon and water pools.

The values are rough approximations and can vary greatly with geographical location and environmental conditions (adopted from Yakir and Sternberg, (2000)).

Hydrogen and oxygen atoms in plant tissues predominantly come from their source water, thus processes that affect the isotopic ratio of source water will also influence the hydrogen and oxygen isotope ratios in plants. If samples of the different water sources of plants – soil water, rain water, groundwater and xylem (branch) water – can be extracted (e.g. by cryogenic vacuum extraction) and analysed for their water isotope signature, it is theoretically possible to investigate the origin of water used by plants by directly comparing their isotopic signature with those of possible water sources as well as quantify the proportional contribution of each different source. For example, for two possible water sources, a simple two end member mixing model can be used with the two sources being the end members, and the plant-water value being somewhere in between and the proportional contribution of these two separate sources can be calculated from the model (Phillips and Gregg, 2001; Phillips and Gregg, 2003).

Beyond that, water isotopes can also be a tool for identifying the difference in water uptake between summer/winter or dry-/wet-season, determining intra- and interspecific resource competition and patterns in community water use. In an early study, for instance, White *et al.,* (1985) showed that eastern white pine (*Pinus strobus*) in eastern America switch between deep and surface soil layers depending on precipitation events (**Figure 1.2**). These authors observed that, following a precipitation event, the surface layers of the soil as well as the water from the white pine trees had similar isotopic composition to that of the precipitation event at both wet sites (with access to groundwater) and dry sites (with no groundwater access). At the dry site, as the soil water gradually dried out after the precipitation event, δ^2H values of branch xylem water decreased gradually, indicating a switch from surface soil water to deeper soil layers. At the wet site with close proximity to groundwater, δ^2H values of branch xylem water switched back to the isotopic signals of the groundwater from that of the deeper soil layers. These data show the capacity of these trees to adjust their patterns of water use according to water availability during precipitation events (with available surface water resources) and during periods of water deficit with no precipitation. Several relatively recent studies have also used stable water isotopes to infer use of different water sources in response to seasonal water availability (Ehleringer *et al.*, 1991; Jackson *et al.*, 1999; Stratton *et al.*, 2000; Weltzin and McPherson, 1997).

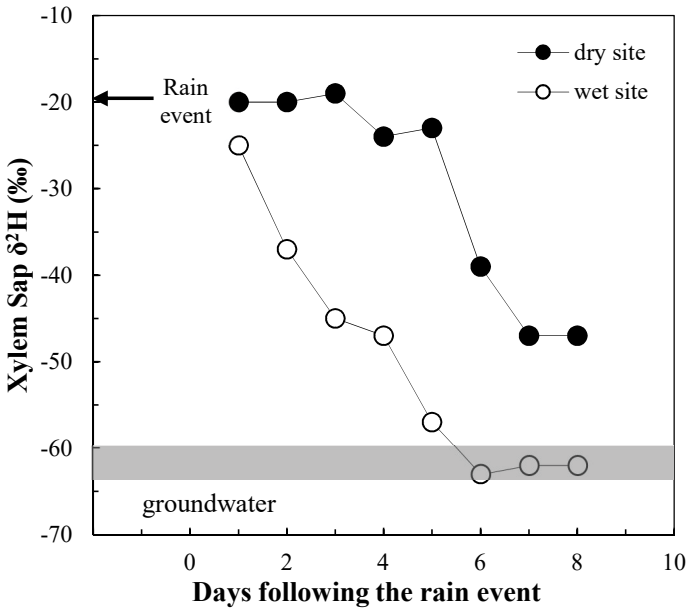

Figure 1.2: Time course of the hydrogen isotope ratio of xylem sap in eastern white pine (*Pinus strobus*) following a summer rain event (from White *et al.*, 1985).

Trees represented by the filled black circles at the wet site had access to a secondary groundwater source, whereas trees represented by open white circles at the dry site did not have access to the groundwater.

In a study at the Daly River catchment in the Northern Territory, Australia, Lamontagne *et al.*, (2005) observed that the δ^2H signature of the xylem sap of the vegetation varied according to the position within the landscape (**Figure 1.3**). At the Oolloo site, these authors investigated two transects extending across the riparian zone from the riverbank to the levee. Trees located at the levee and the upper terraces had relatively depleted δ^2H signatures of the xylem sap, whereas, trees closer to the river had more enriched signatures (**Figure 1.3**) and more similar to the groundwater signature. The authors concluded that some species found along different points of the transect showed facultative dependence on groundwater, i.e., they use groundwater when available but can survive without it. However, *Melaleua argenta*, another species predominantly found on the river banks, was found to be obligate users of groundwater because isotopic signatures of their xylem sap remained consistently similar to that of groundwater and did not vary among samplings. In another study in *Banksia* woodland on the northern Swan Coastal Plain, Western Australia in a Mediterranean climate, Zencich *et al.*, (2002) also used stable water (δ^2H) isotope to trace source water uptake and these authors concluded that groundwater is taken up by the species at all sites throughout the annual cycle when it was within the rooting zone of the vegetation. Further examples include, (a) differentiating contrasting water use strategies of

juvenile riparian plants and mature trees (Dawson and Ehleringer, 1991) where soil and surface water were the dominant source of water for juvenile plants, in contrast to groundwater for mature trees and (b) determination of the mountainous source of groundwater and opportunistic use of that groundwater by riparian trees (Chimner and Cooper, 2004). Thus, stable water isotopes have emerged especially over the last couple of decades as a powerful tool to provide insights into the water movement within plants and their water use strategies.

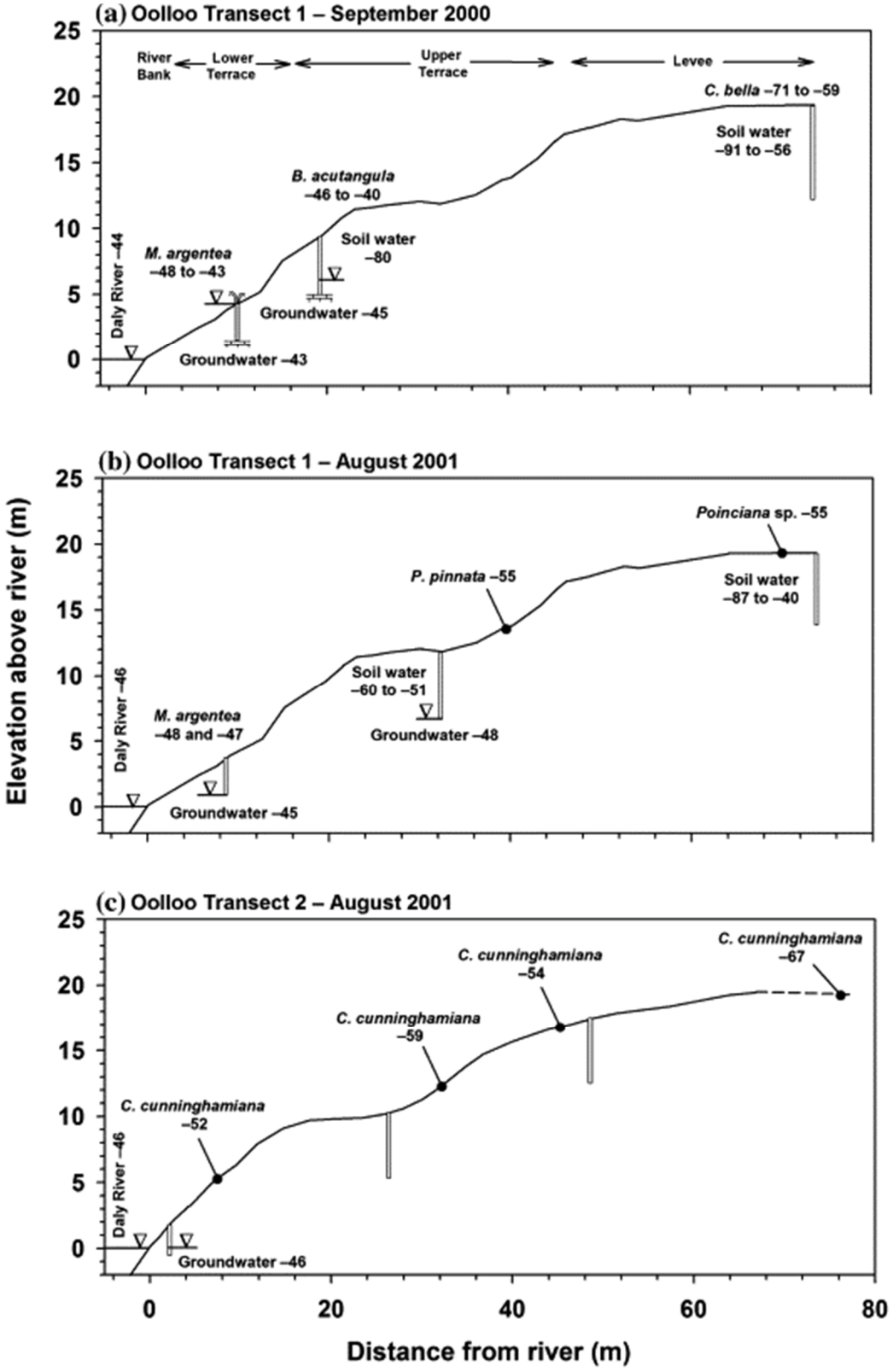

Figure 1.3: Cross-section of the riparian zone for three transects sampled at Oolloo in 2000–2001.

Deuterium values (‰) of xylem sap, river, soil water and groundwater are shown. When present, the height of the water table in test holes is shown with an inverted triangle (from Lamontagne *et al.*, 2005).

Application of stable carbon isotopes in determining plant water-use-efficiency

Discrimination against ^{13}C

Researchers in early studies of carbon isotope ratios among broad plant communities observed that the carbon isotopic ratio of C3 and C4 plants fall into a bimodal distribution of two non-overlapping categories (Bender, 1971; Smith and Epstein, 1971). An example of $\delta^{13}C$ (‰) compositions of C3 and C4 grasses is shown in **Figure 1.4** (adopted from Cerling *et al.*, (1997)). The $\delta^{13}C$ composition of atmospheric CO_2 is approximately -8‰ when there is no considerable nearby industrial activity; therefore, there exists ~5‰ fractionation in the C4 group and this increases to as large as ~19‰ in the C3 group (Saugier *et al.*, 2012). This variation in the relative abundances of stable carbon isotopes between plants and the atmosphere suggests that plants discriminate against ^{13}C isotope during photosynthesis which is also related to the two distinct metabolic pathways of C3 and C4 plants.

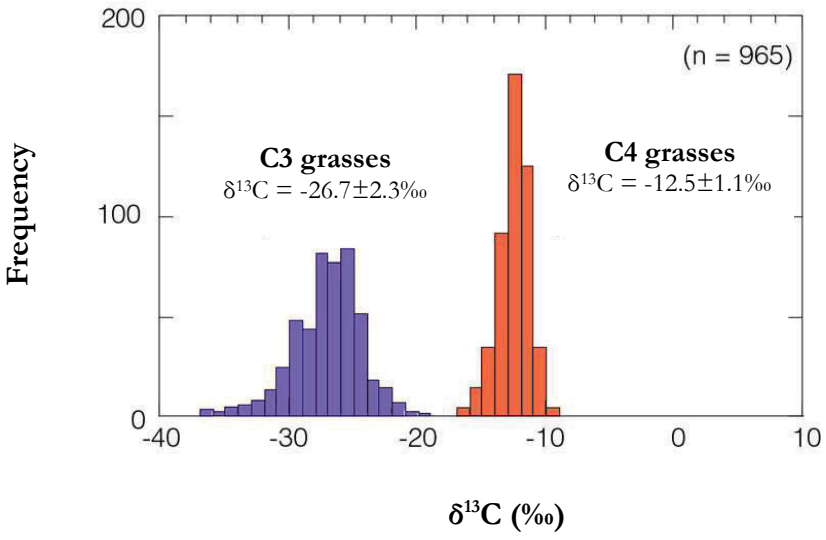

Figure 1.4: Histograms of $\delta^{13}C$ for modern C3 and C4 grasses (from Cerling *et al.*, 1997).

This fractionation arises because of the differences between the atomic masses of heavier and lighter carbon isotopes which affects the diffusion of CO_2 into leaves as well as the kinetic parameters of the chemical reactions involved in carbon fixation. The physical and biochemical phenomena underpinning these fractionation effects are generally well

understood and consequently enable us to incorporate carbon isotopic methods in investigations of a range of problems in plant physiology, ecology or other fields of research (O'Leary, 1993).

The isotopic ratio of ^{13}C to ^{12}C in plant tissue is generally much less than that in the atmosphere, indicating that plants discriminate against ^{13}C during photosynthesis. Farquhar and Richards, (1984) defined this discrimination as:

$$\Delta^{13}\mathrm{C}\ (‰) = \frac{R_a - R_p}{R_p} = \frac{\partial^{13}C_a - \partial^{13}C_p}{1 + \frac{\partial^{13}C_p}{1000}} \qquad (1)$$

Where, R_a is the $^{13}C/^{12}C$ ratio of CO_2 in air, and R_p is that of plant carbon. In the above equation, $\delta^{13}C_a$ is the $\delta^{13}C$ value of CO_2 in air and $\delta^{13}C_p$ is that of the plant.

The most widely applied model of discrimination against ^{13}C in C3 plants is that of Farquhar *et al.*, (1982). This model relates discrimination to variation in the ratio of intercellular to ambient CO_2 mole fractions (C_i/C_a), in addition to a number of other parameters. This model has been updated in more recent years to add the effects of dissolution and diffusion from the intercellular air spaces to the sites of carboxylation in the chloroplasts, fractionation during day respiration and photorespiration and "ternary effects" (where the term "ternary" refers to three interacting gases - CO_2, water vapour and air) etc. (Evans and Von Caemmerer, 2013; Farquhar and Cernusak, 2012; Tcherkez *et al.*, 2011). However, a simplified form of this model that omits effects other than those of diffusion through stomata and carboxylation and is the most widely used model of discrimination against ^{13}C. Although this simplified version is an approximation of the actual discrimination, it has been sufficient for a substantial number of applications (Cernusak *et al.*, 2013).

Before proceeding to more quantitative aspects of the discrimination model, a simple physical explanation of fractionations associated with carbon isotope in a C3 plant is now presented.

Fractionation of carbon isotope in plant tissues takes place before the first irreversible step during the photosynthesis process (Craig, 1954), i.e., the carboxylation reaction, which is essentially irreversible in both C3 and C4 pathways (Saugier *et al.*, 2012)

A simple, two-step CO_2 uptake scheme for C3 plants is as follows:

$$CO_2 \text{ (external)} \overset{\textit{Diffusion}}{\leftrightharpoons} CO_2 \text{ (internal)} \overset{\textit{Carboxylation}}{\rightarrow} R\text{--}CO_2^-$$

The first step induces an isotope fractionation through a physical process (i.e., diffusion) and the second step induces fractionation through an enzymatic process. At the first step, CO_2 enters the leaf through stomata and diffuses to the site of carboxylation and at the next step, an appropriate carboxylase enzyme takes up the CO_2 (which is also an irreversible process). The fractionation associated with diffusion is 4.4‰ (Hesterberg and Siegenthaler, 1991; O'Leary, 1981). In C3 plants, the first step in CO_2 fixation is catalysed by Ribulose-1, 5-bisphosphate carboxylase/oxygenase (RuBisCo) in the following equation:

$$CO_2 + \text{RuBP} \rightarrow 2\ \text{3-PGA}$$

Here, RuBP = Ribulose-1, 5-bisphosphate and 3-PGA = 3-phosphoglycerate.

The larger source of fractionation in C3 plants is this enzymatic process catalysed by RuBisCo, which has been quantified using a variety of methods (Roeske and O'Leary, 1984) showing a consistent result of ~29‰ compared with dissolved CO_2, with an uncertainty of less than 1‰, at 25℃, pH 8 (Saugier *et al.*, 2012). In C4 plants, however, the first step of carboxylation is carried out by PEP carboxylase which catalyses the following equation:

$$PEP + HCO_3^- \rightarrow OAA + P_i$$

Here, PEP = Phosphoenolpyruvate, OAA = oxaloacetate and P_i = inorganic phosphate.

A number of investigations using different methods measured ~2‰ fractionation associated with PEP carboxylase (O'Leary, 1984; Schmidt *et al.*, 1978; Whelan *et al.*, 1973; Winkler *et al.*, 1983).

Simplified $\Delta^{13}C$ model of C3 plants

A simplified form of the ^{13}C discrimination model of Farquhar *et al.*, (1982), as mentioned in the previous section, can be described as follows:

$$\Delta^{13}\mathrm{C}\ (‰) = a + (b - a)\frac{C_i}{C_a} - d \qquad (2)$$

Where, C_i and C_a is the intercellular and atmospheric concentration (mole fraction) of CO_2, *a* is diffusional fractionation (4.4‰) and *b* is carboxylation fractionation (29‰). In this simplified form of the model, *b* is usually taken as 27‰, which allows for a reduction in fractionation caused by the terms that are omitted in the above equation accounting mainly for the drawdown in CO_2 mole fraction from the intercellular mole fraction of CO_2 to mole fraction of CO_2 at the sites of carboxylation (Cernusak *et al.*, 2013). The term *d* as discussed in Farquhar *et al.*, (1989), allows contribution from respiration, liquid-phase diffusion, isotopic changes due to carbon export, CO_2 fixation in C3 plants by PEP carboxylase and a variety of other factors. However, the value of *d* is usually very small and therefore is usually neglected within a single series of studies without significant variation in results (Saugier *et al.*, 2012).

The focus in this thesis was on calculating the discrimination against ^{13}C from leaf dry-matter primarily from C3 plants. Equation (1) and (2) predicts that, $\delta^{13}C_p$ should vary as a function of C_i/C_a in C3 plants provided that $\delta^{13}C_a$ is constant. Although $\delta^{13}C_a$ may vary in

closed canopy forests, glasshouses, and other situations where the turbulent exchange of air between the plant canopy and the free troposphere is impeded, it is generally relatively constant in the atmosphere where CO_2 is well-mixed (Cernusak *et al.*, 2013). Consequently, $\delta^{13}C_p$ generally varies significantly as a function of C_i/C_a in C3 plants. For example, in 44 species of well-watered tree seedlings of angiosperms (circles in **Figure 1.5**) and conifers (triangles) grown either outdoors or in well-ventilated shade houses (Orchard *et al.*, 2010), the geometric mean regression through the dataset yields the equation: $\delta^{13}C_p$ (‰) = -12.1 - 22.0 C_i/C_a, which is close to the predicted relationship assuming $\delta^{13}C_a$ = - 8‰, a = 4.4‰ and b = 27‰, i.e., $\delta^{13}C_p$ (‰) = -12.4 - 22.6 C_i/C_a (Cernusak *et al.*, 2013).

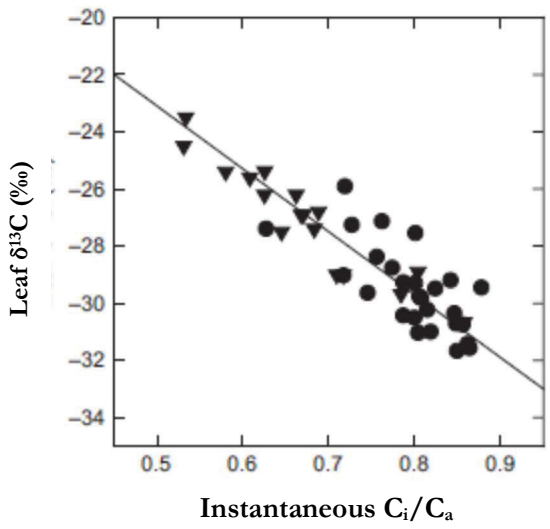

Figure 1.5: Bulk-leaf $\delta^{13}C$ plotted against the instantaneous C_i/C_a ratio during photosynthesis for seedlings of 44 tree species (from Cernusak *et al.*, 2013).

Each data point represents the average of several individuals of one species. Species' identities are detailed in Orchard et al., (2010). The solid line is a geometric mean regression: leaf $\delta^{13}C$ (‰) = -12.1-22.0 C_i/C_a.

Water-use-efficiency in relation to $\Delta^{13}C$

The definition of water-use-efficiency (WUE) depends upon the particular context in which it is being discussed. For example, the time-scale over which WUE is measured (e.g. instantaneous exchange of water vapour for CO_2 gas *versus* biomass accumulation or yield) or water loss in relation to carbon gain at the leaf-level (Eamus, 1991). In most of the

current literature, WUE is discussed either in terms of an instantaneous measurement of the efficiency of carbon gain for water loss; or as an integral of such an efficiency over time, (commonly expressed as ratio of water use to biomass accumulation, or harvestable yield) (Bacon, 2009). In agronomy, WUE is the measure of a plant's capacity to convert water into plant biomass. It includes both the use of water stored in the soil and rainfall during the growing season.

$$\text{WUE} = \frac{\text{Dry matter production or crop yield per unit land area } (\frac{\text{kg}}{\text{ha}})}{\text{Water consumed as transpiration per unit land area } (\frac{\text{kg}}{\text{ha}})}$$

Plant physiologists, however, have defined WUE in a fashion that is somewhat similar to the photosynthesis to transpiration ratio, i.e.:

$$\text{WUE} = \frac{\text{Net } CO_2 \text{ uptake } (\mu\text{mole}/\text{m}^2\text{sec})}{\text{Transpiration rate } (\mu\text{mole}/\text{m}^2\text{sec})}$$

This is often termed the instantaneous transpiration ratio (Barton *et al.*, 2012). For example in well-watered C3 plants, about 500 molecules of water are lost for every molecule of CO_2 fixed by photosynthesis. This gives a WUE of 1/500 or 0.002 for C3 plants. Plants with C4 photosynthesis generally transpire less water per molecule of CO_2 fixed; a typical WUE for well-watered C4 plants is therefore about 1/250 or 0.004.

A simpler concept of WUE also often used is that of *instantaneous water-use-efficiency*, WUE_{inst}, defined as the ratio of the fluxes of net photosynthesis (A) and transpiration (E) (Eamus, 1991). This is commonly measured at leaf-scales (e.g. Moreno-Gutiérrez *et al.*, (2012)). Since A and E share a diffusion pathway, i.e., the stomata, WUE_{inst} can be determined without an estimate of stomatal conductance (g_s). However, stomatal response to leaf-to-air vapour pressure deficit (VPD, defined as the difference in water vapour pressure between the interior of the leaf and the surrounding atmosphere) is likely to result in the

optimization of plant water use in relation to carbon gain. At the leaf-level, carbon fluxes involved in net photosynthesis (A) is measured as CO_2 uptake, and water fluxes (transpiration, E) is measured as water loss. In a steady state, these fluxes can be quantified by Ohm's law analogy relationships:

$$E = v * g_w \qquad (3)$$

And,

$$\mathrm{A} = (C_a - C_i) * g_c = \frac{(C_a - C_i) * g_w}{1.6} \qquad (4)$$

Here, *v* is the gradient in water-vapour pressures between the inside of the leaf and the atmosphere outside the boundary layer (e_i - e_a) divided by the total atmospheric pressure (P), g_c is stomatal conductance to CO_2, g_w is leaf-conductance to water vapour = 1.6 * g_c where 1.6 is the ratio of gaseous diffusivities of CO_2 and water vapour in air and C_i and C_a are the intercellular and atmospheric concentration of CO_2, respectively

From equation (3) and (4), WUE_{inst} can be written as:

$$WUE_{inst} = \frac{A}{\mathrm{E}} = \left(1 - \frac{c_i}{c_a}\right).\frac{c_a}{1.6\ v} \qquad (5)$$

Expressing the vapour pressure gradient between the inside and outside the leaf using *v* (i.e., $v = \frac{(e_i - e_a)}{\mathrm{P}}$ eliminates the effects of elevation changes (P) and temperature on diffusion on the estimates of the stomatal conductance (g_s)) (Saugier *et al.*, 2012). Also, e_i - e_a in the numerator of the term *v* in the equation (3) represents the difference in water vapour pressure between the interior of the leaf and the surrounding atmosphere which is essentially the leaf-to-air vapour pressure deficit (VPD).

Another measure of plant water-use-efficiency is the *intrinsic water-use-efficiency* (WUE_i) defined as A/g_w, i.e., the ratio of net photosynthesis to stomatal conductance to water vapour. This is essentially WUE_{inst} multiplied by *v*. WUE_i is a better measure of leaf-level water-use-efficiency because it allows direct comparison of intrinsic physiological considerations, eliminating the confounding effects of differences induced by temperature and humidity gradients or evaporative demands between plants (Osmond *et al.*, 2012; Saugier *et al.*, 2012). From equation (2), (3) and (4) WUE_i for C3 plants can be calculated using the discrimination against ^{13}C ($\Delta^{13}C$) calculated from bulk-leaf $\delta^{13}C$ using the following equation (Werner *et al.*, 2012):

$$WUE_i = \frac{c_a(b - \Delta^{13}\mathrm{C})}{1.6(b - a)} \qquad (6)$$

Equation (6), therefore, is often applied as an indicator of *long-term* trends in the internal regulation of carbon uptake and water loss of plants.

Stomatal conductance (of both CO_2 and water vapour), WUE_{inst} and WUE_i are important ecophysiological traits that have rarely been examined in relation to hydraulic strategies of co-occurring species (Moreno-Gutiérrez *et al.*, 2012; Werner *et al.*, 2012). In this thesis, Equation (6) has been used to calculate WUE_i at the leaf-level using the bulk-leaf $\Delta^{13}C$. An understanding of the drivers of changes in $\Delta^{13}C$ and WUE_i at leaf scales will advance our understanding of the alternate hydraulic strategies of co-existing species (Moreno-Gutiérrez *et al.*, 2012) across water availability gradients.

Stomatal regulation in relation to water availability

Stomata in leaves of plants act as gate between the interior of the plant and the atmosphere and play a vital role in determining vegetation responses to environmental conditions. Considerable research efforts are currently directed towards investigating stomatal responses to external/environmental conditions ranging from molecular levels to whole plant levels as well as to ecosystem levels (Nilson and Assmann, 2007). It is essential that stomata remain open for CO_2 to penetrate the leaf in order to continue photosynthesis and

this also allows substantial amount of water loss in the form of transpiration. The driving force for water loss to the atmosphere from the sub-stomatal cavity is typically 100 times larger than the driving force for CO_2 uptake into the sub-stomatal cavity for photosynthesis (Bacon, 2009). In a typical C3 plant, the outward fluxes of water vapour may reach 2000 to 3000 μmol m^{-2} s^{-1}, whereas, the inward fluxes of CO_2 may range between 20 and 30 μmol m^{-2} s^{-1} under well-watered conditions. Consequently there is an inherent dominance of water loss to carbon gain in all plants. When water availability is a limiting factor, however, excessive water loss (via transpiration) must be minimized in order to prevent desiccation, drought stress or even plant death. Hence, a coordinated regulation of gas-exchange to maximise carbon gain whilst simultaneously minimising water loss is integral to plant survival (Cowan and Farquhar, 1977; Medlyn *et al.*, 2011).

Each stoma consists of microscopic pores surrounded by a pair of guard cells. Guard cells can increase or decrease the size of the pore by changing their turgor status, therefore, stomata can regulate the diffusive mass transfer of both water vapour and CO_2 between environment and the leaf interior. In this process, stomata maximize CO_2 entry into the leaf and transpiration while minimizing loss of water from the leaf during stressful environmental conditions. When stomatal pores remain open and conductance is high, the intercellular concentration of CO_2 (C_i) also remains high, closer to the concentration of atmospheric CO_2 (C_a) and a larger C_i/C_a ratio. In contrast, a lower stomatal conductance results in a much lower concentration C_i and a smaller C_i/C_a ratio. For example, in a well-watered plant, C_i/C_a might approximate 0.8, whereas, it can be as small as 0.3 during extreme water-stress (Farquhar and Sharkey, 1982; Seibt *et al.*, 2008).

Under any particular set of conditions, equation (2) suggests that, as C_i/C_a ratio decreases, discrimination against ^{13}C ($\Delta^{13}C$) also decreases and *vice versa*. Considering two limiting cases as described in O'Leary, (1993), when stomata are nearly closed, C_i becomes very small and the overall CO_2 uptake is limited only by the initial diffusion process. Under these circumstances virtually all available C is taken up during the carboxylation process without significant enzymatic discrimination and therefore, only the diffusional fractionation is expressed and $\delta^{13}C$ of C3 plants should approach -8 -4.4‰ = -12.4‰. In contrast, when stomata are relatively open, C_i approaches C_a and transfer can occur between the intercellular and atmospheric pools of CO_2. Under these circumstances diffusion approaches equilibrium and the diffusional fractionation of ^{13}C is not expressed, however,

enzymatic fractionation takes place and $\delta^{13}C$ of C3 plants approaches -8-30‰ = -38‰. Bulk-leaf $\delta^{13}C$ can therefore be expected to range between these two extremes.

Net photosynthetic rate is a result of the interaction of source-atmospheric CO_2 and stomatal regulation with sink-intercellular CO_2 during assimilation in the mesophyll. Theoretically from equation (5) and (6), WUE (like $\Delta^{13}C$) will be inversely proportional to C_i/C_a. When C_i is low (smaller C_i/C_a ratio), the driving force for CO_2 uptake will be enhanced while the driving force for water loss will remain relatively unchanged both ultimately resulting in an increase in WUE (Bacon, 2009).

To summarize, C_i/C_a ratio is determined by interaction of CO_2 assimilation rate and the extent of stomatal opening, i.e., by the supply and utilization of CO_2 at sites of carboxylation in the mesophyll of the leaf (Pate, 2001). Thus, a photosynthetically active plant with relatively closed stomata will tend to exhibit low C_i/C_a ratios and accordingly less negative $\delta^{13}C$ values, smaller $\Delta^{13}C$ and increased WUE for the photosynthate which it is producing compared to a corresponding plant with relatively open stomata having higher C_i/C_a ratio, and hence a more negative $\delta^{13}C$ values, larger $\Delta^{13}C$ and decreased WUE.

Scope and structure of this thesis

The overall objective of this thesis is to incorporate stable hydrogen, oxygen and carbon isotope analysis techniques in investigating sources of water uptake by plants as well as discrimination against ^{13}C and water-use-efficiency in relation to varying degrees of water availability across moisture and temperature gradients in Australia. There is a clear need to better understand how vegetation responds to water stress, particularly in Australia, the driest of all permanently inhabited continents. My research aimed at providing a better understanding of contrasting water uptake and water use strategies of dominant overstorey and understorey species across contrasting ecosystems in Australia and also how these species respond to variation in water availability. I hypothesized that spatial and temporal variability of plant water sources and access to these sources by plants, or the lack thereof, will also be reflected in their water-use-efficiency at the leaf-level. To test this hypothesis I specifically focused on using stable isotope analyses to trace possible water sources accessed by vegetation across different sites, quantified proportional contributions of these sources and investigated concomitant water-use-efficiencies at the leaf-level. The findings presented in this thesis will provide assistance in predicting the nature and scale of

ecosystem responses to water stress as well as valuable insights on the effectiveness of using stable isotope analysis techniques in investigating such processes.

This thesis consists of six chapters including this chapter (**Chapter 1**), which provides a general background for the work described in subsequent chapters. In **Chapter 2** and **Chapter 3**, I investigated contrasting water uptake and water use strategies of two very structurally and climatically different ecosystems. The first site was located in NSW, a temperate mesic site (mean annual rainfall of >1000 mm) across a naturally occurring gradient in depth-to-groundwater. The second site was tropical, located in the Northern Territory in a semi-arid region with extremely seasonal and low mean annual precipitation (<350 mm). This site also had a natural gradient in depth-to-groundwater. In these two chapters, I aimed at providing insights on the nature and extent of groundwater dependency across sites and also investigated whether spatial and/or seasonal variation of groundwater uptake was reflected at the leaf scale.

In **Chapter 4**, I moved my focus from groundwater gradients in a particular region to a climate gradient across multiple sites and across a much larger spatial/species scale at a continental scale in Australia. In addition to investigating seasonal and/or spatial variability in $\Delta^{13}C$ and intrinsic water-use-efficiency and their relationships with water availability, I also examined to what extent $\Delta^{13}C$ reflects variations in leaf structural, functional and nutrient traits in this chapter. In addition, this chapter looked at the effectiveness $\Delta^{13}C$ as an integrative ecological tracer to explain environmental constraints at a continental scale.

The ability of vegetation to respond to adverse or changing environments may also to some degree be constrained by their evolutionary history of the species involved. However, the ancestral history of the species is generally not included in comparative ecophysiological studies that focus on interspecific patterns of leaf-traits. In **Chapter 5**, I aimed at re-evaluating the traditional cross-species relationships of $\Delta^{13}C$ with climate variables as well as other leaf structural, functional and nutrient traits from an evolutionary perspective by formally including phylogenetic information of the extant taxa involved in the comparative analysis.

Finally, **Chapter 6** provides a general discussion of the collective outcomes of this research and its relevance to understanding water uptake and water use strategies of vegetation

across a range of sites in Australia using stable isotope techniques and suggests avenues for further research.

Chapter 2 Sources of water uptake, discrimination against ^{13}C and water-use-efficiencies in mesic *Eucalyptus* woodlands sampled along a natural gradient of depth-to-groundwater

Introduction

Australia is the driest continent on the Earth and the majority of its land area is classified as semi-arid and arid (O'Grady *et al.*, 2006c). Mean annual rainfall in Australia is only about 350-450 mm yr^{-1} and evapotranspiration typically accounts for about 90–98% of available rainfall (Eamus, 2009). Annual evaporation, however, frequently exceeds annual rainfall across most of the continent (O'Grady *et al.*, 2011). For example, annual tree water use exceeds rainfall by 30–300% across a number of sites in South Australia (Benyon *et al.*, 2006), a result made possible by access to groundwater at these sites. Consequently groundwater plays a significant role in many of Australia's ecosystems (Eamus *et al.*, 2006a; Evans and Hatton, 1998) and this role can vary from minor to essential. Technically groundwater is defined as the saturation zone of the regolith and its associated capillary fringe (Eamus *et al.*, 2006b) and is the largest global store of liquid fresh water, accounting for about 96% of all liquid fresh water (Shiklomanov, 1998). Owing to being hidden from view, the importance of groundwater is generally not well understood nor fully appreciated. There also exists an ever increasing need for fresh water for drinking, irrigation and other human consumption and this has created an increasing demand for groundwater extraction in Australia. Thus groundwater usage has doubled over 1983-1996 and in New South Wales and Western Australia this increase is even larger (Eamus *et al.*, 2006b). Consequently, there is considerable concern about the potential impacts of over-extraction of groundwater on ecosystems dependent on groundwater within Australia and globally.

It was not until the 1990s that Groundwater Dependent Ecosystems (GDEs) were widely recognized as a separate class of ecosystems by the hydrological and ecological communities in Australia (Eamus *et al.*, 2006b). Their conservation, biodiversity, cultural, economic and social values are increasingly being recognized. Ecosystems that partially or seasonally, if not solely, rely on groundwater for their water requirements are classified as GDEs. In other words, GDEs are "ecosystems whose current composition, structure and function are reliant on a supply of groundwater" (Eamus, 2009). Terrestrial vegetation may exhibit complex spatial and temporal patterns of groundwater use (Evans and Hatton, 1998; O'Grady *et al.*, 2006a); for example, their reliance on groundwater might be expressed every day of the year or only for a few months each year or every few years and this only becomes observable when the supply of groundwater is removed for a sufficient length of time to affect plant function (typically rates of water use) (Eamus, 2009). Several studies over the last few decades have investigated the role of groundwater in Australian ecosystems. Evans and Hatton, (1998) showed that groundwater plays a minor to major role in most of Australia's wetlands; whilst some wetlands may be completely dependent on groundwater discharge under all climatic conditions, others may have very limited dependence, such as only under dry conditions (Mudd, 2000; Thorburn *et al.*, 1994). Around Australia, groundwater dependence has been demonstrated in a large range of terrestrial vegetation communities which includes tropical woodlands and tropical forests (Drake and Franks, 2003; O'Grady *et al.*, 2006a), arid woodlands (O'Grady *et al.*, 2009), *Melaleuca* forests (Kelley *et al.*, 2007), woodlands in Mediterranean environments (Groom *et al.*, 2000), riparian (Lamontagne *et al.*, 2005; Thorburn *et al.*, 1993) and some temperate plantations (Benyon and Doody, 2004).

The complexity associated with establishing a degree of groundwater usage in order to allocate *environmental flow*[3] represents a significant challenge to water-resources managers (Eamus *et al.*, 2006b; O'Grady *et al.*, 2006a). One powerful approach is the use of stable isotopes at natural abundance levels which can provide information about variation in groundwater dependency within and between species and ecosystems. Use of stable isotopes has increasingly been recognized as a tool for understanding a number of physiological process and environmental interactions in ecology. Especially in ecophysiology, a large number of studies investigated the main sources or possible

[3] An allocation of water to the environment, expressed as the minimum flow (volume of water) required through a specific location within a specified time to maintain the health of an ecosystem (Eamus *et al.*, 2006b).

combinations of sources of water uptake of vegetation by comparing δ^2H and/or $\delta^{18}O$ composition of vegetation branch (xylem) water with those of possible sources of water available for uptake (surface water, groundwater, soil water, rain water; see **Chapter 1**) (Busch *et al.*, 1992; Ehleringer and Dawson, 1992; Jobbágy *et al.*, 2011; Kray *et al.*, 2012; Lamontagne *et al.*, 2005; O'Grady *et al.*, 2006b; Smith *et al.*, 1998; Thorburn *et al.*, 1993; Zencich *et al.*, 2002). For example, (O'Grady *et al.*, 2006c) showed that trees located at the junction of the Douglas and Daly Rivers in the Northern Territory varied their principal source of transpired water according to position within the landscape. Species (*Melaleuca argentea* and *Barangtonia actuangula*) located closer to the river showed a more enriched signal of δ^2H consistently similar to that of groundwater indicative of their *obligate use* of groundwater. A similar study conducted using isotopes in *Banksia* woodlands on the northern Swan Coastal Plain in Western Australia found that *Banksia attenuata* and *Banksia ilicifolia* species derived some of their water from groundwater throughout the dry-wet-seasonal cycle (Zencich *et al.*, 2002). However, the majority of such studies have been conducted in arid and semi-arid climates (Jobbágy *et al.*, 2011; Kray *et al.*, 2012; O'Grady *et al.*, 2006c; Smith *et al.*, 1998) because of the lack of rainfall and surface water stores in such climates. The work described in this chapter is unusual in that it was conducted in a mesic environment where mean annual rainfall was consistently larger than 1000 mm for the period 1990 – 2014 (Bureau of Meteorology Station No: 068243) in Kangaloon bore-field site in the Southern Highlands, NSW.

The Kangaloon bore-field site is a relatively undisturbed *Eucalypt* woodland occurring along a natural depth-to-groundwater gradient. Knowledge of proportional use of groundwater by the vegetation at sites with different depths to the water table in this region is crucial for land and water resources managers and would contribute to our understanding of the effects of groundwater drawdown in this region. To address this issue, the present study investigated the proportional use of potential water sources used by dominant overstorey and understorey species using stable isotope mixing models (SIMMs). SIMMs, increasingly being used over the past few decades, can quantify source contributions to a mixture and naturally occurring stable isotopes are used to determine water, carbon or nutrient sources and trace element fluxes and cycling in a variety of systems (Phillips and Gregg, 2003). Nearly all SIMMs extensively used in ecological research use basic mass balance principals and the distinct isotopic signatures of various sources in order to determine their relative contributions to the mixed signature in an end product (Hopkins III and Ferguson, 2012;

Phillips and Gregg, 2003). In the context of the present study, if the mixing subspaces are defined by two tracers (for example, δ^2H and $\delta^{18}O$) and three possible sources (e.g., groundwater, soil water, recent rain water etc.), the sources are plotted as vertices of a triangle in the mixing subspace and any point bound by the triangle represents a tree using a combination of these sources. This approach of estimating proportional contribution of potential sources is particularly advantageous over direct comparison to trace source water uptake. This is because vegetation with roots throughout the soil profile is unlikely to obtain water from a single source from a particular depth with the most similar isotopic composition (Cramer *et al.*, 1999) and may utilize other possible sources, for example, soil water from deeper soil layers, groundwater or recent rain water represented by soil water signatures from the upper soil layers.

Another naturally occurring stable isotope, that of carbon, ^{13}C, and discrimination against ^{13}C ($\Delta^{13}C$) calculated from ^{13}C in leaf dry-matter can also be used as a proxy to calculate leaf intrinsic water-use-efficiency, WUE_i (this is discussed in more detail in **Chapter 1**). Like δ^2H and $\delta^{18}O$, $\Delta^{13}C$ (and WUE_i) has also been increasingly used for identifying strategies of water use in terrestrial plants both globally (Diefendorf *et al.*, 2010; Kohn, 2010) and regionally in Australia (Cernusak *et al.*, 2011; Cernusak *et al.*, 2013; Miller *et al.*, 2001; Schulze *et al.*, 1998b; Stewart *et al.*, 1995). However, it has not, to-date, been applied to GDEs to this author's knowledge. Several studies previously documented decrease in $\Delta^{13}C$ and associated increase in WUE_i with decreasing water availability in a number of plant functional types (Dawson and Ehleringer, 1993; Diefendorf *et al.*, 2010; Ehleringer and Cooper, 1988; Kohn, 2010; Leffler and Evans, 1999; Livingston and Spittlehouse, 1996). Based on the well-documented influence of water availability on WUE_i, I hypothesise that the $\Delta^{13}C$ of vegetation using groundwater will differ at sites that have shallow, compared to sites with deeper depth to water table.

Dendrochronology, the study of growth in tree rings, has a long history in ecological research spanning many decades (Drew and Downes, 2009; McCarroll and Loader, 2004) and a substantial number of both early and recent dendrochronological studies have documented good correlations of seasonal water availability and tree height with annual diameter growth (Carter and Klinka, 1990; Giles *et al.*, 1985; Robertson *et al.*, 1990; Spittlehouse, 1985). Quantification of growth rates from tree rings have been used to reconstruct fluctuations in the supply water from precipitation and groundwater (Bogino and Jobbágy, 2011; Oberhuber *et al.*, 1998; Perez-Valdivia and Sauchyn, 2011; Xiao *et al.*,

2014). Application of isotope analyses to tree rings (isotopic dendroclimatology) is a relatively recent field and has increasingly been applied over the last few decades (McCarroll and Loader, 2004). Tree-rings act as archives of the carbon, hydrogen and oxygen extracted from the environment each year and provide a record of the past in the annual rings (McCarroll and Loader, 2004). Variations in isotopic composition across different tree rings have been associated with changes in water availability in a number of studies based on the principle that, wood formed during water-stress is enriched in ^{13}C, reflecting the decreased stomatal conductance relative to photosynthesis arising from water stress. As a consequence, the ratio of $[CO_2]$ within and outside of the leaf (C_i/C_a) changes and this is recorded in the cellulose of tree rings (Cocozza *et al.*, 2011; Horton *et al.*, 2001; Máguas *et al.*, 2011; McCarroll and Loader, 2004). In addition, isotope ratios in tree-rings have an added advantage that the physiological controls on variation of these isotopes are reasonably well understood as well as relatively simple compared to the myriad factors controlling annual growth increment. Several studies observed a good relationship between discrimination/WUE_i calculated tree-ring ^{13}C content and accumulated transpiration/transpiration deficit (Dupouey *et al.*, 1993; Livingston and Spittlehouse, 1996). In another study, variations in ^{13}C content across growth rings in pine and maple were found to be related to changes in soil water during the growing season (Leavitt, 1993). Relatively recent application of isotopes in dendroclimatology of GDEs have provided an insight into the importance of access to groundwater on plant growth. Thus Hultine *et al.*, (2010) identified rapid, large and reversible responses of tree ring width to draining and refilling of a nearby reservoir. Long-term trends in depth-to-groundwater have also been observed to impact the dendrochronology of vegetation (Bogino and Jobbágy, 2011; Lageard and Drew, 2008). Determination of the link between variations of ^{13}C content in tree rings with water availability should therefore improve the reliability of results obtained from foliar isotopic analysis of the GDEs as well as increase our understanding of tree water use.

This study investigates proportional use of groundwater (and other possible sources of water) by dominant overstorey and understorey species along a naturally occurring depth-to-groundwater (DTGW) gradient in mesic *Eucalyptus* woodlands in south-western Australia. A combination of $\delta^{18}O$ and $\delta^{2}H$ signatures of groundwater, soil water and xylem branch water and $\delta^{13}C$ signatures from leaves and tree-cores were used in this study. Although a number of studies have examined patterns of water use/ hydraulic architecture

of vegetation in several different types of ecosystems, for example, comparing mesic and xeric habitat (Addington *et al.*, 2006) or spatially extensive environmental gradients e.g., across precipitation gradients (Schulze *et al.*, 1998a), few studies have examined variation in patterns of water uptake arising from differences in depth-to-groundwater (DTGW), especially in mesic environments where water availability is generally not a limiting factor. The focus of this chapter was to compare and contrast how differences in DTGW influence patterns of uptake of water and leaf intrinsic water-use-efficiencies of dominant overstorey and understorey species in a mesic remnant *Eucalyptus* forest. Patterns of several structural and functional attributes in these forests have previously been shown to differ significantly across this gradient in DTGW (Zolfaghar *et al.*, 2014). Thus, the three shallowest groundwater sites (DTGW ≤ 5.5 m) contained taller trees, maintained a larger stand basal area, larger leaf area index, larger above-ground biomass, larger annual rates of leaf litterfall production and consequently larger above-ground net productivity than the sites with deeper water tables (Zolfaghar *et al.*, 2014).

Specifically, this study aimed at answering the following questions:

1. Do the dominant overstorey and understorey species in the study site take up water from different sources?
2. What proportion of groundwater is used by the dominant overstorey and understorey species in the study site?
3. Can stable isotope signatures ($\Delta^{13}C$ and WUE_i calculated from $\Delta^{13}C$) of leaf and sap wood be used to identify groundwater use?

Materials and methods

Site description

Sampling of the mesic *Eucalypt* woodland was conducted in March 2013 at five locations along a naturally occurring depth-to-groundwater gradient in relatively undisturbed native woodlands of the Kangaloon bore-field site in the Southern Highlands, NSW. The site is located in the Upper Nepean catchment 110 km south-west of Sydney (between 34°29' S 150°34' E and 34°32' S 150°37' E). DTGW in this area has been monitored by the Sydney Catchment Authority (SCA) on a daily basis since 2006 and average DTGW fluctuated minimally (<10%) across all sites during 2006-2012. The closest BoM station to the project site was the Burrawang (Spurfield) meteorological station (station no: 068243, elevation 685

m, http://www.bom.gov.au/) operated from 1961 to the present. The study area received a mean annual rainfall of 1067 mm; rainfall in 2011 and 2012 however, was 1561 and 1188 mm respectively representing 46% and 11% larger rainfall above the long-term mean (Zolfaghar *et al.*, 2015). Mean monthly rainfall is largest in February in recent years (186 mm) and smallest in August (51 mm). Mean minimum temperature occurs in July (2.7°C) and mean maximum temperature in January (24.3°C) for the period of 2010-2013.

The study site has a natural gradient in DTGW, enabling measurement of the influence of DTGW on vegetation. Five specific study sites were selected to encompass a full range of depths (2.4 m to 37.8 m), thereby allowing the potential for variation in sources of water uptake and water-use-efficiency of the vegetation. The selected study site numbers, GPS locations of the bores and approximate DTGW are listed in **Table 2.1**.

Table 2.1: Specific study sites, GPS locations and depth-to-groundwater at each study sites

SCA* Site ID	GPS location of the existing bore	Date of observations of GW depths	No of observations	Average DTGW (± SE) (m)	Distance from Site (km)
3J	S 34° 32' 23.2" E 150° 37' 49.9"	12/10/2007-29/11/2012	1876	2.4 (0.008)	11.91
3F	S 34° 31' 48.4" E 150° 37' 37.9"	10/09/2007-29/11/2012	16	4.3 (0.19)	12.08
3A	S 34° 31' 43.7" E 150° 37' 18.9"	21/12/2006-29/12/2012	2171	9.8 (0.02)	11.72
8A	S 34° 30' 43.9" E 150° 36' 34.9"	02/05/2011-22/05/2012	04	14.6 (0.43)	11.84
10A	S 34° 29' 1.9" E 150° 34' 0.2"	16/03/2006-13/11/2012	2435	37.8 (0.24)	11.89

*Data from Sydney Catchment Authority (SCA).

Sampling protocol

At each DTGW site, dominant overstorey and understorey species were selected based on the data collected by the Terrestrial Ecohydrology Research Group (TERG), University of Technology Sydney (UTS). Three replicate plots (20 m x 20 m) were established and within each replicate plot, three trees of the two dominant overstorey species and the two dominant understorey species were sampled based on the total basal area of each species. Dominance in this protocol means the two species that account for the largest basal areas

in the replicate plots at each DTGW site. **Table 2.2** shows the dominant overstorey and understorey species selected for the study:

Table 2.2: Selected overstorey and understorey species based on the basal area (m^2) estimated from three 20 m X 20 m plots.

Site ID	DTG W (m)	Dominant overstorey	Basal Area (m^2)	Dominant understorey	Basal Area (m^2)
3J	2.5	*Eucalyptus piperita*	1.74	*Persoonia linearis*	0.14
		Eucalyptus radiata	2.56	*Pultenaea blakelyi*	0.04
3F	4.3	*Eucalyptus globoidea*	3.17	*Banksia spinulosa var. spinulosa*	0.02
		Eucalyptus sieberi	1.02	*Acacia longifolia*	0.04
3A	9	*Eucalyptus sclerophylla*	1.26	*Persoonia levis*	0.06
		Eucalyptus sieberi	0.65	*Banksia spinulosa var. spinulosa*	--
8A	13.5	*Eucalyptus piperita*	2.27	*Acacia longifolia*	0.003
		Eucalyptus sieberi	1.53	*Acacia terminalis*	0.003
10A	37	*Eucalyptus sclerophylla*	1.60	*Leptospermum polygalifolium*	0.20
		Eucalyptus piperita	0.95	*Persoonia levis*	0.02

Data collected by Terrestrial Ecohydrology Research Group (TERG), UTS.

Three trees located within ~50 m radius of the bore for each dominant overstorey and understorey species were selected for sampling. Terminal branches and leaves of the overstorey trees were harvested from the top of the canopy using an elevated work platform. From each tree, two branch samples of about 5 cm length and 10 mm in diameter were collected for δ^2H and $\delta^{18}O$ analysis. Sampling strategy was designed so as to collect all branch samples without altering the isotopic ratio by fractionation caused by evaporation (see **Chapter 1**). While only a few microliters are needed for δ^2H and $\delta^{18}O$ analysis, sampling of branches (and soil) was designed to collect ~2 ml water by cryogenic vacuum extraction (see below), to avoid evaporation problems with small samples. Large sample sizes can minimize the influence of inadvertent fractionation arising during collection and storage of sample. All branch samples had the bark stripped off, were sealed in small plastic centrifuge tubes and wrapped in parafilm, refrigerated in a portable cooler and stored at -20 ℃ in the laboratory until cryogenic distillation. Soil samples were collected at each of the five sampling sites from soil surface to up to ~1 m at 10 cm interval to determine variations in δ^2H and $\delta^{18}O$ across different depths of the soil profile. Samples of bulk soil were extracted with a hand operated soil corer and were also immediately stored

in the same type but larger plastic centrifuge tubes as the branch samples, sealed with parafilm and stored in a portable cooler. Branch, leaf and soil samples were collected in March 2013. Rain water samples were collected from a rain water collector installed near the automated weather station in the study area in July, August, September and October 2013. Groundwater samples were also collected from the bores located at each site using HydraSleeve™ no-purge groundwater sampler, GeoInsight, USA (Cordry, 2003).

Healthy well-exposed mature leaves were collected for ^{13}C analysis from three different branches of three different trees for each species and stored in paper bags. At each site, sampling of stem, leaves, soil and groundwater was performed on the same day. Wood cores (one core per tree and two-three cores per species) were also collected from *Eucalyptus sclerophylla* species which was available at all sites except for the shallowest site (DTGW 2.4 m) for which *Eucalyptus piperita* cores were collected. Cores were collected using a power corer in a slow speed up to the centre of the tree. After collection, each core was transferred in an appropriately sized PVC pipe for shipment and air-dried and stored in the laboratory until analysis. To avoid the inclusion of wood $\Delta^{13}C$ from different years, trees of similar size were selected for wood core sampling, with DBH ranging between 60-70 cm.

Procedure of branch (xylem) water extraction and analysis

Branch water and soil water in this study was extracted by cryogenic vacuum distillation. In this method, water from stem and soil sample is extracted by evaporation and the vapour is captured in a cold trap and frozen cryogenically with liquid nitrogen (based on the principals described in Ingraham and Shadel, (1992)). This method requires a complex vacuum system and the duration of the extraction process is longer than some of the other methods of water extraction, for example, the azeotropic or centrifugation method (Vendramini and Sternberg, 2007). However, it provides consistent high precision and accuracy for water distilled from various plant tissues and soil, especially for stable isotope analyses (Orlowski, 2010). All stem and soil samples were extracted using the cryogenic vacuum distillation system constructed by Dr Tomek Wyczesany and myself in the TERG research laboratory in University of Technology Sydney (UTS). The design of this system was based on the vacuum extraction device outlined in West *et al.*, (2006). It consists of six independent glass units each consisting of two L-shaped tubes connected to an extraction unit and an U-shaped collection unit, all attached to a stainless steel vacuum manifold through the collection unit (**Figure 2.1**). Each unit can be isolated from the manifold by a

plug valve. The required vacuum is generated by a vacuum pump connected to the stainless steel manifold.

Figure 2.1: Cryogenic distillation system to extract water for stable isotope analysis.

The silver flasks in the front of the system contain liquid nitrogen to capture water vapour from the samples (soil or branch). Samples are heated to 60℃ in the flasks sitting in individual heating mantles at the rear of the apparatus. The lines connecting the liquid nitrogen flasks and sample flasks are under a hard vacuum to facilitate removal of water from the samples.

Branch water and soil water were extracted based on the methodology described in (Orlowski, 2010). Each soil/stem sample was weighed and the weight was recorded before starting the extraction process. First, an evacuated extraction unit (usually under vacuum for 10-15 minutes prior to the analysis) was isolated from the vacuum manifold to insert a sample in the extraction tube. The centrifuge tube used for sample storage was opened and immediately inserted in the extraction tube with the sample inside to minimize fractionation induced by handling and evaporation due to exposure followed by the reconnection of the unit to the manifold. For soil samples, glass wool was packed above

the inserted centrifuge tubes to prevent the spread of soil particles through the stainless steel manifold. The extraction tube containing the sample was again frozen for 10 minutes using small liquid nitrogen Dewars. Next, the Dewars were transferred below the U-shaped collection tubes to freeze out the evaporating waters from the samples and the extraction tube was placed in a beaker containing water in a heating element at 60 ℃. After inserting six individual samples in the system and subsequent steps mentioned above, the whole unit was pumped down to a pressure of approximately 10 milliTorr. Throughout the whole extraction process, the sample in the extraction tube was heated in a beaker at 60 ℃ while the tip of the collection tube was placed in a liquid nitrogen Dewar which was refilled as required to ensure constant freeze-out of the evaporating water.

Water from each branch sample was extracted for a minimum of 60-75 minutes and each soil samples for 30-45 minutes following the extraction time suggested by West *et al.*, (2006) to ensure a complete extraction of water. After completing the extraction, the vacuum pump was turned off and the boiling water and liquid nitrogen were removed from under the collection tube and the extraction tube, respectively. The system was then left to defrost all the while under vacuum for ~45 minutes. The extracted water in the collection U-tubes was pipetted into vials for analysing their isotopic signatures. Each branch/soil sample after extraction was oven dried for 48 hours and the dry weight was recorded, which was then deducted from the weight of samples measured prior to extraction to get the weight of water contained in the sample. Percentage of extracted water was then calculated and the sample was discarded and re-extracted if the percentage of extraction was < 90%.

The δ^2H and $\delta^{18}O$ analysis of all soil and branch water was performed using the Picarro L2120-i Analyser for Isotopic H_2O in the TERG research laboratory at UTS. Five laboratory standards were calibrated against IAEA VSMOW2– SLAP2 scale, where Vienna Standard Mean Ocean Water 2 (VSMOW2, $\delta^{18}O$ =0 ‰ and δ^2H =0 ‰), Standard Light Antarctic Precipitation 2 (SLAP2, $\delta^{18}O$ = - 55.5 ‰ and δ^2H = - 427.5 ‰) and Greenland Ice Sheet Precipitation (GISP, $\delta^{18}O$ = - 24.8 ‰ and δ^2H = - 189.5 ‰) were used as quality control references (IAEA, 2009). The standard deviation of the residuals between the VSMOW2–SLAP2 value of the internal standards and the calculated values based on best linear fits was ~ 0.2 ‰ for $\delta^{18}O$ and ~ 1.0 ‰ for δ^2H.

^{13}C isotope composition of leaves and wood cores

Leaf samples stored in paper bags were completely dried in an oven at 60℃ for five days. After drying, each leaf sample was ground with a Retsch MM300 bead grinding mill (Verder Group, Netherlands) until finely and homogeneously ground. Between one and two milligrams of ground material was sub-sampled in 3.5 mm X 5 mm tin capsules for analysis of $\delta^{13}C$ giving three representative independent values per tree.

To determine the ^{13}C profiles of the tree cores, I first polished the outer surface with sandpaper to aid identification of tree rings. However, as is often observed in *Eucalypts* (Brookhouse, 2006), no tree rings could be identified consistently nor easily. Therefore, I sliced each core with a sledge Leica SM2010R microtome to obtain 20-25 samples at two locations, a) from sapwood formed in recent years obtained from a roughly 6-mm outer segment of the cores (no bark was sampled, sapwood depth for these species were estimated from Zolfaghar 2014) and b) from heartwood at r/2 distance from the bark (**Figure 2.2**). The thickness of one slice was selected to be 1/1000 of the diameter of the tree usually between 300-700 μm depending on tree diameter. Each slice was ground finely in the bead grinding mill and 1-2 mg of ground material was transferred into tin capsules for $\delta^{13}C$ analysis.

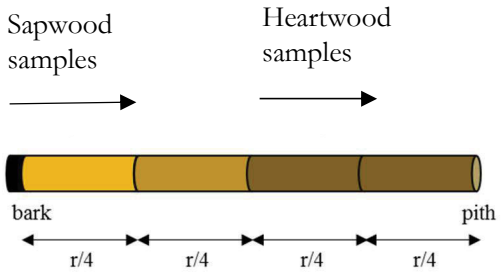

Figure 2.2: Sampling locations from tree cores for ^{13}C analysis

All $\delta^{13}C$ analysis was performed Picarro G2121-i Analyser (Picarro, Santa Clara, CA, USA) for isotopic CO_2 in the UTS TERG research laboratory. Atropine and Acetanilide were used as laboratory standard references and results were normalised with the international standards Sucrose (IAEA-CH-6, $\delta^{13}C_{VPDB}$ = -10.45 ‰), Cellulose (IAEA-CH-3, $\delta^{13}C_{VPDB}$ = -24.72 ‰) and Graphite (USGS24, $\delta^{13}C_{VPDB}$ = -16.05 ‰). Standard deviation of the

residuals between the IAEA standards and the calculated values of $\delta^{13}C$ based on best linear fit was ~ 0.5 ‰.

Data analyses

The local meteoric water line, LMWL; (Dansgaard, 1964) was fitted using simple linear regression. At each site, means of $\delta^{18}O$ and $\delta^{2}H$ signatures of overstorey and understorey species, discrimination against ^{13}C (and water-use-efficiency) calculated at leaf/core level was compared using a one-way analysis of variance (ANOVA) followed by a Tukey's *post-hoc* test for multiple comparisons. Data for both overstorey and understorey species were checked for homogeneity of variance (Bartlett test) and data were homogeneous in both cases.

Potential sources of water uptake by overstorey and understorey species were investigated using two approaches, a) from direct comparison by plotting $\delta^{18}O$ and $\delta^{2}H$ signatures of both stem and sources together and b) using the *siar* (stable isotope analysis in R) package in R (Parnell *et al.*, 2010). This package uses the basic methodology for estimating proportional source contributions, for example in context of this study, a dual isotope (δ_1, δ_2, i.e. , two isotope signatures obtained from branch water), three-source, mass balance, linear mixing model can be described by the following equations (Schwarcz, 1991):

$$\delta_1 \text{(branch water)} = X_1\, \delta_1 (S_1) + X_2\, \delta_1 (S_2) + X_3\, \delta_1 (S_3)$$

$$\delta_2 \text{(branch water)} = X_1\, \delta_2 (S_1) + X_2\, \delta_2 (S_2) + X_3\, \delta_2 (S_3)$$

$$1 = X_1 + X_2 + X_3$$

Where, δ_1 and δ_2 are known isotopic signals from branch water, S_1, S_2 and S_3 are three sources and $\delta_i(S_j)$ denotes isotopic signature of element i for source j and X_i denotes proportional contribution of source i. The *siar* package uses a Bayesian approach based on Gaussian likelihood to fit probability models to isotopic data and estimates the most likely proportion of water taken up from each source in plant water (Parnell *et al.*, 2010). Specifically *siar* allows incorporation of variability and uncertainty between sources as well

as any number of sources in the model (Hopkins III and Ferguson, 2012; Parnell *et al.*, 2010). Models were applied to the isotope data to infer the relative contribution of each water source in the branch water, producing 500,000 simulations (of which the first 50,000 were discarded) of plausible contributing values from each source using Markov chain Monte Carlo (MCMC) methods. Groundwater, soil water (mean of stable soil layers usually 30 cm - 60 cm) and rain water were considered as potential sources of water uptake in the model. Isotopic signatures of the surface soil were considered as the rain water signal because of ongoing rain at the time of sampling. The isotopic signatures and standard errors of each potential source were used as the input in the model and the branch water isotopic signals were used as the "target" values (Parnell *et al.*, 2010). The trophic enrichment factor (TEF) of the model was set to 0, because no enrichment of isotopes occurs during water uptake from soil by roots (Ehleringer and Dawson, 1992). The concentration dependence was also set to 0. A model was run for the overstorey and understorey species at each DTGW site producing four groups of plants (two overstorey and two understorey species) and the mean of the posterior distribution of the MCMC simulations was reported as the most probable contribution of each source for every overstorey and understorey species.

Results

Groundwater, soil water and rain water isotopic compositions

A plot of δ^2H *versus* the $\delta^{18}O$ values of obtained from rainfall water sampled in July (two rain-events), August, September and October 2013 (**Figure 2.3**) fell in a line with a slope of 8.66 and an intercept of 12.60 (Adj $r^2 = 0.95$, $p<0.0001$) and was not significantly different from the global meteoric water line (GMWL, $\delta^2H = 8.13\ \delta^{18}O + 10$, Bartlett-corrected likelihood ratio test statistic for common slope: LR=0.05, p>0.05) (Rozanski *et al.*, 1993) and the local meteoric water line (LMWL) for the Botany Basin ($\delta^2H = 8.22\ \delta^{18}O + 15.41$) (Jankowski 2005 unpublished data, (SCA, 2009)). Isotopic composition of groundwater sampled from the bore at each site ranged from -6.34‰ to -5.49‰ for $\delta^{18}O$ and -33.61‰ to -30.24‰ for δ^2H. The range of $\delta^{18}O$ and δ^2H values in bore water samples from five study sites was narrow (0.85‰ for $\delta^{18}O$ and 3.37‰ for δ^2H) and all bore samples plotted close to the LMWL; indicating that groundwater is recharged at these sites without any major transformation (for example, fractionation due to evaporation) and/or chemical reactions. A likelihood ratio test for common slope also could not identify any significant

difference between bore water and local rain water isotopic signal (LR=2.89, p>0.05). Soil water isotopic composition varied widely between depths and between sites and the δ^2H - $\delta^{18}O$ signatures of surface soil in all sites were enriched compared to the sub-surface layers. Patterns in soil water isotopic signals for the five study sites are discussed individually for each site in the following sections.

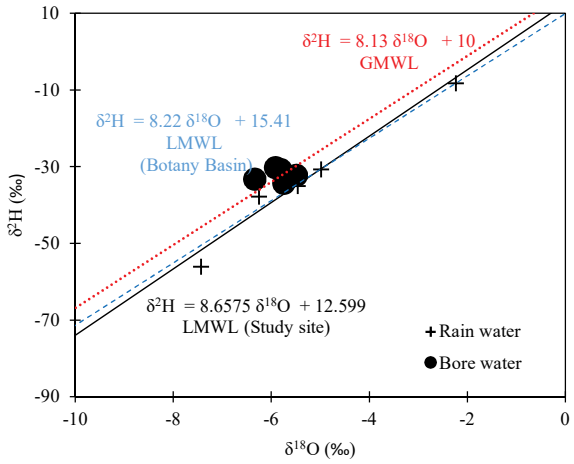

Figure 2.3: Local meteoric water line, LMWL (black solid line) at the study area.

The blue dashed line is the local meteoric water line of Botany basin and the red dotted line is the Global meteoric water line (GMWL). The crosses and the circles denote the rain water and bore water isotopic composition respectively.

Comparison of isotopic compositions of branch (xylem) water with possible sources

Site with 2.4 m DTGW

This site was the shallowest site (i.e., the site with the smallest DTGW from the soil surface) among the five sites in this study and was characterized by a dense woodland of very tall (26 ± 0.66 m) trees (Zolfaghar *et al.*, 2014). *Eucalyptus radiata* and *Eucalyptus piperita* were the two dominant overstorey species and *Pultanaea blakelyi* and *Persoonia linearis* were the two dominant understorey species sampled within the 50 m radius of the bore at this site. Soil water from the top 10-30 cm depth showed large variability in δ^2H - $\delta^{18}O$ signatures than those in deeper layers at this site; while δ^2H and $\delta^{18}O$ values approached to values closer to that from the bore water at about 70 cm depth from the surface (**Figure**

2.4). Branch xylem water isotopic compositions of all species sampled at this site matched very closely with the sub-surface soil water signal at the depth of 20 cm and 60 cm (**Figure 2.4**). A one-way ANOVA performed as the type of species sampled (i.e. overstorey/understorey species) as the grouping variable and mean δ^2H - $\delta^{18}O$ values as the response variables also could not identify any significant differences in branch xylem water isotopic values between overstorey and understorey species ($\delta^{18}O$: $F=0.009$, $p>0.05$; δ^2H: $F=0.792$, $p>0.05$).

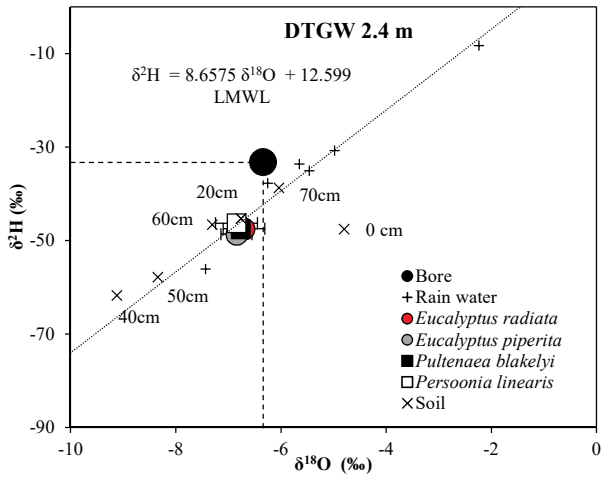

Figure 2.4: Rain, soil and xylem water isotopic composition of the DTGW 2.4 m site

Regression line for rainfall water shows the local meteoric water line (LMWL): $\delta^2H = 8.66\ \delta^{18}O + 12.60$, Adj $r^2 = 0.95$, $p < 0.0001$.

Site with 4.3 m DTGW

The next site was a site with a 4.3 m DTGW and *Eucalyptus globoidea* and *Eucalyptus sieberi* were the two dominant overstorey and *Banksia spinulosa* and *Acacia longifolia* were the two dominant understorey species sampled at this site. Soil water δ^2H - $\delta^{18}O$ values varied widely at the top 0-20 cm with relatively more stable values from 20 cm to the deeper soil layers. The overstorey species showed isotopic compositions (especially $\delta^{18}O$ values) that fell closer to the bore water signal compared to all species sampled at this site (**Figure 2.5**). Considering the rain water signal (represented by surface water isotopic signal), the bore water signal and the mean sub-surface soil water signal as three vertices of the mixing triangle in the δ^2H - $\delta^{18}O$ space, the overstorey species sampled at this site fell inside the

triangle, theoretically indicative of using a mix of all three available water sources. Branch xylem water isotopic signal of the understorey species matched closely with sub-surface soil water at the depth of 10-20 cm (**Figure 2.5**). Overstorey species at this site showed significantly different branch water $\delta^{18}O$ values compared to the understorey species (ANOVA: F=8.57, p<0.05), however, a statistically significant difference between overstorey and understorey species could not be identified from the $\delta^{2}H$ values (F=3.0, p>0.05).

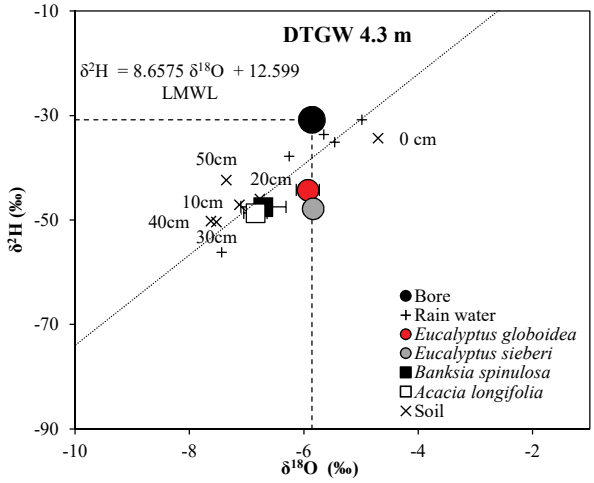

Figure 2.5: Rain, soil and xylem water isotopic composition of the DTGW 4.3 m site

Regression line for rainfall water shows the local meteoric water line (LMWL): $\delta^{2}H = 8.66\ \delta^{18}O + 12.60$, Adj $r^2 = 0.95$, $p < 0.0001$.

Site with 9.8 m DTGW

The third site along the groundwater gradient was a site with 9.8 m DTGW. This site was characterized by relatively shorter (15.84 ± 0.2 m) trees compared to the two shallower sites (DTGW 2.4 m and 4.3 m) (Zolfaghar *et al.*, 2014). *Eucalyptus sclerophylla* and *Eucalyptus sieberi* were the two dominant overstorey species and *Banksia spinulosa* and *Persoonia levis* were the two dominant understorey species present within the 50 m radius of the bore at this site. Soil water isotopic signals varied largely at the top 20 cm soil layer and became relatively stable from 30 cm to the deeper soil layers at this site. The overstorey species at this site showed very similar branch xylem water $\delta^{18}O$ values to bore water as observed at the DTGW 4.3 m site (**Figure 2.6**) and also appeared to use a mixture of surface water,

sub-surface water and groundwater. Among the understorey species, branch xylem water signals of *Banksia spinulosa* matched closely with isotopic signatures at the depth of 50 cm and *Persoonia levis* matched more closely to soil water values at the depth of 10-20 cm. Branch water signal of the two overstorey species were found to be significantly different from understorey species for both δ^2H and $\delta^{18}O$ isotopes at this site (ANOVA for $\delta^{18}O$: $F=7.77$, $p<0.05$ and δ^2H: $F=5.44$, $p<0.05$).

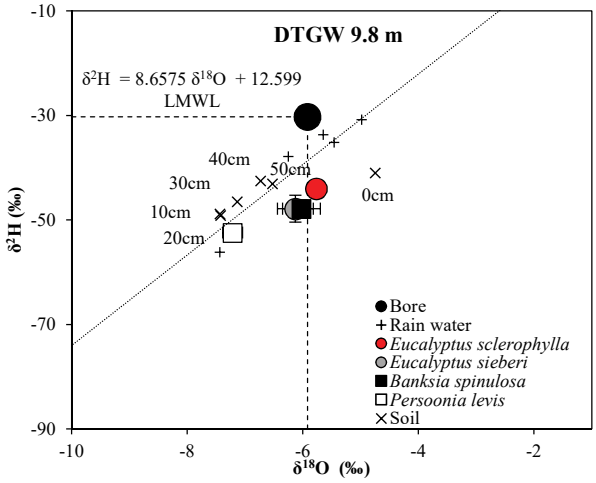

Figure 2.6: Rain, soil and xylem water isotopic composition of the DTGW 9.8 m site

Regression line for rainfall water shows the local meteoric water line (LMWL): $\delta^2H = 8.66\ \delta^{18}O + 12.60$, Adj $r^2 = 0.95$, $p < 0.0001$.

Site with 14.6 m DTGW

The next site along the gradient was a site with 14.5 m DTGW with *Eucalyptus piperita* and *Eucalyptus sieberi* as the dominant overstorey species and *Acacia longifolia* and *Acacia terminalis* as the dominant understorey species. As observed in the other sites, soil water δ^2H - $\delta^{18}O$ values showed larger variation in the top 20 cm of the soil profile and showed more stable values from 30 cm downwards (**Figure 2.7**). Branch xylem water values of neither δ^2H nor $\delta^{18}O$ from the overstorey species nor understorey species at this site matched closely with bore water signal and these species appeared to match more closely with sub-surface water and water from recent rainfall events represented by the soil-surface (0 cm) signature (**Figure 2.7**). This finding was further supported by the findings from an ANOVA

performed where unlike the DTGW 4.3 m (for $\delta^{18}O$) and 9.8 m sites, branch water signatures of the overstorey species were not significantly different from those of understorey species at this site (ANOVA $\delta^{18}O$: F=0.32, p>0.05, $\delta^{2}H$: F=0.14, p>0.05).

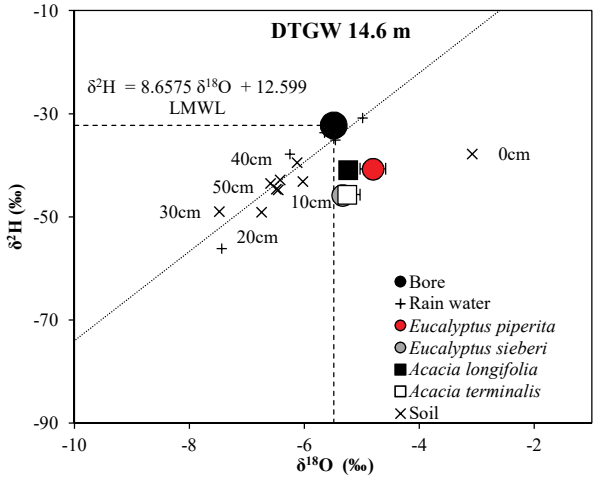

Figure 2.7: Rain, soil and xylem water isotopic composition of the DTGW 14.6 m site

Regression line for rainfall water shows the local meteoric water line (LMWL): $\delta^{2}H = 8.66\ \delta^{18}O + 12.60$, Adj $r^2 = 0.95$, $p < 0.0001$.

Site with 37.8 m DTGW

The DTGW 37.8 m site was the site having the deepest groundwater across the gradient in this study and was characterized by *Eucalyptus sclerophylla* and *Eucalyptus piperita* as the dominant overstorey species and *Leptospermum polygalifolium* and *Persoonia levis* as the dominant understorey species. Soil water $\delta^{2}H$ - $\delta^{18}O$ signatures showed large variation up to 30 cm depth at this site (**Figure 2.8**). Branch water isotopic signal of the all overstorey species sampled at this site matched closely with that of soil water from 50 - 60 cm depth (**Figure 2.8**). Isotopic signatures of *Persoonia levis* matched more closely with soil water signatures at 10 - 20 cm depth. *Leptospermum polygalifolium* appeared to match more closely with the sub-surface and recent rain water represented by soil-surface signature (0 cm). No significant difference between branch xylem water signals of overstorey and understorey species was identified at this site (ANOVA $\delta^{18}O$: F= 3.52, p>0.05, $\delta^{2}H$: F=3.02, p>0.05).

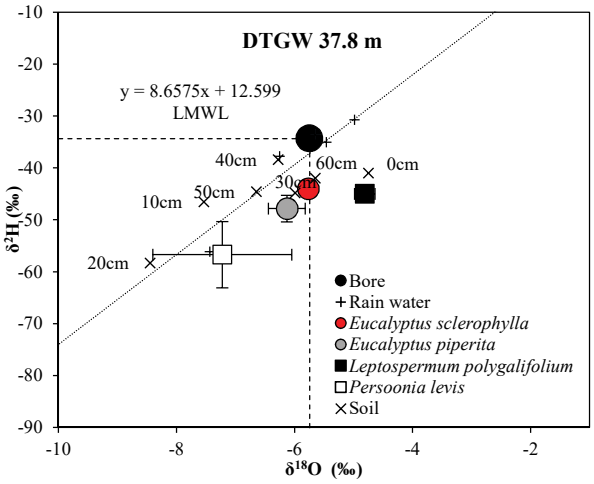

Figure 2.8: Rain, soil and xylem water isotopic composition of the DTGW 37.8 m site

Regression line for rainfall water shows the local meteoric water line (LMWL): $\delta^2H = 8.66\ \delta^{18}O + 12.60$, Adj $r^2 = 0.95$, $p < 0.0001$.

Proportional contribution of sources of water uptake along the DTGW gradient

Isotopic composition of δ^2H and $\delta^{18}O$ of three possible sources (i.e. groundwater, sub-surface soil water and recent rain water in the upper soil profile) were used to estimate proportional contributions sources of water accessed by each individual overstorey and understorey species at each site using the *siar* package (Parnell *et al.*, 2010) of R. **Figure 2.9** shows the relative contributions of each source of water to plant branch water obtained from *siar* models. Results from *siar* models suggest that, the overstorey and understorey species took up water simultaneously from the three well-defined water pools, recent rain water available in the upper soil profile at the time of sampling (represented by water extracted from the top 0-10 cm), water from stable sub-surface layers (>30 cm) of the soil profile and groundwater. At the shallowest site (DTGW 2.3 m), the mean probability of proportional contribution was 26% for groundwater, 44% for sub-surface soil water and 31% for recent rain water for both overstorey and understorey species. At the DTGW 4.3 m site, over 40% of water acquired by the dominant overstorey species originated from recent rain water and the understorey species were found to be relying more on water from sub-surface soil layers. The probability of proportional contribution of groundwater was 24% for overstorey and 15% for understorey species at this site. At the DTGW 9.8 m, both dominant overstorey and understorey species depended mostly on water from sub-surface soil layers. The two deepest sites along the gradient were found to be more reliant

on sub-surface water and recent rain water than groundwater, for example, the proportional contribution of sub-surface water in the branch xylem water was approximately 43% for overstorey and understorey species at the DTGW 14.6 m site while recent rain water contributed more than 40% to branch xylem water for both species at the DTGW 37.8 m site.

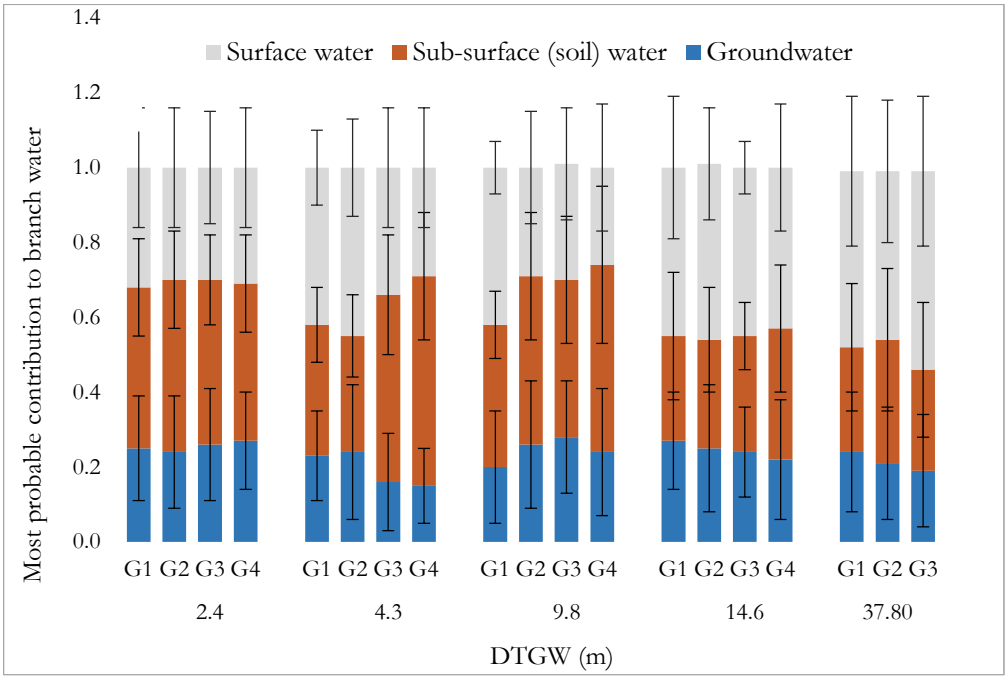

Figure 2.9: Most probable contributions of sources of water obtained from *siar* Bayesian mixing models.

The error bars are the standard deviations of the means. G1- G4 denotes groups 1- 4, i.e., G1 = overstorey species 1, G2 = overstorey species 2, G3 = understorey species 1 and G4 = understorey species 2.

Variation in WUE_i along the DTGW gradient

Figure 2.10 shows foliar discrimination against carbon-13 ($\Delta^{13}C$) and leaf intrinsic water-use-efficiency (WUE_i, calculated from bulk-leaf $\Delta^{13}C$) for overstorey and understorey species at each site, plotted against DTGW. Among all five sites, overstorey species from DTGW 4.3 m site showed the largest $\Delta^{13}C$ and smallest WUE_i. The understorey species showed the largest $\Delta^{13}C$ and smallest WUE_i at the shallowest site and $\Delta^{13}C$ decreased and WUE_i increased gradually as DTGW increased (linear regression for understorey species: Adj r^2= 0.11, $p<0.05$). The overstorey species, however, did not exhibit any such pattern with increasing DTGW (Adj r^2 in linear regression = 0.04, $p>0.05$). A one-way ANOVA with DTGW of all five sites as the grouping variable and $\Delta^{13}C$ (and WUE_i) as the response variable also could not identify any significant difference between sites (overstorey: F=1.39, $p>0.05$, understorey: F=1.35, $p>0.05$).

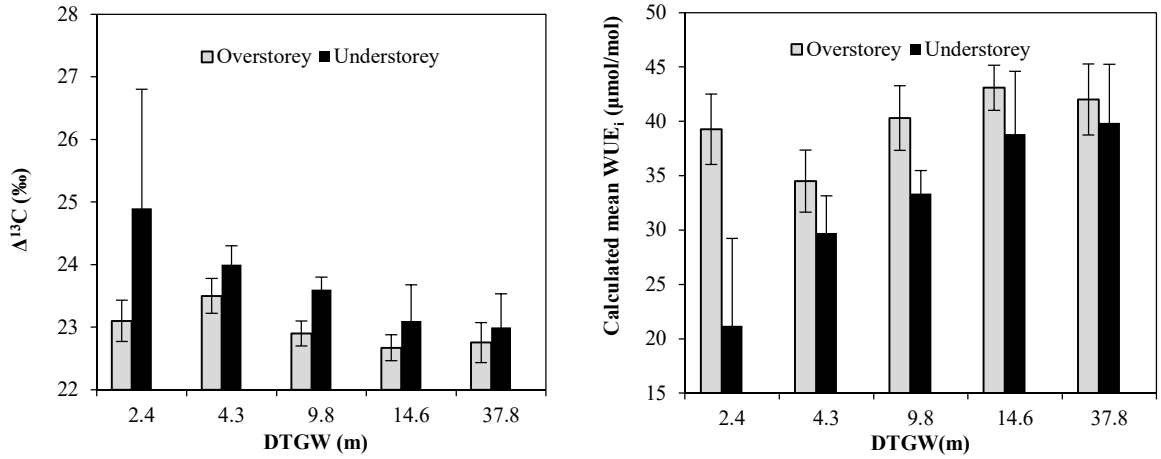

Figure 2.10: Discrimination against ^{13}C ($\Delta^{13}C$) and calculated leaf intrinsic water-use-efficiency (WUE_i) in five study sites across the DTGW gradient.

Dominant overstorey and understorey species are represented by grey and black columns respectively.

Variation in $\Delta^{13}C$ in tree-cores along the DTGW gradient

A one-way ANOVA followed by Tukey's *post-hoc* tests performed with DTGW as the grouping variable and tree-core $\Delta^{13}C$ as the response variable identified significant differences between sites along the DTGW gradient. Results from recent sapwood sampled from the outermost part of each tree-core (**Figure 2.11a** and **2.11c**) and from heartwood at r/2 distance from the bark of each core (**Figure 2.11b** and **2.11d**) are shown in **Figure 2.11**. Mean $\Delta^{13}C$ of the recent sapwood was the largest and mean calculated WUE_i was the smallest at the 9.8 m site. Mean $\Delta^{13}C$ and WUE_i of sapwood from the DTGW 4.3 m site was not significantly different from the DTGW 9.8 m site. Sapwood $\Delta^{13}C$ decreased and WUE_i increased at the two deepest site with the DTGW 14.6 m site showing the smallest mean $\Delta^{13}C$ and largest WUE_i with a larger variation. Consistent with foliar $\Delta^{13}C$ analysis, the shallowest site (DTGW 2.4 m) showed smaller $\Delta^{13}C$ values than the DTGW 4.3 m site in the tree-core analysis. Results from heartwood sampled at r/2 distance from the bark of each core (**Figure 2.11b** and **2.11d**) showed that $\Delta^{13}C$ of heartwood was the largest and calculated mean WUE_i was the smallest at the 4.3 m site while $\Delta^{13}C$ decreased and WUE_i increased significantly from 4.3 m to 14.6 m site (one way ANOVA: $F=104.3$, $p<0.0001$). As observed from the sapwood analysis, the shallowest site (DTGW 2.4 m) showed smaller $\Delta^{13}C$ values (and larger WUE_i) than the DTGW 4.3 m site in the heartwood analysis as well. $\Delta^{13}C$ values were consistently larger and calculated mean WUE_i was consistently smaller in tree cores from recent sapwood than in heartwood samples representing larger discrimination against ^{13}C and consequently smaller WUE_i in recent wet-years.

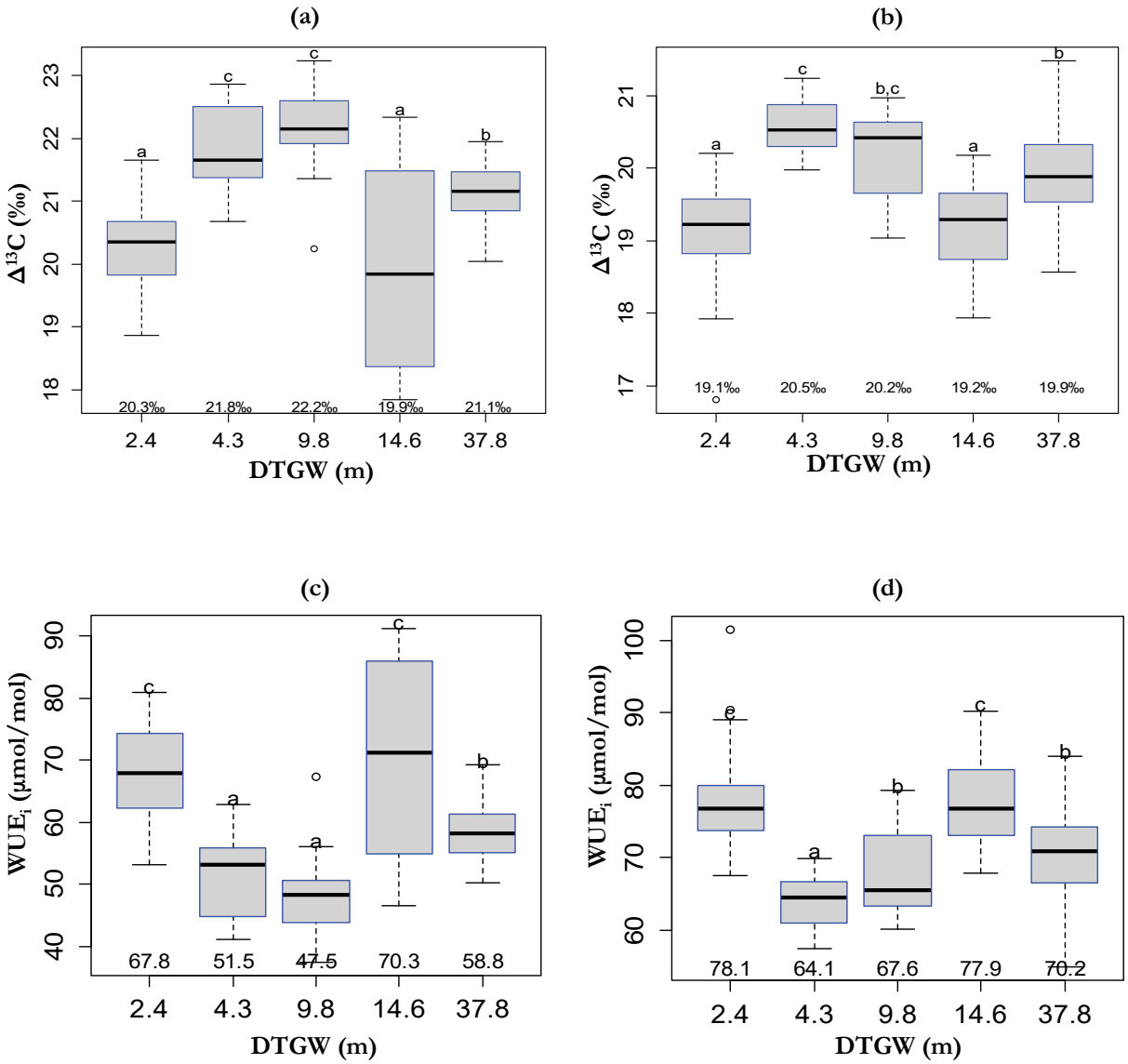

Figure 2.11: Δ¹³C (‰) and calculated mean WUEᵢ (µmol/mol) of sapwood and heartwood of trees sampled along the DTGW gradient.

Eucalyptus sclerophylla was sampled at all sites except for the shallowest site (DTGW 2.4 m), where *Eucalyptus radiata* was sampled. Panels a and c show results from sapwood of tree cores closest to the bark representing recent growing seasons and panels b and d show results from heartwood of cores (at r/2 distance further from the bark) representing growing seasons in the more distant past. The box plots present the maximum and minimum values, the inter-quartile range, and the median (solid centreline) values and the open circles indicating outliers from 2-3 cores at each sites. Letters above bars indicates the differences between means (Tukey HSD, confidence level of 0.05) across sites and sites not connected by same letter are significantly different from other sites. Values under the boxes presents the mean values of $\Delta^{13}C$ for each site.

Discussion

Determination of proportional use of water sources

I hypothesized that, even at mesic sites with a large mean annual precipitation of > 1000 mm as experienced at my study sites, increased access to groundwater still exerts an influence on trees growing at these sites. Specifically, I hypothesized that in sites with relatively shallow depths-to-groundwater (< 10 m), trees will be accessing groundwater and as DTGW increases from shallower to deeper sites, the proportional use of groundwater will decrease. Two approaches were used to trace the tree water uptake in the present study, using a direct comparison by plotting $\delta^{18}O$ and $\delta^{2}H$ signatures of both branch xylem water and recent rainfall, sub-surface soil water and groundwater sources and using the *siar* package in R (Parnell *et al.*, 2010) to quantify the proportional use of each source.

Direct comparison of branch $\delta^{2}H$ and $\delta^{18}O$ isotopic compositions with groundwater, sub-surface soil water and recent rain water in the uppermost soil layers in five study sites indicated that, in most cases these three different sources contributed simultaneously to plant-water use (**Figure 2.4-2.8**). While the direct comparison method is a reliable method of tracing source water uptake and has extensively been used in a number of studies (Busch *et al.*, 1992; Ehleringer and Dawson, 1992; Goldsmith *et al.*, 2012; Kray *et al.*, 2012; Lamontagne *et al.*, 2005; O'Grady *et al.*, 2006c; Smith *et al.*, 1998; Thorburn *et al.*, 1993; Zencich *et al.*, 2002), it gets more complicated to speculate proportional use of possible water sources, particularly when plants access water from different sources simultaneously. Stable isotope mixing models, for example *siar* is a more suitable approach to obtain proportional contribution of each source and can also characterize the variation between the isotopic signatures between the sources as well as incorporate prior knowledge in the analysis (Hopkins III and Ferguson, 2012; Leng *et al.*, 2013; Parnell *et al.*, 2010). Direct comparison of $\delta^{18}O$ and $\delta^{2}H$ signatures of branch and water sources indicated that at the shallowest site of DTGW 2.4 m, plants extracted water from deeper soil layers (closer to 60 cm, **Figure 2.4**) and no significant differences could be identified between branch water signatures of overstorey and understorey species. Also isotopic values through the soil profile showed that as depth increased to about 70 cm, $\delta^{2}H$ and $\delta^{18}O$ gradually approached values observed from the bore (groundwater). Groundwater at this site was shallow, being only ~2 m from the soil surface. Approach of sub-surface soil $\delta^{2}H$ and $\delta^{18}O$ signatures to that of groundwater at the depth of 70 cm suggest that the sub-surface water in the

capillary fringes at the deeper soil layers at this site originated from groundwater and both overstorey and understorey species at this site significantly relied on this water source. At the DTGW 4.3 m and 9.8 m sites, one way ANOVA identified significant differences between branch water δ^2H and $\delta^{18}O$ signatures of overstorey and understorey species (for $\delta^{18}O$ at DTGW 4.3 m and for both δ^2H and $\delta^{18}O$ at DTGW 9.6 m sites), indicative of water uptake from different pools for overstorey and understorey species at these two sites. Consistent with this finding, branch δ^2H and $\delta^{18}O$ for deep rooted overstorey species for these two moderately deep sites matched more closely with bore water isotopic signal, whereas, shallower rooted understorey species showed branch δ^2H and $\delta^{18}O$ values closer to values from sub-surface soil layers. Unlike the three shallowest sites, no significant differences could be identified between the overstorey and understorey species at the two deepest sites (13.5 and 37 m) and branch water isotopic signals were closer to sub-surface soil water/recent rain water signals than bore water signals from direct comparison for both overstorey and understorey species, indicating that both species at the two deepest sites mostly accessed water from surface/sub-surface soil layers. Similar differentiation between source water uptake of sites with different depth to groundwater has previously been observed in Rossatto *et al.*, (2012). These authors also observed that plant water uptake, even at sites with water tables very close to the surface was limited by its presence and was also constrained to the shallower wet-season unsaturated zone of the soil profile. They also suggested that plants growing in areas with a deeper wet-season unsaturated soil profile have greater variability and potentially opportunistic water uptake strategies as observed in this present study.

Consistent with the conclusions from the direct comparison approach, results from mixing model suggested that the overstorey and understorey species took up water simultaneously from the three well-defined water pools, i.e., the recent rain water available at the time of sampling (represented by water extracted from the upper soil surface), water from stable sub-surface layers of the soil profile and groundwater. However, plants from the sites with a relatively shallow water table (DTGW $\leq$ 10 m) extracted more water from deeper soil layers ($\geq$ 30 cm) than plants growing at sites with a deeper water table, where the most probable proportional contribution of rain water (at the time of sampling) was $\geq$ 50% (**Figure 2.9**) for both overstorey and understorey species. At the shallowest site (DTGW 2.4 m), the most probable proportional contribution of groundwater, sub-surface soil water and rain water was ~26%, ~44% and ~31% respectively for both overstorey and

understorey species. However, at the DTGW 4.3 m site, the most probable proportional use of groundwater for the overstorey species still remained ~25% while it decreased to ~15% for the understorey species. Except for the shallowest site, the probable contribution of groundwater was larger in all overstorey species than understorey species at all sites with one exception (the understorey *Banksia spinulosa* at the DTGW 9.8 m site). While it is unlikely that this species had access to groundwater at the depth of 9.8 m at this site, this result from the model had occurred because both soil water at the depth of ~60 cm and branch water δ^2H and $\delta^{18}O$ values fell close to bore water values at this site. It is also noteworthy that, the *siar* mixing models attributed ~20% probability of the total extracted water to be from groundwater even for the DTGW 14.6 m and 37.8 m sites for overstorey species (and smaller probabilities for understorey species) though it is unlikely that vegetation had access to groundwater at these sites. These results might have been obtained because overstorey species at these two deepest sites accessed water from capillary fringes deeper than the soil sampled at 1 m depth that had similar signals to bore water isotopic signal. Overall, results from the *siar* mixing model suggest that the deeper (≥ 30 cm) soil layers at three shallowest sites and recent rain water at the two deepest sites were the most probable sources of the plant water uptake in summer of 2013 when the vegetation received more than average rainfall consistently for over 12 months.

In a study to investigate the influence of DTGW in this particular study area, Zolfaghar *et al.*, (2015) identified that, the shallowest sites in the gradient had significantly larger aboveground biomass and net primary productivity. Since putative access to groundwater appeared to influence the structural and functional traits of trees in this area, my initial hypothesis was that the proportional use of groundwater will decrease as DTGW increase and this will be picked up from stable isotope mixing models. The results from the mixing models, however, could not identify any significant decrease of groundwater-uptake with increasing DTGW for this current study. Instead, I found that vegetation appear to rely mostly on soil water from relatively deeper sub-surface soil layers for the DTGW 2.4, 4.3 and 9.8 m sites and on the rain water represented by superficial soil layers at the two deepest sites, at least during very wet conditions with frequent rains before and during the sampling. Similar results have previously been observed in several studies where the shallow/moderately deep soil layers were the most dominant sources of uptake of water for woody species especially during wet conditions (Dodd *et al.*, 1998; Leng *et al.*, 2013; Verweij *et al.*, 2011), even when groundwater was in the close proximity (Rossatto *et al.*,

2012). Also, water uptake from shallower sub-surface soil layers is more energy efficient particularly for very tall overstorey trees investigated in this present study because, shallower uptake means the path length for the transport of water to the canopy is smaller. As distance required to move water increases, the required water potential gradient increases which is unfavourable to canopies because too low a canopy water potential results in reduced stomatal opening and eventually can lead to xylem embolism (Zolfaghar *et al.*, 2015). Findings from the stable isotope mixing models were also consistent with previous studies investigating the groundwater dependent ecosystems in this particular area, which concluded that the threshold access of groundwater was 9.8 m, beyond which there were minimal changes in vegetation structure and function in response to DTGW (Zolfaghar *et al.*, 2014; Zolfaghar *et al.*, 2015). Groundwater resources in these sites could be more important during the dry-season, as previously observed in Australian savannas, where at least 50% of water used for transpiration in some species came from deeper water sources during dry conditions (Lamontagne *et al.*, 2005). Goldstein *et al.*, (2008) also found that several cerrado woody species in sites with more dense vegetation rely on water sources from deeper (around 1.5–3 m) regions of the soil profile during the dry-season and these authors suggest that there is a niche separation between woody plants and grasses in which the latter only use water from the upper soil layers, whereas trees can use water from both upper and deeper layers. A differentiation in sources of plant water-uptake (i.e. deep sub-surface layers for shallow DTGW sites and recent rain water for deeper DTGW sites) even when water was not a limiting factor suggests that that trees at deeper DTGW sites have a larger range in depth of soil water extraction which will enable different species at these sites to coexist, particularly during drier conditions (Rossatto *et al.*, 2012).

Variation in discrimination against ^{13}C and WUE_i

Another objective of this study was to investigate whether groundwater use, or the lack thereof, can be identified from leaf-level discrimination against ^{13}C and WUE_i. I hypothesized that, as DTGW increased, water will be less available to roots and therefore leaves will discriminate less against ^{13}C, resulting in a decreasing trend of $\Delta^{13}C$ and an increasing trend of WUE_i with increasing DTGW. Consistent with the findings from direct comparison and mixing models of $\delta^{18}O$ and $\delta^{2}H$, mean overstorey WUE_i showed no significant trend with increasing DTGW (one-way ANOVA: $F=1.66$, $p>0.05$). Mean understorey WUE_i, however, showed a significant increase as expected with increasing DTGW (Adj $r^2= 0.13$, $p<0.05$) (**Figure 2.10**) although means were not significantly

different among sites (one-way ANOVA: $F=2.02$, $p>0.05$). The absence of a significant trend in $\Delta^{13}C$ and WUE_i for the overstorey species may have arisen because of the exceptionally wet summer with 46% and 11% larger rainfall above the long-term mean experienced at all sites in two consecutive years prior to sampling for the current study. Bulk-leaf $\Delta^{13}C$ (and WUE_i calculated from $\Delta^{13}C$) is modulated by the intercellular and atmospheric concentration of CO_2 (C_i/C_a) at the time when the leaf dry matter was synthesized and therefore is likely to represent the wet environmental conditions during leaf formation at all sites. Because all sites received above-average rainfall, the influence of groundwater availability was likely to have been minimal and was reflected in the non-significant trend of $\Delta^{13}C$ (and WUE_i) with increasing DTGW for overstorey species at these sites. A statistically significant increase in WUE_i for the understory may reflect the shallower maximum rooting depth for understory species compared to deeper rooted overstorey species indicating that the impact of above average rain on bulk-leaf $\Delta^{13}C$ (and WUE_i) was less pronounced for understory species.

In order to investigate to what extent recent rainfall affected the bulk-leaf $\Delta^{13}C$ and WUE_i calculated from $\Delta^{13}C$, I measured ^{13}C content of stem-wood from *Eucalyptus sclerophylla* as a function of depth through the wood. $\Delta^{13}C$ (and WUE_i) of leaves reflected the water status of the wet summer in 2013 whilst measurements of $\Delta^{13}C$ (and WUE_i) of heartwood in the stem was expected to reflect the environmental conditions experienced by the trees further back into the past, before the wetter-than-average years associated with the 2010/2011 global land sink anomaly (Poulter *et al.*, 2014). The methodology was therefore designed to sample recent sapwood as well as heartwood before the very wet period experienced immediately prior to 2013. Consistent with patterns observed from foliar $\Delta^{13}C$ analysis, recent sapwood samples did not show any statistically significant trend with increasing DTGW. However, $\Delta^{13}C$ was consistently larger and WUE_i smaller at the DTGW 4.3 and 9.8 m sites than the two deepest sites (**Figure 2.11**). Most importantly, for the heartwood samples, $\Delta^{13}C$ decreased and WUE_i increased significantly as DTGW increased across the range of 4.3 –18.4 m depth (**Figure 2.11**) and WUE_i was significantly larger at the 14.6 m site (77.9 μmole/mole) than the 4.3 m and 9.8 m sites (64.1 and 67.6 μmole/mole respectively) suggesting that in drier conditions, trees in these two shallower sites were able to successfully tap into groundwater and therefore were less efficient in using water (indicated by smaller values of WUE_i) than the trees at the deeper 14.6 m site.

The shallowest site (DTGW 2.4 m) consistently showed smaller $\Delta^{13}C$ and larger WUE_i from both sapwood and heartwood samples. Trees at this site had much smaller soil volume for root growth available because of the close proximity to the water table to the soil surface. This site also experienced water-logging and visibly saturated soil conditions due to the above-average rainfall received during this study. Saturation of the upper soil profile results in anoxia (oxygen-stress) which inhibits root water uptake, often causing reduced stomatal opening similar to the effect of water deficits and has been extensively documented in several studies (Brolsma and Bierkens, 2007; McAinsh *et al.*, 1996; Rodriguez-Iturbe *et al.*, 2007; Schuur and Matson, 2001; Zegada-Lizarazu and Iijima, 2005). Thus, flooding, and the shallow water table combined to result in a smaller uptake of water (because of anoxic conditions) for the much taller trees (compared to the 4.3 m and 9.8 m sites) and hence an increase in WUE_i at the shallowest site. Maximum rates of water uptake have previously been observed at sites having intermediate depths-to-groundwater rather than at the shallowest depths, in agreement with the current study (Baird *et al.*, 2005; Zolfaghar *et al.*, 2014).

Conclusions

The aim of this chapter was to examine sources of uptake of water and proportional contribution of each possible water source for vegetation growing in the mesic sites in the southern highlands of NSW along a naturally occurring DTGW gradient using stable isotope analysis. This chapter also investigated whether access to groundwater influenced the water-use-efficiency of the vegetation at the leaf and stem-wood level. A differentiation of most probable water sources between the three shallower and two deeper sites despite consistent wet conditions experienced by the vegetation suggest that groundwater level *does* affect plant water uptake patterns and soil water partitioning among woody species in these sites even during persistent wet conditions but that these influences might be more distinct during drier rather than wetter conditions at these sites. These findings were further supported by intrinsic water-use-efficiencies calculated from the heartwood that showed significant increase from shallower to deeper sites. Stable isotope analysis also supported the ~10 m threshold of groundwater access for trees at these sites as have been observed in a previous study (Zolfaghar *et al.*, 2015). These findings fill a gap in our understanding of the mechanisms of water use by groundwater dependent vegetation especially during humid conditions.

Chapter 3 Seasonal patterns of sources of water uptake, discrimination against ^{13}C and water-use-efficiencies along a natural gradient of depth-to-groundwater in semi-arid tropical savanna and *Acacia* woodlands

Introduction

Drylands, defined as "areas where precipitation is scarce and typically more-or-less unpredictable", cover 41% of the earth's total land area and are sub-categorized as arid, semi-arid and dry humid areas (Reynolds *et al.*, 2007). Arid and semi-arid regions are further characterized by regions with chronic water shortage (Clarke, 1991). In Australia 70% of the land is classified as semi-arid or arid (Eamus *et al.*, 2006b; O'Grady *et al.*, 2011; O'Grady *et al.*, 2006a) and annual evaporation exceeds mean annual rainfall across most of the continent (Donohue *et al.*, 2009) predominantly categorizing the Australian landscapes as "water-limited" according to the widely accepted Budyko framework (Budyko, 1974). Some regions in Central Australia consistently receive rainfall less than 300 mm $year^{-1}$ making water a limiting resource in these areas (Eamus *et al.*, 2006b). Also, the surface water bodies in this region (particularly in the Ti Tree basin) are ephemeral in nature (NRETAS, 2009). Hence, groundwater in such areas play an important role as a potential source of water for maintaining ecosystem structure and function of terrestrial and riparian vegetation (Evans and Hatton, 1998). Owing to the remoteness of much of Australia's interior, few studies have investigated groundwater use by vegetation communities in its semi-arid regions.

This chapter investigates differences in source of uptake of water and water-use-efficiency in the dominant overstorey species across a depth-to-groundwater (DTGW) gradient in a water limited basin in Central Australia. This contrasts the study at mesic sites in Kangaloon, New South Wales reported in **Chapter 2**. The present study was located in the Ti Tree basin, the location of an important groundwater resource in Central Australia

(Cook *et al.*, 2008), where mean annual precipitation is ~300 mm and occurs mostly in large events during summer, thus there is zero rainfall available for vegetation for prolonged periods. The dry-season in this region is characterized by declining soil water availability and high vapour pressure deficits (O'Grady *et al.*, 2009). A number of previous studies have documented some unique characteristics of vegetation in this region. For example, O'Grady *et al.*, (2009) observed that, despite being in an extremely water limited environment, the wood density and specific leaf-area (SLA) of dominant deep-rooted species in this region were similar to those from more mesic environments. Furthermore, they observed that daily rates of water use also remained similar across seasons in deeper rooted species despite significant differences in water availability during dry- and wet-seasons. In a separate study along the Northern Australian Tropical Transect (Koch *et al.*, 1995), Eamus *et al.*, (2000) also observed tree water use of *Eucalyptus* species to be similar in the dry-season compared to the wet-season and these authors proposed that, in seasonally dry environments, the hydraulic architecture required to tolerate long periods of drought potentially limits tree water use when water availability is high. In this present study, the first aim was to investigate the sources of water accessed by vegetation along a groundwater gradient in semi-arid Central Australia and to identify whether there was variation in potential water sources during dry- and wet-seasons.

The resource supply rates, especially pertaining to water availability, are highly heterogeneous in space and time due predominantly to pulsed rainfall patterns as is often observed in water limited regions (e.g., mean annual rainfall can vary eightfold in Central Australia). This heterogeneity provides an axis of distinct ecological differentiation facilitating stable co-existence of a diverse range of species in these regions. Ecologists have long been investigating this fundamental question - how do co-existing plant species co-exist? (Silvertown, 2004; Vandermeer, 1972). An important mechanism that can influence the stable co-existence of plant communities especially in arid and semi-arid habitats with pulsed water-resources availability is the "hydrological niche segregation" among co-occurring species (Dawson, 1990; Silvertown *et al.*, 1999). In 1999, Silvertown showed that differences in access to, and use of, water in space and time is a "potent force that structures many types of plant community" globally. In another study, Araya et al., (2011) examined 96 species in eight plant communities in South Africa and 99 species across 18 plant communities in the UK to quantify their hydrological niches and concluded that hydrological niche segregation is a fundamental process underlying species co-

existence (Araya *et al.*, 2011). However, there has been no examination of hydrological niche separation in Australian water-limited ecosystems to this author's knowledge. The identification of differential source water uptake and/or water-use-efficiency of co-occurring plant species in the Ti Tree basin will help to fill this gap in our understanding of the mechanisms of species co-existence in water-limited habitats.

Stomatal conductance is regulated to maximise carbon gain whilst simultaneously minimising transpiration (this is discussed in more detail in **Chapter 1**) and is sensitive to both soil and atmospheric water content (Prior *et al.*, 1997; Thomas and Eamus, 1999). Leaf intrinsic water-use-efficiency (WUE_i), defined by the ratio of leaf-scale carbon gain to stomatal conductance, can therefore provide valuable insights on how vegetation respond to variation in water availability. Discrimination against stable carbon-13 isotope ($\Delta^{13}C$) is increasingly being used to calculate leaf intrinsic water-use-efficiency, which can also be used as a proxy of water-use-efficiency calculated from gas-exchange measurements (see **Chapter 1**). A second aim of this study was to calculate WUE_i of the dominant tree species across the DTGW gradient in order to examine whether access to groundwater was reflected at the leaf-scale as well as to identify any existing patterns between dry- and wet-seasons in WUE_i in this semi-arid ecosystem.

Differential access to water between species has been manifested as changes in morphological traits of plants in a number of previous studies, for example, changes in SLA (Warren *et al.*, 2005), ratio of leaf area to sapwood area (Eamus *et al.*, 2000; Sperry, 2000) or wood density (Bucci *et al.*, 2004; Hacke *et al.*, 2000). Particularly in arid habitats, plant species are subjected to numerous selective pressures in addition to low or zero precipitation, such as high temperatures, high solar radiation and high vapour pressure deficit. Collectively these selective pressures influence a number of plant traits which is often reflected at the leaf-level, for instance, on SLA (Eamus *et al.*, 2006b; Fonseca *et al.*, 2000; Turner, 1994) or on stomatal conductance of water and CO_2 (Gates, 1968). Even within a site, plant traits exhibit seasonal variations due to changes in water availability. In a study in northern Australia, O'Grady *et al.*, (1999) demonstrated a 30–40% decline in leaf area of evergreen *Eucalypts* during the dry-season. The ratio of leaf area to sapwood area has also been observed to decline in the dry-season across the Northern Australian Tropical Transect (Eamus *et al.*, 2000) and these authors suggested that reduction in leaf area during the dry-season represents an optimization response to increased evaporative demand (O'Grady *et al.*, 1999). Like SLA, leaf vein density (LVD), defined as length of

veins per unit area (mm mm^{-2}), is another leaf-trait that influences the whole-plant performance (Uhl and Mosbrugger, 1999). As an inherent leaf structural trait, LVD has increasingly been gaining attention to examine the influence of environmental variation on morphological features. A review by Uhl and Mosbrugger, (1999) lists abiotic factors such as temperature, light interception, soil dryness, humidity and nutrient availability, in addition to leaf morphological factors such as leaf insertion level and leaf size, as key variables that influence LVD. Leaf veins are essentially composed of xylem and phloem embedded in parenchyma which carry the same water that exits the plant through stomata. In principle, therefore, the propensity for leaves to lose water should match the capacity of the xylem to deliver the same water (Brodribb and Holbrook, 2007; Meinzer and Grantz, 1990; Sperry, 2000) and consequently exhibit a positive correlation between leaf-hydraulic conductance (K_{leaf}, determined by the hydraulic conductance of the vein xylem and the hydraulic conductance outside the xylem) and LVD (Brodribb *et al.*, 2007; Sack and Holbrook, 2006; Sack and Scoffoni, 2013). LVD provides a direct estimate of K_{leaf} because it gives the distance water in the transpiration stream must traverse as it travels from the termini of the xylem-network to the sites of evaporation (Brodribb *et al.*, 2010). Since transpiration is directly linked with available water accessed by vegetation, one might speculate that LVD would also be influenced by availability of water. Furthermore, a number of studies have demonstrated increased LVD with increasing aridity (Brodribb *et al.*, 2010; Brodribb and Holbrook, 2003; Sack and Holbrook, 2006; Scoffoni *et al.*, 2011; Sommerville *et al.*, 2012). Consequently a final aim of the studies described in this chapter was to examine patterns in LVD with water availability across the DTGW gradient in the semi-arid regions of Central Australia. With evidence of LVD being strongly associated with leaf hydraulic conductance, K_{leaf} and leaf-level gas-exchange rates (Brodribb *et al.*, 2007; Sack *et al.*, 2003; Sack and Frole, 2006; Sack and Holbrook, 2006), the relationships of LVD with $\Delta^{13}C$ was also investigated in the present study.

To summarize, this chapter specifically addresses the following questions:

1) Can analyses of stable oxygen, hydrogen and carbon isotopes provide insights on the nature and extent of groundwater dependency along a depth-to-groundwater gradient across the tropical Ti Tree basin?
2) If so, which of the dominant overstorey species across the gradient are groundwater dependent?

3) Is there a seasonal pattern in sources of water uptake of the dominant overstorey species across the Ti Tree basin?
4) Can bulk-leaf $\Delta^{13}C$ and leaf intrinsic water-use-efficiency (WUE_i) be used to identify groundwater use and seasonal variation in sources of water uptake across the gradient?
5) Is the vein investment of dominant overstorey species affected by increasing DTGW? And finally,
6) Can we identify a relationship between LVD and bulk-leaf $\Delta^{13}C$?

Materials and methods

Site description

The study was conducted in the Ti Tree Basin; a 5500 km^2 basin located approximately 200 km north of Alice Springs, NT and 180 km north of the Tropic of Capricorn (22.28°S, 1933.25°E, 549 m asl). The climate of this site is characterized by a tropical arid zone with hot summers and warm winters. The nearest Bureau of Meteorology station on the Territory Grape Farm (Station 015643; 1987- May 2016) recorded a mean and median annual precipitation of 319.9 and 299 mm, respectively (http://www.bom.gov.au/). Of the annual median rainfall, 72% falls during the summer months (December - February) and 86% falls during the monsoon season (November - April), placing the site just inside the Australian Monsoon Tropics (Bowman *et al.*, 2010; Hutley *et al.*, 2011). Mean minimal and maximal temperatures are in the range of 5°C and 22.6°C in July to 22°C and 37.5°C in January. Summer maximal temperature of 46.2 °C was recorded on 5 January 1994 and winter minimal temperature of –4.0 °C was recorded on 11 August 1994 (http://www.bom.gov.au/).

The soil is characterized as a "red kandosol" (74:11:15 sand: silt: clay) (Eamus *et al.*, 2013), which is typical of large portions of semi-arid Australia with high potential for drainage (Morton *et al.*, 2011; Schmidt *et al.*, 2010). Patches of hard siliceous soil is often observed and are likely surface expressions of the hardpan (Cleverly *et al.*, 2013), which is also a common formation in the top meter and deeper in this type of soil (Cleverly *et al.*, 2013; Morton *et al.*, 2011). The major source of water for domestic, stock and irrigation use for this region is a large underground reservoir, recharged mainly by seepage from river

channels and their flood-out areas and by occasional very heavy rainfall events (NRETAS, 2009). The Ti Tree basin also has a natural depth-to-groundwater gradient with an overall flow of groundwater towards the northern and north-eastern parts of the Ti Tree basin aquifer. The depth of the water table below ground level is sufficiently shallow in the northern part that groundwater is lost through transpiration and evaporation; whereas DTGW reaches as high as 49 m in the southern and western parts of the basin. Four study sites in an east-west transect (groundwater depth ranging from 4.4 m to 49.4 m) and four sites in a north-south transect (groundwater depths from 8.3 m to 49.5 m) were selected to capture the variability of the sources of water uptake and water-use-efficiency of the vegetation across the DTGW gradient (a detailed site description is listed in **Table 3.1**). In addition to a site near the Woodforde River flood-out area in the east-west transect, three additional (up to 2 km) transects near the Allungra Creek waterhole in the southern part of the basin were also sampled. This was done to capture variation in $\Delta^{13}C$ and WUE_i of frequent recharge zones near the hills *versus* the distal reaches of the Woodforde River that receive flood-outs only following rare occurrences of heavy rainfall. A map of the Ti Tree Basin with selected study sites is presented in **Figure 3.1**.

The selected study sites were characterized by three distinct types of vegetation, (1) low *Acacia* Mulga woodland with an understorey of shrubs, herbs and C3 and C4 grasses and (2) taller, open *Corymbia* savanna with extensive Spinifex grass (*Triodia spp.*) and sparse *Corymbia* (and *Eucalyptus*) trees (Cleverly *et al.*, 2016; Eamus *et al.*, 2013; O'Grady *et al.*, 2009). Along the east-west transect, one specific site with a DTGW of 4.4 m (bore no: 18889) was selected as a representative of the third vegetation type: riparian vegetation predominantly consisting of the River Red Gum (*Eucalyptus camaldulensis var. obtusa*) lining the banks of the Woodforde River. A detailed description of the selected sites for this study are presented in **Table 3.1**.

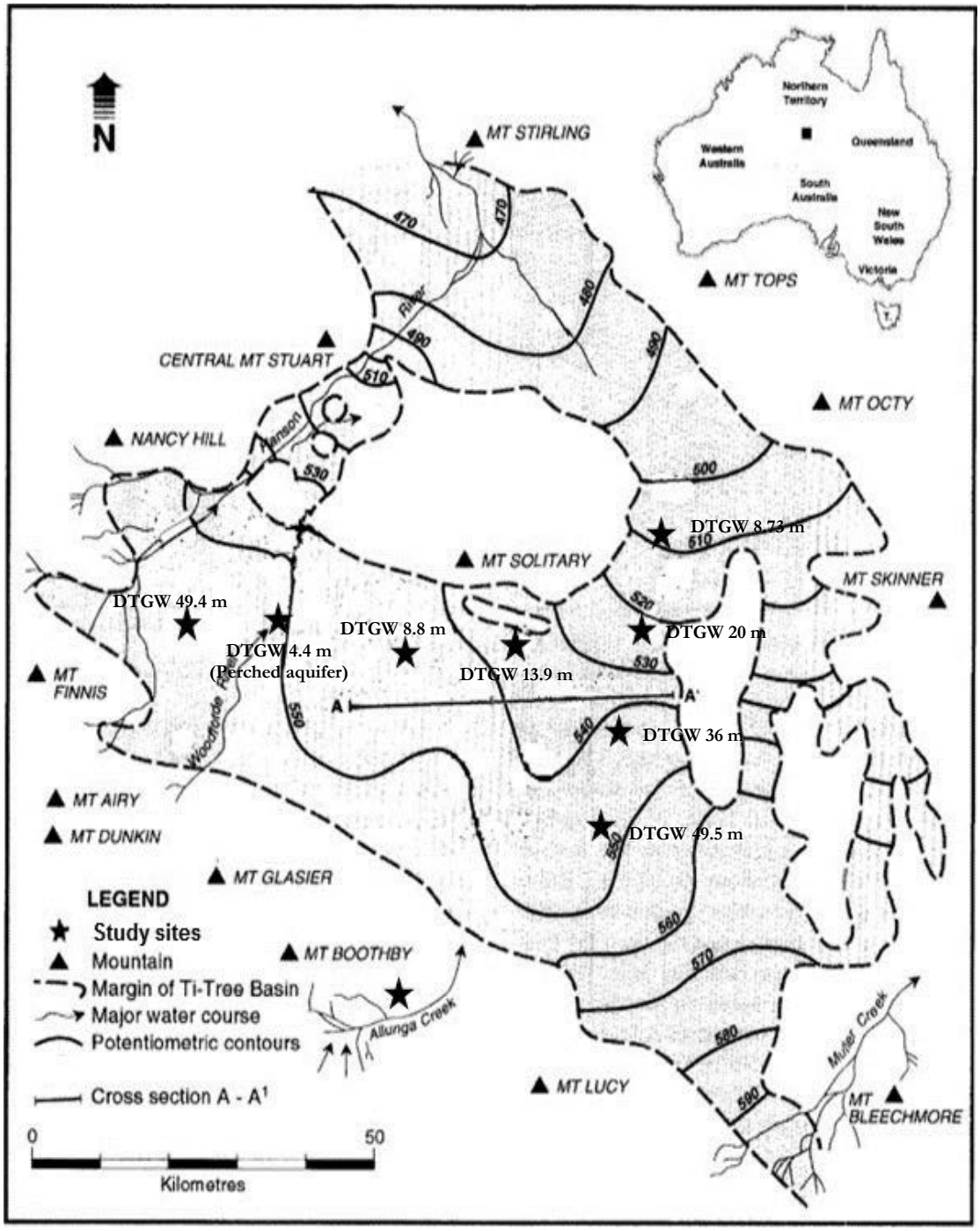

Figure 3.1: The Ti-Tree Basin, Central Australia (shown in the small black square on inset map) and the study sites (modified from Harrington *et al.*, (2002)).

Potentiometric contours indicate the general direction of groundwater flow is to the east and north from the western and southern margins, respectively. Star symbols represents the sites along the east-west and north-south transect selected in this study.

Table 3.1: Specific study sites (Bore ID and name), GPS locations, depth-to-groundwater and brief descriptions of each study site.

Bore ID*	Bore Name	GPS Location of the existing bore	Average DTGW (m)	Description
East-west transect				
RN 18889	Monitoring Bore Ti Tree Station	133° 19' 37.1" E 22° 20' 44.4"S	4.4	Riparian vegetation
†18830	East eddy covariance tower	133° 38' 22" E 22°17'37" S	8.8	*Corymbia* savanna
RN 17353	Investigation/monitoring bore Ahakeye land trust	133° 48' E 22° 17' S	13.9	*Corymbia* savanna
RN 16684	West eddy covariance tower	133° 14' 57.2" E 22° 16 ' 55.3" S	49.4	*Acacia* (Mulga) woodland
North-south transect				
RN 013543	Monitoring bore Ti Tree area railway corridor	133° 54' 55" E 22° 16' 17" S	8.73	*Acacia* (Mulga) woodland
RN 017424	Monitoring bore Woodgreen station	133° 52' 45.73" E 22° 28' 12.77" S	20	*Corymbia* savanna
RN 013545	Monitoring bore Bushy Park station	133° 51' 16" E 22° 36' 15" S	36	*Corymbia* savanna
RN 017708	Adrail camp domestic bore, Aileron station	133° 49' 38" E 22°44' 10" S	49.5	*Corymbia* savanna

* Bore ID, locations and DTGW were obtained from NR MAPS, Department of Natural Resources, Environment, the Arts and Sport, Northern Territory Government (NRETAS), http://nrmaps.nt.gov.au/;jsessionid=8bqnlwnwdf501h4x0jc4675q6.
†Eddy covariance tower establisher by University of Technology Sydney (UTS).

Sampling protocol, stable isotope and leaf vein density analysis

At each selected study site, two dominant overstorey and understorey species, typically *Acacia* and *Corymbia spp*., were selected and sampling was performed twice from the selected trees in September 2013 (late dry-season) and in April 2014 (late wet-season). Often the *Acacia* and *Corymbia spp*. were the only two dominant overstorey species present in a *Corymbia* savanna, whereas *Acacia* woodlands were dominated mainly by *Acacia spp*. The same sampling protocol described in **Chapter 2** was followed for sampling stems, leaves and soil and bore water.

Three distinctly different micro-habitats were identified at the 8.8 m DTGW site of the east-west transect. These micro-habitats were identified as (a) within the *Acacia* patch; (b) the transition zone between the *Acacia* and the *Corymbia* savanna; and (c) within the

Corymbia savanna (discussed in details in the next section). Branch (xylem) samples from *Acacia aneura* and *Corymbia opaca* trees were collected from each of these three habitats for xylem water isotope analysis.

Three trees of two dominant overstorey species present at a particular site were selected within a 50 m radius of the bore. Three leaves from each tree were collected during the April 2014 sampling for ^{13}C and leaf vein density analysis. First, leaf areas for the leaves were measured and then leaves were oven dried for 72-96 hours in oven at 60 ℃. For the broad leaved species, each dried leaf was halved using a razor blade and the first half was ground finely for ^{13}C analysis. A small sub-section (approximately 1 cm^2) from the other half was used for leaf vein density analysis giving three leaf subsections per tree and nine per species. For the *Acacia* phyllodes due to their small size, several phyllodes were combined and ground for ^{13}C analysis and one whole phyllode was used for leaf vein density analysis.

Each leaf section selected for leaf vein density analysis was cleaned and stained following the approach described in (Gardner, 1975). This method uses a 5% (w/v) NaOH solution as the principal clearing agent and leaf-sections immersed in clearing agent were placed in an oven at 40 ℃ overnight (Gardner, 1975). More sclerophyllous leaves, particularly *Acacia* phyllodes, proved difficult to clear effectively and were placed in the oven longer to aid the clearing process. Once cleared, the straw-coloured and partially translucent leaf sections were stained with a 1% (w/v) safranin solution. Most leaf sections were stained for up to three minutes and then soaked with a 95% (w/v) ethanol solution until the vein network was sufficiently stained and the majority of colour was removed from the lamina tissue. After staining, the cuticular layer(s) were removed using a combination of approaches (for example, small paint brush, fine-tipped tweezers and razor blades etc.) to aid in identifying the vein network for subsequent imaging and analysis. Following staining and cuticle removal, leaf sub-sections were photographed (away from the major veins), using a Nikon microscope (model: SMZ800) at 40X magnification. Finally, minor veins were traced by hand for all photographed vein images and leaf vein density was calculated as total vein length per unit area (mm/mm^2) using ImageJ version 1.48 (National Institutes of Health, USA).

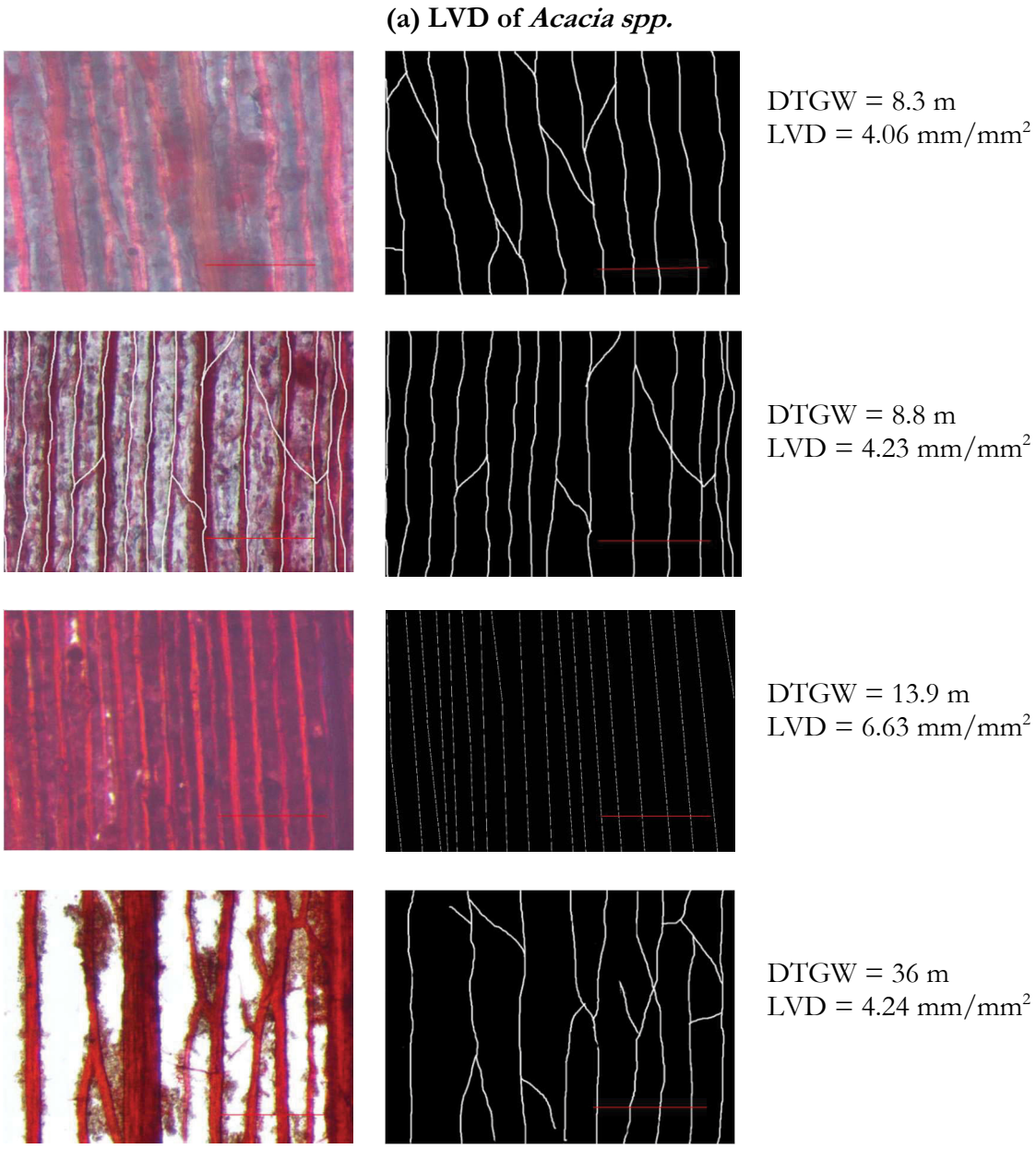

Figure 3.2(a): Leaf vein density (LVD) patterns in *Acacia* phyllodes of (top to bottom) (i) *Acacia kempana*, (ii) *Acacia aneura*, (iii) *Acacia sericophylla* and (iv) *Acacia aneura var. tenius*.

Left panels show the original vein images and right panels show the traced images of minor veins. Only one of the two layers typically observed in *Acacia* species are shown here. DTGW and the calculated LVD are shown in the right column for each vein image. Scale bar equals to 1 mm.

(b) LVD of *Eucalyptus* and *Corymbia spp.*

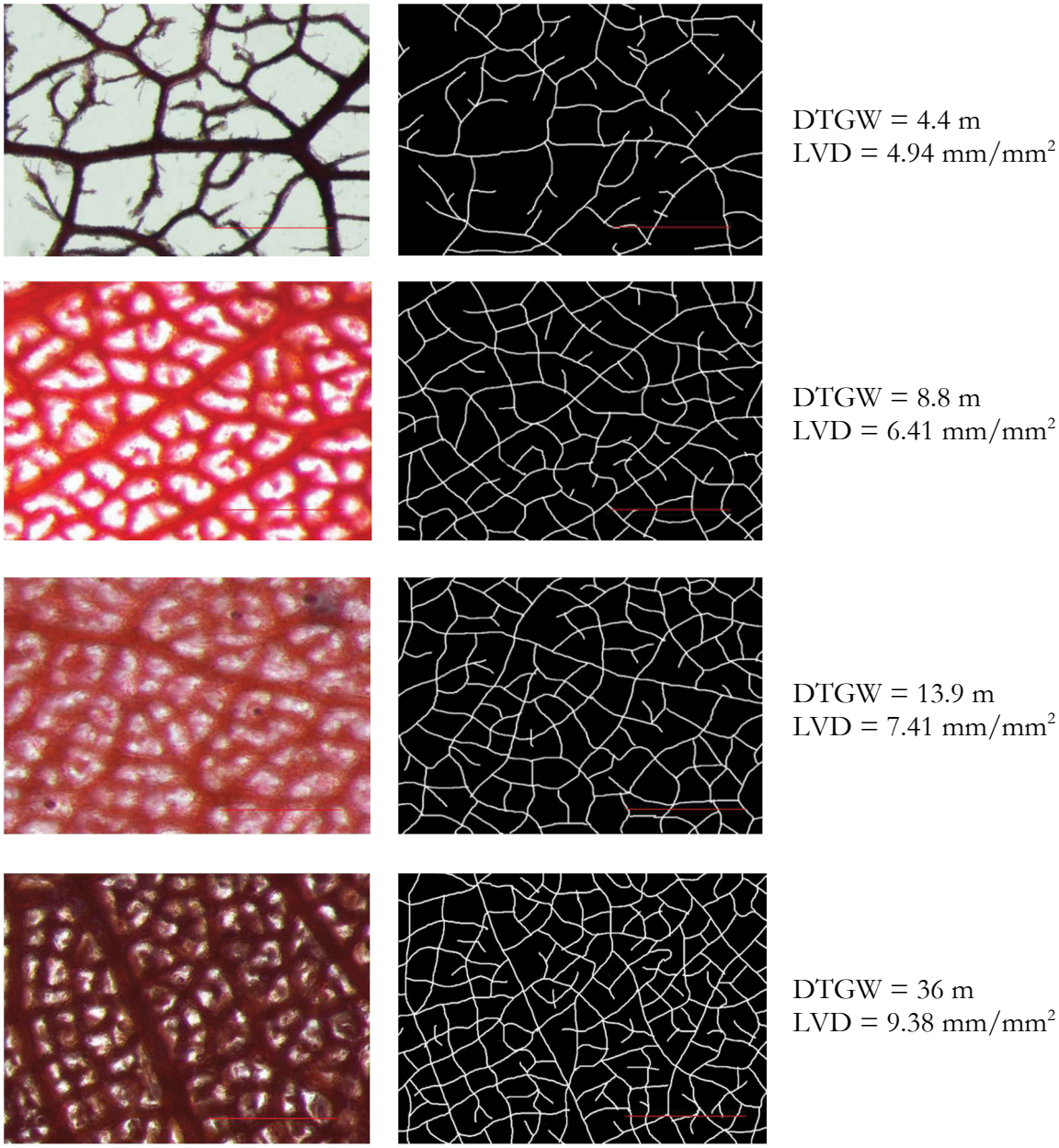

Figure 3.3(b): Leaf vein density (LVD) patterns in leaves of (top to bottom) (i) *Eucalyptus camaldulensis var. obtusa*, (ii) - (iv) *Corymbia opaca*.

Left panels show the original vein images and right panels show the traced images of minor veins. Low to high LVD is arranged from top to bottom. DTGW and the calculated LVD are shown in the right column for each vein image. Scale bar equals to 1 mm.

Data and statistical analysis

The local meteoric water line (LMWL) (Dansgaard, 1964) was fitted using simple linear regression. Species-mean values (obtained from three leaves sampled per trees and three individual trees per species) for the dominant overstorey species at each were calculated for δ^2H, $\delta^{18}O$, $\delta^{13}C$ and leaf vein density to account for inter-species variability. The relationships between discrimination against ^{13}C (and water-use-efficiency, WUE_i) with depth-to-groundwater were tested using regression analysis after testing for non-normality (Shapiro-Wilk test, $\alpha = 0{\cdot}05$) and homogeneity of variances (Bartlett test). At each site, mean WUE_i of overstorey species, was compared using a one-way analysis of variance (ANOVA) followed by a Tukey's *post-hoc* test for multiple comparisons.

Results

Meteorological conditions during the study period

Figure 3.4 shows the meteorological conditions from the data obtained from the UTS eddy covariance towers installed at the DTGW 8.8 m and 49.4 m in the east-west transect. These two towers are approximately 50 km apart in an east-west direction. Mean daily temperature and mean daily vapour pressure deficit (VPD) showed the expected seasonal pattern, with larger mean temperature and VPD recorded in summer (December–February) than winter (June–August) (**Figure 3.4**). Total rainfall recorded from January 2013 to June 2014 was 363 mm at the DTGW 8.8 m site and 376.4 mm at the DTGW 49.4 m site. Daily sums of rainfall showed that the DTGW 8.8 m and 49.4 m site received 265 mm and 228 mm rainfall respectively between the September 2013 and April 2014 sampling which is over 73% and 60% of the total rainfall received from January 2013 to June 2014 respectively at these sites.

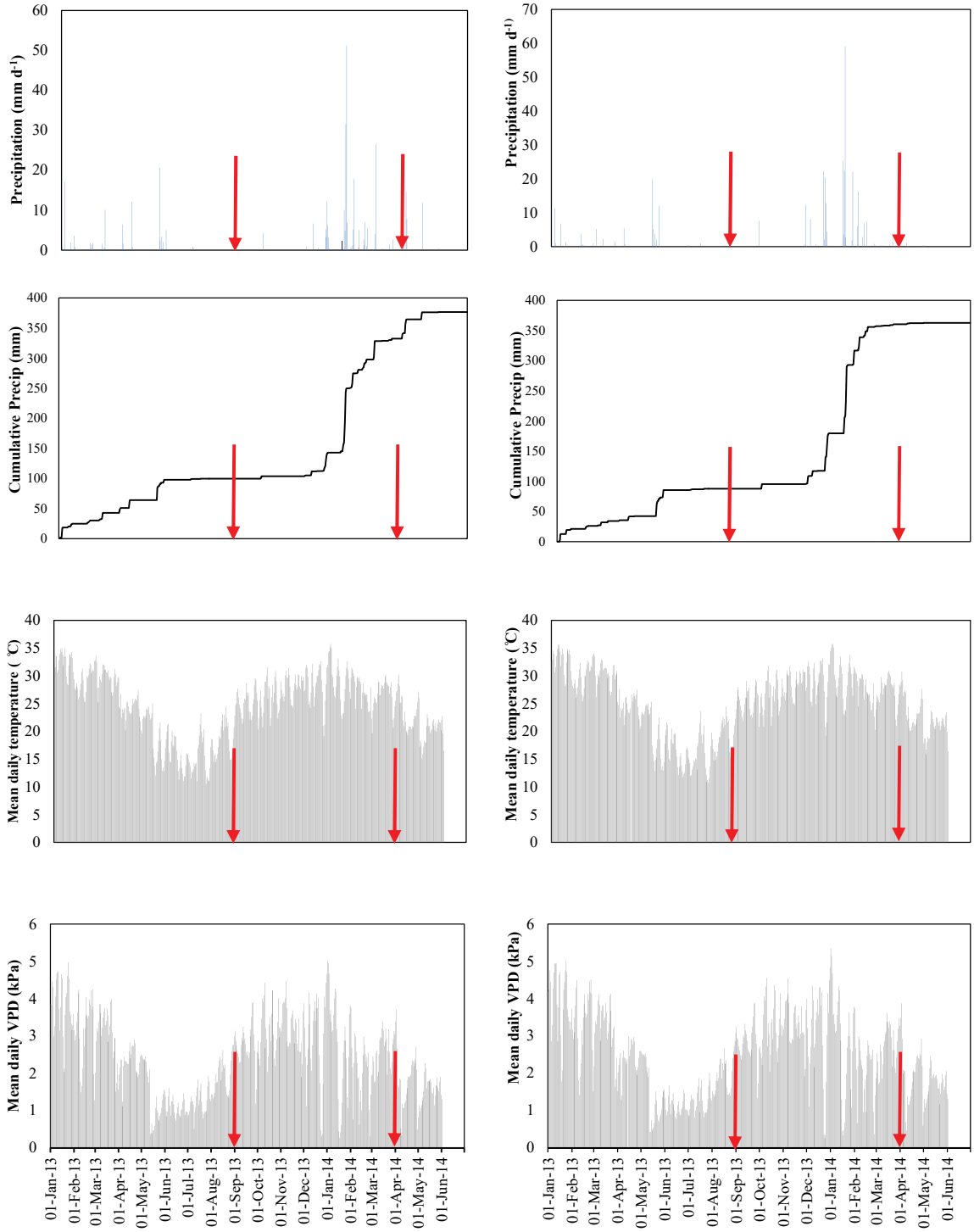

Figure 3.4: Mean daily meteorological conditions of daily precipitation, cumulative precipitation, mean air temperature and vapour pressure deficit from Jan 2013 - Jun 2014 from the eddy-covariance data.

Left panels show data for DTGW 49.4 m and right panels show data for DTGW 8.8 m. Red lines show the two sampling periods in September 2013 (late dry-season) and April 2014 (late wet-season).

Local meteoric water line (LMWL) of Ti Tree

δ^2H versus the $\delta^{18}O$ values of rain water (**Figure 3.5**) fell in a line with a slope of 4.53 and an intercept of 3.03. Liu *et al.*, (2010) have previously recorded a mean value of this slope of 6.9 for 1962–2002 from the Global Network of Isotopes in Precipitation (GNIP) station in Alice Springs (Liu *et al.*, 2010). All rain samples fell inside the ranges suggested by Liu *et al.*, (2010) (i.e., -5.01‰ to +0.03‰ for $\delta^{18}O$ and ~-24‰ to ~+2‰ for δ^2H). Deuterium excess, *d* (calculated from the equation: $d = \delta^2H - 8 * \delta^{18}O$ and a measure of the deviation of the given data point from a line with slope of 8) was much smaller in the precipitation in April 2013 (6.14 ± 3.29) compared to winter precipitation in June 2013 (118.69 ± 19.86).

Comparison of soil and xylem water δ^2H-$\delta^{18}O$ signals: east-west transect

A comparison of δ^2H-$\delta^{18}O$ signals of branch (xylem) water and soil water between the sites of the east-west transect is described below. Sites are ordered from the west (largest DTGW) to the east (gradually smaller DTGW up to 8.8 m except for the DTGW 4.4 m site formed due to the presence of a perched aquifer at the Woodforde River and then increasing to 13.9 m DTGW) at the end of the transect.

Site with 49.4 m DTGW

The first site from the west end of the east-west transect was the deepest site of this transect with a DTGW of 49.4 m. This site was located in a Mulga woodland characterised by a discontinuous canopy of short (3 – 7 m), evergreen *Acacia aneura* and *Acacia aptaneura* trees with relatively shallow rooting depth (Eamus *et al.*, 2013). The understorey consists of shrubs, herbs and C3 and C4 grasses that are conditionally active depending upon moisture availability and season (Cleverly *et al.*, 2013; Eamus *et al.*, 2013). This site was one of the two sites in this transect that had an eddy-covariance system.

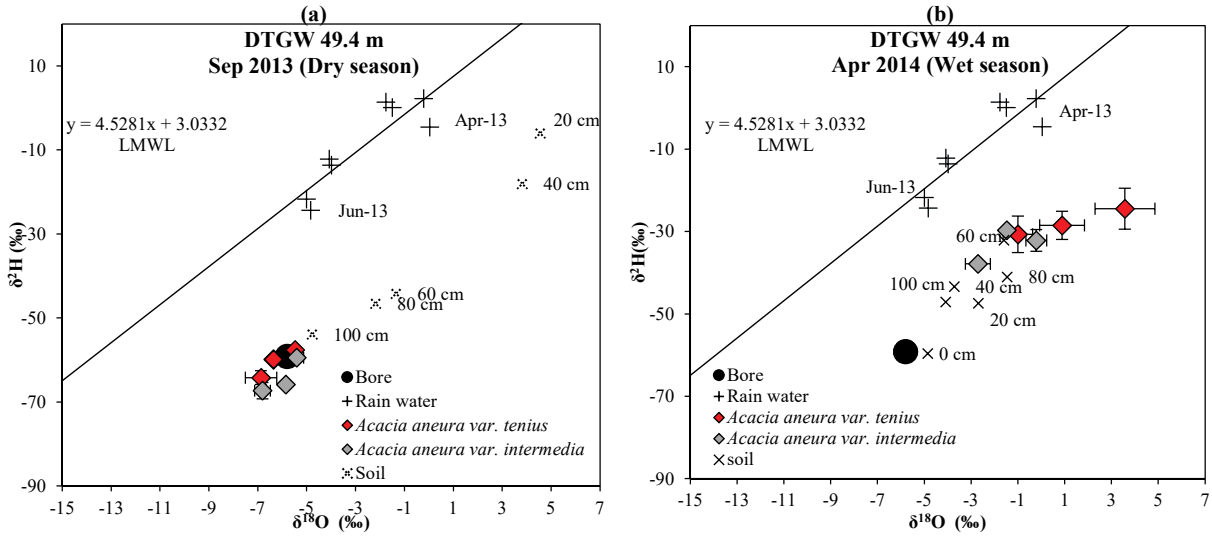

Figure 3.5: Rain, soil and xylem water isotopic compositions at 49.4 m DTGW site (east-west transect).

Panel a and b show Sep-2013 and Apr-2014 sampling respectively. Regression line for rainfall water sample (from April 2013 and June 2013) shows the local meteoric water line (LMWL): $\delta^2H = 4.5281\ \delta^{18}O + 3.0332$, $r^2 = 0.79$, $p < 0.01$.

δ^2H and $\delta^{18}O$ compositions of soil water gradually became increasingly depleted throughout the 1 m depth, with very enriched values at the top 40 cm of the upper soil profile during Sep-2013 sampling consistent with soil evaporation during dry periods (**Figure 3.5a**). Not enough water sample was obtained from cryogenic distillation from the soil surface for isotopic analyses during the dry-season sampling (Sep-13). However, no such pattern could be identified during the Apr-2014 sampling, at the end of the wet-season (**Figure 3.5b**).

During Sep-2013, isotopic signatures of both dominant overstorey (*Acacia*) species appeared to have accessed soil water from below 100 cm depth (**Figure 3.5a**). A consistently decreasing pattern of soil water isotopes in Sep-2013 also suggest that these values were approaching isotopic values of water sitting on the hardpan at around 100 cm depth at this site (Cleverly *et al.*, 2013; Cleverly *et al.*, 2016) and this water was accessed by most of the species sampled during this period. After the wet period in January-March 2014, isotopic compositions of branch water was more enriched than the Sep-2013 sampling (**Figure 3.5b**) and branch water isotopic composition of some of the *Acacia* trees

sampled matched more closely with soil water isotopic compositions from the depth of 60 – 80 cm during the April-2014 sampling.

Site with 4.4 m DTGW

This site had the shallowest DTGW among all the sites in the east-west transect adjacent to the Woodforde River (and bore no 18889) and is one of the three most important recharge areas in Ti Tree Basin (NRETAS, 2009). The river bank was lined with deep rooted *Eucalyptus camaldulensis var. obtusa* over a shallow perched aquifer but not connected to the main and deep (up to ~49 m deep) Ti-Tree basin aquifer (NRETAS, 2009). The soil water isotopic profile for this site showed large variation between the two sampling periods, and showed no significant patterns during the Apr-2014 sampling (**Figure 3.6**). However, xylem water δ^2H and $\delta^{18}O$ of deep-rooted *Eucalyptus camaldulensis* did not vary seasonally at this site and ($\delta^{18}O$ =~-6 ‰ and δ^2H=~-60‰ during both seasons) and were also very close to the isotopic signal of the bore water sampled at this site (**Figure 3.13b**). The δ^2H and $\delta^{18}O$ of understorey *Eremophila latrobei* species varied between the two sampling dates with relatively more enriched values and larger standard errors during Apr-2014 than Sep-2013.

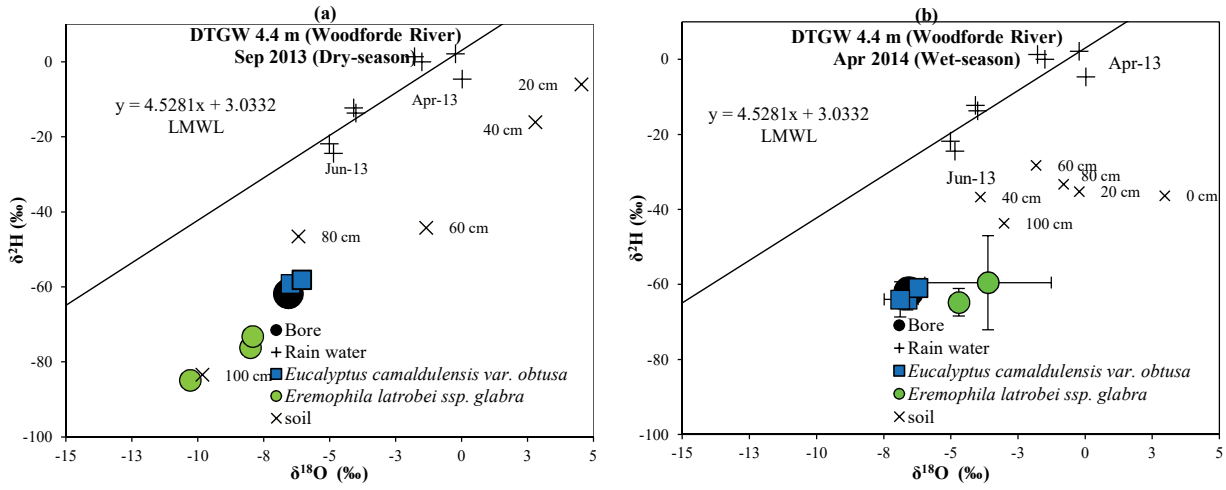

Figure 3.6: Rain, soil and xylem water isotopic composition at the 4.4 m DTGW site (east-west transect).

Panel a and b show Sep-2013 and Apr-2014 sampling respectively.

Site with 8.8 m DTGW

The next site from west to east along this transect was a site with 8.8 m DTGW (measured from bore no 18830) and the second of the two sites in this transect that had an eddy-covariance system installed. This site was characterized by two dominant species of trees: a patches of short *Acacia spp. (Acacia aneura*, *Acacia sericophylla* and *Acacia malleodora*) canopies with an understorey of shrubs and grasses dominantly *Eremophila latrobei subsp. glabra* and *Aristida holathera* and b very tall (> 15 m) and widely spaced *Corymbia opaca* trees over patches of *Triodia schinzii* grasses.

Within 100 m radius around the bore, there were three distinctly different micro-habitats at this site, the first habitat was a small patch of *Acacia spp.* with occasional *Corymbia* trees close to the eddy-covariance tower within the *Corymbia* savanna (hereafter referred to as habitat 1); the second habitat was the transition between the *Acacia* patch and the extensive *Corymbia* savanna (habitat 2) and the third habitat was the *Corymbia* savanna *per se* (habitat 3) (Cleverly *et al.*, 2016).

Figure 3.7 shows variation in isotopic compositions of branch (xylem) water across the three different habitats at the 8.8 m DTGW site. Trees sampled from micro-habitats 1, 2 and 3 are labelled with corresponding numbers in red. Isotopic signal of branch water from the *Acacia spp.* sampled during Sep-2013 did not differ significantly from each other and showed similar δ^2H-$\delta^{18}O$ compositions to soil water close to a depth of 100 cm. *Corymbia* branches sampled from habitat-1 showed varying isotopic signals (larger standard errors) and branches from habitat-2 showed similar signals to soil water from depths close to 80 – 100 cm. Soil water isotopic signals varied during the Apr-2014 sampling. *Corymbia* branches sampled from both habitat-1 and habitat-2 showed very similar values (close to 100 cm soil water isotopic values) during this sampling. Interestingly, branch-water isotopic signal of *Corymbia* branches sampled from habitat-3 showed consistent values during both Sep-2013 and Apr-2014 sampling (Sep-2013: $\delta^{18}O$=-5.81‰, δ^2H=-66.85‰ and Apr-2014: $\delta^{18}O$=-5.83‰, δ^2=-66.80‰) and these values were the closest to the bore-water isotopic signals ($\delta^{18}O$=-6.25‰, δ^2H=-60.95‰), among all other trees sampled at this site.

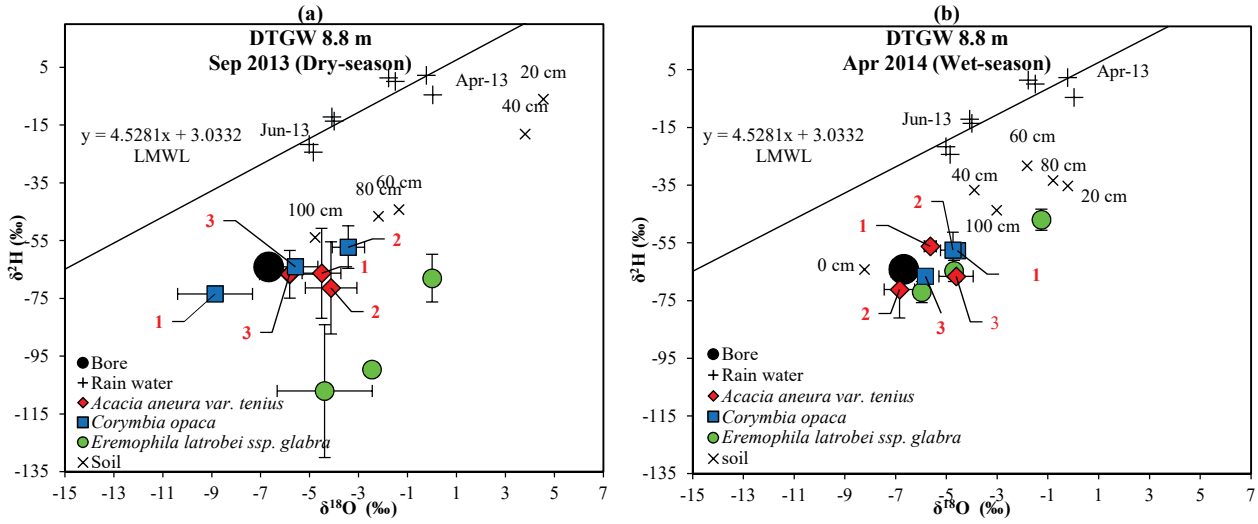

Figure 3.7: Rain, soil and xylem water isotopic composition at the 8.8 m DTGW site (east-west transect).

Panel a and b show Sep-2013 and Apr-2014 sampling respectively. Trees sampled from micro-habitats 1, 2 and 3 are labelled with corresponding numbers in red colour. *E. latrobei* was sampled randomly and not from specific micro-habitats.

Site with 13.9 m DTGW

The fourth and last site along the east-west transect was the site with 13.9 m DTGW; a large open *Corymbia* savanna, characterized by widely spaced and very tall *Corymbia opaca* and short (~2 m) *Acacia sericophylla* species. The soil water isotopic profile for this site also varied between the two sampling periods, with gradually depleting values of δ^2H-$\delta^{18}O$ with increased soil depth during the Sep-2013 sampling and no such patterns during the Apr-2014 sampling. δ^2H - $\delta^{18}O$ of xylem water from *Acacia sericophylla* showed similar signatures to soil water at the depth of ~100 cm during the Sep-2013 sampling and varied more between branches during Apr-2014 sampling with larger standard errors (**Figure 3.8b**) matching closely with isotopic signal of the soil-surface (0-10 cm). Xylem water δ^2H - $\delta^{18}O$ from *Corymbia* trees at this site remained very similar during both Sep-2013 and Apr-2014 sampling (Sep-2013: mean $\delta^{18}O$=-6.05‰, δ^2H=-63.08‰ and Apr-2014: mean $\delta^{18}O$=-6.48‰, δ^2=-65.61‰) also similar to the bore water isotopic signals ($\delta^{18}O$=-6.25‰, δ^2H=-60.95‰, **Figure 3.13b**).

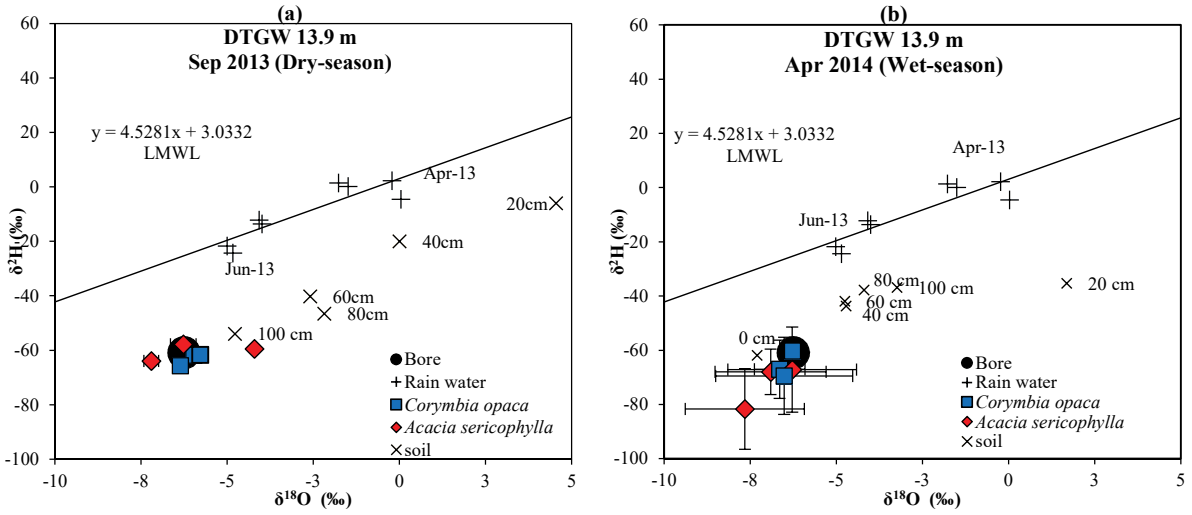

Figure 3.8: Rain, soil and xylem water isotopic composition at the 13.9 m DTGW site (east-west transect).

Panel a and b show Sep-2013 and Apr-2014 sampling respectively.

Comparison of soil and xylem water δ^2H-$\delta^{18}O$ signals: north-south transect

A comparison of δ^2H - $\delta^{18}O$ signals of branch (xylem) water, soil water and groundwater between the sites of the north-south transect is described below. Sites are ordered from the north (smallest DTGW) to the south (largest DTGW) end of the transect.

Site with 8.3 m DTGW

The first site from the north end of the north-south transect was the shallowest site of this transect with an 8.3 m DTGW. This site was characterized by short *Acacia* species, predominantly *Acacia aneura var. tenuis* and *Acacia kempana* with relatively broader phyllodes and an understorey of C3 and C4 herbs and grasses. Branch water isotopic signal did not vary significantly at this site between the two sampling periods of Sep-2013 and Apr-2014 or between the two species. The soil water isotopic profile for this site however varied largely between the two sampling periods. Most of the trees sampled appeared to match more closely with the isotopic signal at the depth of 60-100 cm during Sep-2013 and the signal of soil-surface water during Apr-2014 (**Figure 3.9**).

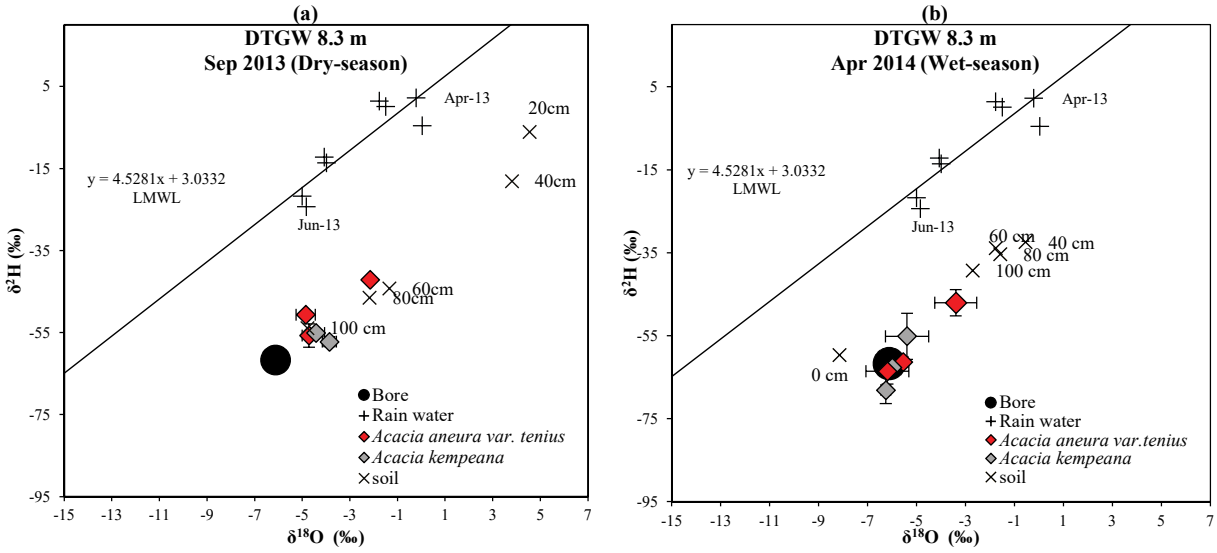

Figure 3.9: Rain, soil and xylem water isotopic composition at the 8.3 m DTGW site (north-south transect).

Panel a and b show Sep-2013 and Apr-2014 sampling respectively.

Site with 20 m DTGW

The next site from north to south along this transect was a *Corymbia* savanna with a 20 m DTGW characterized by two dominant species of trees – a) short *Acacia aneura* and b) very tall and widely spaced *Corymbia opaca*. δ^2H - $\delta^{18}O$ signals of soil water varied largely between the two sampling periods. Branch water isotopic signal of the *Acacia* species also varied between the two sampling periods; matching closely with soil water signal of depth 60 - 100 cm during the Sep-2013 sampling and with depth 20 - 40 cm during the Apr-2014 sampling (**Figure 3.10**). Two of the three *Corymbia* trees sampled at this site did not vary much during either sample periods ($\delta^{18}O$ =~-6 ‰ and δ^2H=~-60‰ during both seasons).

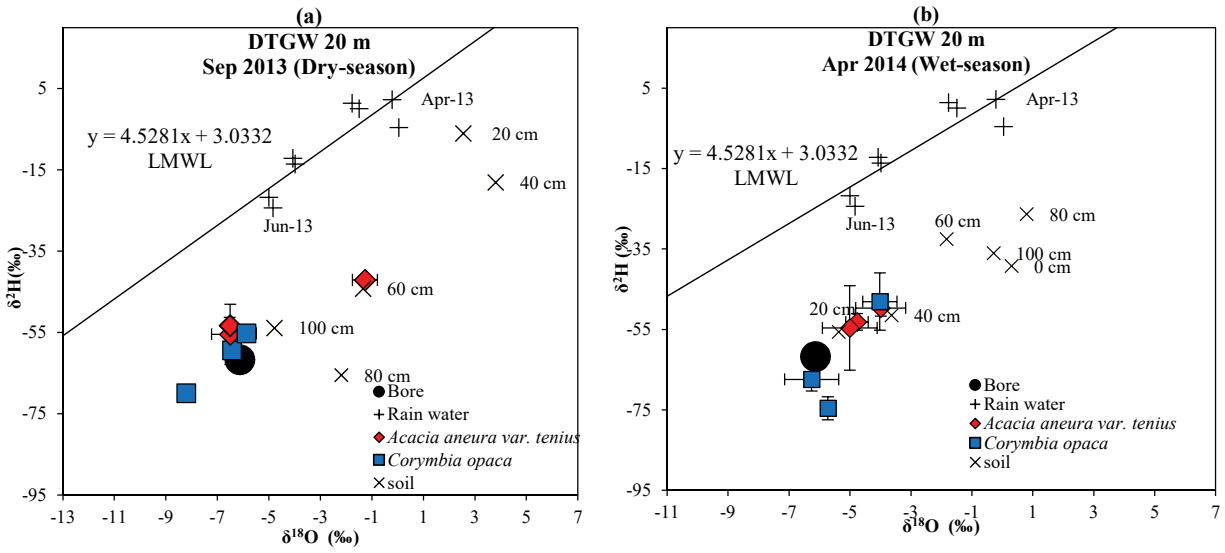

Figure 3.10: Rain, soil and xylem water isotopic composition at the 20 m DTGW site (north-south transect).

Panel a and b show Sep-2013 and Apr-2014 sampling respectively.

Site with 36 m DTGW

The next site along the north-south transect was the site with a 36 m DTGW. This site was characterized by ~5 - 6 m tall *Acacia* spp. (predominantly *Acacia aneura*), widely spaced *Corymbia* trees and C3 and C4 herbs and grasses. During the Sep-2013 sampling, branch-water isotopic signal of the *Acacia spp*. varied largely at this site. The *Corymbia* trees appeared to have accessed water from below 100 cm depth (**Figure 3.11a**). During the Apr-2014 sampling at this site, the xylem water δ^2H - $\delta^{18}O$ in both *Acacia* and *Corymbia* species showed similar values (although with larger standard errors between branches) and more closely matched with soil surface water isotopic signal, indicative of the use of water from recent rains. This was also the first site among all the sites in two transects where the deeper rooted *Corymbia* species showed the most variation in δ^2H - $\delta^{18}O$ compositions between the two sampling dates (Sep-2013: $\delta^{18}O$ =~-6 ‰ and δ^2H=~-65‰; Apr-2014: $\delta^{18}O$ =~-8 ‰ and δ^2H=~-90‰).

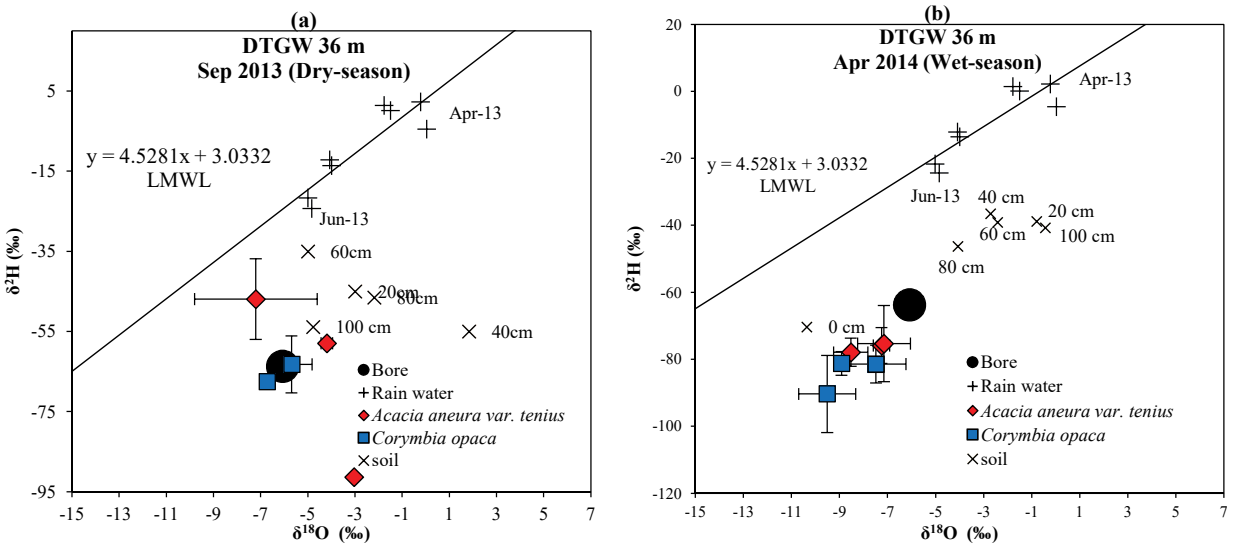

Figure 3.11: Rain, soil and xylem water isotopic composition at the 36 m DTGW site (north-south transect).

Panel a and b show Sep-2013 and Apr-2014 sampling respectively.

Site with 49.5 m DTGW

The last site along the north-south transect was the site with a 49.5 m DTGW characterized by ~5 - 6 m tall *Acacia spp.* (predominantly *Acacia aneura*), *Corymbia opaca* and C3 and C4 herbs and grasses. Both *Acacia* and *Corymbia* trees sampled during Sep-2013 at this site showed similar branch water δ^2H - $\delta^{18}O$ composition and appeared to have accessed soil water from ~100 cm depth (**Figure 3.12**). During the Apr-2014 sampling, soil water as well as branch water isotopic signal showed more depleted values where branch water appeared to match more closely with soil water signal of the depth of 20 - 40 cm. This was another site in this transect, other than the site with DTGW 36 m, where the δ^2H - $\delta^{18}O$ composition *Corymbia* trees differed between the two samplings - closely matching with soil water δ^2H - $\delta^{18}O$ of ~100 cm during Sep-2013 and 20-60 cm during Apr-2014 sampling.

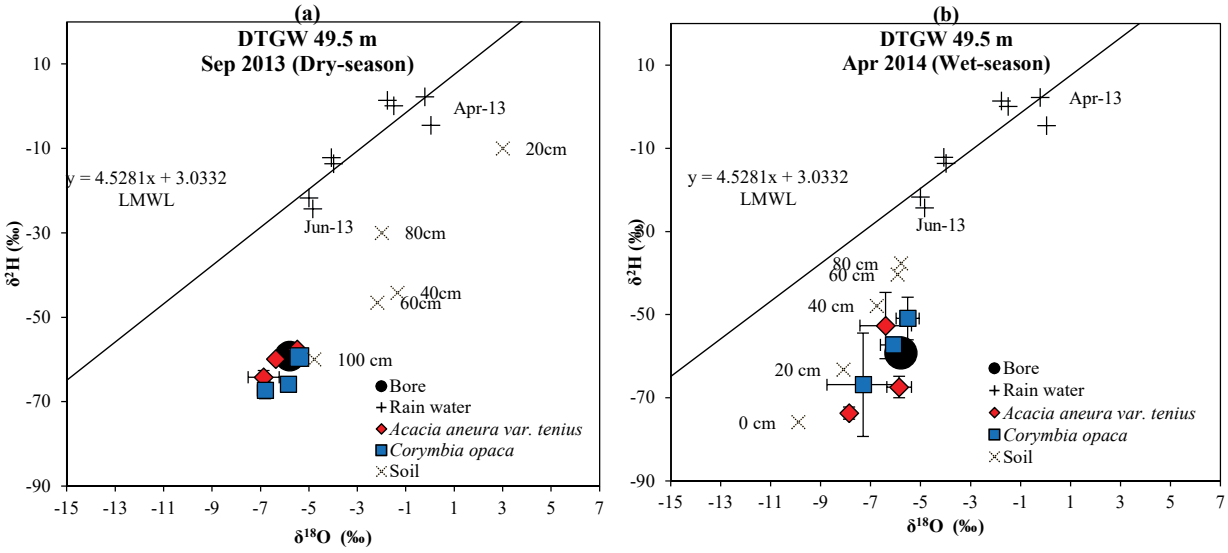

Figure 3.12: Rain, soil and xylem water isotopic composition at the 49.5 m DTGW site (north-south transect).

Panel a and b show Sep-2013 and Apr-2014 sampling respectively.

Comparing bore and xylem water isotopes

Figure 3.13a shows that the δ^2H-$\delta^{18}O$ composition of xylem water for *Acacia aneura* at the two shallowest sites where *Acacia* was present, did not match that of bore water for either sample times (i.e., both wet-season and dry-season). In marked contrast, the δ^2H-$\delta^{18}O$ composition of xylem water for the two deep rooted species, *Eucalyptus camaldulensis* and *Corymbia opaca* at the two shallowest sites where these two species were present were tightly clustered around the values for bore water and this was observed for both sample times (**Figure 3.13b**).

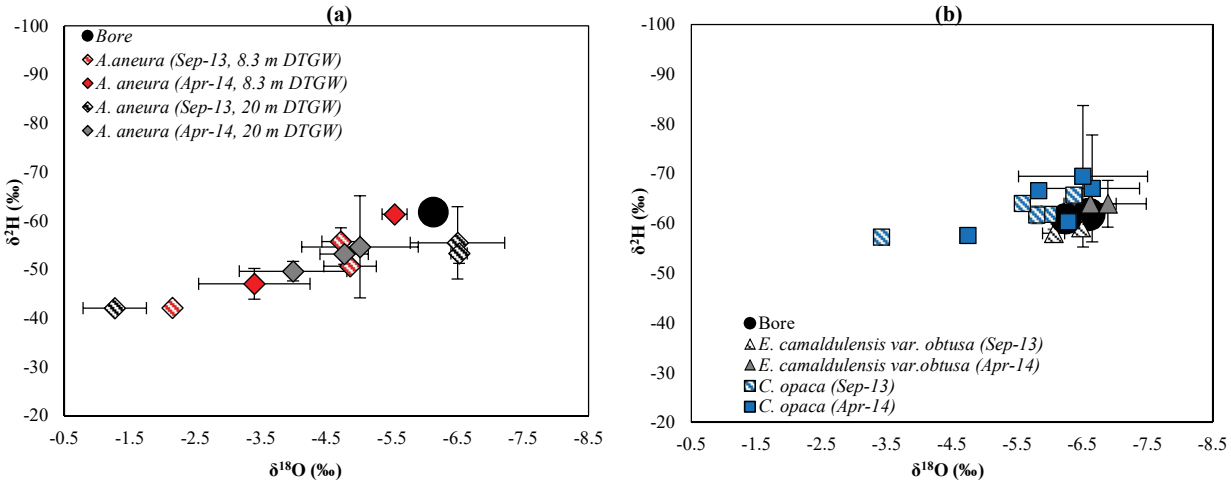

Figure 3.13: Comparison of xylem and bore water δ^2H-$\delta^{18}O$ plots for *Acacia aneura var. tenuis* sampled from 8.3 m and 20 m DTGW (panel a) and *Eucalyptus camaldulensis var. obtusa* and *Corymbia opaca* sampled from 4.4 m, 8.8 m and 13.9 m DTGW (panel b).

Bore water samples were available only for 8.3 m DTGW site (panel a) and for 4.4 m and 13.9 m DTGW sites (panel b).

Variation of $\Delta^{13}C$ across the DTGW gradient

Discrimination against carbon-13 ($\Delta^{13}C$) calculated from bulk-leaf $\delta^{13}C$ of shallow-rooted *Acacia spp.* across a DTGW gradient in the Ti Tree basin did not show any statistically significant pattern during the Sep-13 or Apr-14 sample periods (**Figure 3.14a and b**). In contrast, $\Delta^{13}C$ values for deep-rooted *Eucalyptus spp.* sampled from DTGW 4.4 m site and the *Corymbia spp.* sampled from all sites with *Corymbia* present across the gradient declined significantly up to a threshold value of DTGW of 13.9 m and then showed non-significant trends from 13.9 m to 50 m DTGW (**Figure 3.14(c) and (d)**). This pattern for the deep-rooted species was observed during both Sep-13 and Apr-14 sampling. At the 8.8 m DTGW site from the Sep-13 sampling (performed after three consecutive months of less than 1 mm rainfall), $\Delta^{13}C$ values of the *Corymbia* trees sampled from habitat-1 showed very positive $\delta^{13}C$ (-25.3 ± 0.07 ‰) and therefore, very small discrimination ($\Delta^{13}C$ = 17.7±0.07 ‰) and consequently were omitted from the regression. Also, no statistically significant trend could be identified for C3/C4 understorey species across the groundwater gradient during either sampling periods (figures not shown).

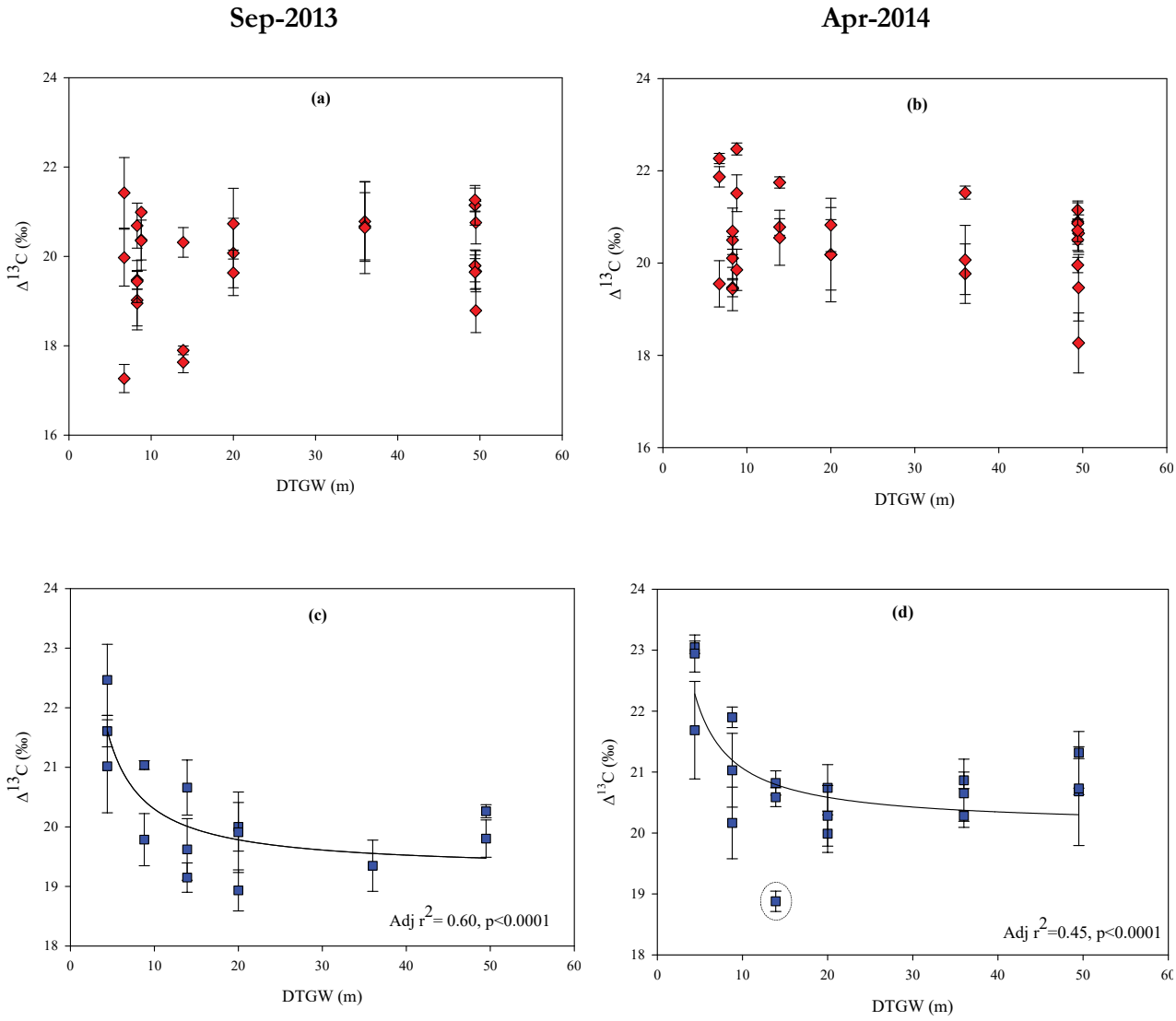

Figure 3.14: Carbon isotope discrimination in leaf dry matter ($\Delta^{13}C$) plotted as a function of DTGW in the Ti Tree basin.

Red points in panel a and b show shallow-rooted *Acacia spp*. and blue points in panel (c) and (d) deep-rooted *Corymbia* and *Eucalyptus* (at site DTGW 4.4 m) species. Left and right panels show Sep-13 and Apr-14 sampling respectively. The circled point in panel (d) was not included in the regression.

Seasonal variation in leaf intrinsic water-use-efficiency (WUE_i)

A one-way ANOVA was used to test for differences between leaf intrinsic water-use-efficiency (WUE_i, calculated from $\Delta^{13}C$) across the DTGW gradient followed by Tukey's *post-hoc* test to determine where any differences lay. ANOVA of WUE_i for shallow-rooted *Acacia spp*. did not identify significant differences between sites during Sep-13 or Apr-14

sampling (**Figure 3.15**) nor across seasons for sites analysed separately. However, when all wet-season data and all dry-season data for *Acacia* were aggregated, a significant difference between the dry-season (Sep-2013) and wet-season (Apr-2014) mean WUE_i was identified between the *Acacia* species (One way ANOVA: $F=9.88$, $p<0.05$). WUE_i for deep-rooted *Corymbia* and *Eucalyptus* species increased significantly with increasing DTGW from 4.4 m to 13.9 m ($F=8.79$, $p<0.001$, **Figure 3.16**) during both sample periods, but did not significantly differ at the deeper sites. Both *Corymbia* and *Eucalyptus* also showed a significant difference between the dry-season (Sep-2013) and wet-season (Apr-2014) mean WUE_i ($F=8.62$, $p<0.01$). For the dry-season and wet-season respectively, species mean WUE_i for *Eucalyptus camaldulensis* was 57.20±3.90 μmol/mol and 47.89±3.57 μmol/mol and for *Corymbia spp.,* 77.19±3.44 57 μmol/mol and 68.15±2.95 μmol/mol.

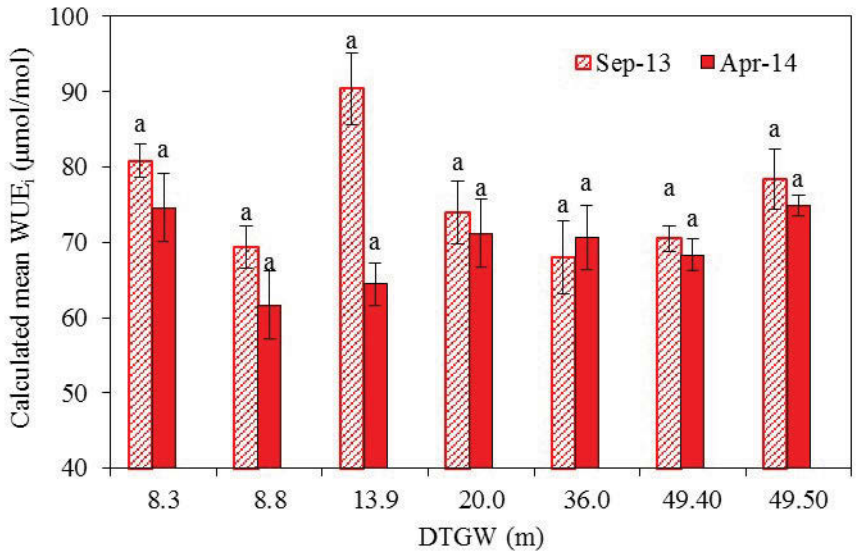

Figure 3.15: Calculated leaf intrinsic water-use-efficiency (WUE_i) in shallow-rooted *Acacia* species across study sites for Sep-13 (patterned column) and Apr-14 (filled column).

Letters above bars indicates the differences between means (Tukey HSD, confidence level of 0.05) across sites in each season.

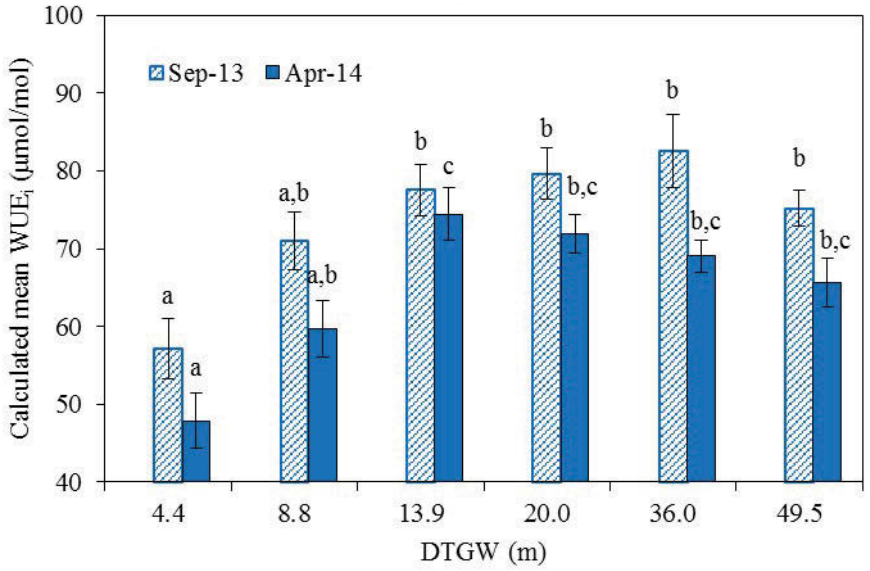

Figure 3.16: Calculated leaf intrinsic water-use-efficiency (WUE_i) in deep-rooted species across study sites for Sep-13 (patterned column) and Apr-14 (filled column).

Column bars at DTGW 4.4 m shows leaf WUE_i calculated from *Eucalyptus camaldulensis*. Leaf WUE_i was calculated for *Corymbia opaca* for the other DTGW sites. Letters above bars indicates the differences between means (Tukey HSD, confidence level of 0.05) across sites in each season and sites not connected by same letter are significantly different from other sites. Species mean WUE_i for the dry-season and wet-season respectively-*Eucalyptus camaldulensis*: 57.20±3.90 µmol/mol and 47.89±3.57 µmol/mol and *Corymbia spp.*: 77.19±3.44 57 µmol/mol and 68.15±2.95 µmol/mol.

Variation in LMA and LVD across the DTGW gradient

Leaf mass per unit area (LMA) and leaf vein density (LVD) of the same leaves used to measure $\Delta^{13}C$ were measured for the Apr-14 sampling. LVD of deep-rooted *Corymbia* species showed a moderately strong and significant relationship with DTGW across the basin (Adj r^2= 0.39, $p<0.01$, **Figure 3.17b**) unlike shallower rooted *Acacia spp.,* which showed no significant relationship with DTGW (**Figure 3.17a**). LVD of the *Corymbia* species increased from DTGW 4.4 m to 13.9 m (one-way ANOVA, F=49.03, $p<0.0001$), with no statistically significant relationship from DTGW 20 to DTGW 40.5 m (F=0.88, $p>0.05$).

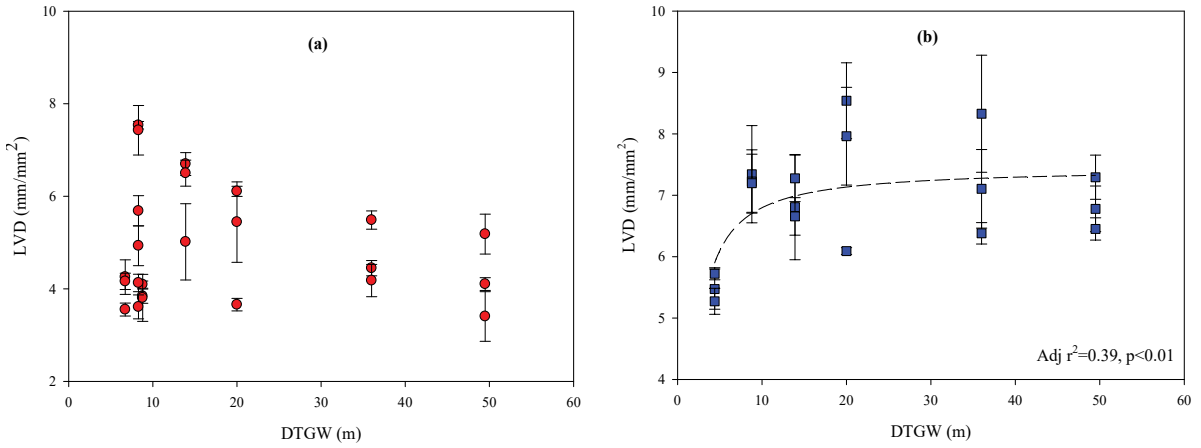

Figure 3.17: Leaf vein density of shallow-rooted *Acacia spp.* (panel a) and deep-rooted *Eucalyptus* (at DTGW 4.4 m) and *Corymbia spp.* sampled across Ti Tree basin plotted as functions of DTGW.

Each symbol represents mean LVD calculated from three individual leaves. Error bars are one standard error. A statistically significant correlation of LVD of deep-rooted species with DTGW is plotted with a dashed line.

A stronger linear and negative relationship between LVD with bulk-leaf $\Delta^{13}C$ was identified for the deep-rooted *Corymbia spp.*, such that, significantly smaller vein-densities were observed in leaves that showed larger discrimination against ^{13}C (Adj r^2= 0.41, $p<0.01$; **Figure 3.18b**). Leaf sampled from *Eucalyptus* species sampled from DTGW 4.4 m showed the largest $\Delta^{13}C$ as well as the smallest LVD. Shallower rooted *Acacia spp.* showed no significant relationships with $\Delta^{13}C$ (**Figure 3.18a**) sampled across the basin. Interestingly, LMA did not show any statistically significant relationships with either DTGW or $\Delta^{13}C$ for both shallow-rooted *Acacia spp.* and deep-rooted *Corymbia spp.* sampled across the Ti Tree basin (figures not shown).

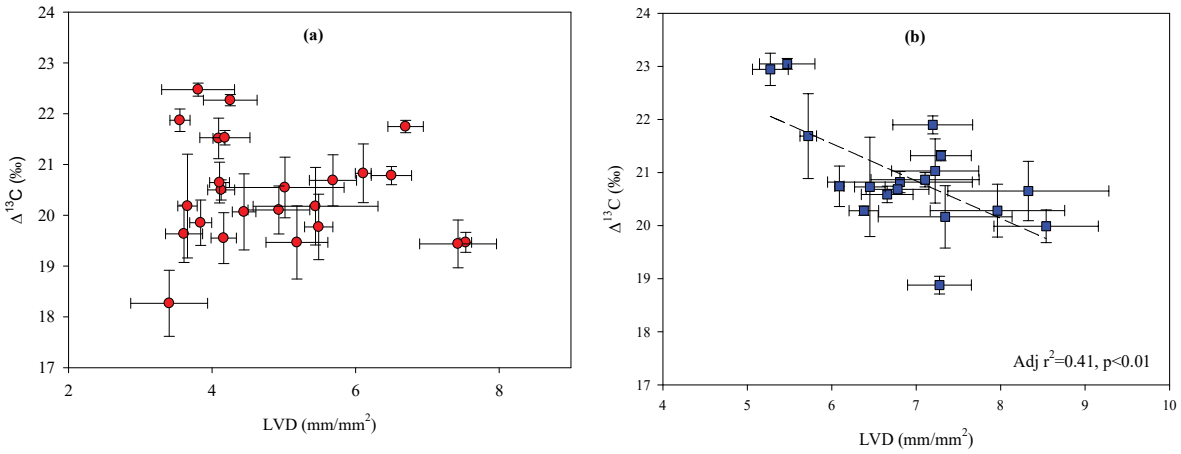

Figure 3.18: Relationships of leaf vein density (LVD) of shallow-rooted *Acacia spp.* (panel a) and deep-rooted *Eucalyptus* (at DTGW 4.4 m) and *Corymbia spp.* with bulk-leaf $\Delta^{13}C$.

Each symbol represents mean LVD and $\Delta^{13}C$ calculated from same three individual leaves. Error bars are one standard error. A statistically significant relationship of LVD and $\Delta^{13}C$ of deep-rooted species is plotted with a dashed line.

Variation in $\Delta^{13}C$ in Allungra creek transects

The Allungra Creek waterhole in the southern part of the Ti Tree basin is a frequent recharge zone that crosses the central part of the underlying Ti Tree aquifer (NRETAS, 2009). Three transects were sampled on March 2015 to capture variation in $\Delta^{13}C$ of frequent recharge zones near the hills at the south of the Ti Tree basin. Each transect perpendicular to the creek extended across the riparian zone along the bank of the creek to the woodlands of slightly higher elevation. Transect-1 was run near the Allungra Creek waterhole and Transect-2 and 3 were run along the creek southeast to transect-1 (**Figure 3.19**). Three leaf samples of three individuals (where available) were collected from *Eucalyptus camaldulensis, Acacia aneura* and *Corymbia opaca* species to measure $\Delta^{13}C$. These were the dominant overstorey species at this site enabling comparison with results from the east-west and north-south transects described earlier in this chapter. *Acacia* was the most dominant species of this particular site and was found to be distributed near the bank of the creek and the distal reaches. *Eucalyptus camaldulensis*, in contrast, was mostly riparian and hence restricted to the banks of the creek. *Corymbia opaca* was predominantly present in Transect-1 near the waterhole.

In general, $\Delta^{13}C$ signatures of trees sampled closest to the creek were significantly larger and WUE_i was significantly smaller, irrespective of species (**Figure 3.19**, $p<0.05$). Trees sampled in the distal reaches had smaller mean $\Delta^{13}C$ and larger WUE_i. *Eucalyptus camaldulensis* along the bank consistently showed larger $\Delta^{13}C$ and smaller WUE_i at all sites. In transect-2, mean $\Delta^{13}C$ and WUE_i of three *E. camaldulensis* sampled within 50 m of the creek did not significantly differ from those sampled along the creek (**Figure 3.19c** and **3.19d**), whereas in transect-3, mean $\Delta^{13}C$ and WUE_i of *E. camaldulensis* sampled along the creek and at a distance of 120 m significantly differed from each other indicative of larger water availability for trees near the creek (**Figure 3.19e** and **3.19f**).

Transect - 1

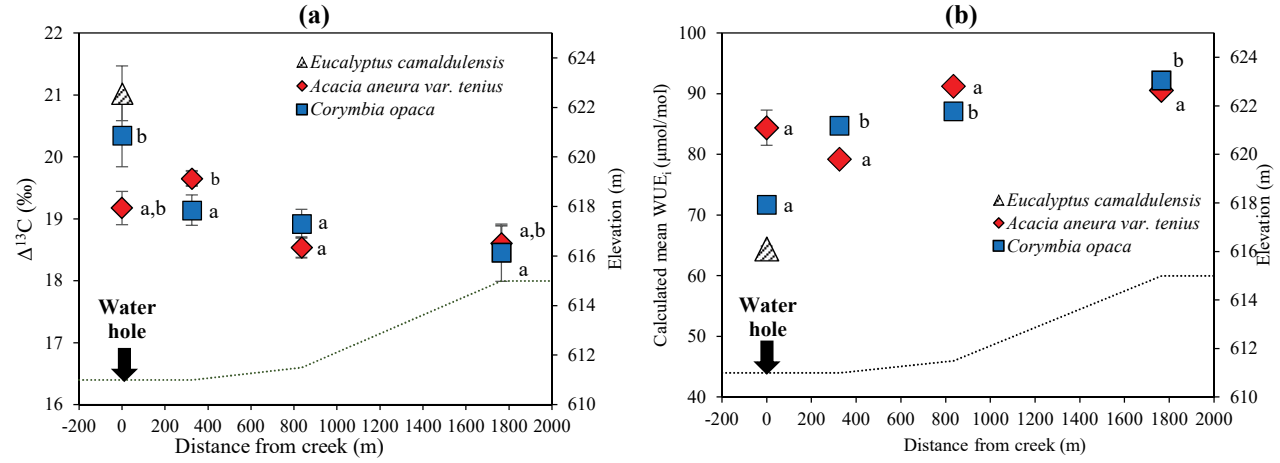

Transect - 2

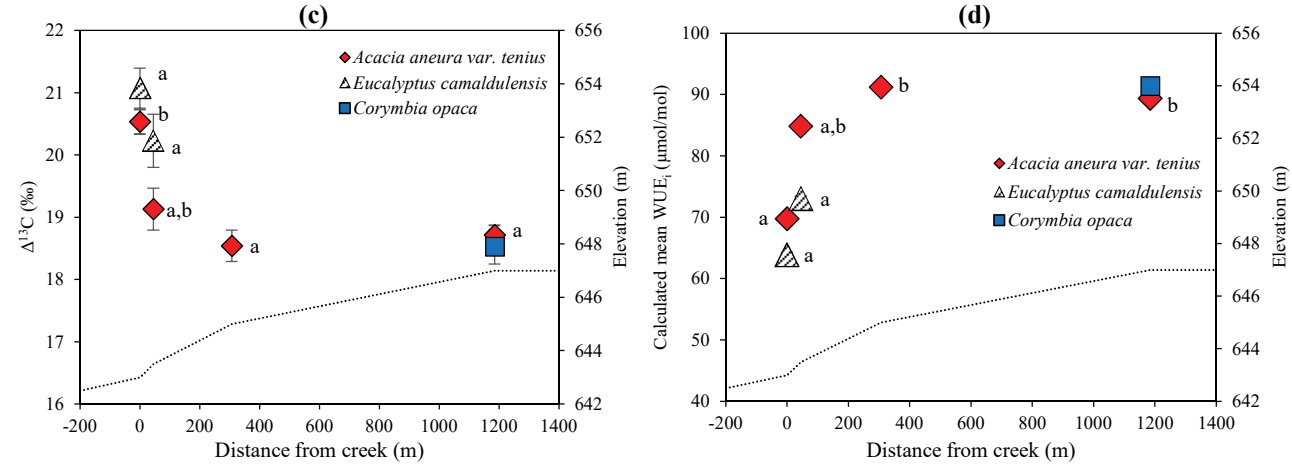

Transect - 3

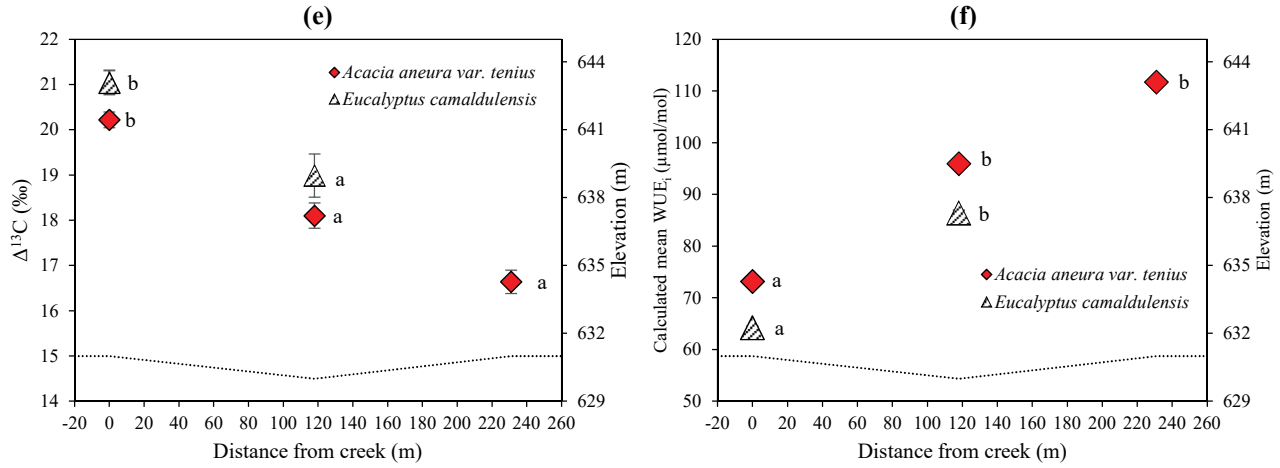

Figure 3.19: Cross sections of the riparian zone towards the distal reaches for three transects sampled at Allungra Creek (March 2015). $\Delta^{13}C$ (left panels) and WUE_i (right panels) values dominant species are also shown.

Letters beside each point indicates the differences between species means for comparison within species (Tukey HSD, confidence level of 0.05) across different points along the transect and points not connected by same letter are significantly different from other points.

Figure 3.20 shows $\Delta^{13}C$ and WUE_i of deep-rooted species (*Eucalyptus camaldulensis* and *Corymbia opaca*) sampled from all three transects plotted as a function of distance from the creek bed. As the distance from the bed increased, there was a significant decline in $\Delta^{13}C$ for both species (*Eucalyptus camaldulensis* and *Corymbia opaca,* **Figure 3.20a**), with concomitant increases in WUE_i with increasing distance from the creek (**Figure 3.20b**). Regressions applied to both species individually (data not shown) resulted in significant (r^2>0.98) negative slopes in **Figure 3.20a** and positive slopes in **Figure 3.20b** for both species. There was no significant relationship between $\Delta^{13}C$ nor WUE_i and distance from creek for the *Acacia* species across the three transects (p>0.05, figure not shown).

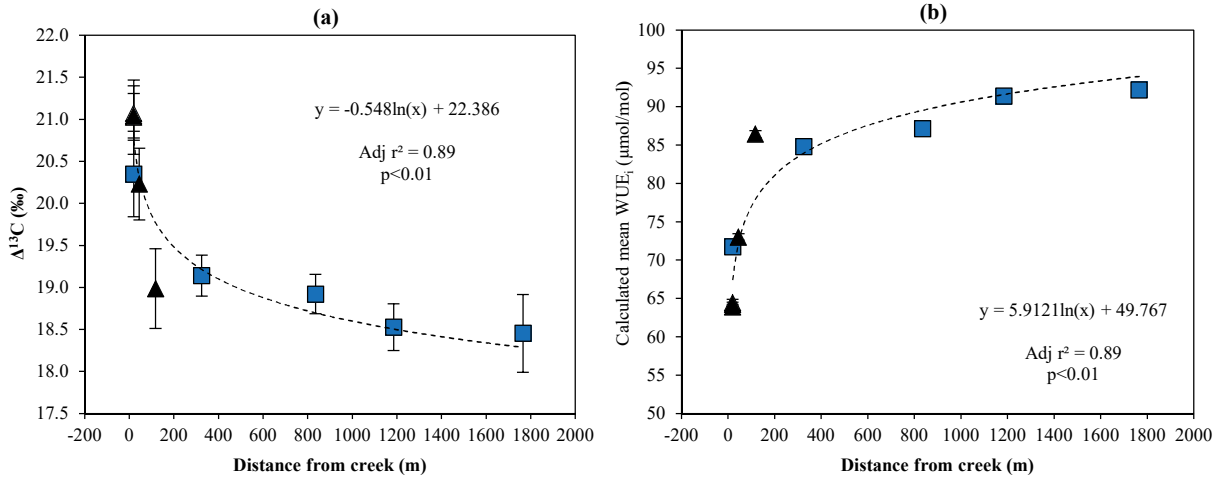

Figure 3.20: $\Delta^{13}C$ (panel a) and WUE_i (panel b) of deep-rooted species sampled across Ti Tree basin plotted as functions of distance from Allungra Creek bed.

Black triangles represent *Eucalyptus camaldulensis var. obtusa* and blue squares represent *Corymbia opaca* species.

Discussion

Variation in source-water uptake

The present study used stable deuterium and oxygen-18 isotopes (δ^2H and $\delta^{18}O$) to investigate the source of water used by vegetation along a depth-to-groundwater (DTGW) gradient in the semi-arid Ti Tree basin in Central Australia. First, the spatial variability in plant water use was investigated by examining the stable deuterium and ^{18}O concentrations in branch (xylem) water in four sites of varying groundwater depth along an east-west transect and four sites along a north-south transect spanning the entire 5,500 km^2 basin. Second, the source of water used by plants at each DTGW was further examined by directly comparing branch deuterium and ^{18}O concentrations with that of soil water and groundwater. Finally, an assessment of the temporal variability in deuterium and ^{18}O concentrations in dominant overstorey species, soil water and groundwater was made by sampling trees, soil cores and bores at the same locations at the late season (Sep-2013) and the late wet-season (Apr-2014).

Stable isotope analysis could distinguish soil water isotopic signals from rain water and ground (bore) water signals across sites. Rain water was sampled from separate rain events during April and June 2013 and consistently showed signals "depleted" in heavier isotopes. Depleted signals of rain water similar to this present study have previously been observed in northern Australia (O'Grady *et al.*, 2002) and these authors characterized the observed depleted signatures as the "rain-out effect", where, rain water contains less of the heavier isotopes of the water molecule because heavier isotopes tend to condense more readily than the lighter isotopes as atmospheric water gradually moves inland causing large event-to event variation in rain water isotopic signal. Deuterium excess *(d)* of the rain water was much smaller in the precipitation in April 2013 (6.14 ± 3.29) compared to winter precipitation in June 2013 (118.69 ± 19.86). This result is consistent with typical characteristic of sites with very low rainfall in every month and consequently the largest *d*-fluctuation (Liu *et al.*, 2010). Winter (June 2013) was the driest season during the study period with the largest *d*. Although with the onset of summer the amount of rainfall increased, the atmosphere beneath the cloud base still remained dry and far from saturated and therefore evaporation occurred during the fall of the rain droplets resulting in enrichment of the δ^2H-values and reduction of *d*-excess of the residual rainwater as observed previously in GNIP Alice Springs station (Liu *et al.*, 2010).

Across eight sites throughout the basin in the present study, bore water (groundwater) did not show significant differences in their δ^2H and $\delta^{18}O$ signatures indicative of being integrated by long-term average precipitation for this given region (O'Grady *et al.*, 2002). In contrast to groundwater isotopic signals, soil water signals showed large differences between Sep-2013 (late dry-season) and Apr-2014 (late wet-season) sampling. For almost all sites during the Sep-2013 sampling after a prolonged period of zero rainfall, δ^2H and $\delta^{18}O$ compositions of soil water showed a gradual depletion throughout the 100 cm depth with enriched values at the top of the upper soil profile. Such large ranges of soil water isotopic signals are suggestive of large event-to-event variability in the isotopic signature of rainfall previously observed in the region (O'Grady *et al.*, 2002). No such pattern of soil water isotopic signals, however, could be identified during the Apr-2014 sampling after all sites received >60% of the annual rainfall. The *Acacia* species showed larger variations in branch water isotopic signals between the two sampling dates compared to deep-rooted *Corymbia* and *Eucalyptus* species. At several sites (for example at DTGW 13.9 m and DTGW 49.4 m in the east-west transect and DTGW 8.3 m in the north-south transect), *Acacia* showed similar branch water δ^2H and $\delta^{18}O$ to those from below 100 cm depth through the soil profile during Sep-2013, which coupled with a consistently decreasing pattern of soil water isotopes might suggest that a possible source of water was created by the existing siliceous hardpans at ≈ 100 cm below the soil at these sites (Cleverly *et al.*, 2013; Cleverly *et al.*, 2016) and this reservoir of soil-moisture storage above the hardpan was accessed by most of the trees sampled during this period. In contrast during Apr-2014 sampling (after summer rains had recharged soil water stores), δ^2H and $\delta^{18}O$ compositions of *Acacia spp.* matched closely with more enriched soil water signals from shallower depths. All these findings suggest that the *Acacia* species across the DTGW gradient adopted an "opportunistic" strategy and were dependent primarily on soil water. This finding is also consistent with previous studies in this region where *Acacia spp.* were found to be very responsive to changes in soil moisture content, which in turn was suggestive of relatively shallow rooting depth of these species (Eamus *et al.*, 2013; Pressland, 1975). Previous studies have also recorded very low predawn leaf-water-potential of *Acacia spp.* in this region (Howe *et al.*, 2007) and these low values of water potentials coupled with the findings from stable isotope analysis confirms that *Acacia spp.* sampled across the basin relied mostly on soil water and did not draw on underlying groundwater.

Two other dominant overstorey species found across the basin were *Eucalyptus camaldulensis* and *Corymbia opaca* which are relatively deeper rooted (8-20 m) and tend to be groundwater dependent in semi-arid regions (Howe *et al.*, 2007; O'Grady *et al.*, 2006a; O'Grady *et al.*, 2006b). Groundwater was in the rooting-zone of these species in at least three of the eight sites (DTGW 4.4 m, 8.8 m and 13.9 m, these three sites are shown in **Figure 3.13b**). *Eucalyptus camaldulensis var. obtusa* lines the river banks at the shallowest site of DTGW 4.4 m and direct comparisons of branch and bore water δ^2H and $\delta^{18}O$ revealed that this species consistently showed similar δ^2H and $\delta^{18}O$ to those of the nearby (shallow) bore water (**Figure 3.13b**). δ^2H and $\delta^{18}O$ compositions also did not vary between the Sep-2013 and Apr-2014 samplings (**Figure 3.13b**) suggesting that this species accessed groundwater at this site during the dry-season in Sep-2013 and did not shift to any other sources despite sufficient soil water availability during (late wet-season) Apr-2014. *Corymbia opaca* at the DTGW 13.9 m site also showed similar behaviour, where branch water isotopic signal matched closely with the (slightly deeper) bore water and did not vary significantly between the two sampling periods (**Figure 3.13b**). These findings from the stable isotope analyses support the observations from a number of previous studies that showed deep rooted *Eucalyptus* and *Corymbia spp.* relying primarily on groundwater as their source of water uptake in these semi-arid regions, especially when groundwater is available within their root zone (Cook *et al.*, 2008; Howe *et al.*, 2007; O'Grady *et al.*, 2006a; O'Grady *et al.*, 2006b).

In this present study, variability among plant habitats was also reflected in plant water sources. For example at the DTGW 8.8 m site, there were three distinctly different micro-habitats; a small patch of *Acacia spp.* with occasional *Corymbia* trees close to the eddy-covariance tower within the *Corymbia* savanna; the transition between the *Acacia* patch and the *Corymbia* savanna and the third was the *Corymbia* savanna *per se* (Cleverly *et al.*, 2016). Groundwater at this site was in the rooting depth *Corymbia* tress of all three habitats, however, branch water δ^2H and $\delta^{18}O$ compositions of only the trees from *Corymbia* savanna (habitat 3) matched closely with bore water isotopic signal indicating groundwater access by these trees, and signals from these trees did not differ significantly during Sep-2013 and Apr-2014 sampling. The *Corymbia* trees from the other two micro-habitats did not show δ^2H and $\delta^{18}O$ compositions similar to bore water and varied between samplings, as was observed in the soil water isotopic signals, indicating that these trees did not access the groundwater and relied more on soil water. It is plausible that these trees in habitat 1 and 2 had some kind of restrictions in their rooting distributions because of the existence of

siliceous hardpan which creates a barrier to root growth, thus they used whatever resource was available (in this case mostly soil water) (Cleverly *et al.*, 2016). It has been suggested by Cleverly et al., (2016) that the *Acacia* trees in the small Mulga patch at the west end of the west-east transect occur directly above a siliceous hardpan and therefore this is likely to be also limiting the access of the *Corymbia* tree to groundwater here.

Proportional contribution of possible water sources

One particular advantage of determining the stable deuterium and ^{18}O signatures of plant branch (xylem) water as well as possible water sources accessed by plants (such as, groundwater, rain water, soil water etc.) is that, stable isotope mixing models (SIMMs) can be used to determine the proportional contribution of each of these possible sources in plant water uptake (Hopkins et al., 2012; Phillips 2003). In **Chapter 2** of this thesis, I used SIMMs to identify the proportional contribution of groundwater, sub-surface soil water and rain water in plant xylem water of the dominant overstorey and understorey species located in the mesic Kangaloon sites in NSW. The theory of mixing models assumes that the mixing sub-space is defined by tracers (such as δ^2H, $\delta^{18}O$ etc.) and generally three or more possible sources (e.g., groundwater, soil water and rain water). The sources are plotted as vertices of a triangle (or a polygon if there are more than three possible sources) in the mixing subspace and any point bound by the triangle (or the polygon) represents a tree using a combination of these sources (Hopkins et. al., 2012; Purnell et. al., 2010). Unlike the mesic Kangaloon sites described in **Chapter 2**, rain water isotopic values at the time of sampling were not available for the trees in the Ti Tree basin described in this chapter. Also in contrast to Kangaloon sites, the deuterium and ^{18}O signatures of the soil-surface were generally much enriched especially during Sep-2013 due to evaporative enrichment in this semi-arid region and does not represent the values for rain water at these sites. Consequently, the deuterium and ^{18}O dataset of possible water sources was too restricted in terms of applying a two-tracer three-source SIMM in this semi-arid Ti Tree basin study. However, SIMMs can also fit a model between only two sources using the *siar* package in R (Purnell et al., 2010). In this particular dataset, there was generally a gradually decreasing pattern of soil water deuterium and ^{18}O signatures during the Sep-2013 sampling and most species appeared to access water from ≈ 100 cm below the soil surface at this time. Deuterium and ^{18}O values at the ≈ 100 cm also fell very close to the bore water isotopic signal in these sites during the dry-season and therefore, models fitted to determine the proportional contribution of groundwater and sub-surface soil water (at the

depth of ≈ 100 cm) as two possible sources of water uptake struggled to differentiate between these two sources (which was represented by a high correlation between the posterior distributions of these two sources) (Inger *et al.*, 2010). In contrast to Sep-2013 sampling, deuterium and ^{18}O signatures varied largely during the Apr-2014 sampling and did not show a gradually decreasing pattern between different depths of soil. Consequently, a particular depth as the "sub-surface layer" that accurately represent a distinct pool of water could not be identified for this sampling period (Apr-2014).

Variation in discrimination against ^{13}C and WUE_i

One specific aim of the present study was to investigate whether discrimination against ^{13}C ($\Delta^{13}C$) and leaf intrinsic water-use-efficiency (WUE_i) calculated from stable isotopes at the leaf-level can accurately identify water availability, more specifically, groundwater use and spatial and/or seasonal patterns of groundwater use in the dominant overstorey species in the semi-arid Ti Tree basin. An increase in foliar $\Delta^{13}C$ represents decreased access to water and increasing WUE_i (Leffler and Evans, 1999; Zolfaghar *et al.*, 2014) and has been previously used to infer access to groundwater (Zolfaghar *et al.*, 2014). I tested the hypothesis that discrimination against ^{13}C ($\Delta^{13}C$) will decrease and leaf-intrinsic water-use-efficiency (WUE_i) will increase as water availability decreases with increasing DTGW, or through the presence of a siliceous hardpan at the western end of the west-east transect underlying the small *Acacia* patch located there. The shallower rooted *Acacia spp*. did not show any significant pattern in regression analysis of $\Delta^{13}C$ with DTGW across the basin during both Sep-2013 and Apr-2014 sampling (**Figure 3.14a** and **3.14b**). Mean WUE_i also showed no significant trend with increasing DTGW (one-way ANOVA: $F=1.78$, $p>0.05$, **Figure 3.15**). This result was consistent with the findings from direct comparison of $\delta^{18}O$ and $\delta^{2}H$, indicating that, *Acacia* species during both Sep-2013 and Apr-2014 sampling were predominantly accessing soil water and therefore $\Delta^{13}C$ did not vary with groundwater availability. In contrast, the $\Delta^{13}C$ of deep-rooted *Eucalyptus camaldulensis* sampled from DTGW 4.4 m site and the *Corymbia opaca* growing under similar atmospheric conditions along the DTGW gradient declined significantly up to a threshold value of DTGW of 13.9 m and then showed non-significant trends from DTGW 13.9 m to DTGW 49.5 m (**Figure 3.14c** and **3.14d**). Site mean WUE_i also increased significantly with increasing DTGW from 4.4 m to 13.9 m (**Figure 3.16**) during both sampling and did not significantly vary at the deeper sites. From these results I conclude that the rooting limit for *Corymbia* at these sites is approximately 14 -16 m. The results from deuterium -^{18}O analysis also demonstrated

access to groundwater for the deep-rooted trees at these three sites (DTGW 4.4 m, 8.8 m and 13.9 m), which coupled with the findings from ^{13}C analysis suggests that, discrimination against ^{13}C and WUE_i calculated from stable isotopes at the leaf-level for these deep-rooted trees accurately identified enhanced water availability (i.e., groundwater uptake) at the shallower end of the DTGW gradient. Furthermore, these findings were consistent with previous observations of rates of sapflow in the Ti Tree basin demonstrating the largest rate of daily water use of *Corymbia* trees at DTGW < 10 m from that decreased as DTGW increased to 20 m (Howe *et al.*, 2007).

Variation in $\Delta^{13}C$ and WUE_i across micro-habitats

One interesting aspect of the deuterium-^{18}O analysis was the identification of within-site variability (across habitats) of sources of water uptake at the DTGW 8.8 m site as discussed in the previous section. This within-site variability was also apparent in the ^{13}C analysis at the leaf-level. As hypothesized, the *Corymbia* trees identified as accessing groundwater from deuterium-^{18}O analysis also showed largest discrimination against ^{13}C (and smallest WUE_i) and also no substantial variation in $\Delta^{13}C$ for these trees was observed during Sep-2013 and Apr-2014 samplings (**Figure 3.21**).

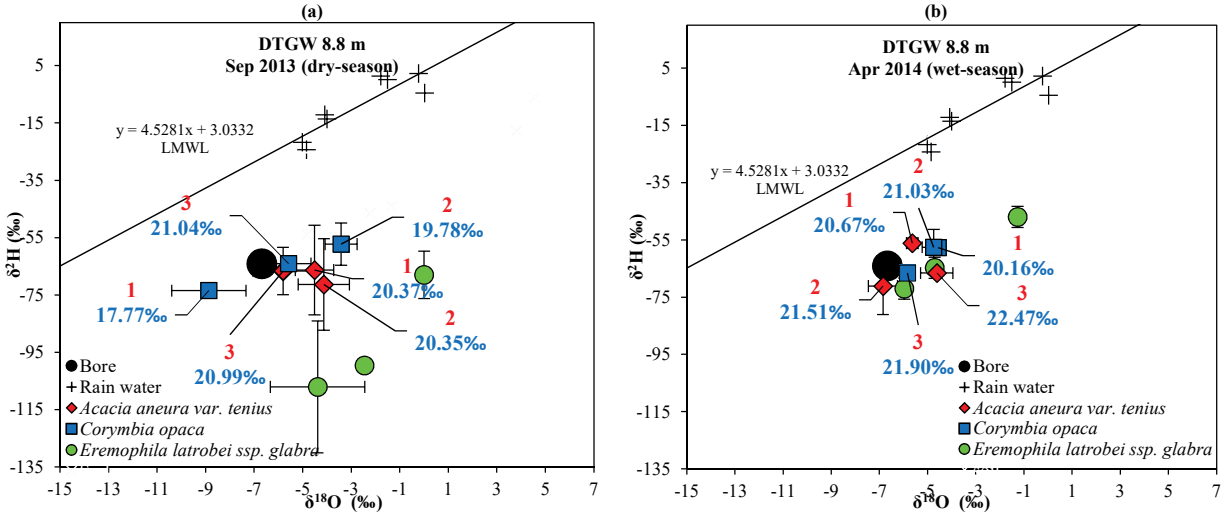

Figure 3.21: Comparison of results from deuterium-^{18}O analysis with ^{13}C analysis at the DTGW 8.8 m site (east-west transect).

Panel a and b show Sep-2013 and Apr-2014 sampling respectively. Trees sampled from micro-habitats 1, 2 and 3 are labelled with corresponding numbers in red colour and the blue numbers indicate calculated discrimination against ^{13}C ($\Delta^{13}C$‰). Deep-rooted *Corymbia opaca* trees closer to the bore (black circle) showed consistently showed larger $\Delta^{13}C$ inferred as access to groundwater.

Comparing the two sites of 49.4 m DTGW and 8.8 m DTGW on the same (east-west) transect, $\Delta^{13}C$ of the *Acacia spp*. was 20.53‰ in Sep-2013 and 21.05‰ in Apr-2014 sampling and these values did not substantially differ across sites and across micro-habitats at the 8.8 m DTGW site (one-way ANOVA: $F=0.4$, $p>0.05$). By contrast at the 8.8 m site, $\Delta^{13}C$ of *Corymbia opaca* trees varied substantially ($F=40.13$, $p<0.0001$) across three micro-habitats in the sequence: $\Delta^{13}C$ of *Corymbia* in the open savanna > *Corymbia* trees in the transition between the *Acacia* patch and open *Corymbia* savanna > Corymbia trees in the *Acacia* patch (**Figure 3.21a and Figure 3.22a**) during Sep-2013. No such variation, however was observed during the Apr-2014 sampling (**Figure 3.21b and Figure 3.22b**). These comparisons further support the interpretation made from deuterium-^{18}O analysis such that, *Corymbia* trees growing in the *Acacia* patch were subjected to restricted root-growth due to the existence of a siliceous hardpan preventing access to groundwater in this micro-habitat and this was reflected by smaller discrimination (larger WUE_i) for these trees. Moving into the extensive open savanna from the *Acacia* patch, *Corymbia* trees showed larger discrimination (and smaller WUE_i) which I interpret as increasing rooting depth of these trees across these habitats potentially enabling them to access groundwater at the depth of approximately 8 m at this site, particularly after prolonged dry periods. Furthermore, there was no evidence of differences in $\Delta^{13}C$ of *Acacia* species sampled across three micro-habitats at the DTGW 8.8 m sites and between those sampled in sites where groundwater exceeded 49 m, which again confirms the findings from deuterium-^{18}O analysis, such that, access to groundwater did not occur for *Acacia* species at the DTGW 8.8 m site. Interestingly, despite not accessing groundwater even during the dry-season in Sep-2013, *Acacia* species exhibited moderately large discrimination against ^{13}C (resulting in smaller WUE_i for this species), consistent with their anisohydric stomatal responses to soil drying extensively documented for these species in a number of studies; that is, their stomata remain open even at very low water potentials (O'Grady *et al.*, 2009; Winkworth, 1973).

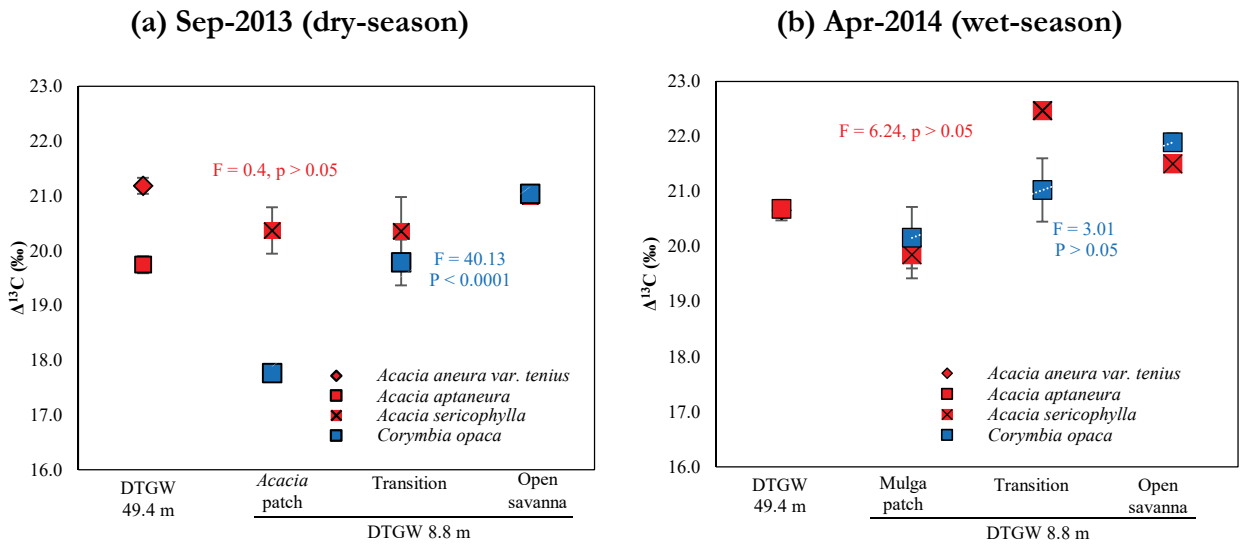

Figure 3.22: Discrimination against carbon-13 ($\Delta^{13}C$) of *Acacia spp.* (red) and *Corymbia opaca* (blue) leaves in the 49.4 m DTGW and across three habitats (open *Corymbia* savanna, transition and *Acacia* patch) within the 8.8 m DTGW site.

Panel a and b show Sep-2013 and Apr-2014 sampling respectively. Symbols show mean ± SE. Results from one-way ANOVA are also listed for corresponding species.

Can $\Delta^{13}C$ be used as an indicator of groundwater use?

There are many previous studies that have used stable isotopes of water to deduce groundwater uptake (Chimner and Cooper, 2004; Lamontagne *et al.,* 2005; White *et al.,* 1985; Zencich *et al.,* 2002); indeed this technique was central to this thesis. Extraction of stable isotopes of water is slow and technically challenging and does not always yield reliable results if distinct differences between bore water and soil water signatures are not apparent (for example in highly sandy soils where percolation rates of rain are rapid). In contract, analyses of foliar $\Delta^{13}C$ is less technically challenging and faster than that of analyses of isotope signatures of water. In three analyses of foliar $\Delta^{13}C$ across rainfall gradients in Australia (Stewart *et al.*, 1995; Miller *et al.*, 2001 and Taylor, 2008) there was a remarkable consistency in the trends of foliar $\Delta^{13}C$ as a function of rainfall (**Figure 3.23**). It is also apparent that for the two deep-rooted species, the foliar ^{13}C values were much larger than predicted from the regressions of foliar ^{13}C *versus* rainfall for any of the three studies (**Figure 3.23**). Thus, I propose that the foliar $\Delta^{13}C$ in the deep-rooted species reflects the larger availability of water arising from access to groundwater for these two species at sites where DTGW ≤ 13.9 m and therefore is an indicator of groundwater use by vegetation.

Eucalyptus camaldulensis and *Corymbia opaca* are 'behaving' as though they are receiving approximately 1500 mm and 900 mm of rainfall indicated by the horizontal dashed line (to the regression line from Taylor, 2008; **Figure 3.23**). Means of $\Delta^{13}C$ of these species were also much larger than previous observations of foliar ^{13}C made in sites with annual rainfall ~300 mm in Northern Australia (Miller *et al.*, 2001; **Figure 3.23**).

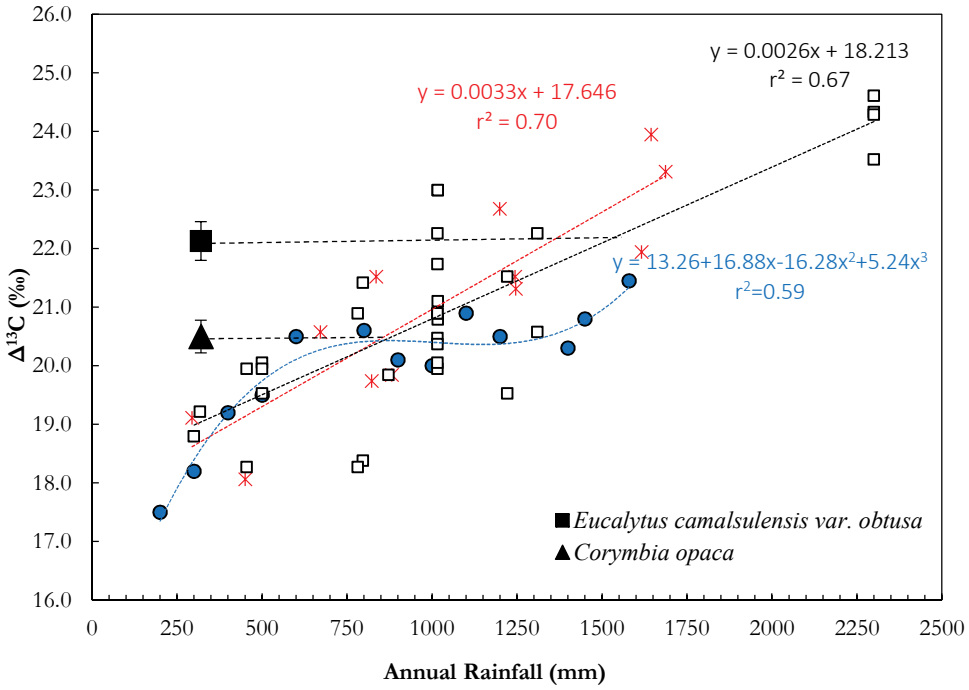

Figure 3.23: Relationships of discrimination against carbon-13 ($\Delta^{13}C$) with annual rainfall observed in different studies across Australia.

The red symbols represent observations made in eastern Australia (Stewart *et al.*, 1995), the blue symbols represents observations made in northern Australia (Miller *et al.*, 2001) and the open squares represents observations made in arid in-land and mesic coastal sites in New South Wales (Taylor, 2008). The black symbols on the left represent mean (±SE) value of $\Delta^{13}C$ of deep-rooted *Eucalyptus camaldulensis var. obtusa* from the Woodforde River site (DTGW 4.4 m) and *Corymbia opaca* sampled across the Ti Tree basin (from sites with DTGW ≤ 13.9 m).

Patterns of ⊿^{13}C and WUE_i along the Allungra creek transects

Three transects (up to 2 km) were run near the Allungra Creek located at the southern boundary of the Ti Tree basin in order to investigate whether the increasing pattern of $\Delta^{13}C$ with decreasing DTGW observed in this present study can be replicated in a frequent

recharge zone of Allungra Creek waterhole, in contrast to the Ti Tree basin where recharge is mainly concentrated in flood-outs following rare occurrence of heavy rainfall.

All species closest to the creek discriminated significantly more against ^{13}C suggesting access to this water source of these species. Interestingly in contrast to *Acacia* species sampled from across Ti Tree basin, $\Delta^{13}C$ of *Acacia*s sampled from along the Creek was significantly larger (and WUE_i smaller) than those sampled further along the perpendicular transect in at least two of the three transects (**Figure 3.19**). This result indicates that *Acacia* species along the Creek were also accessing this relatively shallow water source. Significantly larger $\Delta^{13}C$ of *Corymbia opaca* trees could also be identified between *Corymbia* trees sampled at the waterhole and at 400 m away from the waterhole. However, no significant difference was detected in *Corymbia* trees further down the transect (**Figure 3.19a** and **3.19b**). As was observed at the 4.4 m DTGW site of the east-west transect in Ti Tree basin, the largest discrimination was detected in the *Eucalyptus camaldulensis* trees mostly restricted to the banks of the Allungra Creek near the waterhole. Overall, dominant species sampled along the Allungra Creek replicated the results obtained from the Ti Tree basin lending further support for the initial hypothesis of decreasing $\Delta^{13}C$ (and increasing WUE_i) with increasing depth-to-groundwater.

Hydrological niche separation in the Ti Tree basin

Results of both deuterium-^{18}O analysis of xylem water and ^{13}C analysis of leaves suggests that the two dominant co-occurring species, i.e., shallower-rooted *Acacia* and deep-rooted *Corymbia spp*. segregated along a continuous depth-to-groundwater gradient. These species maintained their relative isotopic rankings in two sampling dates (i.e., the late dry- and wet-season) with contrasting water availability. The shallower-rooted *Acacia* species adapted a "profligate / opportunistic" water use strategy characterized by anisohydric behaviour of these species and consequently, high $\Delta^{13}C$ and low WUE_i (Moreno-Gutiérrez *et al.*, 2012) and appeared to have relied mostly on shallow and highly fluctuating water pool of the sub-surface soil. Species like *Acacia*, which have a relatively narrow window of opportunity of water uptake from superficial soil layers due to pulse water availability are able to maximize their photosynthesis and growth by profligate water use strategies (Hernández *et al.*, 2011; Orians and Solbrig, 1977). In contrast to these shallower-rooted species, stable isotope analyses revealed that deep-rooted *Eucalyptus* and *Corymbia* species depended mostly on groundwater when groundwater was available in their rooting-zone and did not shift to any

other sources despite sufficient soil water availability during the wet-season. However, when groundwater was beyond the rooting-depth, the water uptake and water use strategies of these deep-rooted species did not vary significantly from that of the shallower-rooted *Acacia* species. These results from stable isotope analyses are suggestive of the existence of "hydrological isotopic niches" that reflect contrasting water uptake and water use strategies of co-occurring species in this water-limited region. These contrasting strategies are driven by the difference in their rooting-depths leading to spatial and temporal partitioning of limiting water-resources that has been frequently observed in severely water-limited regions like the Ti Tree basin (Orians and Solbrig, 1977; Peñuelas *et al.*, 2011; Schwinning and Ehleringer, 2001).

LVD across the DTGW gradient

Leaves are composed primarily of two components - the mesophyll that carries out photosynthesis and the leaf vein network. Investment in leaf vein networks is underpinned by within-leaf resource allocation strategies (Niinemets *et al.*, 2007; Niinemets *et al.*, 2006; Niklas *et al.*, 2007). The biological and/or mechanical properties of leaf support structures largely co-varies with leaf-size (Poorter and Rozendaal, 2008; Westoby and Wright, 2003; Wright *et al.*, 2006). A number of studies demonstrate that larger leaves require larger investments in construction of primary and secondary veins to meet the hydraulic demands of the photosynthetic mesophyll tissue as well as to provide sufficient bio-mechanical support to ensure effective light interception (Givnish, 1988; Niinemets and Kull, 1999; Niklas, 1999). Leaf vein density (LVD, length of veins per unit area) is increasingly being recognized to be influenced by a number environmental variables such as temperature, light interception, soil dryness, humidity and nutrient availability and morphological variables, such as, leaf insertion level and leaf size (Uhl and Mosbrugger, 1999). Furthermore, there is a growing body of evidence that LVD is positively associated with leaf hydraulic conductance, maximum photosynthetic rate and leaf-level gas-exchange rates (Brodribb *et al.*, 2007; Sack *et al.*, 2003; Sack and Frole, 2006; Sack and Holbrook, 2006). Based on global-scale correlations between LVD and environmental, morphological and gas-exchange variables, one aim of this present study was to investigate whether vein investments of dominant overstorey species in semi-arid Ti Tree basin were affected by decreasing water availability i.e., increasing DTGW, as well as to identify relationships between LVD and bulk-leaf $\Delta^{13}C$, if such exist.

In a critical review of a substantial number of LVD studies, Uhl and Mosbrugger, (1999) attributed water availability to be the most important factor that influences venation density. These authors reviewed an early study that investigated 93 species of mostly herbs and some deciduous trees that also demonstrated that venation density is higher in plants from xeric habitats than in plants from mesic habitats (Zalenski, 1902 cited in Uhl and Mosbrugger, 1999). In a more recent meta-analysis of LVD compiled from a global database of 796 species, Sack and Scoffoni, (2013) also observed a negative relationship between LVD and mean annual precipitation. Based on these findings I hypothesized that trees able to access groundwater would demonstrate smaller LVD and *vice-versa*. By sampling trees growing under similar climate conditions of temperature, rainfall and VPD in the Ti Tree basin, it will be possible to ignore these variables as possible causes of variation in LVD. Indeed, LVD of deeper rooted *Eucalyptus* and *Corymbia* species that showed groundwater access from stable isotope analyses increased as DTGW increased from 4.4 m to 13.9 m (one-way ANOVA, $F=49.03$, $p<0.0001$) and no statistically significant relationship from DTGW 20 to DTGW 40.5 m ($F=0.88$, $p>0.05$) was observed where depth of the water table had presumably exceeded the rooting depth of these trees. This correlation is further supported by the fact that there was no relationship between DTGW and LVD of the shallower rooted *Acacia* species, which did not access groundwater at these sites, as concluded from stable isotope analyses. Both *Acacia* and *Corymbia* species in this present study, however, showed vein-densities generally close to the higher end of the global spectrum (from Figure 4, Sack and Scoffoni, (2013)) consistent with higher LVDs obtained from "semi-desert" species. Overall, higher LVDs in species from arid/semi-arid regions allow more even spatial distribution of water across the phyllode/lamina during water-stress, which further contributes to a greater consistency of mesophyll hydration (Sommerville *et al.*, 2012); and a more consistent mesophyll hydration may, in turn, allow continued photosynthetic carbon assimilation during water-stress (Sommerville *et al.*, 2010). Higher LVDs of *Acacia* species, in particular in semi-arid regions in Australia, have also been previously associated with a more rapid upregulation of phyllode function with the return of precipitation following drought (Sommerville *et al.*, 2010), and rapid upregulation mechanisms are crucial for vegetation in regions with unpredictable and pulse-like rainfall as is observed in the Ti Tree. This is required because vegetation in these areas are provided with only a few opportunities for carbon and water gain (Byrne *et al.*, 2008; Grigg *et al.*, 2010).

An interesting result obtained from the vein density study was the identification of a strong negative linear relationship of LVD of deep-rooted *Corymbia spp*. with bulk-leaf $\Delta^{13}C$ (and WUE_i) such that, $\Delta^{13}C$ significantly decreased (and WUE_i increased) as LVD increased (**Figure 3.18b**). In contrast, no such relationship was found with *Acacia* species. Albeit being sampled from a range of DTGW sites and from individuals with varying LVDs, $\Delta^{13}C$ values for *Acacia* in the present dataset remained fairly stable with >70% values ranging between 19-21‰, ultimately resulting in a non-significant relationship of LVD with $\Delta^{13}C$ (**Figure 3.18a**). A possible explanation could be the well-documented anisohydric behaviour of these species (O'Grady *et al.*, 2009; Winkworth, 1973) resulting in a non-significant pattern of $\Delta^{13}C$ with water availability and therefore with LVD. Compared to *Acacia*, deeper rooted *Eucalyptus* and *Corymbia* species showed larger variation in $\Delta^{13}C$ and also in LVD. So, what possible mechanism can explain the significant relationship observed between a structural leaf-trait like LVD with a functional trait like $\Delta^{13}C$ (and WUE_i) in these groundwater accessing deep-rooted species? The optimal carbon gain for water use model assumes that transpiration (E) and CO_2 assimilation a are linked, because, in order to gain carbon most economically with respect to water loss (i.e., optimization of the ratio A/E = water-use-efficiency, see **Chapter 1**), stomata should function in such a manner that the marginal water cost of carbon assimilation ($\frac{\partial A}{\partial E}$) remains constant (Cowan and Farquhar, 1977; Farquhar and Sharkey, 1982). This particular feature of stomatal control effectively couples structural traits involved with water-flow with traits associated with primary production (Brodribb and Holbrook, 2007). This explains the observed correlations between K_{leaf} and A_{max} in a number of studies (Brodribb *et al.*, 2007; Brodribb *et al.*, 2010; Brodribb *et al.*, 2005; Brodribb and Jordan, 2008; Sack and Holbrook, 2006; Sack and Scoffoni, 2013). LVD is directly proportional to K_{leaf} and the A/g_s ratio influences the $\Delta^{13}C$ (and WUE_i) signatures in leaves; therefore, a coordination between these two distinct physiological processes in an expected pattern observed in this present study suggests that these plants (having access to groundwater) have converged on a common solution for optimizing water supply through veins with respect to assimilation related loss of water (Brodribb and Holbrook, 2007).

Conclusions

The focus of this chapter was to examine sources of uptake of water by vegetation, spatial/seasonal variation of water sources and water-use-efficiencies along a depth-to-

groundwater (DTGW) gradient in the semi-arid Ti Tree basin in Central Australia. Results from stable deuterium and ^{18}O analysis revealed difference in sources of water and water uptake strategies of dominant shallow and deep-rooted overstorey species across the naturally occurring groundwater gradient in this region. The shallower rooted *Acacia spp.* were found to be opportunistic in their water use utilising the available soil water from the upper soil horizons, with some evidence of utilisation of "ponded" water collecting above the siliceous hardpan at ≈100 cm depth. These species also showed large variability in their δ^2H- $\delta^{18}O$ reflecting local small-scale differences in the depth of the hardpan and hence rooting depth. In contrast, deep-rooted *Eucalyptus* and *Corymbia* species consistently relied on groundwater during both dry- and wet-seasons when groundwater was available in their rooting-depth (up to DTGW 13.5 m). Seasonal variation was identified in water accessed by *Acacia spp.* at all sites and water accessed by *Corymbia spp.* at sites > DTGW 13.5 m sites from stable isotope analysis, associated with seasonal variation in soil water. In contrast to mesic ecosystem investigated in **Chapter 1**, stable ^{13}C analysis at the leaf-level could reliably and consistently identify access to groundwater by vegetation in this semi-arid region. Discrimination against ^{13}C and WUE_i calculated from stable ^{13}C isotopes at the leaf-level for deep-rooted trees accurately mirrored access to groundwater inferred from deuterium - ^{18}O analysis at the shallower end of the DTGW gradient. Bulk-leaf analysis of ^{13}C also captured the within-site variability of source water uptake by vegetation across micro-habitats and also seasonal variation in water availability. $\Delta^{13}C$ was significantly associated with leaf vein-densities in groundwater accessing deep-rooted trees, further indicating the influence of water availability in assimilation related loss of water. Overall, the findings from this chapter reinstates that stable isotope analysis can be a powerful tool to investigate contrasting water use strategies, specifically groundwater dependence in semi-arid regions of Central Australia. This differential utilisation of water from various depths (including groundwater) is likely to contribute to the hydrological niche separation of co-occurring species in the Ti Tree basin.

Chapter 4 Variation in bulk-leaf ^{13}C discrimination, leaf-traits and discrimination-trait relationships along a continental-scale climate gradient in Australia

Introduction

Vegetation structure and function is largely modulated by climate and understanding plant physiological responses to climate gradients is critical for understanding spatial variation in ecosystem processes (Koch *et al.*, 1995; Schulze *et al.*, 1996). In Australia there are several climatic zones. The amount and timing of rainfall and the average summer and winter temperatures determine the key differences among these zones (Eamus *et al.*, 2006b). Mean annual precipitation in Australia (MAP) is about 350-450 mm yr^{-1}- which makes it the driest of all permanently inhabited continents; although precipitation is highly variable across the continent. In some regions (for example Central Australia), MAP is low to very low (< 300 mm yr^{-1}) whereas the north-eastern coast receives very high MAP (>2500 mm). Mean maximum temperature increase with decreasing latitude and distance from the coast and mean minimum temperature decreases with increasing distance inland (Eamus *et al.*, 2006b). Thus, Australia's climate is highly heterogeneous both spatially and temporally across the continent and this provides an axis of distinct ecological differentiation across which we can examine how physiological characteristics of vegetation vary.

Functional and structural attributes of vegetation often change in a predictable manner along gradients in water-availability. For example in a range of sites with varying depth-to-groundwater, vegetation showed significantly larger aboveground biomass and net primary productivity and decreasing water-use-efficiency with increasing water availability (Zolfaghar *et al.*, 2014). Schulze *et al.*, (1998a) showed increased tree water use with increased MAP in a range of species across Australia. Access to water resources also significantly influence sap velocity of trees (Dragoni *et al.*, 2009; Rossatto *et al.*, 2012;

Whitley *et al.*, 2013; Zeppel *et al.*, 2008). Vegetation adapted to low rainfall shows a suite of traits- for example, they tend to have sclerophyllous[4] leaves (Eamus *et al.*, 2006b; Fonseca *et al.*, 2000; Turner, 1994) and a high concentration of nitrogen per unit leaf area (Cunningham *et al.*, 1999; Schulze *et al.*, 1998b; Taylor and Eamus, 2008; Wright *et al.*, 2001). From an ecohydrological perspective it is important to understand how leaf-level physiological and structural characteristics change from strongly water-limited ecosystems with pulsed water-resource availability to extremely wet ecosystems with water surplus throughout the year - at a continental-scale in Australia.

Measurements made at leaf-scale have long gained attention to estimate phenomena at an ecosystem-scale. Schulze *et al.*, (1994) concluded that leaf-level maximum stomatal conductance can be a strong predictor of ecosystem-level surface conductance and maximum carbon assimilation rate. The worldwide leaf economics spectrum (Wright *et al.*, 2004) highlights the importance of quantifying correlations among leaf-traits (for example leaf mass per unit area, leaf life-span, leaf nitrogen and phosphorus concentrations, rate of photosynthesis) and how these traits differ between plant functional types. These key leaf attributes, particularly leaf mass per unit area, scale strongly with several whole-plant properties (for example, relative growth rate, rate of carbon assimilation) and ecosystem properties (for example, aboveground net primary productivity) (Lambers and Poorter, 1992; Reich *et al.*, 1992). However, leaf stomatal conductance and leaf intrinsic water-use-efficiency (the ratio of rate of carbon assimilation and stomatal conductance, see **Chapter 1**) and their correlation with other key leaf structural/nutrient attributes have rarely been examined at a large spatial scale. An examination of leaf-level stomatal regulation (i.e., a tight *versus* loose stomatal regulation on photosynthesis and transpiration) and leaf-level intrinsic water-use-efficiency of dominant tree species across several contrasting ecosystems may provide a novel understanding of how different plant species respond to environmental stress in different climatic zones.

Difference in natural abundance of stable carbon isotope ($\delta^{13}C$) in leaf dry matter has increasingly been recognized as a powerful tool for identifying strategies of water use in terrestrial plants both in individual and within-community levels (Cernusak *et al.*, 2013; Diefendorf *et al.*, 2010; Kohn, 2010). Early work in the 1980's demonstrated the relation of $\delta^{13}C$ of leaves of C3 plants with the ratio of the partial pressures of CO_2 within the leaf

[4] A sclerophyllous leaf is thick, stiff and leathery with low water content per unit dry mass of the leaf (Eamus et al., 2006).

(hereafter termed as intercellular concentration of CO_2, C_i) and in ambient air (C_i/C_a) (Farquhar *et al.*, 1989; Farquhar *et al.*, 1982; O'Leary, 1981; O'Leary, 1988). Carbon isotope composition measured from leaf tissue and hence, the calculated discrimination[5] ($\Delta^{13}C$) against ^{13}C (Brugnoli and Farquhar, 2000; Farquhar *et al.*, 1982; Farquhar and Richards, 1984) therefore can provide a good proxy of an important gas-exchange characteristic, i.e., leaf-level intrinsic water-use-efficiency (WUE_i) - given by the ratio between leaf net photosynthetic rate (A) and stomatal conductance (Dawson *et al.*, 2002; Farquhar, 1991; Farquhar *et al.*, 1989; Livingston and Spittlehouse, 1996). Theoretically therefore, more water-use-efficient plants should have more positive $\delta^{13}C$ values (thus smaller discrimination against ^{13}C) and therefore smaller values of $\Delta^{13}C$ (O'Leary, 1988). Consequently, variation in $\delta^{13}C$ and $\Delta^{13}C$ has been applied to several studies that look at how these variations are manifest along environmental gradients.

Variations in $\Delta^{13}C$ have been examined in two recent meta-analyses (Diefendorf *et al.*, 2010; Kohn, 2010) at a global scale. Diefendorf *et al.*, (2010) combined 3,310 published leaf $\Delta^{13}C$ values for 334 woody plant species at 105 locations across the world (although this meta-analysis did not include data for trees sampled in Australia) whereas, the Kohn, (2010) global-study encompasses all types of C3 plants, including trees, shrubs, herbs, and grasses from approximately 570 individuals. Both of these studies have documented decreasing $\Delta^{13}C$ with decreasing MAP, and MAP explains about half of the variation in $\Delta^{13}C$ across the globe. In Australia, several studies at smaller spatial scales examined variation in $\Delta^{13}C$ in response to variation in MAP. Stewart *et al.*, (1995) examined 348 species from 12 plant communities in along a 900 km-long rainfall gradient in southern Queensland and found a strong response of averaged $\delta^{13}C$ to rainfall. In contrast, several studies in northern Australia (Cernusak *et al.*, 2011; Miller *et al.*, 2001; Schulze *et al.*, 1998b) and in south-western Australia (Schulze *et al.*, 2006; Turner *et al.*, 2008) observed only weak community-level responses of $\delta^{13}C$ to MAP. However, most of these studies only investigated species within the closely related genera of *Eucalyptus*. There is, therefore, a need to examine how $\Delta^{13}C$ responds to environmental stress at the community-level with samples from a larger range of genera. Furthermore, few studies have examined relationships of $\Delta^{13}C$ with other leaf-traits encompassing a broad taxonomic range of dominant woody plant species at a continental scale.

[5] Discrimination against ^{13}C describes change in isotopic composition induced by the plant, eliminating variation as a result of the starting value of the atmospheric CO_2 used for photosynthesis (Cernusak et al., 2013)

Cross-species analysis performed across multiple sites located in distinctly different climate biomes not only provides an opportunity to investigate responses of $\Delta^{13}C$ (and consequently WUE_i) with water availability, but also enables a comparison of $\Delta^{13}C$ responses across a wide range of other climate attributes that largely vary across sites, such as temperature, evapotranspiration, solar radiation or vapour pressure deficit. The "Budyko framework" introduced by Budyko, (1974) elegantly couples complex patterns of a number of climate attributes such as potential/actual evapotranspiration and runoff into a general function of two variables: MAP and net radiation. A wide range of catchment hydrological studies have used the Budyko framework to examine the interactions of climate, vegetation and water yield in a number of sites across Australia (Donohue *et al.*, 2010; Donohue *et al.*, 2009) and at a larger global scale (Gentine *et al.*, 2012; Jones *et al.*, 2012; Troch *et al.*, 2013; Wang and Hejazi, 2011; Williams *et al.*, 2012). The Budyko framework describes the relationship of potential and actual evapotranspiration of a catchment normalized by precipitation, i.e., the evaporative index (ε, defined as ratio of actual evapotranspiration to precipitation) as a function the dryness index (Φ, the ratio of potential evapotranspiration to precipitation). Evapotranspiration in a catchment is influenced by both the drying power of the atmosphere (determined by climate, specifically, net radiation and vapour pressure deficit) and the water availability in a catchment (intercepted by the canopy or stored groundwater or soil water) (Creed *et al.*, 2014). The Budyko framework, therefore, incorporates two catchment states, with evapotranspiration being limited by either energy supply or water supply, where, a value of $\Phi < 1$ indicates a humid, energy-limited catchment and a value of $\Phi > 1$ indicates a dry, water-limited catchment. Incorporating quantitative measures of key vegetation characteristics in the Budyko framework has also increasingly been gaining attention. For instance, Donohue *et al.*, (2007) argued that vegetation dynamics integrated explicitly within the Budyko framework could potentially increase its utility for addressing land and water resources management issues. A specific aim of this present study was to examine the distribution of sites with contrasting climate/ecosystem attributes across the Budyko framework as well as to investigate whether the variability of $\Delta^{13}C$ across these contrasting ecosystems was captured in this framework.

Interpretation of $\Delta^{13}C$, however, is not always straightforward due to the complex interactions between plant performance and environmental conditions. For example, if leaf size and structure adapt due to water stress, the mesophyll conductance of the leaf might

also be altered leading to changes in the ratio of chloroplast to ambient concentration of CO_2 (Seibt *et al.*, 2008). Nutrients can also influence the intercellular concentration of CO_2 through its effect on photosynthetic capacity (Lamont *et al.*, 2002; Radin, 1984). The level of sclerophylly is also directly influenced by internal levels of nutrients (Groom and Lamont, 1999) which is reflected in the nutrient concentrations at leaf-level (Lamont *et al.*, 2002). All of these therefore can influence $\Delta^{13}C$ signatures obtained from leaf dry matter. Leaf structural and nutrient attributes if available can provide additional insights about their effects (if any) on $\Delta^{13}C$ at individual species level as well as site-specific species assemblage level. A large, comparative study across a broad taxonomic spread of dominant species would also provide an important test of relationships between functional and structural traits, nutrient related traits of leaves and bulk-leaf $\Delta^{13}C$.

In this chapter, variation in bulk-leaf $\Delta^{13}C$ signature and its relationships with gas-exchange, structural and nutrient traits of the dominant overstorey species from seven sites across Australia have been assessed. The objective of this chapter was to address the following questions:

1) How does discrimination against ^{13}C at the leaf-level and intrinsic water-use-efficiency calculated from $\Delta^{13}C$ vary with climate at a continental scale? These relationships were assessed using (a) means of individual species at each site and (b) mean values calculated for each biome.
2) To what extent is leaf-level discrimination against ^{13}C modulated by seasonality of precipitation?
3) What is the relationship between actual and potential evapotranspiration with respect to the theoretical Budyko framework and how is the seasonal variation in $\Delta^{13}C$ across sites captured in this framework?
4) Is there seasonal and/or spatial variability in $\Delta^{13}C$ and intrinsic water-use-efficiency across a wide range of sites and species across Australia?
5) To what extent does $\Delta^{13}C$ reflect variations in leaf structural, functional and nutrient traits across a climate gradient?
6) How effective is $\Delta^{13}C$ as an integrative ecological tracer to explain environmental constraints at a continental scale in Australia?

Materials and methods

Study area

The study area of this study includes a subset (seven out of ten SuperSites and two nodes for the Far North Queensland rainforest SuperSite) of SuperSites of the Australian SuperSite Network across the continent. The Australian SuperSite Network (http://www.tern-supersites.net.au/) a part of the Terrestrial Ecosystem Research Network (TERN), is a federally funded initiative of the Australian government to conduct research in a number of "SuperSites" located across the country. Each of these SuperSites is a distinctly different type of ecosystem. Multiple data streams collected from these SuperSites in this study provides a novel opportunity to combine and compare contrasting ecosystems across the whole continent. It is important to note that leaf samples were collected by the research team managing each SuperSite and sent to the author for analyses of ^{13}C.

The location, mean annual precipitation, and mean annual temperature for each of the seven SuperSites distributed across the continent, their location, mean annual precipitation and mean annual temperature are given in **Table 4.1**.

Table 4.1*:* Site characteristics

Name, latitude, longitude, mean annual precipitation, mean annual temperature and site visits are listed for the sites studied across the continent. Long term average climate data was obtained from the WorldClim database.

Site	Lat °	Long °	MAP (mm)	MAT (°C)	visit/season	
Calperum Mallee	-34.0373	140.6738	255	17.3	summer/ dry	winter/wet
Great Western Woodlands	-30.2640	120.6917	273	18.5	summer/ dry	winter/wet
Alice Mulga	-22.2828	133.2493	321	22.4	summer/ wet	winter/dry
Cumberland Plain	-33.6190	150.7382	900	17.7	summer/ wet	winter/dry
Warra Tall Eucalypt	-43.0888	146.6512	1474	10.1	summer/ dry	winter/wet
Litchfield Savanna*	-12.4853	131.1461	1714	27.8	summer/ wet	winter/dry
FNQ - Cape Tribulation†	-16.1000	145.4500	2087	25.2	summer/ wet	winter/dry
FNQ - Robson Creek†	-17.1195	145.6323	2140	21.0	summer/ wet	winter/dry

* $\Delta^{13}C$, leaf-trait and meteorological data from (Cernusak *et al.*, 2011) for Howard Springs was used as a representative of Litchfield Savanna SuperSite. †Data were collected from two nodes for the Far North Queensland (FNQ) rainforests SuperSite.

Site description

These seven SuperSites represent six biomes with mean annual temperature (MAT) ranging from 10°C to ~28°C and mean annual precipitation (MAP) from 255 to 2,140 mm per year. A brief description of each of these sites is now given.

Calperum Mallee

The Calperum Mallee SuperSite is in the mallee semi-arid ecosystem located approximately 25 km north of Renmark in South Australia. The landscape is an extensive plain with undulating mallee woodland and riverine vegetation that fringes the River Murray and its anabranches. The vegetation is dominated by upper storey Eucalypt trees of four species (*Eucalyptus dumosa, Eucalyptus incrassata, Eucalyptus oleosa* and *Eucalyptus socialis*) (Meyer *et al.*, 2015). Mean annual rainfall is ~255 mm at this site.

Great Western Woodlands

The Great Western Woodlands located in south-west Western Australia is the largest remaining intact semi-arid temperate woodland in the world. The vegetation comprises a 16-million hectare mosaic of mallee, scrub–heath and woodland and is locally determined by edaphic factors and influenced by historic disturbances (Gosper *et al.*, 2013). Mean annual rainfall is ~250 mm with the highest-mean rainfall months in winter. *Eucalyptus salubris* constructs the dominant crown layer in association with other *Eucalyptus* species (*E. salmonophloia, E. longicornis and E. moderata)* (Gosper *et al.*, 2013).

Alice Mulga

The semi-arid Alice Mulga SuperSite is located approximately 200 km north of Alice Springs, in the Northern Territory of Australia. The climate is characterized as having hot summers and warm winters. Mean annual rainfall is ~300 mm and is highly seasonal, mostly occurring in large rainfall events during summer. Vegetation is dominated by Mulga (*Acacia aneura* and related species) woodlands, occasionally with large areas of spinifex under sparse woodland of *Corymbia* and other *Acacia* species.

Cumberland Plain

The Cumberland Plain is a sclerophyll *Eucalyptus* woodland west of Richmond in New South Wales. The soil is characterized by nutrient-poor alluvium from sandstone and shale

bedrock in the Blue Mountains deposited by the Nepean River. Despite being nutrient poor, this SuperSite supports high regional biodiversity and endemic biota and is dominated by *Eucalyptus fibrosa*, *Eucalyptus moluccana* and *Eucalyptus tereticornis* in the overstorey. Mean annual rainfall is ~900 mm at this site.

Warra Tall Eucalypt

The Warra Tall Eucalypt SuperSite is a cool and wet temperate forest located in Tasmania. The vegetation is dominated by tall *Eucalyptus obliqua* occurring in a full range of successional stages from young regrowth forests to old-growth mixed forests (Hickey *et al.*, 1999). Mean annual temperature in this site is the lowest (~10°C) and has a mean annual precipitation of 1474 mm.

Litchfield Savanna

The Litchfield Savanna SuperSite is a ~1.5 km^2 tropical savanna 70 km south of Darwin in northern Australia. This site is representative of the dominant ecosystem of that region. Climate of this site is typical of northern Australia with extremely seasonal and high rainfall (mean annual rainfall ~1800 mm) and approximately 56% of this site is burnt annually (Murphy *et al.*, 2010). However, in this study, data collected from Howard Springs (approximately 65 km north of Litchfield SuperSite from Cernusak *et al.*, 2011) have been used as a representative of this particular SuperSite. This approach is justified because both of these sites had very similar vegetation and climate conditions as well as frequency of occurrence of fire. The stand structure in these two sites are sufficiently similar as to not shift physiological properties at a leaf-scale given the species occurring at both sites largely overlap (Bowman *et al.*, 2001; Hutley and Beringer, 2010; Murphy *et al.*, 2010).

FNQ Rainforest

The FNQ Rainforest SuperSite is located in a tropical wet forest ~140 km north of Cairns in Far North Queensland. This SuperSite is structurally divided into two transects – a) the lowland rainforest based in the Daintree rainforest near Cape Tribulation (MAT = 25.2 °C, MAP = 2087 mm) and b) the upland rainforest based around Robson Creek (MAT = 21 °C, MAP = 2140 mm). Precipitation is highly seasonal with most of it occurring during summer (Weerasinghe *et al.*, 2014). FNQ supports 10% of Australian flora despite of occurring in only 0.2% its landmass. Consequently a substantial number of the species in this study come from this SuperSite. Data from Cape Tribulation and Robson Creek were

collected and analysed independently in this study because of significantly different environmental clines (altitude, MAT and MAP) that exists in these two transects of FNQ.

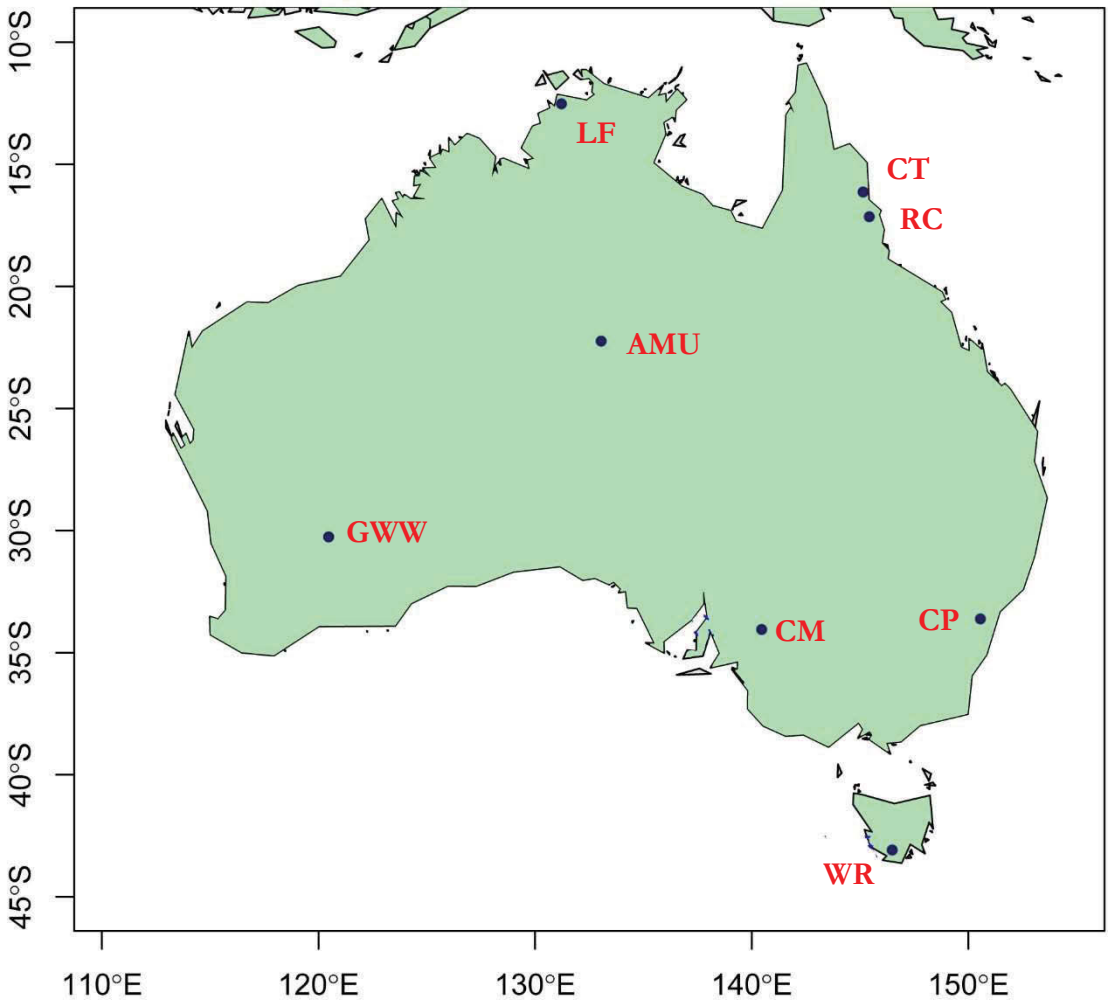

Figure 4.1: Location of seven SuperSites (two sampling nodes for FNQ) sampled across Australia.

Abbreviations: CM = Calperum Mallee, GWW = Great Western Woodlands, AMU = Alice Mulga, CP = Cumberland Plain, WR = Warra Tall Eucalypt, LF = Litchfield Savanna, CT = Cape Tribulation and RC = Robson Creek. CT and RC are the two nodes sampled for the Far North Queensland (FNQ) SuperSite.

Biome types

The SuperSites in this study fall into seven distinctly different biomes. Temperate woodlands CM and GWW were grouped into a single biome whereas, the two lowland and upland transects of FNQ SuperSite were treated as two separate biomes in the analysis. SuperSite and biome abbreviations further used in this study are listed in **Table 4.2**.

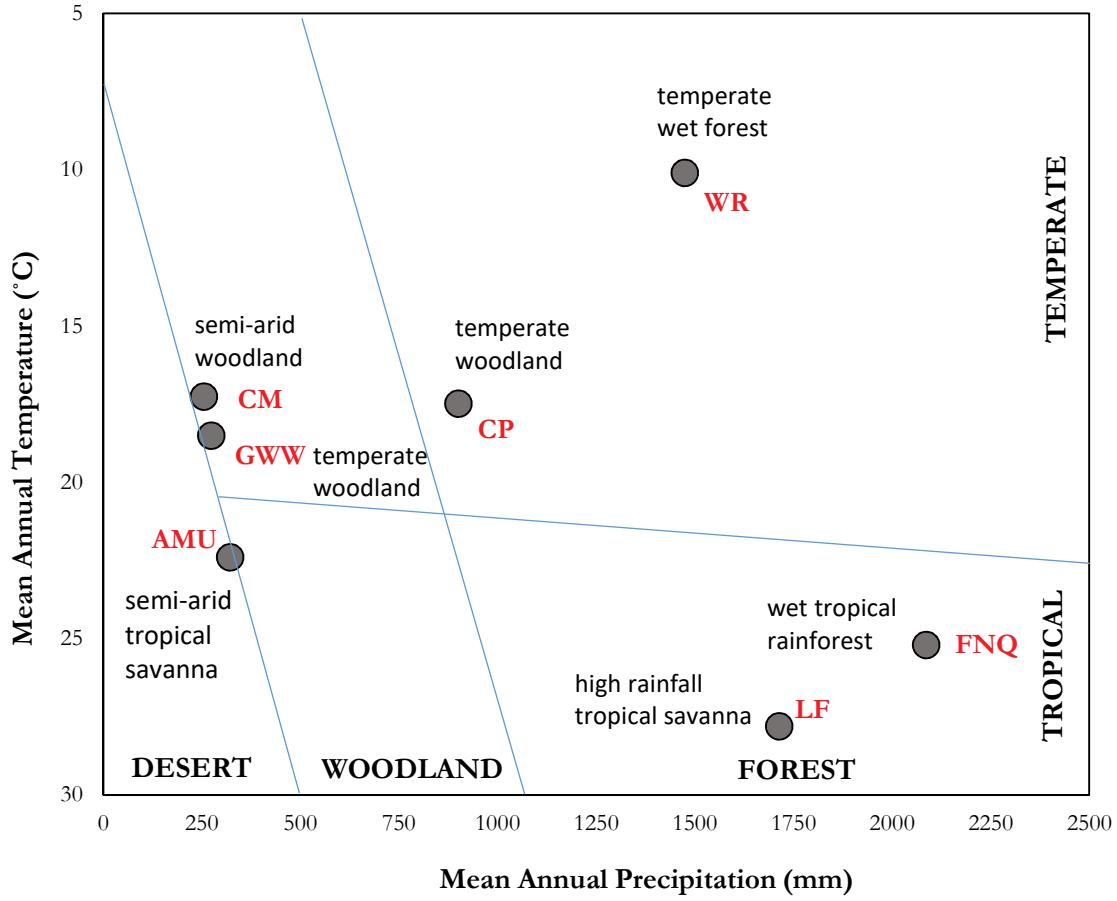

Figure 4.2: Mean annual temperature, mean annual precipitation, and biomes of the study sites.

Each SuperSite is plotted in the Whittaker Biome Diagram (Whittaker, 1975) using the MAT and MAP observations generated for each site from the WorldClim data. The vertical blue lines separate the biomes in terms of vegetation type and the horizontal blue line separates the biomes in terms of climate type. See **Table 4.2** for site abbreviations.

Table 4.2: SuperSite and biome abbreviations used in the study

SuperSite		Biome	
Name	**Abbreviation**	**Name**	**Abbreviation**
Calperum Mallee	CM	Semi-arid woodland	SW
Great Western Woodlands	GWW	Temperate woodland	TW
Alice Mulga	AMU	Semi-arid tropical savanna	STS
Cumberland Plain	CP	Temperate woodland	TW
Warra Tall Eucalypt	WR	Temperate wet forest	TWF
Litchfield Savanna	LF	High rainfall tropical savanna	HRT
FNQ - Cape Tribulation	CT	Lowland wet tropical rainforest	LTR
FNQ - Robson Creek	RC	Upland wet tropical rainforest	UTR

Data and analysis

Study species

At each site a one hectare plot within the footprint of the flux tower was established and replicated measurements of foliar $\Delta^{13}C$ were made on dominant and mostly broadleaf evergreen overstorey species that collectively made up ~ 80% of the (aboveground) biomass. A total of 55 plant species from the dry-season and 44 species from the wet-season sampling (417 individual trees from 27 plant families) were assessed. Four to six selected individuals of each species and three samples per individual were sampled for measurement of $\Delta^{13}C$ and other leaf-traits. A standard protocol and the same equipment was used for all eight sites. An average of $\Delta^{13}C$ values for all species sampled was also calculated for each biome to remove within-species variability. Variation in 16 additional leaf attributes (gas-exchange characteristics, structural and nutrient traits, see **Table 4.4** for details; additional to $\Delta^{13}C$) across the SuperSites and their correlations with $\Delta^{13}C$ were also examined. The gas-exchange and foliar structural and nutrient status data were collected by researchers at each SuperSite as part of a larger federally funded project of the Terrestrial Ecosystem Research Network (TERN). $\Delta^{13}C$ was analysed by me as part of this PhD project. Gas-exchange, leaf structural and nutrient data were collected by Dr Keith Bloomfield and colleagues, and analysed by me as part of this PhD project.

Environmental variables

In order to quantify the climatic conditions for each of the seven SuperSites, 19 variables have been considered (11 temperature related and eight precipitation related parameters,

see **Table 4.3**). Long term average data was obtained from the WorldClim database (http://www.worldclim.org/, (Hijmans *et al.*, 2005) with a spatial resolution of 1 km.

Table 4.3: List of climate variables used in climate analysis

WorldClim Code	Variables
BIO_1	Mean Annual Temperature
BIO_2	Mean Diurnal Range
BIO_3	Isothermality
BIO_4	Temperature Seasonality
BIO_5	Max Temperature of Warmest Month
BIO_6	Min Temperature of Coldest Month
BIO_7	Temperature Annual Range
BIO_8	Mean Temperature of Wettest Quarter
BIO_9	Mean Temperature of Driest Quarter
BIO_{10}	Mean Temperature of Warmest Quarter
BIO_{11}	Mean Temperature of Coldest Quarter
BIO_{12}	Mean Annual Precipitation
BIO_{13}	Precipitation of Wettest Month
BIO_{14}	Precipitation of Driest Month
BIO_{15}	Precipitation Seasonality
BIO_{16}	Precipitation of Wettest Quarter
BIO_{17}	Precipitation of Driest Quarter
BIO_{18}	Precipitation of Warmest Quarter
BIO_{19}	Precipitation of Coldest Quarter

Leaf-trait data

In this chapter, variation in 16 leaf attributes (listed in **Table 4.4**) in addition to $\Delta^{13}C$ values for multiple species across the SuperSites and their correlations with $\Delta^{13}C$ were examined. Leaf-traits data were collected as part of a larger federally funded project across all the SuperSites by the research teams operating each of the SuperSites and analysed by me as part of this PhD project.

Table 4.4: List of leaf-traits used in this study

Abbreviation	Units	Leaf-traits
A400.a	μmol CO_2 m^{-2} s^{-1}	Net assimilation at [CO_2] 400 ppm
E400.a	mmol H_2O m^{-2} s^{-1}	Transpiration rate at [CO_2] 400 ppm
vpdL400	KPa	Vapour pressure deficit based on leaf temp.
g_s400	mmol H_2O m^{-2} s^{-1}	Stomatal conductance at [CO_2] 400 ppm
C_i/C_a	-	Intercellular [CO_2] : ambient [CO_2]
C_i400	μmol CO_2 mol^{-1}	Intercellular [CO_2] with CO_2 reference at 400 ppm
LDMC	-	Ratio leaf dry to fresh mass
LMA	g m^{-2}	Leaf mass per unit area
FMA	g m^{-2}	Fresh mass per unit area
$LeafN_{mass}$	mg g^{-1}	Total leaf [N]
$LeafP_{mass}$	mg g^{-1}	Total leaf [P]
RatioNP	-	Ratio of total leaf [N] : [P]
$LeafN_{area}$	mg m^{-2}	Total leaf [N], (area basis)
$LeafP_{area}$	mg m^{-2}	Total leaf [P], (area basis)
PNUE	μmol CO_2 s^{-1} g^{-1} N	Photosynthetic nitrogen use efficiency (Net assimilation at [CO_2] 400 ppm, per unit N)
PPUE	μmol CO_2 s^{-1} g^{-1} P	Photosynthetic phosphorous use efficiency (Net assimilation at [CO_2] 400 ppm, per unit P)

Isotope analysis

See **Chapter 2** of this thesis for detailed methodology on ^{13}C analysis.

Methodology and statistical analyses

Species-mean values (obtained from leaves sampled from four to six individuals) for the dominant overstorey species for each SuperSite were calculated for each trait to account for inter-species variability. The distribution of species means for each season was tested for non-normality (Shapiro-Wilk test, $\alpha = 0{\cdot}05$) and homogeneity of variances (Bartlett test). All of the 19 climate variables were approximately normally distributed (except for maximum temperature of warmest month, BIO_5). Bulk-leaf $\Delta^{13}C$ values were also normally distributed. The distributions of five out of 16 traits were deemed normal and left untransformed in all subsequent analyses (see **Table 4.9** for details). Other traits showed approximately normal distribution after natural log/square root distribution and were therefore transformed appropriately (**Table 4.9**). Ordinary least square regression analysis was performed to investigate relationships between bulk-leaf $\Delta^{13}C$ /leaf-traits and MAP at the site level, where MAP was treated as an independent variable and species mean values were treated as a continuous response variable. Assumptions of the models were checked

for normality and homoscedasticity of the residuals. Bivariate partial regression models were constructed to assess the influence of temperature-related climatic parameters as secondary predictors on bulk-leaf $\Delta^{13}C$ (accounting for the covariance of MAP). Relationships between traits were explored by fitting standardized major axis (SMA) (Legendre and Legendre, 1998; Warton *et al.*, 2006) and slopes were fitted individually for both dry- and wet-season using the *smatr* library in R (Warton *et al.*, 2012). SMA slope-fitting techniques are appropriate for describing bivariate relationships where X as well as Y variables have variation associated with them due to measurement error and species sampling (Sokal and Rohlf, 1995). First, robust SMA regression slopes were fitted separately for dry-season and wet-season for each bivariate relationship between bulk-leaf $\Delta^{13}C$ and a leaf-trait. For a given bivariate relationship, if SMA regressions were significant for both seasons, the existence of a common slope of the relationships was tested for using a Bartlett-corrected likelihood ratio test. If the slopes were not significantly different ($p>0.05$, i.e. there was a common slope), Wald tests were performed to identify significant differences in elevation between the common fitted slope and for significant shifts along the common fitted slope. Means of the $\Delta^{13}C$ were compared one-way ANOVA and significant differences between sites were determined by Tukey HSD tests (confidence level of 0.05). Principal component analysis (PCA) was used to identify which of the climate variables (MAP, MI), the gas-exchange parameters (A400.a, g_s400, C_i/C_a etc.), the nutrient (P, N) related traits or the structural traits (LMA, FMA etc.) were more closely associated with variations in $\Delta^{13}C$. All analyses were performed using R software package (R Development CORE Team, 2009).

The theoretical Budyko framework was used to examine the relationship between the potential evapotranspiration (ET_p) and actual evapotranspiration (ET_a) of each of the sites, each normalized by precipitation (P). Each SuperSite was plotted on the Budyko curve based on its dryness index (Φ) and evaporative index (ε). These indices were calculated from SILO patched point data constructed from observational records provided by the BoM (see details in http://www.longpaddock.qld.gov.au/silo). For each SuperSite, the nearest meteorological station that had long term (125-years) climate data was selected (a list of meteorological stations is provided in Appendix **Table A2**). Morton's potential and actual evapotranspiration over land (Morton, 1983) obtained from the SILO data were used to calculate the long-term *annual* and *seasonal* averages of Φ and ε using the following equations (Baldocchi and Ryu, 2011; Gerrits *et al.*, 2009):

$$\Phi = \frac{ET_p}{P} \text{ and } \varepsilon = \frac{ET_a}{P}$$

Following the BoM convention, May to September in the north and October to April in the south were considered as "dry-season" and "wet-season" was defined as October to April in the north and May to September in the south. Another climatic indicator of moisture availability in addition to MAP, the moisture index (MI), was calculated as a ratio between precipitation and potential evaporation for each of these SuperSites (Togashi *et al.*, 2015). MI is a dimensionless number conceptually related to the Budyko curve and can provide valuable insights when comparing sites that have very different climate conditions.

Leaf intrinsic water-use-efficiency (WUE_i) (defined as the ratio of carbon assimilation and stomatal conductance to water, ((Beer *et al.*, 2009) see **Chapter 1** for details) was calculated using the species mean $\Delta^{13}C$ based on a simplified leaf-level model of C3 photosynthetic isotope discrimination (Werner *et al.*, 2012) using the following equation:

$$WUE_i = \frac{c_a(b - \Delta^{13}\mathrm{C})}{1.6(b - a)}$$

Here, *a*, *b* are fractionation factors (the change of ratio in molar concentrations) occurring during diffusion of CO_2 through stomata pores (4.4‰) and enzymatic carbon fixation by Rubisco (27‰), respectively. The value of C_a was assumed to be 390 μmol mol^{-1}.

Results

Variation in $\Delta^{13}C$ with climatic parameters

Linear regression models were used (**Table 4.5**) to examine relationships of each temperature and precipitation related variable with $\Delta^{13}C$ of corresponding season (for example, mean T of wettest quarter was analysed only with $\Delta^{13}C$ of the wet-season and not with $\Delta^{13}C$ of the dry-season). $\Delta^{13}C$ was most strongly associated with MAP among all the

precipitation related parameters in this dataset. Interestingly, the regression with mean annual temperature (MAT) could not adequately capture the variability of $\Delta^{13}C$ across sites (dry-season: Adj r^2=0.104, $p<0.05$; wet-season, non-significant), although both dry- and wet-season $\Delta^{13}C$ have strongly and significantly relationship with three other temperature related parameters; i.e. isothermality, temperature seasonality and temperature annual range (see **Table 4.5**).

Table 4.5: Linear regression of $\Delta^{13}C$ with climate parameters

Relationships of $\Delta^{13}C$ of dry- and wet-season with temperature and precipitation parameters of corresponding season. R^2 values were adjusted for the number of predictors in the model.

Variables	Dry-season		Wet-season	
	Adj r^2	**slope**	**Adj r^2**	**slope**
Mean Annual Temperature	0.104•	+	0.016	NS
Mean Diurnal Range	0.201***	-	0.380***	-
Isothermality	0.395***	+	0.358***	+
Temperature Seasonality	0.400***	-	0.487***	-
Max T (Warmest Month)	0.016	NS	0.011**	-
Min T (Coldest Month)	0.198***	+	0.134**	+
T Annual Range	0.308***	-	0.434***	-
Mean T (Wettest Quarter)	N/A	N/A	0.147**	+
Mean T (Driest Quarter)	0.049•	+	N/A	N/A
Mean T (Warmest Quarter)	-0.011	NS	-0.013	NS
Mean T (Coldest Quarter)	0.153**	+	0.107*	+
Mean Annual Precipitation	0.483***	+	0.571***	+
Precip. (Wettest Month)	N/A	N/A	0.428***	+
Precip. (Driest Month)	0.026	NS	N/A	N/A
Precip. (Seasonality)	0.238***	+	0.258***	+
Precip. (Wettest Quarter)	N/A	N/A	0.432***	+
Precip. (Driest Quarter)	0.014	NS	N/A	N/A
Precip. (Warmest Quarter)	0.407***	+	0.404***	+
Precip. (Coldest Quarter)	-0.019	NS	0.116*	+
Moisture index	0.449***	+	0.523***	+

***p<0.0001, **p<0.001, *p<0.01, •p<0.05, NS=non-significant, N/A= not analysed.

Variation of $\Delta^{13}C$ and WUE_i with MAP

Linear regression analysis shows significant increase in $\Delta^{13}C$ with increasing MAP along the rainfall gradient for both seasons (**Figure 4.3**, **Table 4.5**). The MAP explained 57% of variation in $\Delta^{13}C$ in (Adj r^2 = 0.571, $p < 0.0001$) for the wet-season sampling and 48% of

variation (Adj r^2 = 0.483, $p < 0.0001$) for the dry-season sampling. Consequently, MAP emerged as the strongest predictor of $\Delta^{13}C$ among the climate parameters in this dataset. Relationships of calculated leaf intrinsic water-use-efficiency (WUE_i) with MAP were similar in magnitude with $\Delta^{13}C$ but with a negative slope, i.e. WUE_i was significantly higher in the drier sites and lower in the wetter sites (dry-season: Adj r^2 = 0.47, $p < 0.0001$, wet-season: Adj r^2 = 0.594, $p < 0.0001$).

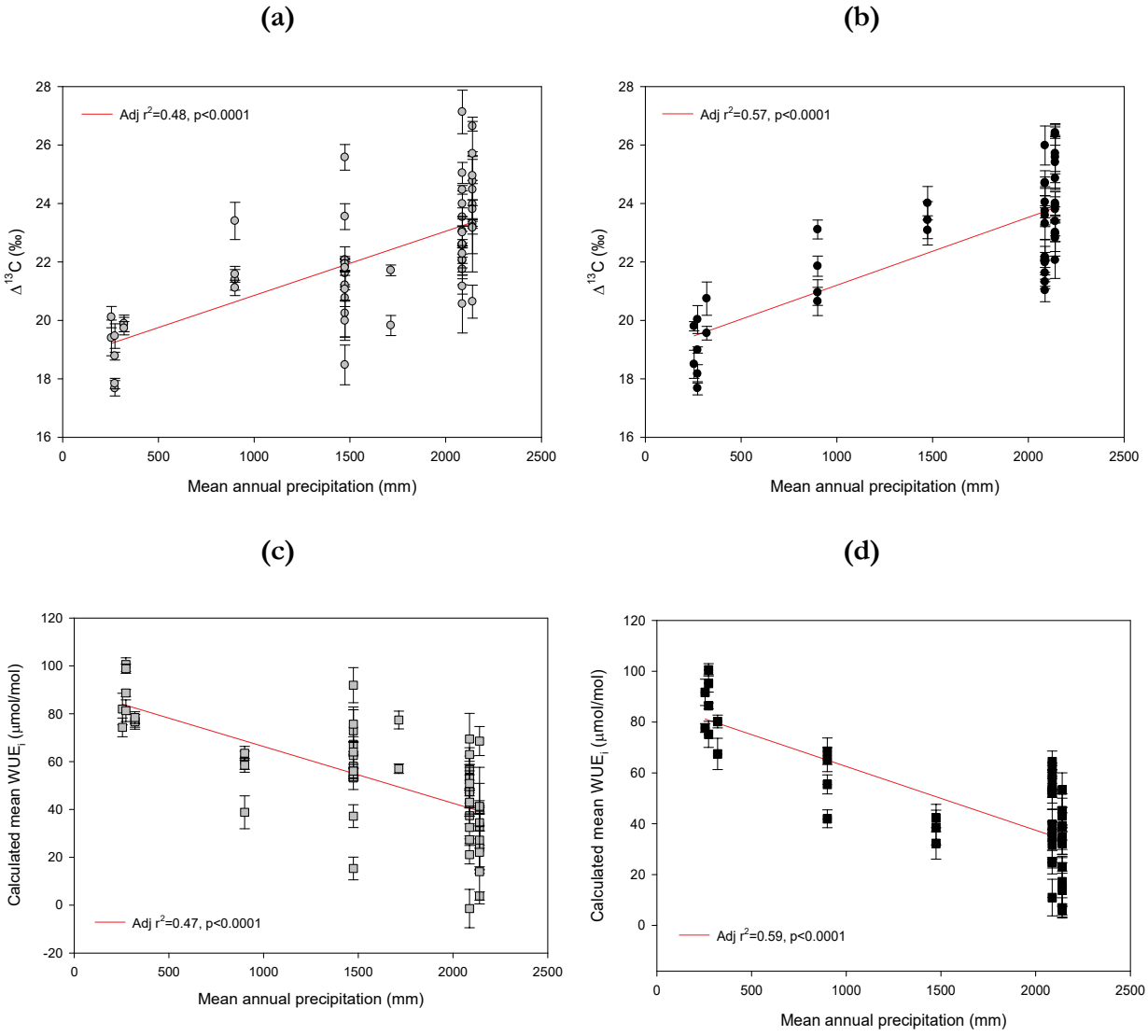

Figure 4.3: Carbon isotope discrimination in leaf dry matter ($\Delta^{13}C$, panels a, b) and leaf intrinsic water-use-efficiency (WUE_i, panels c, d) calculated from $\Delta^{13}C$ plotted as a function of mean annual precipitation (MAP).

Grey and black symbols represent sampling for dry- (panels a, c) and wet-season (panels b, d) respectively- each symbol representing the species mean of four to six individuals. Error bars represent standard errors.

Variation in ∠^{13}C with temperature related parameters

In addition to MAP, isothermality (i.e., the day-to-night temperature oscillation relative to the mean summer-to-winter oscillation), temperature seasonality and temperature annual range were the three next strongest predictors of $\Delta^{13}C$ in the single factor linear regression models (**Table 4.5**). These three potential predictors therefore were separately included as secondary predictors in addition to MAP and multiple regression models were constrained to evaluate the additional influence of these predictors on $\Delta^{13}C$. One violation of assumptions in these multiple regression models was the existence of strong colinearity between the predictor variables (for example: isothermality was strongly and significantly associated with MAP, r^2=0.917, p<0.0001). To account for the covariance of MAP with other predictors, bivariate partial regression models were used and partial r^2 values of each secondary predictor were reported (which gives the additional influence of secondary predictors on $\Delta^{13}C$ that is statistically independent of MAP).

Table 4.6 shows the result from the multiple linear regression and partial r^2 values from partial regression models. Although inclusion of secondary predictors slightly improved the r^2 values for all the predictors in both seasons, the regression model with isothermality as a secondary predictor in the wet-season is the only model with notable explanatory power (r^2 = 0.13, p<0.0001). This result indicates that, isothermality had a weak but significant influence on $\Delta^{13}C$ in addition to MAP during the wet-season that was statistically independent of its covariance with MAP. Also across all SuperSites, isothermality had a significant relationship with MAP (Pearson's correlation coefficient between MAP and isothermality was 0.917, p<0.0001) and wetter sites appeared to have higher isothermality than the drier sites. Thus the wetter sites had more "temperature even-ness" over the course of a year compared to the drier sites which (other than MAP) also had the largest positive relationship with $\Delta^{13}C$, particularly for the wet-season sampling among all the other secondary predictors in the multiple regression model.

Table 4.6: Multiple linear regression of $\Delta^{13}C$ with MAP and other climate parameters as secondary predictors and partial r^2 from bivariate partial regression

	Dry-season			Wet-season		
	Multiple r^2	**Partial r^2 (MAP)**	**Partial r^2 (secondary predictor)**	**Multiple r^2**	**Partial r^2 (MAP)**	**Partial r^2 (secondary predictor)**
MAP + Isothermality	0.475***	0.15	0.004	0.615***	0.42	0.13
MAP + Temperature Seasonality	0.501***	0.18	0.05	0.576***	0.20	0.04
MAP + T Annual Range	0.516***	0.32	0.083	0.575***	0.27	0.04

Variation of $\Delta^{13}C$ and WUE_i with moisture index

The entire dataset was divided into dry- and wet-season based on sampling time. However, from a climatic point of view, wet-season at the wetter sites (for example, in FNQ) represents very different conditions than that of the drier sites (for example, in AMU). Moisture indices (MI) for each of these SuperSites were therefore calculated as the ratio of annual precipitation to annual potential evapotranspiration and used in the analysis as an additional measure of moisture availability. Linear regression analysis showed significant increase in $\Delta^{13}C$ with increase in MI (similar to MAP) with the adjusted r^2 values slightly smaller than those obtained from linear regression of $\Delta^{13}C$ with MAP (**Table 4.5**). MI explained 52% of variation in $\Delta^{13}C$ in (Adj $r^2 = 0.523$, $p < 0.0001$) for wet-season sampling and 45% of variation (Adj $r^2 = 0.449$, $p < 0.0001$) for the dry-season sampling (**Table 4.9**). Similar relationships of MI and WUE_i with opposite (negative) slopes were obtained from linear regression analysis such that significantly larger water-use-efficiency was obtained in the sites with smaller MI and MI explained 53% and 45% of variation in WUE_i during wet and dry-season respectively (dry-season: Adj $r^2 = 0.449$, $p < 0.0001$, wet-season: Adj $r^2 = 0.526$, $p < 0.0001$).

Effect of precipitation seasonality on $\Delta^{13}C$ and WUE_i

The most significant positive relationship of both the dry- and wet-season $\Delta^{13}C$ was observed with MAP (as previously described) and wet-season $\Delta^{13}C$ also associated

significantly with most of the climate parameters except MAT and mean T of the warmest quarter (see **Table 4.5**). The relationship of dry-season $\Delta^{13}C$ was non-significant with precipitation of the driest month and precipitation of the driest quarter. In contrast, wet-season $\Delta^{13}C$ was significantly associated with precipitation of the wettest month (Adj r^2 = 0.428, $P < 0.0001$) and precipitation of the wettest quarter (Adj r^2 = 0.432, $P < 0.0001$). These results suggest that, although MAP *does* capture the variation of $\Delta^{13}C$ across the continent both for dry- and wet-season, $\Delta^{13}C$ is to some extent modulated by precipitation seasonality. **Figure 4.4** shows variation between the dry- and wet-season of mean $\Delta^{13}C$ and WUE_i across sites. Site mean values of $\Delta^{13}C$ were larger during the wet-season than dry-season sampling by 0.01 to ~ 2‰ in all but two sites (CM and CP, **Figure 4.4a**) suggesting that, as water availability increases in the wet-season, discrimination against ^{13}C of also increased. Calculated mean WUE_i was larger in the dry-season (except for CM and CP) than the wet-season sampling by 0.04 to 21 μmol/mol and in drier sites than wetter sites (**Figure 4.4b**).

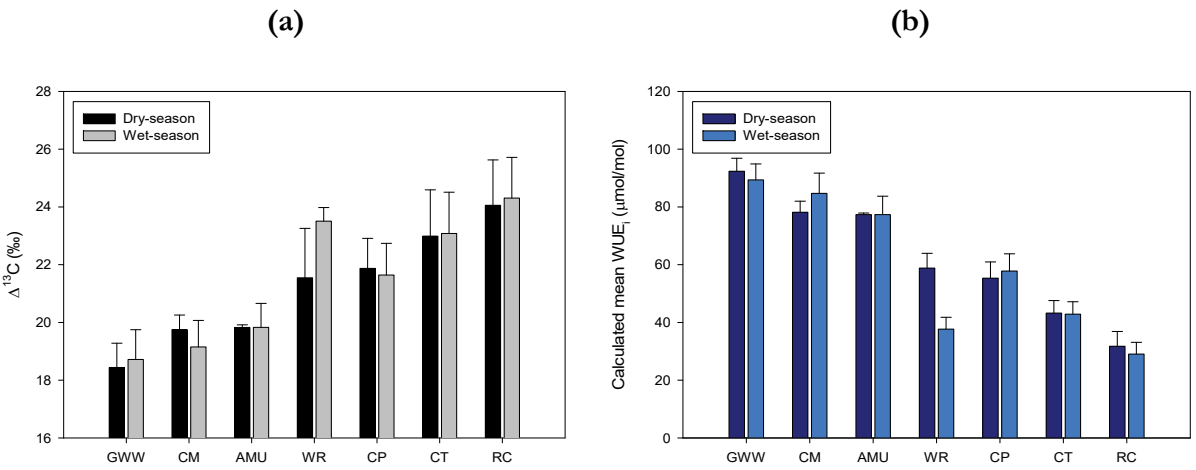

Figure 4.4: Site mean values of (a) $\Delta^{13}C$ and (b) WUE_i across all sites.

Dark and light bars represent mean of dry- and wet-season respectively and the error bars represent standard errors. Only dry-season data was available for the site LF (not shown in the figure).

Variation in $\Delta^{13}C$ and WUE_i across biomes

Mean $\Delta^{13}C$ and calculated mean WUE_i values grouped by biome **Figure 4.5** varied highly significantly across both seasons (see **Table 4.2** for biome descriptions). The smallest discrimination and the largest WUE_i occurred in semi-arid woodlands (SW; mean $\Delta^{13}C_{dry\text{-}season}$ = 19.75‰, mean $WUE_{i\ dry\text{-}season}$ = 78.14 μmol/mol, mean $\Delta^{13}C_{wet\text{-}season}$ = 19.15‰ and mean $WUE_{i\ wet\text{-}season}$ = 84.6 μmol/mol) and the largest discrimination and the smallest WUE_i occurred in the tropical rainforests (LTR, UTR; mean $\Delta^{13}C_{dry\text{-}season}$ = 23.42‰, mean $WUE_{i\ dry\text{-}season}$ = 31.74 μmol/mol, mean $\Delta^{13}C_{wet\text{-}season}$ = 23.64 ‰ and mean $WUE_{i\ wet\text{-}season}$ = 29.04 μmol/mol), p values <0.0001 for both seasons. Data were available only for the dry-season for the HTS biome. Discrimination against ^{13}C and WUE_i appeared to vary more significantly from biome-to-biome during the wet-season than the dry-season sampling (F values for wet-season = 12.12 and for dry-season = 7.36 from one-way ANOVA). Also, mean $\Delta^{13}C$ calculated for each biome were larger during the wet-season than the dry-season in all climate biomes across the continent, with the exception of semi-arid woodlands. Overall, biome type explained similar variation in $\Delta^{13}C$ (and also WUE_i) when compared to MAP (and MI) for both seasons from the ANOVA model ($\Delta^{13}C$ for dry-season: Adj r^2_{MAP} = 48.3%, r^2_{biome} = 45.0% and wet-season: Adj r^2_{MAP} = 57.1%, r^2_{biome} = 55.8).

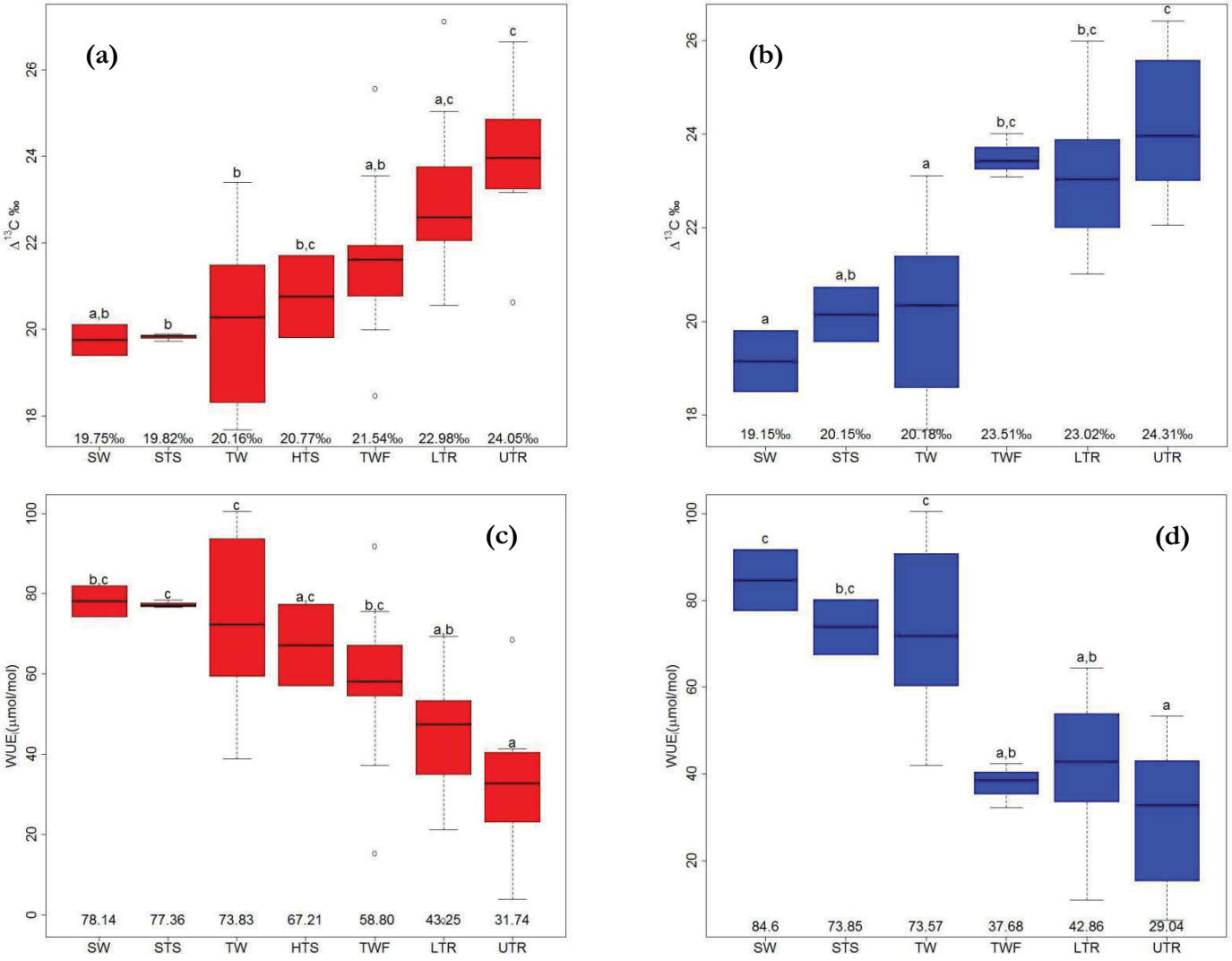

Figure 4.5: Variation in $\Delta^{13}C$ and WUE_i by biome types.

Red and blue plots respectively represent dry- and wet-season sampling. The box plots present the maximum and minimum values, the inter-quartile range, and the median (solid centreline) values and the open circles indicating outliers. Letters above bars indicate the differences between means (Tukey HSD, confidence level of 0.05) across sites in each season and biomes not connected by same letter are significantly different from other biomes. Values under the boxes present the mean values of $\Delta^{13}C$ and WUE_i for each biome (see **Table 4.2** for biome descriptions).

Variation in potential and actual evapotranspiration across sites

The widely-used Budyko theoretical framework was employed to explore the relationships between potential and actual evapotranspiration across the seven SuperSites. ET_p, ET_a and precipitation data for 125 years (1890-2014) were used to calculate long-term annual averages of the dryness index (Φ) and evaporative index (ε). In addition to 125-year long-term Φ and ε, values of five 25-year tiles from 1890-2014 (i.e., 1890-1914, 1915-1939, 1940-1964, 1965-1989 and 1990-2014) were also calculated to examine long-term trends in Φ and ε. Data from each year were divided into two (dry and wet) seasons. As per BoM convention, May to September was considered as dry-season and October to April was considered as wet-season in four SuperSites (AMU, CP, LF and FNQ) and May to September was considered as wet-season and October to April was considered as dry-season in the other three sites (CM, GWW and WR). Seasonal average (both 125-year average and five 25-year averages) of Φ and ε were then calculated and plotted against the Budyko curve to examine any seasonal patterns/variations in long-term Φ and ε values. SILO data was available only from one site in FNQ (approximately 30 km Northeast of RC and 90 km Southeast of CT), hence, CT and RC are grouped into one site. A list of meteorological stations from which data were obtained are listed in **Table A2** in the Appendix.

Variation in long-term annual average Φ and ε

When Φ and ε values (mean of 125-years) were plotted, the distribution of some SuperSites deviated from the theoretical Budyko curve more than others. FNQ is the only site ($\Phi \approx 1$) that fell on the curve. LF and WR are the other two high-rainfall sites and fell slightly above the curve. All other sites had moisture deficit ($\Phi > 1$) and fell above the curve with higher than expected evapotranspiration values except for AMU which fell below the curve.

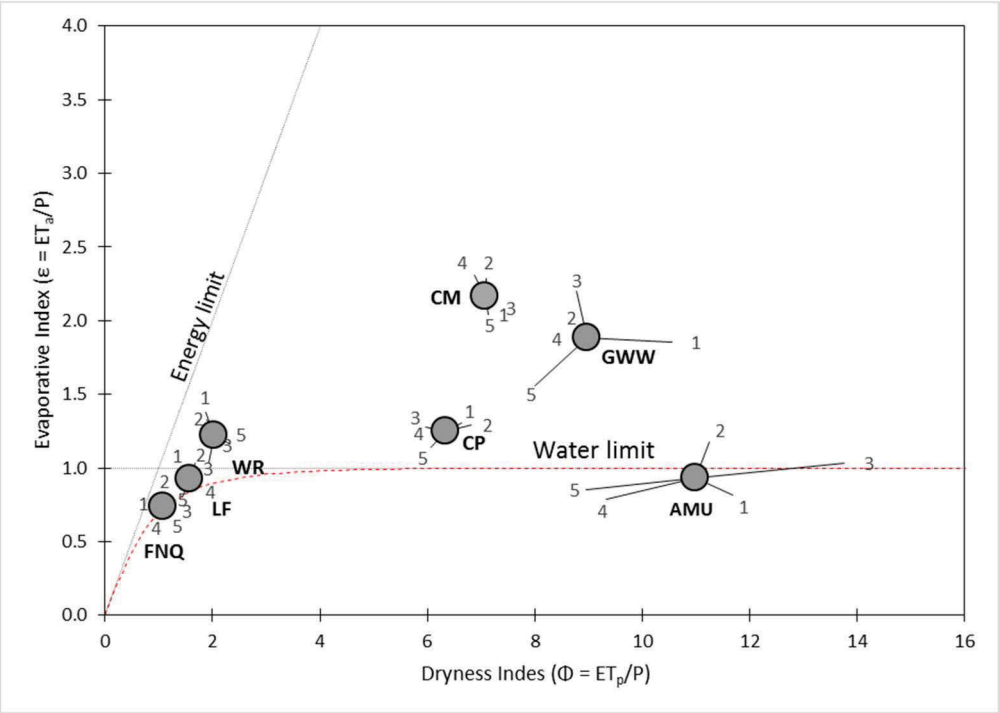

Figure 4.6: Long-term annual average ε plotted against Φ for each of the SuperSites.

Each SuperSite is represented by grey circles. Red dashed line indicates the theoretical Budyko curve- a plot of evaporative index as a function of dryness index. Values of Φ>1 indicate a water-limited (arid) climate, whereas values of Φ <1 indicate an energy limited (humid) climate. Each value of ε as a function of Φ calculated from 25-year mean is connected to the 125-year mean by radial lines – number 1 to 5 indicating Φ-ε values of five 25 year tiles of 1890-1914, 1915-1939, 1940-1964, 1965-1989 and 1990-2014 respectively. Site abbreviations are listed in Table 4.2.

The variation between Φ and ε values calculated from each 25-year tile also differed among SuperSites. Variation in long-term ε was less than that of Φ in the water-limited sites (AMU, CP and GWW, **Figure 4.6**, **Table 4.7**) and AMU and GWW showed the largest variation in both ε and Φ among all the SuperSites. Sites in the wetter end of the rainfall spectrum did not show significant variation in long-term ε relative to the variation in Φ (**Table 4.7**).

Variation in long-term seasonal average Φ and ε

Long-term seasonal averages of Φ and ε showed interesting differences in their distribution when plotted in the theoretical Budyko curve. All the sites had significantly larger values of both Φ and ε during dry-seasons than during wet-seasons (**Figure 4.7**). **Figure 4.7** shows

that dominant tree species also discriminated more against ^{13}C during wet-season than dry-season and also more in wetter sites than drier sites during both seasons.

Although the site FNQ fell on the theoretical Budyko curve when the long term annual averages were plotted in **Figure 4.6**, it was above the curve when the long-term average of only dry-season Φ- ε values were plotted (**Figure 4.7(a)**). Both FNQ and WR fell on the curve during wet-season despite being above the curve during dry-season (**Figure 4.7(b)**). Also FNQ and WR during wet-season were energy limited (Φ<1); all other sites during both seasons fell on the water limited side (Φ>1) of the curve. Among the dry sites, only AMU fell below the curve during the wet-season sampling. For all these sites, evaporative indices were closer to the theoretical Budyko curve in the wet-season than the dry-season. Dry-season average, wet-season average and annual average Φ and ε calculated for 1890-2014 and standard deviation of five calculated 25-year means are shown in **Table 4.7**. From **Figure 4.7** and **Table 4.7,** variation (indicated by standard deviation, σ) between five 25-year means of Φ and ε values were larger at the drier sites than the wetter sites and also larger during the dry-season than during the wet-season. Long-term evaporative index (ε) for five 25-year tiles varied less during dry-seasons (**Table 4.7**) when compared to variation in long-term dryness index (Φ), whereas, ε compared to Φ was not very different for the same five 25-year tiles during wet-seasons.

Table 4.7: Dryness index (Φ) and evaporative index (ε) for dry-season average, wet-season average and annual average for 1890-2014 and standard deviations (σ) of five 25-year means from 125-year mean.

SuperSite	Annual average				Dry-season				Wet-season			
	mean Φ	σ	mean ε	σ	mean Φ	σ	mean ε	σ	mean Φ	σ	mean ε	σ
CM	7.1	0.1	2.2	0.1	11.3	0.8	3.2	0.3	2.9	0.2	1.1	0.1
GWW	8.9	0.9	1.9	0.2	12.8	2.4	2.4	0.4	4.6	0.4	1.3	0.1
AMU	11.0	1.9	0.9	0.2	19.0	2.8	1.6	0.5	9.3	1.8	0.8	0.1
CP	6.3	0.4	1.3	0.1	20.1	1.6	2.4	0.2	4.4	0.3	1.1	0.0
WR	2.0	0.2	1.2	0.1	3.1	0.4	1.8	0.1	0.7	0.1	0.5	0.1
LF	1.6	0.1	0.9	0.1	33.4	8.4	13.9	4.4	0.9	0.1	0.6	0.1
FNQ	1.1	0.1	0.7	0.0	3.3	0.6	1.8	0.2	0.8	0.0	0.6	0.0

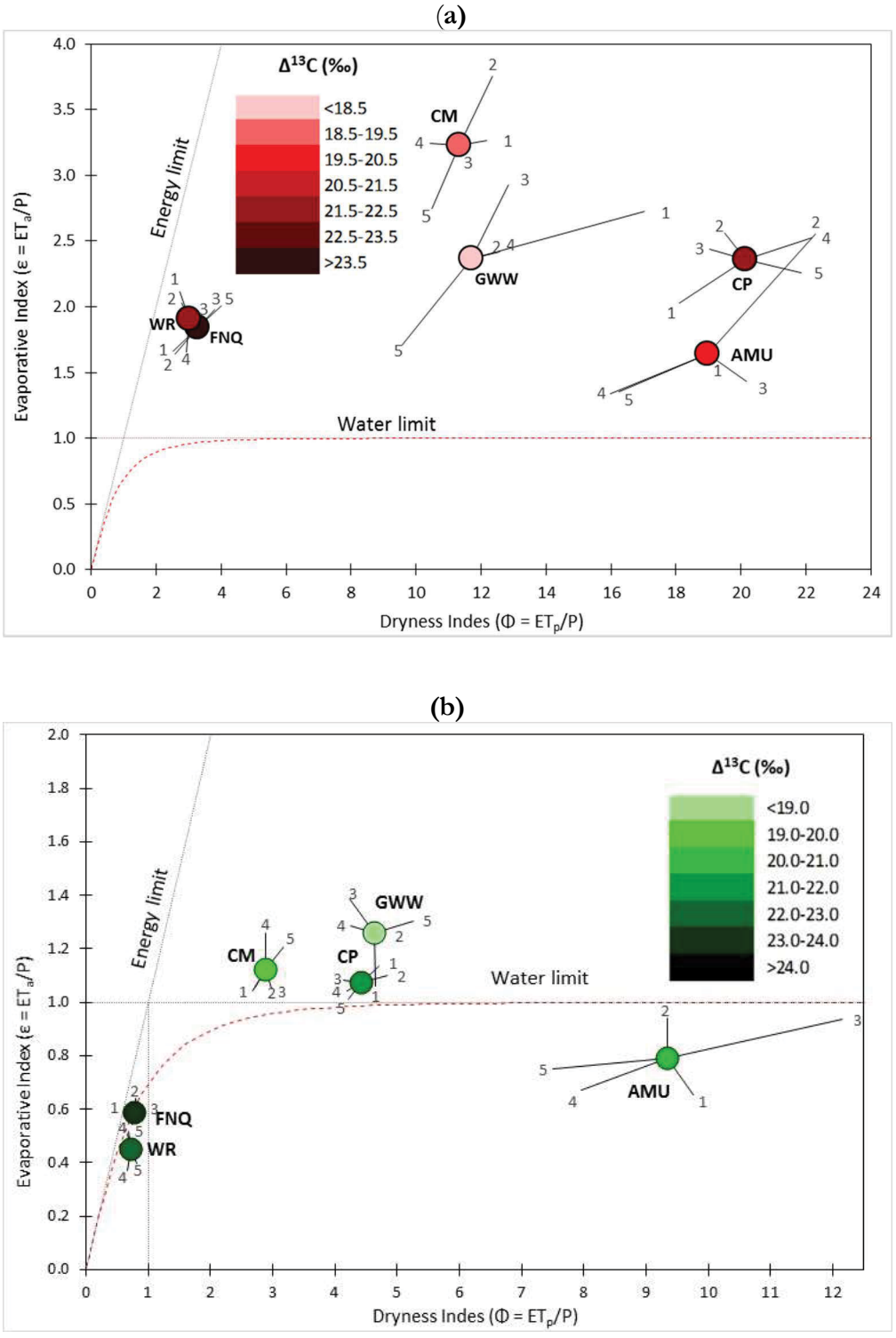

Figure 4.7: Long-term seasonal average ε plotted against Φ for each of the SuperSites for (a) dry-season in red circles and (b) wet-season in green circles.

Site mean value of $\Delta^{13}C$ is indicated by the shade of its data point. In AMU, CP, and FNQ, May to September was considered as dry-season and October to April was considered as wet-season. In CM, GWW and WR, May to September was considered as wet-season and October to April was considered as dry-season. Red/green circles indicate the 125-year mean values of ε as a function of Φ calculated for dry/wet-season respectively; connected by radial lines to Φ- ε values calculated for dry- and wet-season for five 25-year tiles. Site LF was not included in the analysis because data from both seasons weren't available.

Variation in gas-exchange parameters across the precipitation gradient

Species mean values of net photosynthetic assimilation, A400.a and stomatal conductance, g_s400 measured at atmospheric concentration of CO_2 of 400 ppm showed a statistically significant positive increase with an 8-fold increase in MAP during the dry-season and g_s400 had a stronger and significant relationship with MAP (Adj r^2: A400.a=0.09, $p<0.01$, g_s400 =0.30, $p<0.0001$, **Figure 4.8a-4.8d**). None of these traits was significantly associated with MAP during the wet-season. The ratio of A400.a to g_s400 (defined as the leaf intrinsic-water-use-efficiency obtained from instantaneous measurements) showed a highly significant negative relationship with MAP across sites during both seasons although stronger correlation with A400.a/g_s400 and MAP was again identified during the dry-season (Adj r^2: dry-season=0.50, $p<0.0001$, wet-season=0.30, $p<0.0001$, **Figure 4.8e-4.8f**). This negative relationship suggests that, dominant species in the sites at the drier end of the spectrum are inherently more efficient in using water and this efficiency was larger during the dry-season than the wet-season.

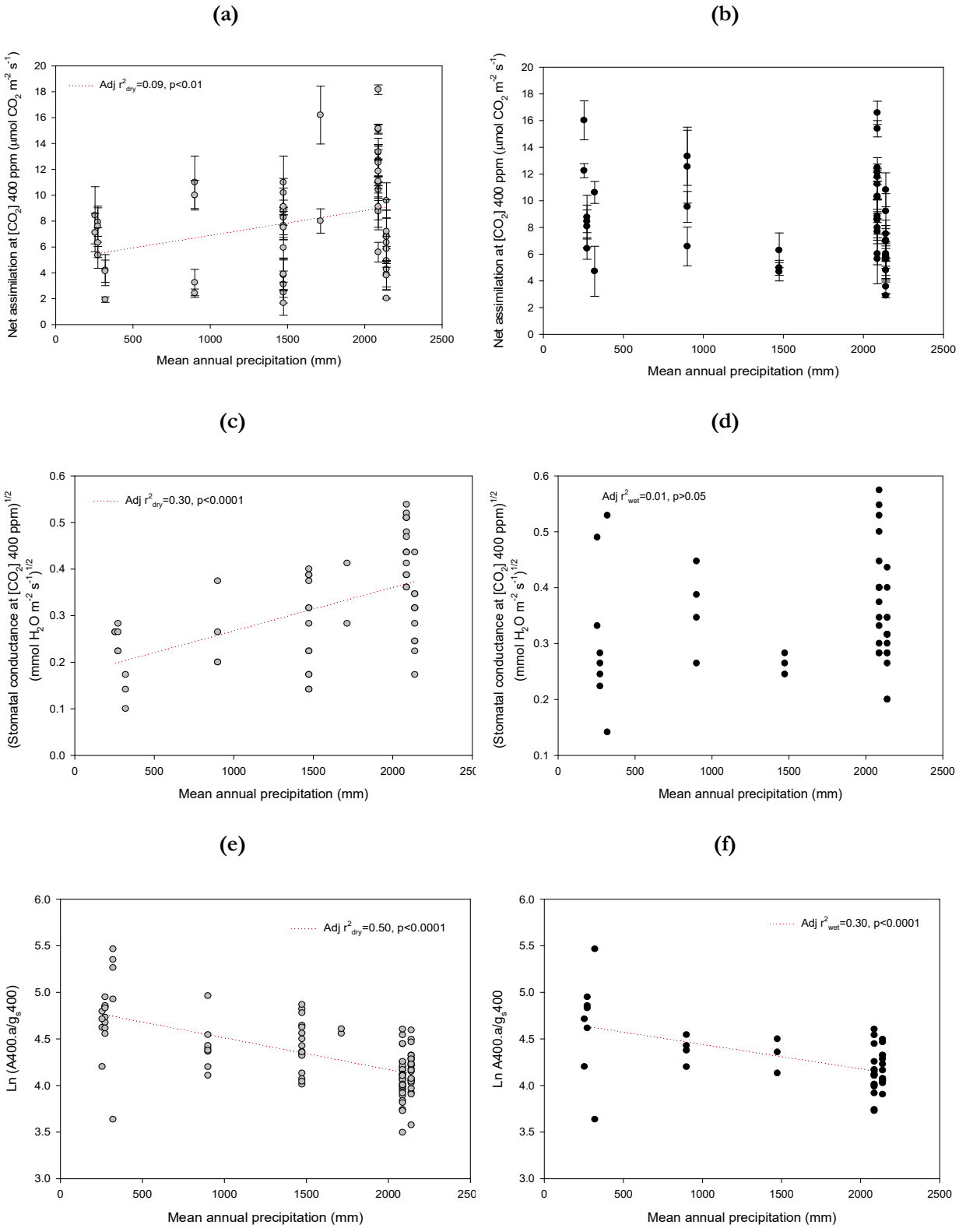

Figure 4.8: Net assimilation, A400.a, stomatal conductance, g_s400 and leaf intrinsic water-use-efficiency (A400.a/g_s400) for both seasons plotted as functions of mean annual precipitation (MAP).

Left and right panels are plotted from dry- and wet-season data respectively. Statistically significant correlations with MAP are plotted with red regression lines. Each symbol represents the species mean of four-six individuals. Error bars are one standard error (not shown when data is transformed due to non-normality). Non-significant regressions are not shown.

Figure 4.9 shows the relationships of the ratio of intercellular and ambient [CO_2] (C_i/C_a) and intercellular [CO_2] with [CO_2] reference at 400 ppm (C_i400). MAP explained 36% of variation in C_i/C_a and 51% of variation in C_i400 during the wet-season (Adj r^2: C_i/C_a = 0.36, $p < 0.0001$ and C_i400 = 0.51, $p<0.0001$). 34% of variation in C_i/C_a and 29% of variation in C_i400 was explained by MAP during the dry-season. Furthermore, the C_i/C_a of the dominant species at the wetter end of the precipitation gradient did not show much variation between dry- and wet-season sampling, but clear seasonal differences in C_i/C_a were observed in the drier sites (rainfall <350 mm). Most of the C_i/C_a values during the dry-season ranged from 0.3~0.6 for drier sites whereas, wet-season sampling for the same sites showed higher C_i/C_a values (0.45~0.75, **Figure 4.9**).

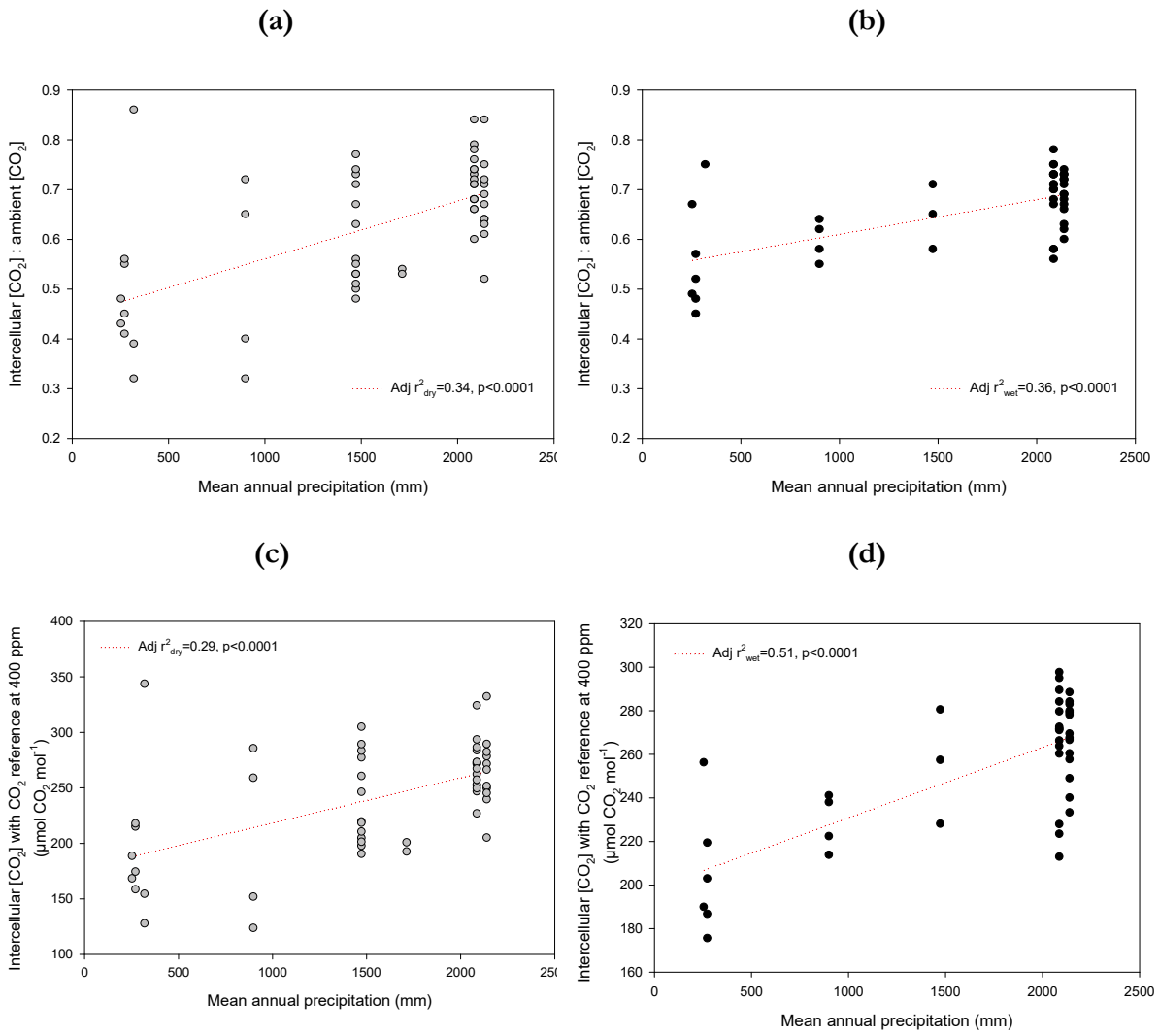

Figure 4.9: Ratio between intercellular and ambient [CO_2] (C_i/C_a) and intercellular [CO_2] with [CO_2] reference at 400ppm (C_i400) for both seasons plotted as functions of mean annual precipitation (MAP).

Left and right panels are plotted from dry- and wet-season data respectively. Statistically significant correlations with MAP are plotted with red regression lines.

Transpiration rate measured at [CO_2] 400 ppm (E400.a) increased and vapour pressure deficit (VPD) based on leaf temperature decreased significantly only during dry-season (r^2: E400.a = 0.061, $p < 0.05$ and VPD = 0.28, $p < 0.0001$, figure not shown) and no significant relationship was identified during the wet-season.

Scaling relationships between $\Delta^{13}C$ and gas-exchange traits

$\Delta^{13}C$ was significantly associated with C_i/C_a (dry-season: $r^2 = 0.20$, $p < 0.001$, slope=0.06, wet-season: $r^2 = 0.19$, $p < 0.001$, slope=0.036) and C_i measured at 400ppm (**Figure 4.10a**,

4.10b, dry-season: r^2 = 0.19, $p<0.001$, slope=22.20, wet-season: r^2 = 0.26, $p<0.001$, slope=14.09). Significant differences between the slopes for dry- and wet-season were identified for both C_i/C_a ($p=0.02$) and C_i400 ($p=0.04$, **Table 4.8**) such that, significantly larger discriminations were found when C_i/C_a (**Figure 4.10a**) and C_i400 (**Figure 4.10b**) were larger and the r^2 values were also higher for both C_i/C_a and C_i400 during the wet-season than the dry-season. Leaf intrinsic water-use-efficiency calculated from the ratio of A400.a and g_s400 was also associated significantly with $\Delta^{13}C$ (dry-season: r^2 = 0.26, $p<0.0001$, slope= -0.17, wet-season: r^2 = 0.17, $p<0.05$, slope=-0.14, **Figure 4.10c**) such that, species that discriminated less against ^{13}C also showed significantly larger instantaneous measurements of intrinsic water-use-efficiency and this relationship was stronger during the dry-season than the wet-season. Standardised major axis (SMA) slopes were homogeneous between dry- and wet-seasons ($p=0.23$) with a significant shift along the slope ($p<0.05$) indicating that, the wet-season sampling shifted towards the more discriminatory end of the spectrum compared to the dry-season sampling (**Figure 4.10c**).

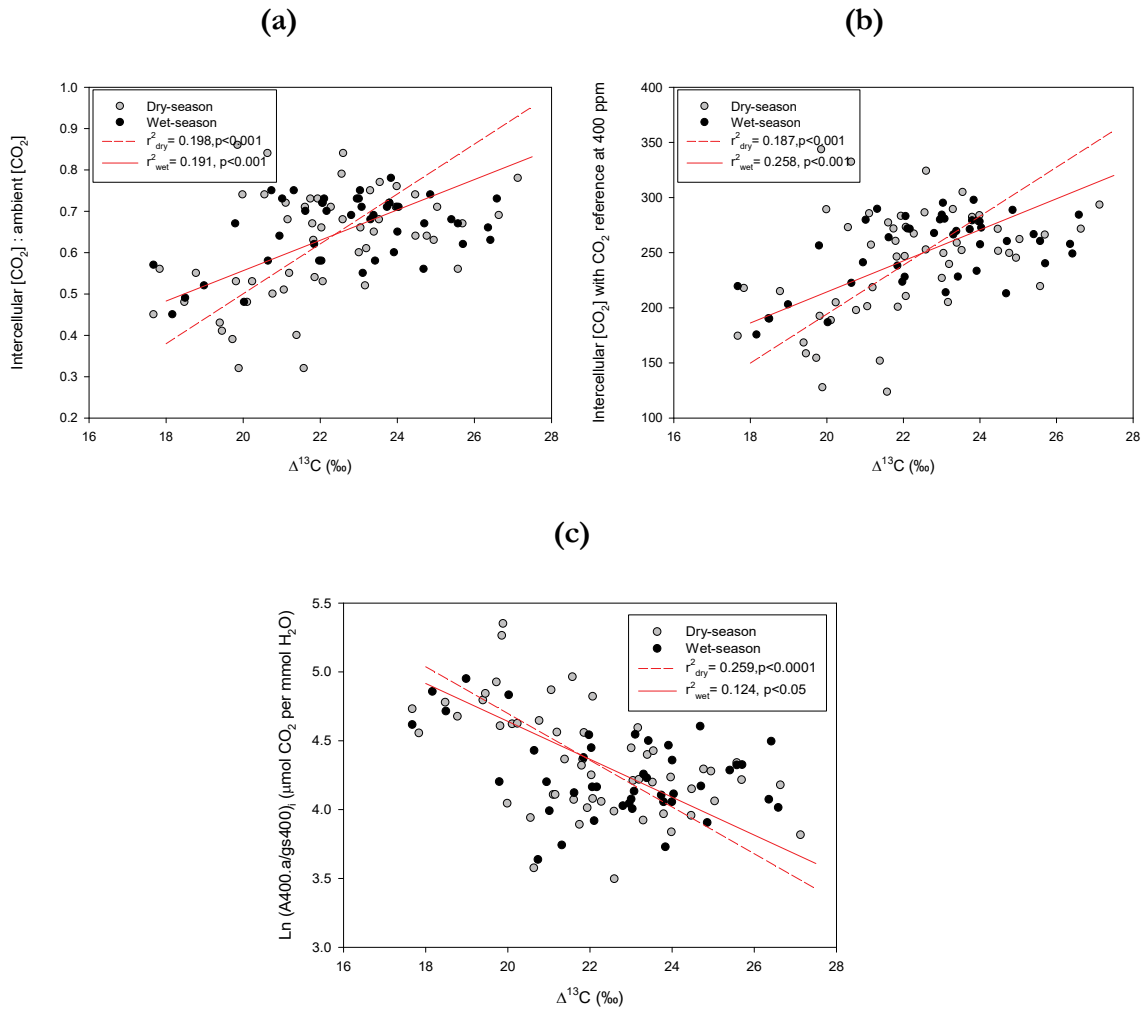

Figure 4.10: Scaling relationships between Δ¹³C and (a) ratio of intercellular and ambient [CO_2] (C_i/C_a), (b) intercellular [CO_2] with [CO_2] reference at 400ppm (C_i400) and (c) Ratio of net photosynthetic assimilation to stomatal conductance (A400.a/gs400).

Dry-season samples are represented by grey circles and dashed lines and wet-season samples by black circles and solid lines. Statistically significant slopes from SMA are plotted with red lines.

$\Delta^{13}C$ was significantly associated with net photosynthetic assimilation during the wet-season (r^2 = 0.14, p<0.01, slope =1.85, **Figure 4.11a**) but not during the dry-season (r^2 = 0.03, p> 0.05), such that, species that discriminated more against ^{13}C during the wet-season sampling had smaller net photosynthetic assimilation. In contrast, $\Delta^{13}C$ was associated significantly with stomatal conductance measured at 400 ppm during the dry-season (r^2 = 0.07, p<0.05, slope =0.06, **Figure 4.11b**) but not during the wet-season (r^2 = 0.003, p>0.05) and showed a negative relationship with vapour pressure deficit during the dry-season (r^2 = 0.23, p<0.01, slope =-0.19, **Figure 4.11c**) but not during the wet-season (r^2 =

0.027, p>0.05). This indicates that, during dry-season, significantly larger discrimination was found in species that had larger stomatal conductance and experienced smaller vapour pressure deficits. Transpiration measured at 400 ppm, however, was not significantly associated with $\Delta^{13}C$ (dry-season: $r^2 = 0.0005$, p>0.05, wet-season: $r^2 = 0.005$, p>0.05; **Figure 4.11d**).

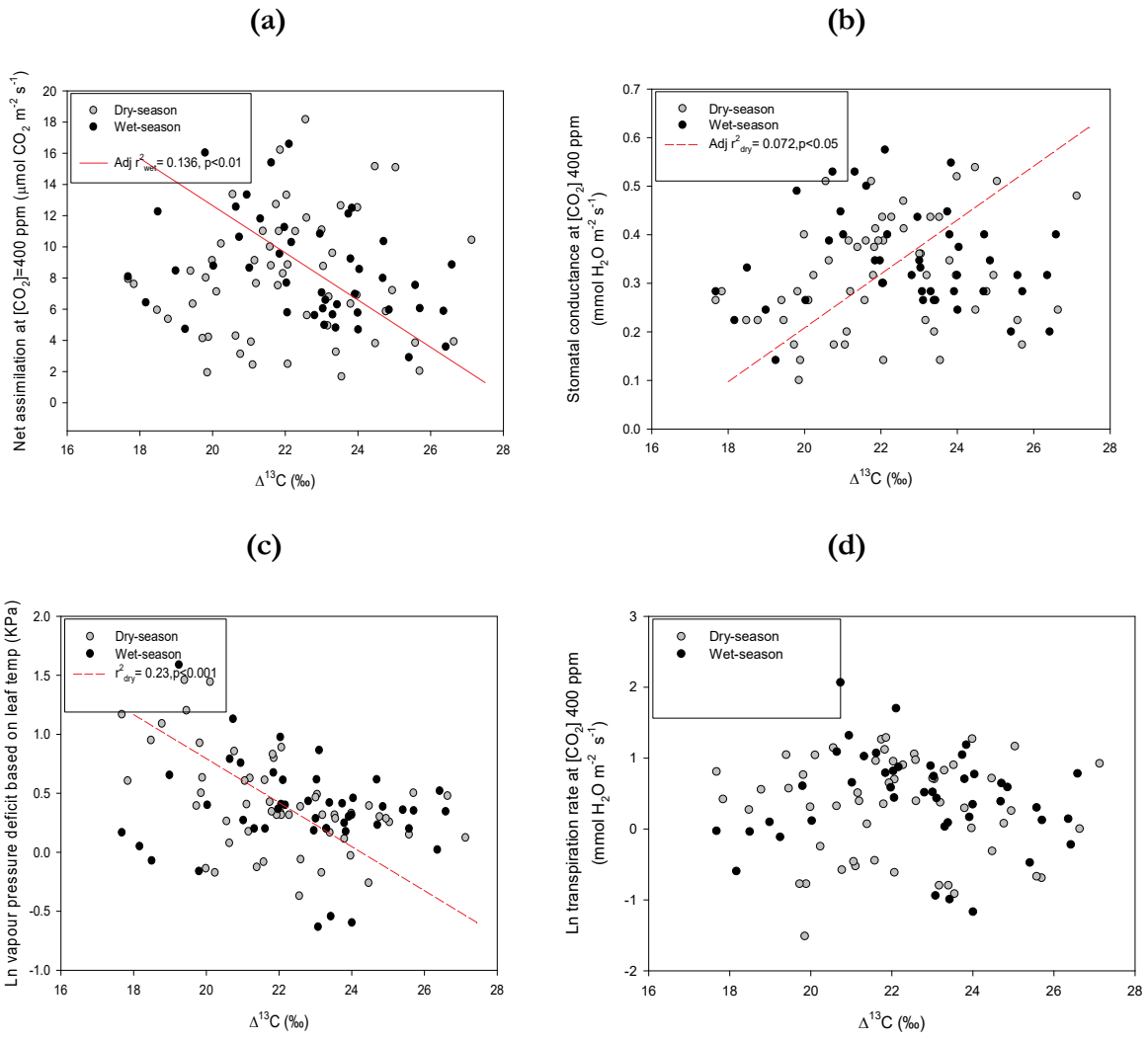

Figure 4.11: Scaling relationships between $\Delta^{13}C$ and (a) net assimilation, (b) stomatal conductance, (c) vapour pressure deficit and (d) transpiration rate.

Dry-season samples are represented by grey circles and dashed lines and wet-season samples by black circles and solid lines. Statistically significant slopes from SMA are plotted with red lines. Non-significant SMA slopes are not shown. In (a) the wet-season regression is significant; in (b) and (c) the dry-season regressions are significant; in (d) none of the regressions is significant.

C_i/C_a showed significant relationships with g_s400 during both seasons (**Figure 4.12b**, dry-season: $r^2 = 0.22$, $p<0.001$, slope=0.91, wet-season: $r^2 = 0.32$, $p<0.0001$, slope=1.21) such that, smaller C_i/C_a during both seasons was associated with smaller g_s400. A400.a however, was not significantly associated with the C_i/C_a ratio (dry-season: $r^2 = 0.02$, $p>0.05$, wet-season: $r^2 = 0.03$, $p>0.05$; **Figure 4.12a**).

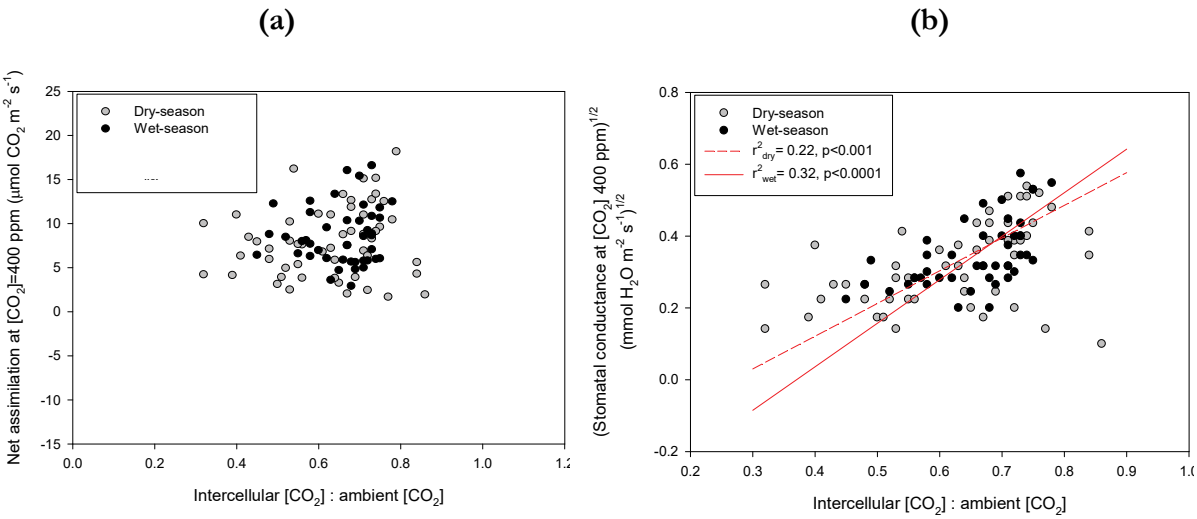

Figure 4.12: Scaling relationships between C_i/C_a and (a) Net assimilation and (b) stomatal conductance.

The dry-season samples are represented by grey circles and dashed lines and the wet-season samples by black circles and solid lines. Statistically significant slopes from SMA are plotted with red lines. Non-significant SMA slopes are not shown.

Table 4.8: Scaling relationships between bulk-leaf $\Delta^{13}C$ and other leaf attributes

trait associated with $\Delta^{13}C$	Season				Statistical tests					
	Dry		Wet		Bartlett's likelihood ratio test for a common slope		Wald tests			
							Shift along common elevation		Shift along common fitted slope	
	r^2	slope	r^2	slope	Y/N	p	Y/N	p	Y/N	p
A400.a	0.006	1.852	0.135*	-1.514	-	-	-	-	-	-
Ln E400.a	0.0005	-0.336	0.005	-0.265	-	-	-	-	-	-
Ln vpdL400	0.229**	-0.187	0.027	-0.146	-	-	-	-	-	-
sqrt g_s400	0.072•	0.055	0.003	-0.045	-	-	-	-	-	-
Ln A400.a/gs400	0.259***	-0.169	0.172•	-0.131	Y	0.234	N	0.837	Y	0.04
C_i/C_a	0.198**	0.060	0.191**	0.036	N	0.017	-	-	-	-
C_i400	0.187**	22.199	0.258**	14.088	N	0.044	-	-	-	-
LDMC	0.177**	-0.038	0.113•	-0.038	Y	0.142	N	0.566	N	0.093
Ln LMA	0.306***	-0.189	0.433***	-0.206	Y	0.632	N	0.663	N	0.168
Ln FMA	0.307***	-0.148	0.445***	-0.144	Y	0.867	N	0.702	N	0.071
Ln $LeafN_{mass}$	0.030	0.188	0.010	0.134	-	-	-	-	-	-
Ln $LeafP_{mass}$	0.135*	0.280	0.003	0.171	-	-	-	-	-	-
Ln Ration NP	0.105	-0.212	0.004	0.091	-	-	-	-	-	-
Ln $LeafN_{area}$	0.191***	-0.176	0.493**	-0.161	Y	0.616	N	0.109	N	0.423
Ln $LeafP_{area}$	0.002	-0.181	0.379***	0.184	-	-	-	-	-	-
PNUE	0.037	0.838	0.025	0.703	-	-	-	-	-	-
Ln PPUE	0.0002	-0.301	0.016	0.229	-	-	-	-	-	-
A400.a ~ C_i/C_a	0.025	30.419	0.008	40.750	-	-	-	-	-	-
sqrt g_s400 ~ C_i/C_a	0.216**	0.911	0.317***	1.211	Y	0.105	N	0.602	N	0.138

***p<0.0001, **p<0.001, *p<0.01, •p<0.05, Y indicates existence if a common slope in which case Wald tests were performed.

Scaling relationships between ⊿^{13}C and leaf structural parameters

$\Delta^{13}C$ showed significant and negatively relationships with leaf mass per unit area, LMA (**Figure 4.13a**, dry-season: r^2 = 0.31, p<0.0001, slope=-0.15, wet-season: r^2 = 0.43, p<0.0001, slope= -0.21), leaf fresh mass per unit area, FMA (**Figure 4.13b**, dry-season: r^2 = 0.31, p<0.0001, slope= -0.15, wet-season: r^2 = 0.45, p<0.0001, slope=-0.14) and the ratio of leaf dry to fresh mass, LDMC (**Figure 4.13c**, dry-season: r^2 = 0.18, p<0.001, slope= -0.04, wet-season: r^2 = 0.11, p<0.05, slope= -0.04), such that, significantly larger discrimination against ^{13}C was found in leaves with smaller LMA (**Figure 4.13a**), smaller FMA (**Figure 4.13b**) and smaller LDMC (**Figure 4.13c**). Slopes were homogeneous between dry- and wet-season for all of these traits, i.e., LMA (p = 0.63), FMA (p = 0.87) and LDMC (p = 0.14) and no significant shift along the elevation or slope were identified (**Table 4.8**).

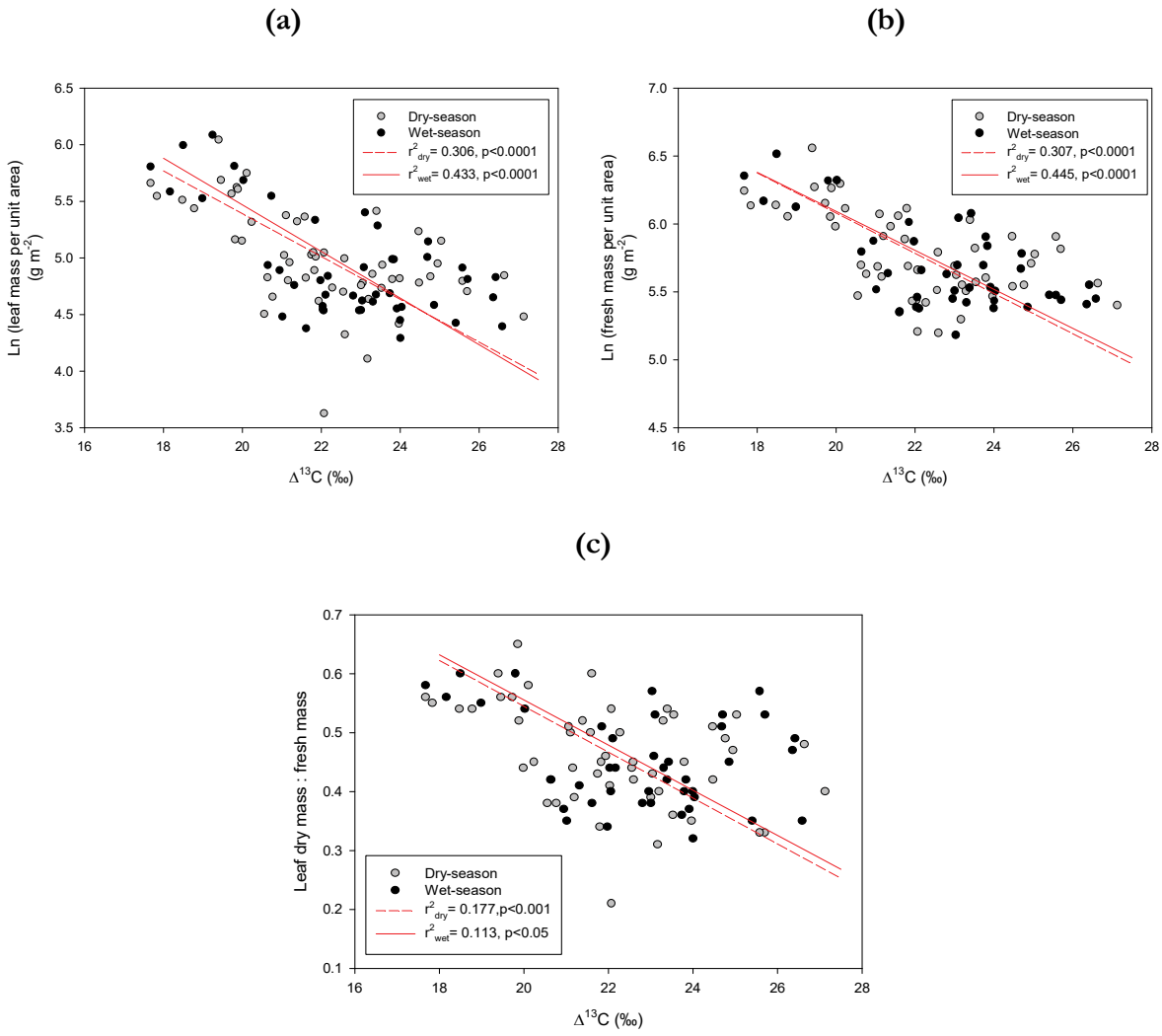

Figure 4.13: Scaling relationships between $\Delta^{13}C$ and (a) leaf mass per unit area, (b) fresh mass per unit area and (c) ratio leaf dry mass to fresh mass.

The dry-season samples are represented by grey circles and dashed lines and the wet-season samples by black circles and solid lines. Statistically significant slopes from SMA are plotted with red lines.

Scaling relationships between $\Delta^{13}C$ and leaf nutrient parameters

Out of all the nutrient related parameters, $\Delta^{13}C$ showed strong (and negative) relationships during both seasons with total leaf N expressed in area basis, $LeafN_{area}$ (**Figure 4.14a**, dry-season: $r^2 = 0.19$, $p<0.001$, slope=-0.18, wet-season: $r^2 = 0.49$, $p<0.0001$, slope= -0.16), such that, significantly larger discrimination was found in leaves that contained smaller nitrogen per unit area. $\Delta^{13}C$ showed a strong and significant relationship with total leaf P expressed in mass basis, $LeafP_{mass}$ only during the dry-season (**Figure 4.14b,** $r^2 = 0.14$, $p<0.01$, slope = 0.28) but not during the wet-season ($r^2 = 0.003$, $p> 0.05$), such that,

species that discriminated more against ^{13}C during dry-season sampling also had lower phosphorus per gram of leaf. In contrast, total leaf P expressed in area basis, $LeafP_{area}$ was significantly associated with $\Delta^{13}C$ only during the wet-season (**Figure 4.14c**, r^2 = 0.38, $p<0.0001$, slope =0.18) but not during the dry-season (r^2 = 0.002, $p> 0.05$) and larger discrimination was associated with smaller phosphorus content per unit area of leaves. No other nutrient related leaf-traits showed any significant relationship with $\Delta^{13}C$ (**Table 4.8**).

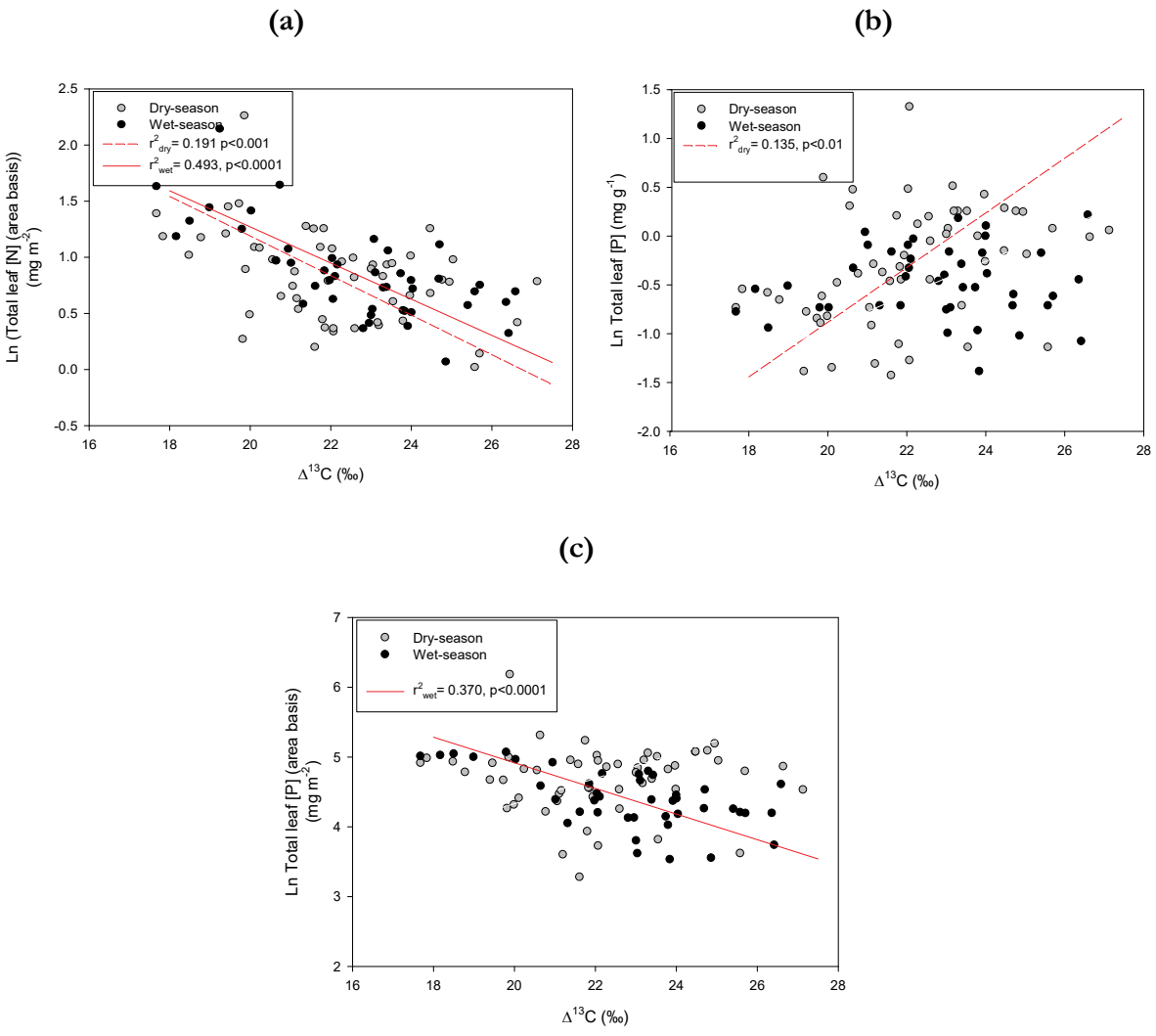

Figure 4.14: Scaling relationships between $\Delta^{13}C$ and (a) total leaf N expressed in area basis, $LeafN_{area}$, (b) total leaf P expressed in mass basis, $LeafP_{mass}$ and (c) total leaf P expressed in area basis, $LeafP_{area}$.

Dry-season samples are represented by grey circles and dashed lines and wet-season samples by black circles and solid lines. Statistically significant slopes from SMA are plotted with red lines. Non-significant SMA slopes are not shown. In (a) regression for both seasons are significant. In (b) only the dry-season regression is significant. In (c) only the wet-season regression is significant.

Variation of leaf-traits with moisture index

In addition to MAP, bivariate linear regression was performed with moisture index (MI) treated as an independent predictor variable and all other leaf-traits treated as continuous response variables. The results of these regressions are compiled in **Table 4.9.** Moisture index was calculated as a ratio of long-term (125-year) mean precipitation and potential evapotranspiration and was considered as another measure of water availability that also takes into account the very different *wet* conditions across different sites. **Table 4.9** shows that, despite taking potential evaporation into account, the correlations of leaf-traits with MI was not very different in strength and nature than those with leaf-traits and MAP.

Table 4.9: Results of bivariate linear regression of leaf-traits with Mean Annual Precipitation and Moisture Index

Traits	Relationship with MAP						Relationship with MI					
	Dry-season			Wet-season			Dry-season			Wet-season		
	Adj r^2	slope	p	Adj r^2	slope	p	Adj r^2	slope	p	Adj r^2	slope	p
$\Delta^{13}C$	**0.474**	+	<0.0001	**0.590**	+	<0.0001	**0.449**	+	<0.0001	**0.523**	+	<0.0001
A400.a	**0.092**	+	<0.05	0.008	-	> 0.05	**0.112**	+	< 0.05	~0	-	> 0.05
Ln E400.a	**0.062**	+	<0.05	-0.005	+	> 0.05	**0.10**	+	< 0.01	0.001	-	> 0.05
Ln vpdL400	**0.281**	-	<0.0001	-0.003	-	> 0.05	**0.236**	-	<0.0001	**-**0.007	-	> 0.05
sqrt g_s400	**0.298**	+	<0.0001	0.002	+	> 0.05	**0.338**	+	<0.0001	0.006	+	> 0.05
Ln WUE_i	**0.500**	-	<0.0001	**0.296**	-	<0.0001	**0.510**	-	<0.0001	**0.279**	-	<0.0001
C_i/C_a	**0.342**	+	<0.0001	**0.364**	+	<0.0001	**0.362**	+	<0.0001	**0.466**	+	<0.0001
C_i400	**0.290**	+	<0.0001	**0.507**	+	<0.0001	**0.301**	+	<0.0001	**0.479**	+	<0.0001
LDMC	**0.399**	-	<0.0001	**0.303**	-	<0.0001	**0.370**	-	<0.0001	**0.243**	-	<0.001
Ln LMA	**0.633**	-	<0.0001	**0.743**	-	<0.0001	**0.605**	-	<0.0001	**0.676**	-	<0.0001
Ln FMA	**0.606**	-	<0.0001	**0.722**	-	<0.0001	**0.579**	-	<0.0001	**0.672**	-	<0.0001
Ln $LeafN_{mass}$	**0.118**	+	<0.01	**0.080**	+	<0.05	**0.170**	+	<0.001	**0.074**	+	<0.05
Ln $LeafP_{mass}$	**0.332**	+	<0.0001	0.004	+	> 0.05	**0.417**	+	<0.0001	-0.006	+	> 0.05
Ln Ratio NP	**0.198**	-	<0.001	0.027	+	> 0.05	**0.239**	-	<0.0001	0.048	+	> 0.05
Ln $LeafN_{area}$	**0.256**	-	<0.0001	**0.621**	-	<0.0001	**0.178**	-	<0.0001	**0.558**	-	<0.0001
Ln $LeafP_{area}$	-0.02	+	> 0.05	**0.546**	-	<0.0001	-0.06	-	> 0.05	**0.526**	-	<0.0001
A400.N	**0.221**	+	<0.001	**0.157**	+	<0.01	**0.287**	+	<0.0001	**0.156**	+	<0.05
Ln A400.P	0.019	+	> 0.05	**0.144**	+	<0.01	~0	+	>0.05	**0.158**	+	<0.01

Results from principal component analysis

Principal components analysis performed separately for the dry- and wet-season sampling identified combinations of variables that best summarized the data. For the data from the dry-season sampling, the first principal component (PC1) accounted for 41.3% of variation in the dataset (**Figure 4.15a**) and represented clear contrasts between environmental constraints and structural traits of the dataset; i.e. (i) MAP, MI and C_i/C_a representing strong positive correlation with $\Delta^{13}C$ and (ii) LMA, FMA and LDMC representing strong negative correlation with $\Delta^{13}C$. Principal component 2 (PC2) accounted for 17.7% of variation and represented a contrast between other nutrient based and gas-exchange traits with two phosphorus related traits $LeafP_{mass}$ and $LeafP_{area}$. In the wet-season data-set, the PC1 and PC2 accounted for 42.4% and 22.6% of variation respectively (**Figure 4.15b**). The first principal component in wet-season data identified a contrast between environmental constraints and structural/ nutrient-based parameters. $\Delta^{13}C$ during both seasons showed strong positive correlation with MAP, MI and C_i/C_a and strong inverse correlation with LMA, FMA and LDMC. When all 16 leaf-traits were considered together with $\Delta^{13}C$, the dominant species from the very low to low MAP (and MI) sites were clearly distinguished from sites with high to very high MAP (and MI, **Figure 4.15a, 15b**).

The distinct separation of the species from drier sites from those from wetter sites was still obtained when only two leaf attributes, $\Delta^{13}C$ and LMA, instead of all 16 other attributes together, were considered in separate PCA models with MAP and MI (compare **Figure 4.15a** with **Figure 4.15c** and **Figure 4.15b** with **Figure 4.15d**). There were variations in relative distance of the points but the grouping pattern was still maintained for both seasons. This result suggests that, $\Delta^{13}C$ like LMA can very reliably provide valuable information for assessing species-specific differences related to water availability at the site level.

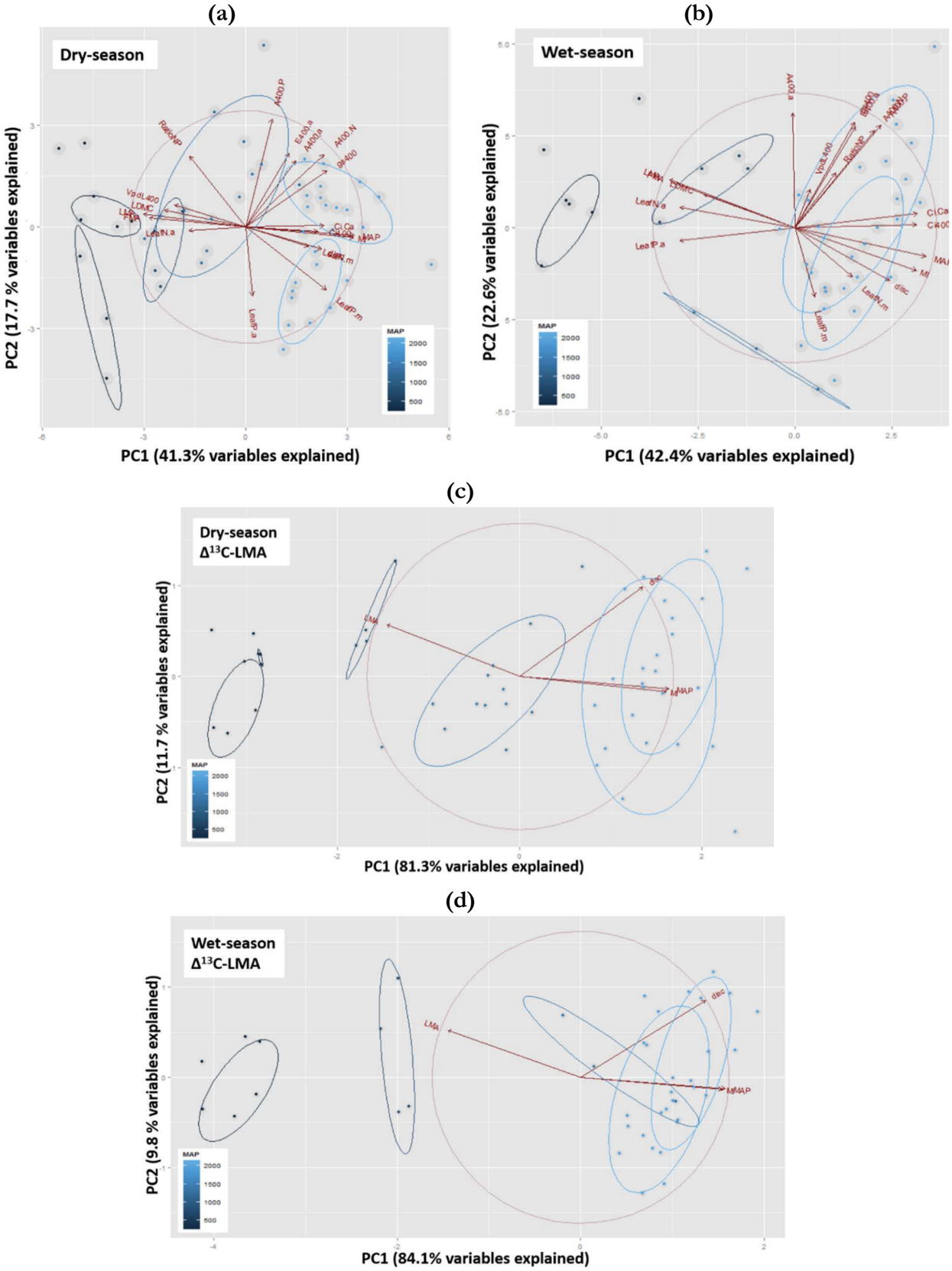

Figure 4.15: Results from principal component analyses to visualize the trait-species data into dimensional axes.

(a) All traits with MAP and MI during the dry-season, (b) during the wet-season, (c) only $\Delta^{13}C$ and LMA with MAP and MI during the dry-season and (d) wet-season. The ellipsoids represent normal data intervals.

Discussion

Characterising climate variability with ⊿^{13}C

The aims of the analyses undertaken in this chapter were to provide better understanding of: (a) how environmental constraints (at a site-level) affect ^{13}C composition of leaves (at a species-level); and (b) cross-species relationships of $\Delta^{13}C$ with other leaf-traits. Discrimination against ^{13}C ($\Delta^{13}C$) as well as 16 other leaf attributes from replicate leaves from four-to-six individuals of the dominant tree species from phylogenetically distant plant families at each site were measured for 55 vascular plant species during the dry-season and 44 species during the wet-season, from seven SuperSites across Australia. The coverage in this study of $\Delta^{13}C$ and cross-species comparisons of other trait values with $\Delta^{13}C$ based on (i) a spatial scale and hence climate zone and biome type, (ii) numbers of phylogenetically distant species and (iii) number of traits considered together is substantially larger than most of those of previous data compilations (Cernusak *et al.*, 2011; Miller *et al.*, 2001; Schulze *et al.*, 1998b; Stewart *et al.*, 1995).

The results in this study indicate that $\Delta^{13}C$ is a powerful tool for characterising the variability in climate across continental Australia. This chapter documents: (i) strong positive correlations of bulk-leaf $\Delta^{13}C$ (and a strong negative correlation of leaf intrinsic water-use-efficiency from calculated $\Delta^{13}C$) of the dominant overstorey species with mean annual precipitation and moisture index during both seasons and (ii) up to 3.7‰ differences during dry-season and 4.5‰ differences during wet-season in $\Delta^{13}C$ among biomes (dry-season: Adj r^2_{MAP} = 48.3%, r^2_{biome} = 45% and wet-season: Adj r^2_{MAP} = 57.1%, r^2_{biome} = 55.8% from one-way ANOVA model). This study presents the largest spatial analyses across Australia to which this correlation has been documented and also takes seasonal availability of water into account. Several studies, for example, at smaller regional scales in northern Australia (Cernusak *et al.*, 2011; Miller *et al.*, 2001; Schulze *et al.*, 1998b) and southern Queensland (Stewart *et al.*, 1995) have previously recorded correlations between $\Delta^{13}C$ and MAP. Miller *et al.*, (2001) and Schulze *et al.*, (1998b) obtained a flat community-level response of $\Delta^{13}C$ to a strong MAP gradient along the Northern Australian Tropical Transect, NATT (Koch *et al.*, 1995). Another non-significant correlation of $\Delta^{13}C$ with MAP was observed in a study in northern Australia ranging in MAP from about 300 mm to about 1700 mm (Cernusak *et al.*, 2011). The results of these studies in northern Australia contrast with the study in eastern Australia (Stewart *et al.*, 1995) and several other

studies for example in north-America (Diefendorf *et al.*, 2010) and in Africa (Midgley *et al.*, 2004); all of these latter studies obtained highly significant correlations of foliar $\delta^{13}C$ or $\Delta^{13}C$ with MAP. Cernusak *et al.*, (2011) concluded that, the non-significant relationship of $\Delta^{13}C$ with MAP resulted from a nearly constant instantaneous measurements of C_i/C_a ratio that was observed in the closely related genera of *Eucalyptus* and *Corymbia* investigated in their study in northern Australia. An increase in C_i/C_a with increasing MAP observed in eastern Australia documented by Wright *et al.*, (2001) can therefore explain a strong response of $\Delta^{13}C$ with MAP obtained in that region (Stewart *et al.*, 1995). In the present study, a significant correlation of C_i/C_a was identified both during the dry- and the wet-season sampling (**Figure 4.9a**, **b**) across an eightfold increase in MAP that consequently resulted in a strong response of $\Delta^{13}C$ to MAP.

Unlike some of the studies in northern Australia that focused mainly on the closely related genera of *Eucalyptus* and *Corymbia* (Cernusak *et al.*, 2011; Miller *et al.*, 2001), Schulze *et al.*, (1998b) encompassed a broad taxonomic range of woody plant species also in northern Australia but these authors still only obtained a weak community-level response of $\Delta^{13}C$ to MAP. Cernusak *et al.*, (2011) and Miller *et al.*, (2001) argued that these contrasting results of strong *versus* flat responses of $\Delta^{13}C$ and C_i/C_a to MAP in northern *versus* eastern Australia could have resulted from differences in seasonality of rainfall in these two regions. Rainfall in monsoonal northern Australia shows a much stronger seasonal distribution and the occurrence of the rainfall is regular from year-to-year whereas, rainfall in eastern Australia is more evenly distributed over the course of the year. Hence the influence of seasonal water availability is an important factor to consider while interpreting the responses of $\Delta^{13}C$ (and WUE_i calculated from $\Delta^{13}C$) and C_i/C_a across a moisture gradient. In the present study, repeated measurements of $\Delta^{13}C$ and other leaf-traits were made during the dry- and wet-season and bivariate linear regression analyses were performed separately for each season. Although mean annual precipitation (and moisture index) could adequately capture the variation of $\Delta^{13}C$ across the continent, it was indeed found to be modulated by precipitation seasonality to some extent. For the same species sampled both during the dry- and wet-season, (i) site mean values of $\Delta^{13}C$ was larger during the wet-season than the dry-season sampling by 0.01 to ~ 2‰ in five of the seven sites (exceptions for CM and CP); and (ii) C_i/C_a showed a stronger increase with increasing MAP during the wet-season (i.e. during the growing season when canopy photosynthesis is the most active) and this was also reflected on $\Delta^{13}C$ by a stronger increase during the wet-season than the dry-season. An

increase in the wet-season from the dry-season $\Delta^{13}C$ indicates that plants are responding to water availability in terms of discriminating against ^{13}C. The smallest increase (0.01‰, **Figure 4.4a** and **Table 4.10**) in community-averaged $\Delta^{13}C$ of the wet- from the dry-season sampling occurred at the site AMU as was expected from the flat-to-no responses of $\Delta^{13}C$ to increasing water availability that is well-documented from several studies in northern Australia (Cernusak *et al.*, 2011; Miller *et al.*, 2001; Schulze *et al.*, 1998b). Schulze *et al.*, (1998b) also recorded a response of $\Delta^{13}C$ to MAP in northern Australia only below the zone of influence of the monsoonal rains, and where conditions were inherently drier. In contrast with AMU, the largest increase in community-averaged $\Delta^{13}C$ of the wet from the dry-season sampling occurred at the site WR (~2‰) this site also had smaller precipitation seasonality (from the WorldClim climate variables BIO_{15}, which gives the precipitation seasonality values as coefficient of variation of inter-annual rainfall, **Table 4.10**). In the site CM, however, the dry-season community-averaged $\Delta^{13}C$ was larger than that of the wet-season. CM also showed the largest actual evapotranspiration from the SILO dataset during the dry-season and this could be attributed to the use of groundwater or stored soil water (this will be discussed further in the next section).

Table 4.10: Comparison of community-averaged $\Delta^{13}C$ from the dry- and wet-season sampling and precipitation seasonality (WorldClim variable BIO_{15})

Site	Community-averaged $\Delta^{13}C$		Precipitation seasonality
	Dry-season	Wet-season	
CM	19.76 ± 0.50	19.15 ± 0.92	17
WR	21.55 ± 1.71	23.51 ± 0.47	24
GWW	18.44 ± 0.84	18.72 ± 1.03	30
CP	21.87 ± 1.04	21.64 ± 1.10	33
AMU	19.83 ± 0.09	19.84 ± 0.83	61
RC	24.06 ± 1.57	24.31 ± 1.41	76
CT	22.99 ± 1.60	23.08 ± 1.43	93

So, what are the mechanisms that underpin the relationship between water availability and $\Delta^{13}C$ that is observed in this study at a continental scale? Essentially, $\Delta^{13}C$ recorded in plant tissues measures the intercellular concentration of CO_2 (C_i) at the time of photosynthesis, which reflects the balance between rates of CO_2 supply to, and demand from, the

intercellular air spaces (Farquhar *et al.*, 1982). $\Delta^{13}C$ of a particular leaf is negatively related to the ratio of net photosynthetic assimilation and the conductance of CO_2 into the leaf (Farquhar *et al.*, 1989; Farquhar *et al.*, 1982) depending also on the plant being able to sustain the co-occurring transpiration that requires the acquisition and transport of water at rates equal to the evaporative demand (Miller *et al.*, 2001). Leaf intrinsic water-use-efficiency (WUE_i) calculated from $\Delta^{13}C$ is defined by the ratio of net photosynthetic assimilation to stomatal conductance of water (g_w). Here, g_w is slightly different to conductance to CO_2 because of the difference in diffusivity of water and CO_2 in air. I calculated g_w by multiplying the conductance of CO_2 into the leaf by a factor of 1.6 (equation 1, "*Methodology and statistical analysis*", also see **Chapter 1** for details). A decrease in $\Delta^{13}C$, indicative of plant discriminating less against ^{13}C (and an increase in WUE_i) can arise either from a decrease in stomatal conductance or an increase in net photosynthetic assimilation and the balance between these two leaf attributes controls the ratio of intercellular and atmospheric concentration of CO_2, C_i/C_a (Cernusak *et al.*, 2011). When water availability decreases, plants respond by imposing increased stomatal limitation, i.e., decreasing stomatal conductance relative to photosynthetic capacity thereby decreasing C_i/C_a ratio (Comstock and Ehleringer, 1992; Miller *et al.*, 2001; Schulze *et al.*, 1998b; Ehleringer and Cooper, 1988) and C_i/C_a ratio being directly proportional to $\Delta^{13}C$, generates a decreasing $\Delta^{13}C$ and an increasing leaf intrinsic water-use-efficiency (WUEi,) with decreasing water availability (Werner *et al.*, 2012; Farquhar and Richards, 1984; Farquhar and Sharkey, 1982; Williams and Ehleringer, 1996).

To investigate the effect of climate variables on $\Delta^{13}C$, 19 climate parameters in addition to MAP were considered in multiple regression analyses. Other than MAP, isothermality as a secondary predictor during the wet-season was the only model with notable explanatory power (**Table 4.6**). This result indicates that isothermality had a weak but significant influence on $\Delta^{13}C$ in addition to MAP during the wet-season and this was statistically independent of its covariance with MAP. It is likely that less stomatal regulation was imposed on leaves in the sites which had more even day-to-night temperature oscillations over the course of the year, thereby generating an influence of isothermality on $\Delta^{13}C$ and this effect was more pronounced during periods of abundant water availability (i.e. during the wet-season).

Seasonal differences in $\Delta^{13}C$

Bulk-leaf $\Delta^{13}C$ is modulated by the canopy C_i/C_a at the time when the leaf dry matter was synthesized. Therefore, an ambiguity associated with interpreting $\Delta^{13}C$ patterns arises in order to determine whether it provides information about C_i/C_a only during favourable conditions in the wet-season when canopy photosynthesis is the most active, or whether it provides information about year-round variation in C_i/C_a along the precipitation gradient, including during the dry-season when water is least available (Cernusak *et al.*, 2011). This ambiguity can be addressed if $\Delta^{13}C$ values from both dry- and wet-season can be compared in addition to complementary information provided by instantaneous gas-exchange measurements. In this study, both C_i/C_a and $\Delta^{13}C$ showed stronger increase with increasing MAP during the wet-season indicating that, growing-season $\Delta^{13}C$ can more reliably predict its responses to water availability. Similar results were previously found in the rainfall gradient study across the northern Australian tropical transect (Schulze *et al.*, 1998b). These authors demonstrated that, $\Delta^{13}C$ was about 2‰ lower in young leaves than in expanded leaves, but this value did not change any further between fully expanded fresh leaves and old leaves that had experienced a full dry-season. Thus they concluded that, $\Delta^{13}C$ represented the conditions during the growing season rather than the conditions over the whole year, despite the fact that leaves start sprouting at the end of the dry-season with deciduous species being earlier than evergreens (Williams *et al.*, 1997).

Plant functional diversity

Bulk-leaf $\Delta^{13}C$ has also been used to identify the functional diversity of water use strategies of co-occurring species in various natural plant communities. Several studies found that $\Delta^{13}C$ is a reliable indicator of water-use-efficiency of co-occurring species of contrasting life forms and phylogenetically distant plant families (Jongen *et al.*, 2015; Moreno-Gutiérrez *et al.*, 2012; Scartazza *et al.*, 2014; Werner and Máguas, 2010). Plant functional types have also explained a considerable amount of variability of $\Delta^{13}C$ within sites in several studies (Diefendorf *et al.*, 2010; Jongen *et al.*, 2015; Werner and Máguas, 2010). In the current dataset, $\Delta^{13}C$ of only the dominant overstorey species was measured; most of these species, however, were broad-leaf evergreen trees. A list of species with species-specific $\Delta^{13}C$ and calculated WUE_i is presented in Appendix **Table A1**. Since there was a very small number of shrubs and needle-leaf trees in comparison with broad-leaf evergreens, $\Delta^{13}C$ values in this particular dataset were too restricted in terms of functional types to obtain a

statistically meaningful comparison and therefore, an analysis based on plant functional types was not included in this study.

Seasonal variation in $\Delta^{13}C$ in reference to Budyko framework

Another objective of this chapter was to look at how the seven SuperSites spread across the continent behave in reference to the widely used Budyko framework of energy and water limitation of evapotranspiration. Measurement of actual evapotranspiration is not as straightforward as measurement of precipitation and is estimated using different models developed over many years using mainly meteorological data. Potential evapotranspiration is generally calculated using the Penman-Monteith equation for a reference crop height assumed to be regulated by energy, atmospheric demand and plant and soil surface conductance (Allen *et al.*, 1998). In this present study, Morton's potential and actual evapotranspiration over land (Morton, 1983) obtained from the SILO patched point data were used to calculate the long-term annual and seasonal averages of Φ and ε. A comparative study investigated the applicability of Morton's environmental evapotranspiration estimates (defined by Morton, (1983) as the evapotranspiration that would occur when the availability of water is not a limiting factor) in comparison to Penman's potential evapotranspiration estimates in 26 meteorological stations across Australia (Chiew and McMahon, 1991). These authors concluded that Morton's environmental evapotranspiration is conceptually a more correct representation of the upper limit of actual evapotranspiration compared to Penman's potential evapotranspiration from different climatic regions throughout Australia and provide similar magnitudes of the upper limit of actual evapotranspiration particularly at moderate climatic conditions. However, Morton's method has also been found not to be very accurate for short periods e.g. daily evapotranspiration estimates (Granger and Gray, 1990). Actual evapotranspiration obtained from eddy covariance measurements for four consecutive years (August 2010 - August 2013) in the site CM, for the year 2013 in GWW and for August 2012 - July 2014 for AMU were available (Cleverly *et al.*, 2016; Macfarlane, 2013; Sun *et al.*, 2015) and compared with Morton's actual evapotranspiration obtained from SILO data as shown in **Table 4.11**. A regression of actual evapotranspiration *versus* Morton's estimate of evapotranspiration yields a significant linear regression ($r^2 = 0.68$) but a slope of 0.71, indicating Morton's estimate was typically 29% lower than that observed from eddy covariance data. Consequently, this is likely to influence the location of each data point in **Figure 4.6** and **Figure 4.7**, making most of the points to move vertically.

Table 4.11: A comparison of ET_a values obtained from eddy covariance measurements and Morton's estimation

Site	Year	Actual evapotranspiration (ET_a)	
		Eddy covariance measurements Σ (mm)	**Morton's estimation Σ (mm)**
CM*	Aug 2010-Dec 2010	283.9	303.8
	Jan 2011-Dec 2011	643.0	581.4
	Jan 2012-Dec 2012	695.9	509.2
	Jan 2013-Dec 2013	394.4	266.2
GWW	Jan 2013-Dec 2013	271.2	420.6
AMU	Sep 2010-Aug 2011	517.5	660.4
	Sep 2011-Aug 2012	203.4	282.8
	Sep 2012-Aug 2013	150.8	182.1
	Sep 2013-Aug 2014	247.6	253.7
	Sep 2014-Aug 2015	244.6	236.8

*Estimated transpiration using (Ritchie, 1972).

The distribution of the SuperSites with reference to the Budyko curve reveals that the observed water use in these sites deviated from its expected dependence on energy and water balances more in some sites than others (**Figure 4.6** and **Figure 4.7**). Relatively more scatter from the theoretical Budyko framework is observed if shorter temporal scales are employed (≤ 1year) due generally to the absence of steady-state conditions (Zhang *et al.*, 2008). In this study, dryness and evaporative indices were calculated for five 25-year tiles from 1890-2014 and mean of 125-year is also reported to eliminate the effect introduced due to short temporal scales. Another assumption of the Budyko curve is that for each site the water balance is adequately described by the relationship:

$$\text{Precipitation} = \text{Runoff} + \text{evapotranspiration}$$

This assumes that there is no significant contribution, i.e., losses to or gains from external sources (for example, groundwater, stored soil water etc.) (Donohue *et al.*, 2007). In this dataset, the highest mean value of annual evaporative index and dry-season evaporative index was observed in the site CM. CM is a site near Chowilla floodplain where groundwater resources are in shallow proximity to the soil surface and vegetation has previously been shown to rely to some extent on saline groundwater during the frequent

and long dry spells (O'Grady and Holland, 2010). Rates of annual evapotranspiration larger than annual precipitation have also previously been recorded in this site and several authors concluded that the vegetation is using water stored in the porous geological substrates from previous wetter periods (Meyer *et al.*, 2015; Swaffer *et al.*, 2014).

The two wettest site, FNQ and WR, fell closest on the theoretical Budyko curve only during the wet-season, whereas, long-term annual average of the drier sites (except AMU) fell above the curve. This might indicate that the ecosystem evaporates and transpires more water than that would be expected for these sites, possibly resulting from groundwater input or run-on of rainwater. Also, all the sites had dryness indices greater than 1 which once again highlights the dominance of water-limited environments in Australia and similar observations in Australian catchments have previously been recorded in Donohue *et al.*, (2007). Interestingly, even for the wettest sites (e.g., FNQ, WR), the evaporative index ε was larger than 1 during the dry-season, indicating that even the wettest sites in this study were not energy limited during the dry-season. The dryness index Φ of Australian rainforests determined in the present study are larger than many other rainforests across the world (Jones *et al.*, 2012), indicating that Australian rainforests are also drier than rainforests on other continents.

Long-term *annual* average of actual evapotranspiration (indicated by evaporative indices) calculated in five 25-year tiles from 1890-2014 varied less in arid sites compared to variation in potential evapotranspiration (indicated by dryness indices). In contrast in humid sites, variation in long-term annual average of actual evapotranspiration was not significantly different than that of potential evapotranspiration. Similar behaviour of desert and grassland ecosystems has previously been recorded in Jones *et al.*, (2012). Long-term *seasonal* average of ε varied less during the dry-season compared to variation in Φ and this variation was more pronounced in the drier sites, whereas, variation in ε was not markedly different compared to variation in Φ during the wet-season. These differences in variation between Φ and ε of arid and humid sites as well as during the dry- and wet-seasons relative to the Budyko curve might suggest that ecosystems regulate their water use (the major component of ET_a) to compensate for climate variability as revealed by variation in potential evapotranspiration (ET_p) at the arid sites and during the dry-season, but this impact was less pronounced at humid sites and during the wet-season at all sites.

Relative contribution of assimilation and stomatal conductance to $\Delta^{13}C$ and WUE_i

Instantaneous gas-exchange measurements were compared with $\Delta^{13}C$ and strong correlations between the bulk-leaf $\Delta^{13}C$ and leaf intrinsic water-use-efficiency calculated from gas-exchange measurements were identified for both seasons (**Figure 4.10c**) such that, species that discriminated less against ^{13}C also showed significantly larger intrinsic water-use-efficiency calculated from the ratio of A400.a to g_s400. This correlation, however, appeared to be stronger with higher r^2 values and levels of significance during the dry-season than the wet-season. There was also a significant shift along the slope of the SMA regression, i.e. a shift of the wet-season sampling towards the more discriminatory end of the spectrum compared to dry-season sampling for the same species sampled during both seasons. This finding confirms of the dominant overstorey across sites discriminating less against ^{13}C at the drier sites than wetter sites and even less during the dry-season.

For C3 plants, where $\Delta^{13}C$ is primarily controlled by C_i/C_a, coordination between stomatal conductance, photosynthesis and leaf area adjustments tends to constrain the potential environmentally driven range of $\Delta^{13}C$ (Cernusak *et al.*, 2013). An ambiguity associated with interpreting the bulk-leaf $\Delta^{13}C$ is to adequately explain the relative contribution of net A400.a and g_s400 that controls the C_i/C_a ratio. From the analyses presented here, an important difference in $\Delta^{13}C$ between dry- and wet-season sampling has been identified. During the dry-season, $\Delta^{13}C$ showed significant a relationship with g_s400 but not with A400.a but during the wet-season, $\Delta^{13}C$ showed significant a relationship with A400.a but not with g_s400. The C_i/C_a ratio, however, was significantly associated with g_s400 during both seasons. Strong positive relationships of g_s400 and C_i/C_a with MAP (**Figure 4.8** and **Figure 4.9**) and a weak but significant relationship of g_s400 with $\Delta^{13}C$ (**Figure 4.11b**) *only* during the dry-season might suggest that during the dry-season, C_i/C_a (and therefore, $\Delta^{13}C$) was more strongly regulated by stomatal conductance than photosynthetic capacity. Similarly Cernusak *et al.*, (2011) concluded that changes in photosynthetic capacity per unit leaf area between the wet- and dry-season were unlikely to account for seasonal changes in rates of canopy photosynthesis. Roussel *et al.*, (2009) also observed that variability of $\Delta^{13}C$ in six genotypes of *Quercus robur* family displaying extreme phenotypic values of $\Delta^{13}C$ can be ascribed to differences in stomatal conductance and stomatal density but not in photosynthetic capacity. However, during the wet-season, a significant correlation between A400.a and $\Delta^{13}C$ (**Figure 4.11a**) was also observed in this present study. This correlation and an apparent lack of correlation between $\Delta^{13}C$ and g_s400 (wet-season, **Figure 4.11b**) in

spite of a highly significant correlation between C_i/C_a and g_s400 (wet-season, **Figure 4.12b** suggest that photosynthetic capacity more strongly regulates the $\Delta^{13}C$ signal than stomatal conductance when canopy photosynthesis is the most active under favourable condition of water availability.

⊿^{13}C and leaf morphology

The results presented in this study demonstrated that leaf morphology at site/species level reflects environmental constraints on plant growth. Several studies have shown that reduced water availability results in thicker and/or denser leaf tissues (Abrams *et al.*, 1994; Groom and Lamont, 1997; Lamont *et al.*, 2002; Witkowski *et al.*, 1992). Species with thicker and denser leaves (resulting in larger values of LMA) are therefore expected to occur where less water is available (Abrams *et al.*, 1994; Reich *et al.*, 1999). Similarly, less discrimination against ^{13}C (i.e. smaller values of $\Delta^{13}C$) is also expected as a response to reduced water availability due to increased stomatal regulation. I found that $\Delta^{13}C$ was most strongly (and as expected, inversely) associated with LMA among all the leaf attributes considered during both the dry- and wet-seasons and this correlation suggests that, there is a physiological relationship between leaf structure and water availability. Lamont *et al.*, (2002) suggested possible ecophysiological mechanisms linking $\Delta^{13}C$ and LMA (smaller $\Delta^{13}C$ being associated with larger LMA) through their effects on decreasing C_i:

(i) with lower soil water availability, stomatal conductance will decrease (decrease in g_s thereby causing a decrease in $\Delta^{13}C$); and

(ii) with thicker palisade and denser tissues (due to increase in LMA), (a) there is greater demand for carbon per unit leaf area (increase in photosynthetic carbon assimilation), (b) internal (mesophyll) conductance will decrease (Hanba *et al.*, 1999) and (c) resistance to water flow will increase, reducing turgor and stomatal conductance.

Among the leaf nutrient traits, $LeafN_{mass}$ showed significant positive relationships with both MAP and MI for both seasons (**Table 4.9**). However, it did not show a relationship with $\Delta^{13}C$. $LeafP_{mass}$ showed a significant positive relationship with both MAP and MI as well as with $\Delta^{13}C$ only during dry-season (**Table 4.9**, **Figure 4.14b**). $LeafN_{area}$ showed significant negative relationships with both MAP and MI (**Table 4.9**) and it was also associated with $\Delta^{13}C$ during both seasons (**Figure 4.14a**). $LeafP_{area}$ showed significant negative

relationships with MAP and MI (**Table 4.9**) and was associated negatively with $\Delta^{13}C$ (**Figure 4.14c**) only during the wet-season. For all these traits, the nature of significant positive or negative relationships obtained from (a) bivariate linear regression with MAP and MI and (b) standardised major axis regression with $\Delta^{13}C$ was consistently similar; indicating that $\Delta^{13}C$ at the species-level reliably reflects the water status at the site-level. The lack of association between the nitrogen concentration on a mass basis and $\Delta^{13}C$ obtained was consistent with weak relationships of the same observed by Schulze *et al.*, (1998b). These results might also suggest that water availability, (and not foliar nutrient content), is the possible factor that have directly influenced $\Delta^{13}C$ signatures (Lamont *et al.*, 2002; Schulze *et al.*, 1998b). The significant correlations with $\Delta^{13}C$ obtained from nutrients expressed on an area basis and not on a mass basis might also have resulted from the significantly strong correlations between $\Delta^{13}C$ and LMA (Lamont *et al.*, 2002).

The predictive power of $\Delta^{13}C$ for the identification of plants' response to water availability was further tested using principal component analysis. When 16 leaf attributes were considered, $\Delta^{13}C$ showed the strongest positive relationship with MAP and MI after LMA and FMA during both seasons, although this relationship appeared to be stronger during the dry-season. The dominant species from the very low to low MAP (and MI) sites could distinctly be identified from those that were from high to very high MAP (and MI) sites (**Figure 4.15**). Since $\Delta^{13}C$ and LMA were two of the most site-stable leaf-traits of all the traits examined, separate PCA models were generated with MAP and MI using only these two leaf-traits. This model however, could explain ~93% variation in the dataset during both dry-and wet-season and a distinct separation of the species from drier and wetter sites was still obtained (**Figure 4.15c and 4.15d**) indicating that $\Delta^{13}C$ like LMA, can provide reliable information about species-specific differences related to environmental constraints. In these PCA models, $\Delta^{13}C$ appeared to be more closely (and inversely) associated with level of sclerophylly than nutrient status among the dominant evergreen species across Australia, with an independent variation of water and nutrient supply at the sites.

Conclusions

Since plant physiology at the leaf-level is important in controlling species distributions along a moisture gradient, interpretable patterns of leaf physiological functions should also be associated with the gradient. The results presented in this chapter indicate that stable carbon isotope ratios of the dominant evergreen overstorey species indeed can provide

meaningful insights on plant water status across diverse habitats and can reliably be used as an indicator of different ecophysiological strategies influenced by environmental constraints in C3 plants at a continental scale in Australia.

Chapter 5 An evolutionary perspective on bulk-leaf ^{13}C discrimination and its correlates

Introduction

Species-specific leaf-traits, for example, leaf stomatal conductance, photosynthetic water-use-efficiency and discrimination against carbon-13 ($\Delta^{13}C$) are often used to characterize plant water relations within ecological communities (Moreno-Gutiérrez *et al.*, 2012). These traits respond to transpirational demand and water availability experienced by a plant in its environment and there has been a substantial volume of research focusing on demonstrating significant correlations between these traits and their correlations with water availability, comparing both within-species and across distantly related species within communities (this is discussed in detail in **Chapter 4**). Results from these studies broadly support the view that there exists a set of "general" relationships between leaf-traits and water availability. These relationships sometimes impose significant constraints on the number of different ways in which a plant might adapt to a given environment, resulting in plant functional convergence at a large scale (Bucci *et al.*, 2004; Edwards, 2006; Meinzer, 2003). Environmental temperature, like water availability, is a fundamental condition linked to the growth and survival of plant species, and most species have evolved some ability to endure drought or stressful temperatures. Indeed, the ability of species to endure adverse climatic conditions plays a crucial role in defining the fundamental niches of species (Addo-Bediako *et al.*, 2000). However, this ability of species to respond to adverse or changing environments may also to some degree be constrained by their evolutionary history (Kellermann *et al.*, 2012). Although much comparative ecophysiological research focuses on interspecific patterns of leaf-traits distributed across ecological communities, few studies focus on how they are distributed across evolutionary lineages.

The primary objective of comparative studies that investigate the relationship between two traits and/or a trait with an environmental or climatic variable across a range of species, is

to assess whether one variable is correlated with another or whether the regression of one variable on another differs significantly from some expected outcome. From a purely statistical point of view, some researchers argue that in cross-species analyses, the species involved are part of a hierarchically structured phylogeny and therefore cannot be regarded as independent data points randomly drawn from the same distribution, thus violating one of the fundamental assumptions of most statistical tests. The lack of independence of two variables involved in any statistical analysis might - a) inflate the degrees of freedom and thereby complicate tests of significance and b) ignore the possibility that the apparent relationship between the two variables obtained from any statistical model might have been altered, sometimes by creating functional relationships where none exist (Felsenstein, 1985; O'Connor *et al.*, 2007). Another issue associated with traits with shared ancestry is that while the effect sizes that are sampled from a population have normal distributions with an expected variance, there are differences in variances when the effect sizes have a phylogenetically correlated structure because lineages within phylogenies may have evolved at different rates (Harvey and Pagel, 1991; Koricheva *et al.*, 2013). Violating these fundamental assumptions can sometimes variously misrepresent the strength of relationships between variables (Felsenstein, 1985; Harvey *et al.*, 1995). For example, Ackerly and Reich, (1999) demonstrated that several strong cross-species correlations between leaf size and other ecophysiological traits like leaf life span, photosynthetic assimilation on a mass basis, total leaf nitrogen on a mass basis and leaf conductance disappeared when evolutionary history was taken into account. They showed that the strong non-phylogenetic association between leaf size and leaf life span in particular resulted because interspecific correlations mainly reflected differences *between* the angiosperms and the conifers while phylogenetic analyses identified no significant correlation between these traits *within* each of these two groups. In **Chapter 4** of this thesis, the cross-species relationship of bulk-leaf discrimination against carbon-13 ($\Delta^{13}C$) with climate variables and leaf structural, functional and gas-exchange traits have been investigated across a continental scale in Australia. The primary objective of this chapter is to formally include phylogenetic information of the extant taxa involved in the comparative analysis in order to re-evaluate some of these relationships from an evolutionary perspective.

For at least a century, ecologists have been highlighting the influence of climate on leaf-traits including the "the worldwide leaf economics spectrum" (Wright *et al.*, 2004). Often

leaf-traits show predictable ecological patterns along gradients of climate. For example, an increase in leaf mass per unit area (LMA) has been demonstrated in species inhabiting arid and semi-arid regions in a number of studies (Eamus *et al.*, 2006b; Fonseca *et al.*, 2000; Niinemets, 2001; Schulze *et al.*, 1998b; Wright *et al.*, 2001; Wright *et al.*, 2004). This pattern suggests that plants exposed to severe water-stress evolve tissues that are more resistant to water loss or less susceptible to drought induced damage (for example xylem embolism). Another leaf-trait that in several studies demonstrated strong responses to climate, particularly availability of water, is discrimination against ^{13}C ($\Delta^{13}C$). **Chapter 4** documented that 57% of variation in $\Delta^{13}C$ in the wet-season and 48% of variation in the dry-season was explained by mean annual precipitation in Australia. Because of the high plasticity observed in some leaf-traits (e.g. LMA and $\Delta^{13}C$) in response to climatic perturbations, it is often assumed that these traits are evolutionarily "labile" (Edwards, 2006). However, interpreting patterns observed in broad ecological communities in response to climatic factors as evidence of *de facto* adaptive evolution can sometimes be misleading (Ackerly and Reich, 1999; Edwards, 2006) since there are a number of processes that underpin the assembly of ecological communities. For instance, reduction in specific leaf area (SLA) has been found repeatedly to be linked with drier climatic conditions across a number of species-pairs in Australia (Cunningham *et al.*, 1999) indicating consistent response of SLA to water availability. Preston and Ackerly, (2003), however, found inconsistent responses of xylem and leaf hydraulic conductivity and Huber value to water availability in several lineages of California chaparrals, suggesting the response of hydraulic pathway to water-stress is more lineage-specific than habitat-specific and probably depends on the physiological characters present in the lineage. Understanding how climatic factors shape current species distributions (Helmuth *et al.*, 2005; Pörtner and Farrell, 2008; Somero, 2010) as well as the degree to which plants-traits are influenced by evolutionary processes (Fu *et al.*, 2012; Little *et al.*, 2010) while predicting the responses of species-specific leaf-traits to environmental constraints can provide valuable insights on the relative importance of these traits in ecological adaptation of plants as well as how traits are evolutionary correlated.

Chapter 4 of this thesis mainly highlighted the relationship with $\Delta^{13}C$ and leaf intrinsic water-use-efficiency (WUE_i) calculated from $\Delta^{13}C$ with climate variables and leaf structural, nutrient and gas-exchange traits. Strong positive correlations of bulk-leaf $\Delta^{13}C$ (and a strong negative correlation of WUE_i calculated from $\Delta^{13}C$) of the dominant overstorey

species with mean annual precipitation (MAP) and moisture index (MI) during dry- and wet-seasons separately across the continent has been documented. $\Delta^{13}C$ has also been found to have statistically significant patterns with climate variables other than MAP (see **Chapter 4**). These findings were underpinned by the core assumption that variation in $\Delta^{13}C$ principally results from adaptive environmental convergence and thus is largely independent of phylogenetic history. Nevertheless, certain observations indicate that while some species demonstrate plasticity for $\Delta^{13}C$ from species-climate interactions, others were inherently stable across environments (Turner *et al.*, 2010; Turner *et al.*, 2008). In one study, Turner *et al.*, (2010) found that some *Eucalyptus* species (for example, *E. ewartiana*, *E. youngiana*, *E. kingsmillii* and *E. leptopoda*) had genetically stable values of $\Delta^{13}C$ under variable environmental conditions, whilst *E. globulus* in contrast demonstrated phenotypic plasticity of $\Delta^{13}C$ pertaining to water availability (Macfarlane *et al.*, 2004).

In this chapter, the focus has moved from ecological communities to closely related species spanning different habitats in order to investigate whether relationships of $\Delta^{13}C$ with climate variables reflect patterns of evolutionary convergence, or whether they emerge principally from the characteristics of major "seed-plant" lineages. Relationships between $\Delta^{13}C$ and climate variables/leaf structural, functional and nutrient traits have been re-evaluated from an evolutionary perspective using phylogenetic comparative methods. In addition, correlated evolutionary changes of $\Delta^{13}C$ with climate variables and $\Delta^{13}C$ with other leaf-traits have also been investigated. Specifically this chapter addresses the following questions:

1) Do species from similar environments tend to have similar values of $\Delta^{13}C$?
2) Is interspecific variation in $\Delta^{13}C$ / leaf structural, functional and nutrient traits and climate variables phylogenetically structured?
3) To what extent are the observed cross-species relationships between $\Delta^{13}C$ and climate variables/leaf-traits similar or different to analyses based on phylogenetic history of seedplants?
4) Do interspecific relationships between $\Delta^{13}C$ and climate variables and leaf-traits observed among cotemporary species provide statistically significant patterns of correlated evolutionary changes leading up to the present day? and finally,
5) Does variation in $\Delta^{13}C$ with climate variables principally results from adaptive environmental convergence?

Methodology

An overview of phylogenetic comparative methods

In this section, phylogenetic comparative methods (PCM) that have been employed in this chapter will be discussed with brief mathematical details. There exist conceptual and mathematical commonalities behind all of the PCMs used in this chapter and a brief explanation of these commonalities will be discussed for convenience of interpretation.

Models of evolutionary changes

A number of models of evolutionary change are employed in different PCMs. One of these models that is commonly used in studying the evolution of continuous features is the constant-variance random walk model of evolution, or, the Brownian motion model (Harvey and Pagel, 1991; O'Meara *et al.*, 2006; Pagel, 1999; Pagel, 2002). A Brownian motion model describes the evolution of a continuous trait as a random walk that continues independently for each of the daughter species after the occurrence of a speciation event. This model has some useful statistical properties, for instance, it results in a normal distribution of trait values across the phylogeny. The simplest version of the Brownian motion model assumes that trait values can increase or decrease at each instant of time with a mean change of zero and a fixed variance. This means that the expected covariance between trait values of two species at the tips of the phylogeny is exactly proportional to their shared history, i.e. the sum of their shared branch lengths, and the expected variance of a trait value for a given species is proportional to total length of the tree, i.e. the summed branch length from the root to the tip for that species (Felsenstein, 1985; Kamilar and Cooper, 2013). An example of a hypothetical phylogeny over which species trait-values can be simulated under Brownian motion is given below.

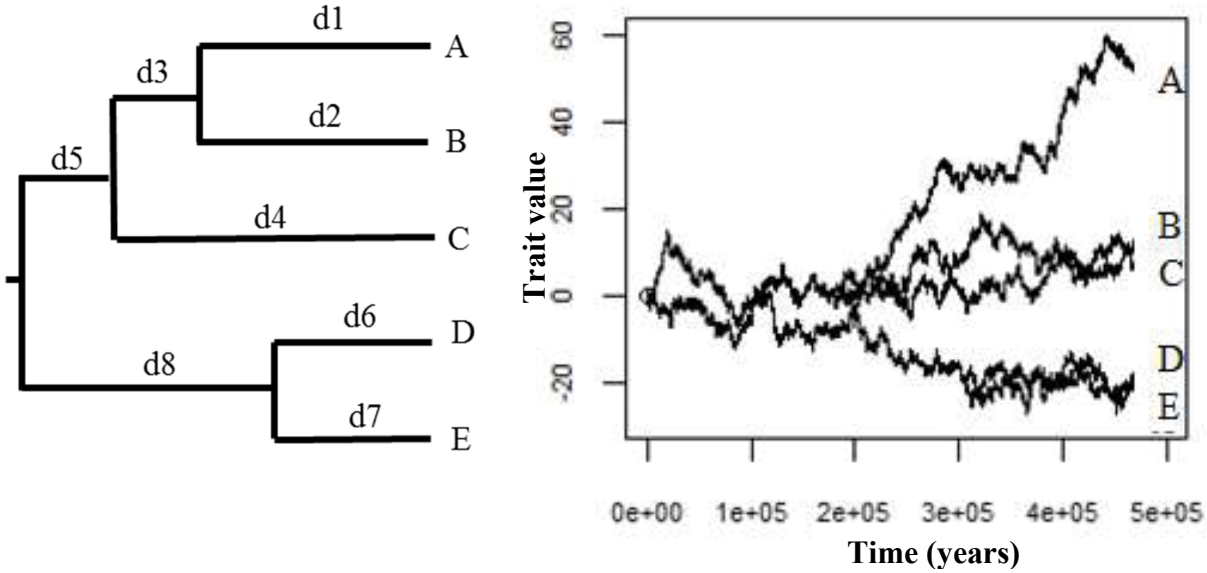

	A	B	C	D	E
A	d5+d3+d1	d5+d3	d5	-	-
B	d5+d3	d5+d3+d2	d5	-	-
C	d5	d5	d5+d4	-	-
D	-	-	-	d8+d6	d8
E	-	-	-	d8	d8+d7

Figure 5.1: An example of a phylogeny and simulation of a trait-value over the phylogeny under Brownian motion evolution with the corresponding variance-covariance matrix.

"-" indicates absence of shared history between two species therefore no covariance between them. d = branch length.

Figure 5.1 shows a hypothetical phylogeny with five extant taxa A, B, C, D and E and a simulation of a trait over the phylogeny under Brownian motion model of evolution. **Figure 5.1** also shows a 5 X 5 variance-covariance matrix calculated from the topology of the phylogeny. Branch lengths of each taxon are given by the letters *d1-d8*. The diagonals of the variance-covariance matrix represent the species variances which is the total length of the tree, whereas, the off-diagonals represent the covariances between each pair of species, which is the sum of their shared branch lengths. The shared history is measured by the ratio of shared branch lengths to the total length from root to tips of the tree. In context of a particular clade being studied, the degree of statistical non-independence in species trait-values can be expressed as a function of exactly how much shared history species exhibit. Employing the Brownian motion model greatly simplifies the maths needed to fit

evolutionary models, and it has been the model best studied to-date from an evolutionary perspective. Phylogenetic generalized least square (pGLS) and phylogenetically independent contrasts (PIC) are two PCMs that have been used in the data analyses part of this chapter, all of which also employ the Brownian motion model. These methods will be discussed further in the following sub-sections.

Testing for phylogenetic signal

In general, before applying any kind of PCM, it is recommended to test whether or not the shared ancestral history of the species involved in the analyses has influenced the distribution of the traits under investigation (Freckleton *et al.*, 2002; Johnson and Stinchcombe, 2007; Swenson *et al.*, 2007). One such approach is to quantify "phylogenetic signal" in order to determine how trait variation is correlated with the phylogenetic relatedness of species (Kamilar and Cooper, 2013). Phylogenetic signal can be defined as the tendency for closely related species to resemble each other, more than they resemble species drawn at random from a phylogenetic tree (Blomberg and Garland, 2002; Blomberg *et al.*, 2003; Kamilar and Cooper, 2013; Losos, 2008; Münkemüller *et al.*, 2012; Wiens and Graham, 2005). More simply, phylogenetic signal is the ecological similarity between closely related species. In context of this chapter for example, if $\Delta^{13}C$ of the leaves of closely related plant species have similar values and this similarity decreases as phylogenetic distance of these species increases, $\Delta^{13}C$ will show non-random and strong phylogenetic signal (Losos, 2008). Conversely, if $\Delta^{13}C$ values vary randomly across a phylogeny or show numerous cases where distantly related species converge on a similar value of $\Delta^{13}C$ while closely related species exhibit notably different values, $\Delta^{13}C$ is will show weak phylogenetic signal (Kamilar and Muldoon, 2010). There are a number of approaches available to test whether or not a particular dataset exhibits a phylogenetic signal; some of these approaches use autocorrelation methods while some use an explicit model of trait evolution. In this chapter, two methods have been employed to test for a phylogenetic signal - Blomberg's K (Blomberg *et al.*, 2003) and Pagel's λ (Freckleton *et al.*, 2002; Harvey and Pagel, 1991; Pagel, 1999). Both of these two parameters explicitly use a constant-variance Brownian motion model of trait evolution. When a strong phylogenetic signal of a particular trait underlying the interspecific variation is detected, this means that the trait concerned is an evolving trait in angiosperms and therefore, differences between species are related to their evolutionary trajectories. When this is the case, it suggests that PCMs might be usefully employed to

study the particular trait, because these methods can take into account the genealogical relationships between the species in a cross-species study.

Blomberg's *K* statistic quantifies the amount of observed variance in trait values relative to the variance expected under Brownian motion (Pagel, 1997). As described in Kamilar and Cooper, (2013), the *K* statistic is precisely a ratio of two mean square errors, MSE_0 to MSE, where, MSE_0 is the mean squared error of the data in relation to its phylogenetic mean and MSE is the mean squared error extracted from a generalized least-squares model that uses the phylogenetic variance-covariance matrix (see **Figure 5.1** for example) in its error structure. MSE_0 to MSE ratio is standardized by the expected mean squared error ratio under Brownian motion to make *K*-values comparable among phylogenies. $K = 0$ indicates no phylogenetic signal, $K = 1$ the trait has evolved exactly according to the Brownian motion model of evolution with strong phylogenetic signal and $K > 1$ indicates that close relatives are more similar than expected under a Brownian motion model of trait evolution. The significance of *K* (i.e., how significantly *K* is different from zero) can also be tested by randomizing the trait values across the tips of the phylogeny and calculating *K* multiple times and then calculating how many times the randomized trait-values produces higher values of *K* than the observed *K*-value. This will be discussed in more detail in the "*Data analyses using phylogenetic comparative methods*" section.

The second parameter that is used in this chapter to measure phylogenetic signal, is Pagel's λ (Freckleton *et al.*, 2002; Pagel, 1997; Pagel, 1999). Pagel's λ is a parameter that quantifies to what extent a dataset depends on the Brownian motion model of evolution given the topology of the phylogeny and scales the branch-lengths of the phylogeny accordingly. Using the maximum likelihood method, the algorithm calculates an optimal value of λ (between 0 and 1) with which the covariances of the variance-covariance matrix determined from a phylogeny is multiplied (see **Figure 5.1** for example). When optimized $\lambda = 0$, all the covariances are multiplied by 0, thereby, erasing all the evidence of shared history. Thus $\lambda = 0$ (or a very small value) indicates that the trait data are not phylogenetically influenced. Optimized $\lambda = 1$, indicates that the trait being studied has evolved exactly along the branches of the phylogeny according to the Brownian motion model of evolution thus there is evidence of phylogenetic history (Pagel, 1999). Any number between 0 and 1 indicates the presence of phylogenetic signal in the trait, but it has evolved according to a process other than pure Brownian motion (Freckleton *et al.*, 2002; Pagel, 1997; Pagel, 1999). Optimized λ can also be larger than 1, but, the upper bound is restricted because

off-diagonal branch lengths cannot exceed diagonal branch lengths in a phylogenetic variance-covariance matrix (**Figure 5.1**) (Freckleton *et al.*, 2002). Since λ is optimized using the maximum likelihood method, it can be tested whether the optimized λ-value is significantly different from a model in $\lambda = 0$ (i.e. no phylogenetic signal) or $\lambda = 1$ (i.e. Brownian expectation) using likelihood ratio tests (Pagel, 1997). If the optimized λ is significantly different from a model in which λ is fixed to be 0 but not significantly different from a model in which λ is fixed to be 1, a statistically significant phylogenetic signal is detected.

Patterns in phylogenetic signal in traits are sometimes used to provide information about evolutionary processes (Kamilar and Cooper, 2013). A weak/random signal is often interpreted as evolutionary lability (Blomberg *et al.*, 2003) because of closely related species developing larger differences in traits than expected due to high rates of trait evolution. Weak signals are also expected to characterize "adaptive radiation" because in this process species diversify rapidly to fill new niches thereby creating larger differences in traits between closely related species (Kamilar and Cooper, 2013). Strong non-random phylogenetic signal on the other hand, is expected to characterize phylogenetic conservatism (Losos, 2008). However, phylogenetic signal in traits can be influenced by many other external processes (for example, scale, taxonomic inflation etc.) (Losos, 2008) and therefore inferring evolutionary processes merely from phylogenetic signal is not always straightforward (Cooper *et al.*, 2010). In this chapter, the aim of testing phylogenetic signal was primarily to explore the potential for the statistical non-independence of trait values, not to infer differences in the rates of evolution solely based on phylogenetic signals.

A K or $\lambda = 0$ for trait values does not necessarily mean that a regression should only be performed non-phylogenetically. In fact, it is the residuals from a regression model that should show no significant phylogenetic signal to preclude the use of a phylogenetic analysis based on the statistical argument of non-independence (Kamilar and Cooper, 2013; Revell, 2010). If both predictor and response variables show strong non-random phylogenetic signal without any indication of phylogenetic pattern in the model residuals, then this particular situation indicates adaptive radiation of the response variable because the residuals of an analysis are not likely to show phylogenetic signal if a lineage rapidly diversifies with the newly formed lineages evolving different adaptations (Hansen, 2014). If related species tend to occur in similar environments (i.e., having similar values of their

predictor variables), the response variable is still expected to show phylogenetic signal (Hansen, 2014).

Testing for correlated evolution

Correlated evolution can be defined as the extent to which change in one variable is associated with change in another from a phylogenetic perspective (Felsenstein, 1985). In the context of this chapter, correlated evolution investigates whether $\Delta^{13}C$ and another climate variable/leaf-trait have evolved together. As discussed earlier, phylogenetic covariance is a property of the data not of the scientific hypotheses under investigation and therefore, wherever it exists, this covariance has to be taken into account if the aim is to avoid overestimation and obtain an unbiased cross-species relationships among variables (Blomberg *et al.*, 2012). It is especially important to use PCMs to investigate this type of analysis, particularly for leaf/plant traits, because of many dependencies of leaf/plant traits that have been found because of their shared ancestral history. Two method of studying correlated evolution have been used in this chapter, i) the Phylogenetic Generalized Least Square (pGLS) method and the ii) the Phylogenetically Independent Contrasts (PIC) method.

Phylogenetic Generalized Least Square (pGLS)

If species share ancestral history, they are likely to produce more similar residuals from the least squares regression line. The Phylogenetic Generalized Least Square (pGLS) method takes the expected covariance structure of these residuals into account and accordingly modifies the slope and intercept estimates (Symonds and Blomberg, 2014) which then can account for interspecific autocorrelation due to phylogeny. For example in a pGLS analysis that tests the relationship of a leaf-trait (*Y*) with another leaf-trait/environmental variable (*X*), the relationship can be given by the following equation:

$$Y = b_0 + b_1 X + \varepsilon$$

where, b_0 is the intercept value of the regression equation, b_1 is the slope for the predictor *X* (i.e., the amount of change in *Y* given the change in *X*) and ε is the residual error. If

individual data points (in this case each plant species) are non-independent because of their shared phylogenetic history, the residuals from closely related species may be of similar values, therefore, the errors may also be non-independent/auto-correlated. In a pGLS regression, the error term ε in this equation is adjusted using the variance-covariance matrix (see again **Figure 5.1**), which accounts for phylogenetic relatedness in the off-diagonal elements of the matrix since the expected covariance will be related to the amount of shared evolutionary history (i.e. shared branch lengths in a phylogeny) between the species (Grafen, 1989). In this chapter, a non-phylogenetic generalized least square regression (non-phylogenetic GLS) and a pGLS of $\Delta^{13}C$ with climate variables/other leaf-traits were estimated and the slopes and the intercepts from these analyses were compared to look at whether shared phylogenetic relationships substantially altered the cross-species relationships (documented in **Chapter 4**).

Phylogenetic Independent Contrasts (PICs)

The second PCM used in this chapter to investigate correlated evolution between $\Delta^{13}C$ and climate variables/other leaf-traits was phylogenetic independent contrasts (PICs). PICs were introduced in a seminal work of Felsenstein, (1985) as a way of integrating shared phylogenetic history in comparative biology. This method is a generalization of "paired comparison" method, where contrasts are taken at each bifurcation (or node) in a phylogeny rather than using only paired tips. Since traits evolve independently in each lineage following speciation, the contrasts represent the outcome of independent evolutionary pathways (Symonds and Blomberg, 2014). This alleviates the problem associated with non-independence of data with shared history as well as providing an opportunity to estimate a relationship that accounts for phylogenetic relatedness among species.

Figure 5.2 shows a phylogeny with five species (*A-E*) with their trait values (X_A-X_E) assigned to the tip of the phylogeny. This phylogeny has three internal nodes *x*, *y* and *z* and a root node *o*. For branch *d3*, the difference between the traits X_A and X_B gives the value of the contrast. The calculation of the contrast value for *d5* requires estimation of trait value for the node *x* (given by X_X in **Figure 5.2**). X_X can be calculated as the means of the daughter species weighted by the daughter branch lengths to reflect amount of time over which divergence has occurred (see the calculation for traits in **Figure 5.2** for the equations). These calculations give the "raw contrasts" that meet the assumption of being

statistically independent, however, they do not conform to another statistical requirement of having been drawn from a normal distribution with the same expected variance. Therefore, each of these contrasts need to be "standardized" by their standard deviation given by the square root of the sum of the branch lengths leading to the two taxa in the contrast – which gives the contrasts equal weighting in subsequent regression analyses (Garland Jr and Ives, 2000). Regressions of contrasts must be forced through the origin because, while taking the differences to obtain the contrast in a regression, the intercept terms are cancelled out (Symonds and Blomberg, 2014). It is noteworthy that although the basic theoretical explanation behind pGLS and PICs are different, ultimately, the results of pGLS, in their raw form, are the same as those derived from independent contrasts (Blomberg *et al.*, 2012; Garland Jr and Ives, 2000; Grafen, 1989; Rohlf, 2001; Symonds and Blomberg, 2014). In this chapter, linear regressions between the contrasts of $\Delta^{13}C$ and climate variables and Standardized Major Axis (SMA) regressions between $\Delta^{13}C$ and other leaf-traits have been performed to obtain the evolutionary correlations (this will be discussed further in the following section).

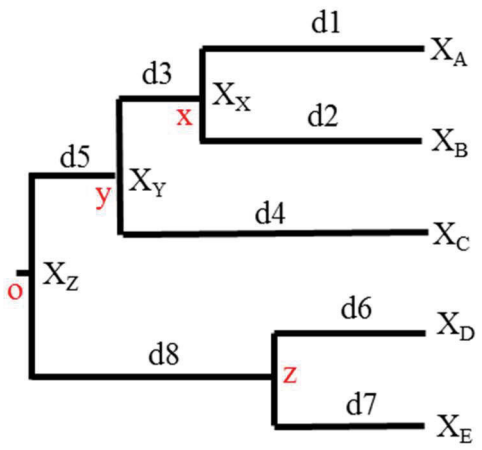

No	Contrasts	Variance
1	X_A-X_B	d1+d2
2	X_D-X_E	d6+d7
3	X_C-X_X	d4+d3'
4	X_Z-X_Y	d5'+d8'

d3' = d3+ d1*d2/(d1+d2)
d5' = d5+ d3'*d4/(d3'+d2)
d8' = d58+ d6*d7/(d6+d7)

$$X_X = \frac{d1X_B * d2X_A}{d1 + d2}$$

$$X_Y = \frac{d3'X_C * d4X_X}{d3' + d4}$$

$$X_Z = \frac{d6X_E * d7X_D}{d6 + d7}$$

Figure 5.2: Calculation involving phylogenetically independent contrasts.

Constructing phylogenetic relationships among plant taxa

A working phylogeny representing the evolutionary relationships of the study taxa was constructed based on the Angiosperm Phylogeny Group III derived megatree R20120829 (Stevens, 2001 onwards). This megatree compiles published angiosperm phylogenies (Davies *et al.*, 2004) and also represents a working hypothesis of relationships between angiosperms. The "BladJ" procedure in the *phylocom* version 4.2 (available at http://phylodiversity.net/phylocom/) (Webb *et al.*, 2007) was used to date the nodes and then attach to the phylogeny using the divergence times estimated by Wikström *et al.*, (2001), hence, estimates of phylogenetic distance are in millions of years. The "multi2di" function from R-library *ape* (Paradis, 2011) was used to transform the working phylogenetic tree structure from multichotomous to dichotomous (binary) format.

Estimating phylogenetic signal and sensitivity analysis

The dated tree obtained from *phylocom* was read into R version 3.1.1 using the *ape* library. Phylogenetic signal (Blomberg's *K* and Pagel's λ) in each leaf-trait was estimated using the "phylosig" function the *phytools* package (Revell, 2012) in R. If there are intraspecific variations for a particular trait and/or the trait is associated with measurement errors, using a single trait measurement per species can underestimate the phylogenetic signal (Blomberg *et al.*, 2003; Ives *et al.*, 2007); therefore, a mean trait value obtained from multiple (four to six) individuals have been used for each species. Although this approach increases the accuracy of the estimates of *K* and λ, it can be improved further if the standard error of trait measurements for each species is also incorporated into the analysis (Baraloto *et al.*, 2010; Ives *et al.*, 2007). Therefore in this study, intraspecific variation (intraspecific standard error) has been incorporated to estimate *K* and λ using the approach described in Ives *et al.*, (2007). To assess the phylogenetic signal of climate variables, *K* and λ were calculated for each the 19 WorldClim variables available for the seven SuperSites (**Chapter 4**). In this dataset, species that occurred at more than one site (three species) were dropped from the phylogeny and then tests were undertaken on the remaining 55 species.

Randomization tests were used to test the ability of Blomberg's *K* to detect deviations from random trait variation using the approach described by Münkemüller *et al.*, (2012). First, observed values of a particular trait were randomly permutated across the tips of the

phylogeny and *K*-values were computed based on this randomized trait pattern. This process was repeated 1000 times which then yielded a distribution of *K*-values under random trait variation. The quantiles of this random trait distribution were extracted and the sensitivity of an observed *K*-value was then tested by a significant deviation from random expectations (indicated by quantiles larger than 0.95) for a significance level of 0.05. Another quantitative approach complementary to *K*-values to characterize phylogenetic signal is to quantify via phylogenetic independent contrasts. First, the variance of independent contrasts (scaled by branch length) was calculated for observed traits on the focal phylogeny. If closely related species tend to have similar trait values (i.e. in the presence of phylogenetic signal), the variance of standardized contrasts will tend to be low. As described for the randomization test for *K*-values, trait values were randomly permuted across the tips of the phylogeny 1000 times and variances of phylogenetic independent contrasts were computed based on this randomized trait patterns. Results were reported if the observed variance of contrasts for a particular trait was significantly lower than expected under random trait variation (for a significance level of 0.05). Variances of independent contrasts were estimated using *picante* package in R (Kembel *et al.*, 2010).

Pagel's λ were estimated using the "maximum likelihood" method. The library *phytools* optimizes the λ-value from a range of λs set between 0 and the theoretical upper limit (determined by the relative height of the most recent internal node on the phylogeny) (Revell, 2012). To test the sensitivity of optimized λ, likelihood ratio tests were performed against a null-hypothesis of $\lambda = 0$ (this is performed by default in the "phylosig" function) and p-values were reported when significant.

Estimating correlated evolution

As mentioned previously, two phylogenetic PCMs were used to account for phylogenetic auto-correlation between species, a regression with pGLS and PIC. The "pgls" function in *caper* library in R was used to conduct the pGLS analysis of both climate-$\Delta^{13}C$ and $\Delta^{13}C$-trait relationships (Orme, 2013) using the maximum likelihood estimate of λ. PGLS in *caper* includes phylogeny of the species as a covariance matrix in a linear model and evaluates multiple causative variables simultaneously incorporating polytomies[6] (Pagel, 1992). Non-phylogenetic generalized least squares (GLS) models were computed using the "nlme" library (Pinheiro *et al.*, 2007). To determine the effects of shared evolutionary history on the

[6] A node on a phylogeny where more than two lineages descend from a single ancestral lineage.

prevailing adaptive interpretations of bulk-leaf $\Delta^{13}C$ and climate/trait variables, the model parameter and fits of non-phylogenetic and phylogenetic GLS models were compared using the Akaike Information Criterion (AIC). AIC evaluates the fit of a model taking into account differences in the number of parameters that are included in the model (Burnham and Anderson, 2004) and therefore, AIC values can be used to interpret how shared ancestry has affected the relationships obtained from the models. The most parsimonious phylogeny for a given dataset is the one with the shortest length (which is equal to the minimum number of changes if there is no homoplasy[7] (i.e., if each character only changes once on the tree) and models that have lower AIC scores can be considered more parsimonious and more strongly supported by the data (Little *et al.*, 2010).

The "pgls" function in *caper* also estimates the parameter λ using the maximum likelihood method when performing the regression analysis (Little *et al.*, 2010; Symonds and Blomberg, 2014). In this case, the strength of the phylogenetic signal of a pGLS model is expressed by λ, ranging between 0 and 1. λ=0 indicates that the variation of a particular trait is modelled as a function of an independent evolution along the branches of the phylogeny leading to the tips. Whereas, λ=1 indicates that variation of a particular trait is modelled exactly as would be expected under the Brownian model. The estimated λ was used for transformation of internal branch lengths for phylogenetic linear model analysis to correct the phylogeny to an appropriate degree. Researchers debate over using the "pseudo r^2" reported in a pGLS analysis that the OLS definition of r^2 does not carry over easily into GLS (Symonds and Blomberg, 2014). Hence, to determine whether the inclusion of phylogenetic information improved model fits, both phylogenetic and non-phylogenetic GLS models were compared only in terms of slope, intercept and AIC scores, with lower AIC score indicating a better fit.

In addition to comparing GLS and pGLS fits, for each climate-variable and $\Delta^{13}C$ relationship, the results from linear regression with and without considering the effect of shared history were compared. This was done by comparing the slope and adjusted r^2 values of an ordinary least square (OLS) regression of each climate - $\Delta^{13}C$ relationship with those of an OLS regression of independent contrasts run through origin. Pearson's correlation between each set of PICs and their standard deviations were calculated and all the correlations were non-significant indicating that the PICs were adequately standardized

[7] When two species have a similar characteristic because of convergent evolution, the feature is called a homoplasy.

as per Garland *et al.*, (1992). Climate variables were treated as independent variables and species mean $\Delta^{13}C$ were treated as continuous response variables in OLS regressions. The non-phylogenetic and phylogenetic relationships of each $\Delta^{13}C$ and a leaf-trait were investigated by comparing the slope and adjusted r^2 values of a Standardized Major Axis (SMA) of the species mean of both $\Delta^{13}C$ and the leaf-trait and an SMA of the independent contrasts run through origin. OLS regressions were performed using the default "lm" function and SMA regressions were performed using the "sma" function in the *smatr* library in R (Warton *et al.*, 2012). Since the signs of independent contrasts are arbitrary, the absolute values were used in the models and the sign of the response-variable was reversed if the sign of the predictor-variable was switched. All non-phylogenetic and phylogenetic models involved in the analysis were checked for normality and homoscedasticity of the residuals and also for outliers that can seriously affect the parameter estimates. Studentized residuals were calculated for each models and all outliers (if any) with residuals $>\pm 3$ was removed from the analysis. Conventional regression diagnostics were also performed including checks for normality of residuals and homogeneity of variance.

It is noteworthy that for each correlation analysis of a climate/trait variable with $\Delta^{13}C$, only species with data available for both variables were used, and consequently, species with any missing data were automatically pruned while performing the analyses using *caper*. Corresponding species were also pruned in presence of outliers. Consequently in some cases, the sample size in the correlation analysis was smaller than the total number of species in the phylogeny (more often due to removal of outliers). Since species composition differed between comparisons, Bonferroni correction could not be applied in the analysis.

Results

Phylogenetic signal of the climate variables

To assess the phylogenetic signal of the climate variables, *K* and λ-statistics for each WorldClim variable was estimated. **Table 5.1** shows the *K* and λ-values of the WorldClim climate variables. A total of 16 out of 19 variables showed significant non-random *K*-values and 10 out of 16 showed significant non-random λ-values indicating that there was more phylogenetic signal in these variables than expected by chance. The highest λ-values were obtained for the variables related to precipitation, namely, MAP, precipitation of the

wettest month and quarter and precipitation of the warmest quarter (the three latter variables had $\lambda > 1$). Among the temperature related parameters, isothermality, temperature seasonality and temperature annual range showed stronger phylogenetic signals both in terms of *K* and λ. Interestingly, all these variables that showed stronger phylogenetic signals among 19 climate variables also had the strongest non-phylogenetic relationships with $\Delta^{13}C$ (non-phylogenetic relationships between $\Delta^{13}C$ and climate variables are discussed in detail in **Chapter 4**).

Randomization tests were performed for *K*-values in order to detect deviations from random trait variations. Climate variables that showed significant non-random *K*-values were also found to have significantly larger *K*s (α=0.05) than 1000 random expectations. Another randomization test was performed using the variances calculated from independent contrasts. Climate variables with significant phylogenetic signals showed significantly smaller variances of contrasts than 1000 random expectations. Histogram bars representing K-values and PIC variances of the traits based on 1000 randomizations are listed in **Appendix B (Figure B1)**.

Table 5.1: Blomberg's *K* and Pagel's *λ* of the climate variables

Climate Variables	Unit	Phylogenetic Signal		Randomization tests	
		K	*λ*	*K* > 95 % random *K*s	PIC variance < 95% random PIC variances
Mean Annual Temperature	℃	**0.38•**	0	Yes	No
Mean Temperature Diurnal Range	℃	**0.44***	**0.63****	Yes	Yes
Isothermality	-	**0.48****	**1.02*****	Yes	Yes
Temperature Seasonality	-	**0.51****	**0.82*****	Yes	Yes
Max T (Warmest Month)	℃	**0.38•**	0	Yes	No
Min T (Coldest Month)	℃	**0.42***	**0.94***	Yes	Yes
T (Annual Range)	℃	**0.45***	**0.75*****	Yes	Yes
Mean T (Wettest Quarter)	℃	0.32	0	No	No
Mean T (Driest Quarter)	℃	0.28	0	No	No
Mean T (Warmest Quarter)	℃	**0.37•**	0	Yes	No
Mean T (Coldest Quarter)	℃	**0.40***	0.8	Yes	Yes
Mean Annual Precipitation	mm	**0.56****	**0.90*****	Yes	Yes
Precipitation (Wettest Month)	mm	**0.57****	**1.04*****	Yes	Yes
Precipitation (Driest Month)	mm	**0.33•**	0.16	Yes	No
Precipitation Seasonality	-	**0.43***	**0.93***	Yes	Yes
Precipitation (Wettest Quarter)	mm	**0.58****	**1.04*****	Yes	Yes
Precipitation (Driest Quarter)	mm	0	0.15	No	No
Precipitation (Warmest Quarter)	mm	**0.52****	**1.05*****	Yes	Yes
Precipitation (Coldest Quarter)	mm	**0.39***	0	Yes	No
Moisture Index	-	0.24	0	No	No

p<0.0001, **p<0.001, *p<0.01, •p<0.05, obtained from randomization tests for *K* and likelihood ratio tests for *λ* simulated from 1000 randomizations

⊿^{13}C-climate relationships and phylogenetic signal of the residuals

In **Chapter 4**, relationships of climate variable with $\Delta^{13}C$ were explored separately for dry- and wet-seasons focusing mainly on seasonal patterns. In the current chapter, species-mean values of $\Delta^{13}C$ were calculated across seasons and used in all analyses. The results of linear regressions of $\Delta^{13}C$ with WorldClim variables are listed in the first two columns of **Table 5.2**. Comparing with the results from the previous chapter (see **Table 4.5, Chapter 4**), the nature/direction of the relationships of $\Delta^{13}C$ for most of the climate variables did not change, although the adjusted r^2 values were always smaller when species mean values across seasons were used in the models instead of seasonal means. Some of the significant relationships observed using seasonal values disappeared when means across seasons were

used, for example, mean T of the driest quarter showed a weak but significant relationship with dry-season $\Delta^{13}C$ (Adj r^2=0.049, $p<0.05$) but this relationship disappeared when annualised species mean $\Delta^{13}C$ was used (Adj r^2=0.03, $p>0.05$). The statistically stronger and more significant relationships (for example, mean diurnal range, isothermality, temperature seasonality, MAP, precipitation of the wettest month/ quarter, precipitation of the warmest quarter etc.) still showed strong and significant relationships when annualised species mean values were used with smaller adjusted r^2 values.

To investigate whether the "residuals" of non-phylogenetic climate-$\Delta^{13}C$ relationships showed any significant phylogenetic signal, *K* and λ of the residuals of each climate-$\Delta^{13}C$ model was estimated (**Table 5.2**). **Table 5.2** shows that, the residuals of the nine climate-$\Delta^{13}C$ relationships showed non-random and significant *K* (mean diurnal range, temperature seasonality, max T of the warmest month, T annual range, mean T of the warmest quarter, MAP, precipitation of the driest month, precipitation of the driest quarter and precipitation of the coldest quarter). Eight climate-$\Delta^{13}C$ relationships showed significant λ for the residuals (mean annual temperature, max T of the warmest month, mean T of the wettest quarter, mean T of the driest quarter, mean T of the warmest quarter, precipitation of the driest month, precipitation of the driest quarter and precipitation of the coldest quarter). Assessment of phylogenetic signals of the residuals of climate-$\Delta^{13}C$ relationships also showed that not necessarily all climate variables that showed significant non-random phylogenetic signal would also have significant signal in the residuals obtained from the climate - $\Delta^{13}C$ relationships. For example, isothermality, one of the strongest predictors of $\Delta^{13}C$ among 19 climate parameters (Adj r^2= 0.44, $p<0.0001$) showed significant phylogenetic signal when the variable itself was tested (*K*=0.48, $p<0.001$ and λ =1.02, $p<0.0001$), whereas, *K* and λ of the residuals of the isothermality-$\Delta^{13}C$ relationship were both non-significant. In contrast, moisture index, (an additional variable calculated as a ratio between precipitation and potential evaporation for each of these SuperSites from SILO data; see **Chapter 4** for details), showed no phylogenetic signal of the variable itself but the residuals of moisture index - $\Delta^{13}C$ relationship showed significant non-random phylogenetic signal in terms of both *K* and λ (*K*=0.34, $p<0.05$ and λ =0.63, $p<0.01$).

Correlated evolution between climate variable and $\Delta^{13}C$

With evidence of significant *K* of the residuals of climate-$\Delta^{13}C$ relationships for at least 10 and significant λ for nine out of 20 climate variables (19 WorldClim variables and moisture

index calculated from SILO data), two methods were used to examine and compare if the association between $\Delta^{13}C$ and climatic variables persisted after controlling for phylogeny: i) phylogenetic generalized least square (pGLS) regression models and ii) ordinary least square (OLS) regression models of the independent contrasts (through origin). The comparison of slopes, intercept, AIC values and λ are reported in **Table 5.2.**

Table 5.2: Phylogenetic signal (residuals) and results from GLS, pGLS and PIC analysis of climate variables-$\Delta^{13}C$ relationships

AIC = Akaike Information Criterion; lower AIC score indicating a better fit. S.E. = standard errors of slopes and intercepts from GLS and pGLS models
***p<0.0001, **p<0.001, *p<0.01, •p<0.05

Climate variable	Phylogenetic signal (residuals)		Non-phylogenetic model							Phylogenetic models								
			Linear regression		GLS					pGLS (caper)							PIC	
	K	*λ*	slope	Adj r^2	Y-int	SE	Slope	SE	AIC	*λ*	Y-int	SE	Slope	SE	AIC	Adj r^2	Slope	Adj r^2
Mean Annual Temperature	0.30	0.50•	0.11	0.05	20.26	1.11	0.11	0.06	218.69	0.57	20.99	1.45	0.06	0.05	206.03	0.009	-0.01	-0.02
Mean Diurnal Range	0.40•	0.31	-0.48	0.23***	27.07	1.28	-0.47	0.12	207.20	0	25.52	1.57	-0.37	0.14	201.32	0.12*	-0.29	0.08•
Isothermality	0.27	0	0.33	0.44***	5.07	2.77	0.33	0.05	193.51	0	5.07	2.76	0.33	0.05	186.39	0.44***	0.33	0.23**
Temperature Seasonality	0.41•	0	-3.69	0.46***	26.45	0.71	-3.69	0.58	187.76	0	26.45	0.71	-3.69	0.58	185.42	0.46***	-3.40	0.29***
Max T (Warmest Month)	0.41*	0.71*	-0.05	-0.01	23.50	1.66	-0.05	0.06	221.38	0.70	22.76	1.86	-0.03	0.05	206.87	-0.01	-0.07	0.04
Min T (Coldest Month)	0.25	0.21	0.18	0.22***	20.57	0.52	0.18	0.05	209.81	0.33	21.04	0.93	0.14	0.05	201.59	0.13*	0.04	-0.01
T Annual Range	0.40•	0	-0.23	0.35***	26.77	0.92	-0.23	0.05	201.13	0	26.78	0.92	-0.23	0.05	193.87	0.35***	-0.18	0.16*
Mean T (Wettest Quarter)	0.29	0.50•	0.09	0.11*	20.39	0.76	0.10	0.04	216.38	0.55	20.88	1.23	0.07	0.03	202.88	0.07•	0.04	0.01
Mean T (Driest Quarter)	0.30	0.43•	0.14	0.03	19.63	1.56	0.14	0.08	218.39	0.61	21.40	1.81	0.03	0.07	207.20	-0.02	-0.01	0.01
Mean T (Warmest Quarter)	0.36•	0.63*	0.02	0.02	21.73	1.41	0.02	0.06	221.76	0.66	21.82	1.68	0.01	0.05	207.33	-0.02	-0.05	0.001
Mean T (Coldest Quarter)	0.26	0.35	0.13	0.16**	19.96	0.78	0.15	0.05	213.18	0.45	20.69	1.17	0.11	0.05	203.03	0.08•	0.03	-0.01
Mean Annual Precipitation	0.44*	0	0.002	0.55***	18.65	0.51	0.002	0.00	193.48	0	18.65	0.51	0.02	0.00	175.83	0.55***	0.003	0.46**
Precip. (Wettest Month)	0.28	0	0.01	0.49***	19.71	0.43	0.009	0.001	196.72	0	19.71	0.43	0.009	0.00	182.21	0.49***	0.009	0.29***
Precip. (Driest Month)	0.49**	0.81*	0.03	0.06*	20.89	0.71	0.03	0.02	220.38	0.79	20.26	1.66	0.03	0.01	203.25	0.07•	0.036	0.15*
Precip. Seasonality	0.24	0.16	0.04	0.27***	19.92	0.60	0.04	0.01	209.78	0.26	20.42	0.90	0.03	0.01	198.83	0.19**	0.02	0.01
Precip. (Wettest Quarter)	0.29	0	0.003	0.49***	19.71	0.43	0.003	0	198.47	0	19.71	0.43	0.003	0	181.86	0.49***	0.003	0.29***
Precip. (Driest Quarter)	0.47**	0.78*	0.008	0.04	21.09	0.70	0.008	0.005	208.42	0.79	20.53	1.64	0.007	0	204.42	0.04	0.009	0.13*
Precip.(Warmest Quarter)	0.27	0	0.004	0.47***	20.04	0.41	0.004	0	200.71	0	20.04	0.41	0.004	0	182.54	0.47***	0.003	0.25***
Precip. (Coldest Quarter)	0.40*	0.69*	0.001	-0.01	21.93	0.58	0.001	0.002	228.12	0.69	21.61	1.49	0.001	0	207.11	-0.02	0.003	0.02
Moisture index	0.34•	0.63*	4.11	0.25***	20.51	0.49	4.11	1.004	201.68	0.67	20.76	1.18	3.43	0.83	192.36	0.25***	3.16	0.26***

Table 5.2 shows that the parameter λ estimated from the residuals of the OLS regressions of each climate - $\Delta^{13}C$ relationships were in general very similar in magnitude to that estimated from the pGLS analysis used in branch length transformation. **Table 5.2** also showed that all climate - $\Delta^{13}C$ models were slightly improved when shared phylogenetic history was incorporated in the analysis as demonstrated by the lower AIC scores for pGLS *versus* non-phylogenetic GLS models. Four temperature related traits (mean diurnal range, isothermality, temperature seasonality and T annual range) and four precipitation related parameters (MAP, precipitation of driest month, precipitation of driest quarter and precipitation of warmest quarter) that showed some of the most significant relationships with $\Delta^{13}C$ in non-phylogenetic analyses, showed no phylogenetic signal from the residuals from pGLS. For all these variables, although the AIC scores were improved after incorporating phylogenetic relationships, the slopes and intercepts of phylogenetic and non-phylogenetic models remained exactly the same in strength and nature (**Table 5.2**, **Figure 5.4**). Climate variables that showed intermediate phylogenetic signals of the residuals also showed larger shifts in slopes and intercepts between non-phylogenetic and phylogenetic models. The standard errors of the intercepts in pGLS regressions of these variables were generally larger than those in non-phylogenetic GLS regressions (**Table 5.2**), indicative of greater uncertainties involved in explaining the variation in $\Delta^{13}C$ explained by these variables evident after phylogenetic relationships were taken into account.

The results of evolutionary correlations using phylogenetically independent contrasts are presented in the last two columns of **Table 5.2**. The nature of all significant climate - $\Delta^{13}C$ relationships were very similar in PIC analyses compared to pGLS analyses. Compared to cross-species climate-$\Delta^{13}C$ correlations, significant evolutionary correlations were overall similar in nature and magnitude (**Figure 5.3**). This was especially true for the climate variables that did not show significant phylogenetic signal of the residuals from pGLS analysis (**Table 5.2**). The most significant discrepancies among cross-species analyses and independent contrast analyses involved relationships of three climate variables, mean T of wettest quarter (Adj r^2=0.11, $p<0.01$), mean T of coldest quarter (Adj r^2=0.16, $p<0.001$) and precipitation seasonality (Adj r^2=0.27, $p<0.0001$); which would be considered significant based on cross-species analyses but found to be non-significant based on independent contrasts (**Table 5.2**, **Figure 5.3**). In contrast, relationships of both precipitation of the driest month and quarter were stronger in independent contrast analysis than from cross-species analysis. The relationship of precipitation of the driest

quarter in particular was non-significant in cross-species analysis (Adj r^2=0.05, p>0.05) but came out stronger and significant from the PIC analysis (Adj r^2=0.13, p<0.01). However, the relationship between $\Delta^{13}C$ and precipitation seasonality disappeared using independent contrasts (see **Table 5.2**). This occurred because the observed positive relationship of $\Delta^{13}C$ with precipitation seasonality was not present in multiple evolutionary divergences throughout the phylogeny; for example, there was no correlation between the contrasts of $\Delta^{13}C$ with precipitation seasonality in the clade "Myrtaceae" but the clade "Rosales" showed significant correlated evolution in $\Delta^{13}C$ with precipitation seasonality.

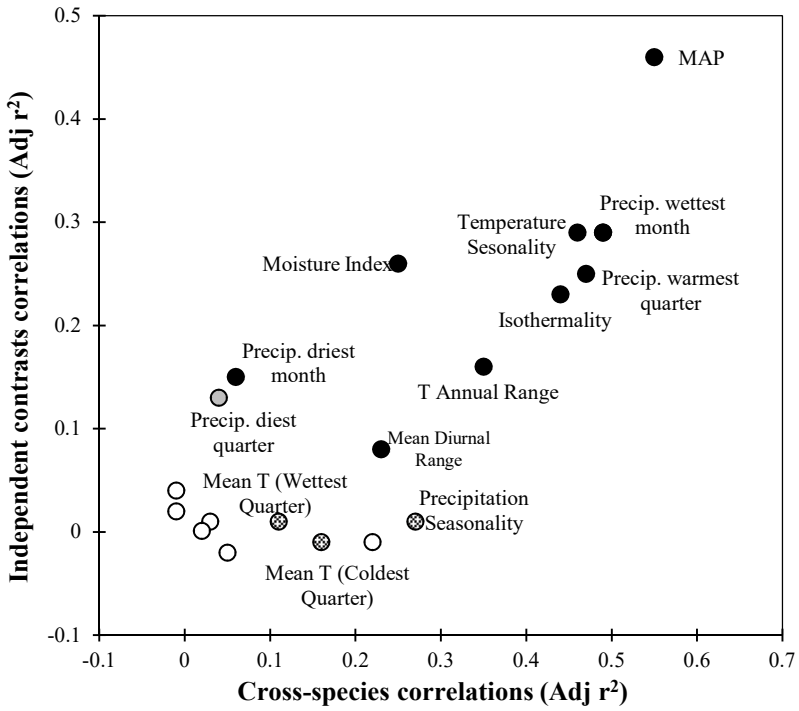

Figure 5.3: Scatterplot of cross-species correlations *versus* independent contrast correlations of the relationships of climate variables - $\Delta^{13}C$.

Closed black circles: correlations significant both in non-phylogenetic and PIC analysis; closed grey circles: correlations significant only in PIC analyses, grey circle with patterns: correlations significant only in non-phylogenetic analysis and open white circles: all other non-significant correlations.

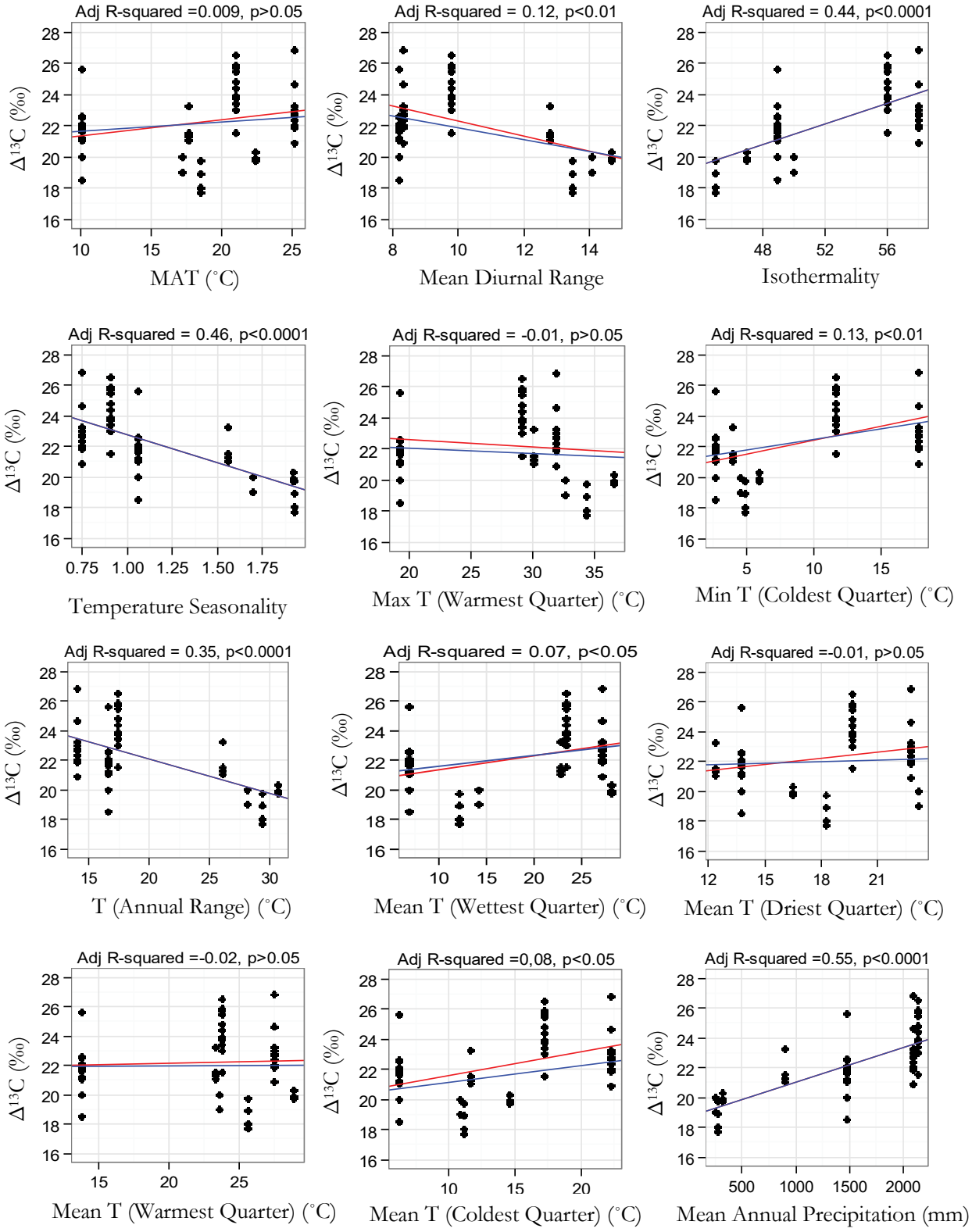
Adj R-squared =0.009, p>0.05
Δ13C (‰)
MAT (°C)
Adj R-squared = 0.12, p<0.01
Mean Diurnal Range
Adj R-squared = 0.44, p<0.0001
Isothermality
Adj R-squared = 0.46, p<0.0001
Temperature Seasonality
Adj R-squared = -0.01, p>0.05
Max T (Warmest Quarter) (°C)
Adj R-squared = 0.13, p<0.01
Min T (Coldest Quarter) (°C)
Adj R-squared = 0.35, p<0.0001
T (Annual Range) (°C)
Adj R-squared = 0.07, p<0.05
Mean T (Wettest Quarter) (°C)
Adj R-squared =-0.01, p>0.05
Mean T (Driest Quarter) (°C)
Adj R-squared =-0.02, p>0.05
Mean T (Warmest Quarter) (°C)
Adj R-squared =0,08, p<0.05
Mean T (Coldest Quarter) (°C)
Adj R-squared =0.55, p<0.0001
Mean Annual Precipitation (mm)

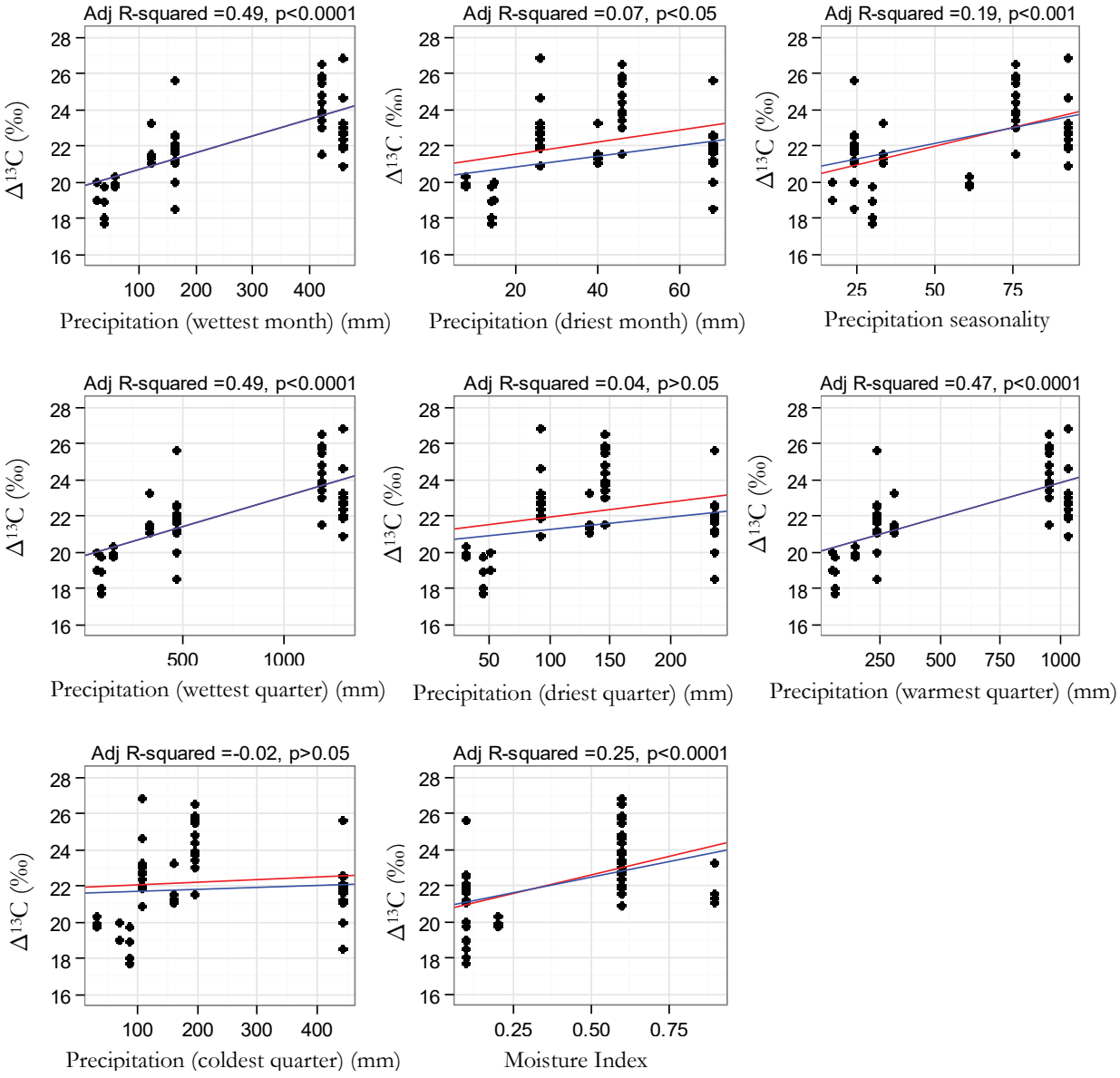

Figure 5.4: Climate variables *versus* carbon isotope discrimination in leaf dry matter ($\Delta^{13}C$).

The best-fit lines for non-phylogenetic GLS (red line) and phylogenetic GLS (blue line) are displayed for each climate variable. Only blue line is shown when slopes and intercepts were exactly same in both GLS and pGLS models. Branch lengths scaled by the maximum likelihood of Pagel's λ parameter were used in the phylogenetic models (**Table 5.1**). Adjusted r^2 and associated p-values from the pGLS analysis are also shown. Units: Discrimination is expressed as per mil (‰), all precipitation related parameters: mm and all temperature related parameters: ℃. Each data point represents an individual species.

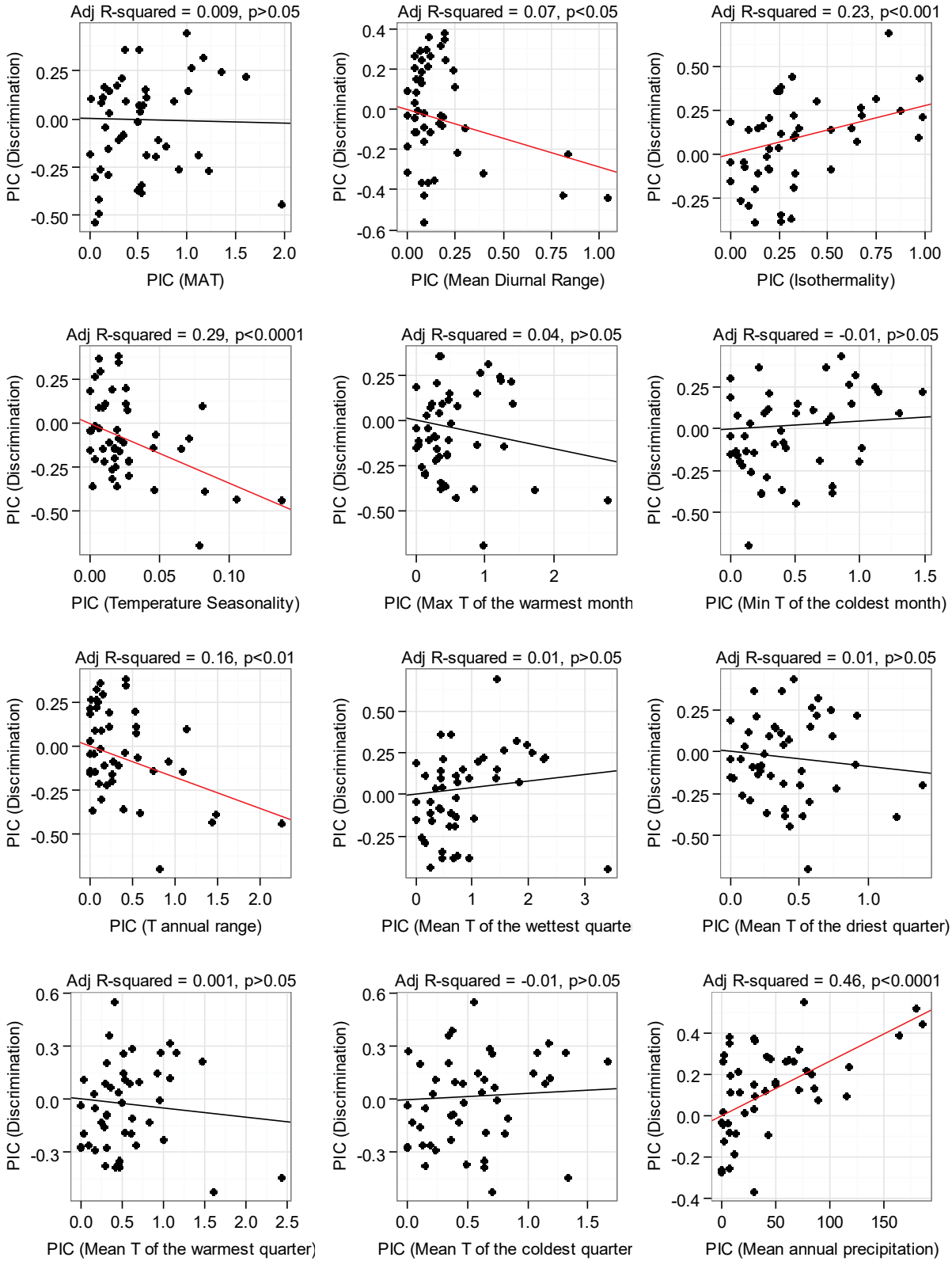
Adj R-squared = 0.009, p>0.05
PIC (Discrimination)
PIC (MAT)
Adj R-squared = 0.07, p<0.05
PIC (Mean Diurnal Range)
Adj R-squared = 0.23, p<0.001
PIC (Isothermality)
Adj R-squared = 0.29, p<0.0001
PIC (Temperature Seasonality)
Adj R-squared = 0.04, p>0.05
PIC (Max T of the warmest month
Adj R-squared = -0.01, p>0.05
PIC (Min T of the coldest month)
Adj R-squared = 0.16, p<0.01
PIC (T annual range)
Adj R-squared = 0.01, p>0.05
PIC (Mean T of the wettest quarte
Adj R-squared = 0.01, p>0.05
PIC (Mean T of the driest quarter)
Adj R-squared = 0.001, p>0.05
PIC (Mean T of the warmest quarter)
Adj R-squared = -0.01, p>0.05
PIC (Mean T of the coldest quarter
Adj R-squared = 0.46, p<0.0001
PIC (Mean annual precipitation)

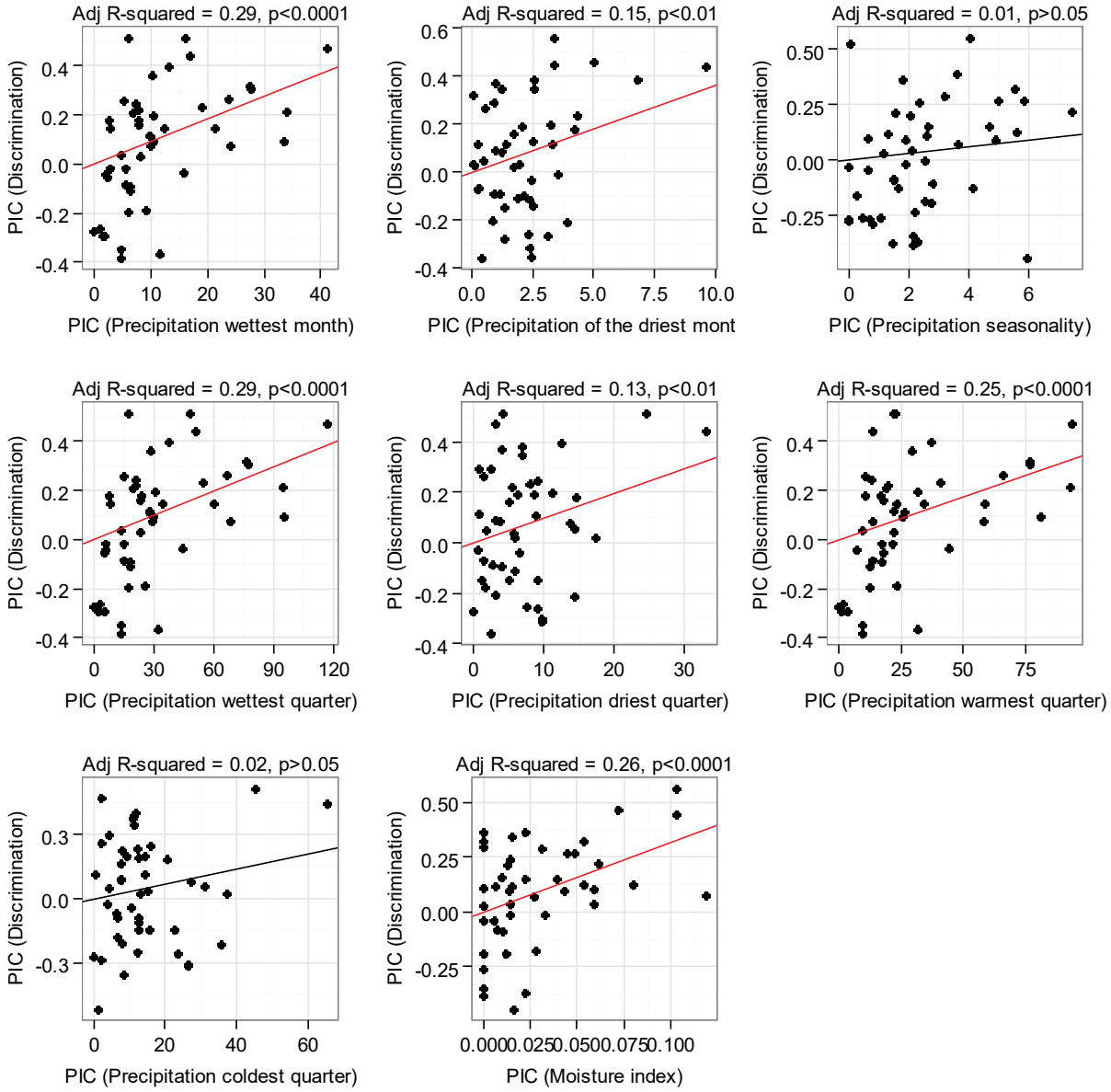

Figure 5.5: Scatterplots of independent contrasts of carbon isotope discrimination ($\Delta^{13}C$) *versus* climate variables.

Correlation analyses using independent contrasts are calculated through the origin. Red-lines: statistically significant best-fit lines for relationships between contrasts of discrimination and climate variables. Black-line: non-significant relationships. Adjusted r^2 and associated p-values are also shown.

Phylogenetic signal of the leaf-traits

The next objective was to determine whether any of the leaf-traits showed significant phylogenetic signals at a continental scale in Australia. Blomberg's *K* and Pagel's *λ* were estimated for each of the 18 traits (**Table 5.3**). The distribution of traits was tested for non-normality (Shapiro-Wilk test, $\alpha = 0{\cdot}05$) and homogeneity of variances (Bartlett test) and appropriately transformed (see **Chapter 4**, "*Methodology and statistical analyses*" section for details). For analyses of leaf-traits, *K* and *λ* values of each trait were estimated twice, first using the species mean values of each trait and then incorporating the intraspecific variation of each trait in the analyses by including the standard errors obtained from four to six measurements of each species. $\Delta^{13}C$ showed significant non-random phylogenetic signal in both *K* and *λ* parameters indicating that there was more phylogenetic signal than expected by chance. Other than $\Delta^{13}C$, eight traits showed significant *K* and *λ* out of 18 traits when only species mean values were used in the code. However, when intraspecific variations were incorporated, 11 traits showed significant *K* and nine traits showed significant *λ*. Also, all *K* and most of the *λ* values increased when intraspecific variations were incorporated in the analyses, indicating that using only the species mean values slightly underestimated the phylogenetic signal in the trait-variables themselves. All three leaf structural traits (LDMC, LMA and FMA) showed significant *K* and *λ*. Among the leaf nutrient traits, total leaf nitrogen ($LeafN_{mass}$) showed significant *K* and *λ* in all tests. Total leaf phosphorus ($LeafP_{mass}$) and photosynthetic phosphorus-use-efficiency (PPUE) showed a significant K and $LeafP_{mass}$ showed significant *K* and *λ* only after accounting for errors. Among the gas-exchange measurements, instantaneous measurements of intrinsic water-use-efficiency calculated from the ratio of A400.a to g_s400, C_i/C_a and C_i400 showed significant phylogenetic signal. None of the other instantaneous gas-exchange measurements showed a significant phylogenetic signal in any test.

In addition to randomization tests performed to test the significance of *K*-values in the trait variables, variances in independent contrasts were also used to characterize the phylogenetic signal of the leaf-traits. The results of these tests are listed in **Table 5.3**. Histogram bars representing *K*-values and PIC variances of the traits based on 1000 randomizations are presented in **Appendix B (Table B2)**.

Table 5.3: Blomberg's *K*, Pagel's *λ* and results from randomization tests for the leaf-traits

Leaf-traits	Phylogenetic Signal				Randomization tests for *K* (Without intraspecific variation)	
	K		***λ***		***K*** > 95% random ***K***s	PIC variance < 95% random PIC variances
	Without intraspecific variation	With intraspecific variation†	Without intraspecific variation	With intraspecific variation†		
$\Delta^{13}C$	**0.38•**	**0.39•**	**0.66***	**0.67***	**Yes**	**Yes**
A400.a	0.23	0.23	0	0	No	No
ln E400.a	0.28	0.34	0	0.51	No	No
ln vpdL400	0.29	0.45	0.26	0.15	No	No
sqrt g_s400	0.24	0.26	0	0	No	No
ln (A400.a/g_s400)	**0.71•**	**0.61***	**1.04*****	**1.02*****	**Yes**	**Yes**
C_i/C_a	**0.41***	**0.53***	**0.81***	**0.82*****	**Yes**	**Yes**
C_i400	**0.39•**	**0.49•**	**0.71***	**0.79****	**Yes**	**Yes**
ln LDMC	**0.43***	**0.44***	**0.85****	**0.54*****	**Yes**	**Yes**
ln LMA	**0.41***	**0.38•**	**0.78*****	**0.65****	**Yes**	**Yes**
ln FMA	**0.37•**	**0.38•**	**0.80*****	**0.73****	**Yes**	**Yes**
ln $LeafN_{mass}$	**0.45***	**0.45***	**0.83****	**0.86****	**Yes**	**Yes**
ln $LeafP_{mass}$	0.34	**0.56•**	0.75	0.22	No	**Yes**
ln Ratio NP	0.28	0.40	0	0.20	No	No
ln $LeafN_{area}$	**0.43•**	0.31	**0.86***	0.67	No	No
ln $LeafP_{area}$	0.36	**1.27***	0.51	**0.89**	No	No
PNUE	0.30	0.36	0.47	0.62	No	No
ln PPUE	0.27	**0.86•**	0	0	No	No

p<0.0001, **p<0.001, *p<0.01, •p<0.05, obtained from randomization tests for *K* and likelihood ratio tests for *λ* simulated from 1000 randomizations
†data was not transformed due to non-linearity to include standard error

Standardized major axis regression was performed on species-mean values of leaf-traits calculated across seasons and the results are listed in **Table 5.2**. Compared with analyses performed separately in dry- and wet-seasons (see **chapter 4**, **Table 4.8** for details), the adjusted r^2 values were always smaller when annualised species mean values were used. Some of the significant relationships identified when analysed separately for dry- and wet-seasons disappeared in the species mean analysis. For example, the relationship of photosynthetic assimilation (A400.a, Adj r^2= 0.135, p<0.01) with $\Delta^{13}C$ was found to be significant in the wet-season but it was non-significant when the species-means were used. The relationship of stomatal conductance with $\Delta^{13}C$, found to be weakly significant during the dry-season sampling (g_s400, Adj r^2=0.072, p<0.05), completely disappeared when species-means were used. The nature/direction of the relationships of $\Delta^{13}C$ with most of

the leaf-traits did not change when means across seasons were used in the SMA models. Tests for phylogenetic signal were also performed on the residuals of the cross-species $\Delta^{13}C$-leaf-trait SMA models. The residuals of only five $\Delta^{13}C$-trait relationships (VPD, C_i/C_a, LDMC, ration of [N] to [P] and $LeafN_{area}$) showed significant *K* and only two (LDMC and $LeafN_{area}$) showed significant λ (**Table 5.4**).

Correlated evolution between $\Delta^{13}C$ and leaf-traits

Correlated evolution between $\Delta^{13}C$ and leaf structural, nutrient and gas-exchange traits was tested using pGLS and independent contrasts. A comparison of slopes, intercepts, AIC values and λ from non-phylogenetic GLS and pGLS models are reported in **Table 5.4**. For $\Delta^{13}C$ - trait relationships, the parameter λ from the pGLS regressions (estimated in *caper* from the residuals of each $\Delta^{13}C$ - trait relationship) overall showed similar phylogenetic signal as was obtained when tests were performed on trait variables themselves (compare **Table 5.3** and **Table 5.4**). For leaf gas-exchange traits (except for C_i/C_a and C_i400), no significant phylogenetic signal was observed in the residuals and slopes and intercepts were exactly the same in non-phylogenetic and phylogenetic GLS models. There was evidence of phylogenetic signal in the residuals of two gas-exchange traits, C_i/C_a (λ=0.61) and C_i400 (λ=0.56) and the slopes and intercepts of these traits were slightly different in pGLS models than non-phylogenetic GLS models (**Table 5.4**). All leaf structural traits showed evidence of non-random phylogenetic signals of the residuals from pGLS (λ>0) and subsequent differences in slopes and intercepts from GLS to pGLS models. Among leaf nutrient traits, total leaf N ($LeafN_{mass}$), total leaf P ($LeafP_{mass}$) and total leaf N on area basis ($LeafN_{area}$) showed λ>0 and subsequent differences in slopes and intercepts in the pGLS models.

From independent contrast analyses, there was evidence of correlated evolution with $\Delta^{13}C$ in four gas-exchange traits: VPD, C_i/C_a, C_i400 and intrinsic WUE_i calculated from the ratio of A400.a and g_s400. All the leaf structural traits and two leaf nutrient traits (Ratio of N to P and $LeafN_{area}$) also showed evidence of correlated evolution. Compared to cross-species $\Delta^{13}C$ - traits correlations obtained from SMA, significant evolutionary correlations from SMA through origin of the independent contrasts were overall similar in nature and magnitude (**Figure 5.6**). There were discrepancies among cross-species analyses and independent contrast analyses in two $\Delta^{13}C$ - trait relationships: the relationship of $\Delta^{13}C$ with $LeafP_{area}$ appeared significant in the cross-species analysis but was non-significant in the

PIC analysis; whereas, the relationship of $\Delta^{13}C$ with ratio of leaf N to P (RatioNP) that was non-significant in the cross-species analysis appeared significant in the PIC analysis (**Table 5.4, Figure 5.6**).

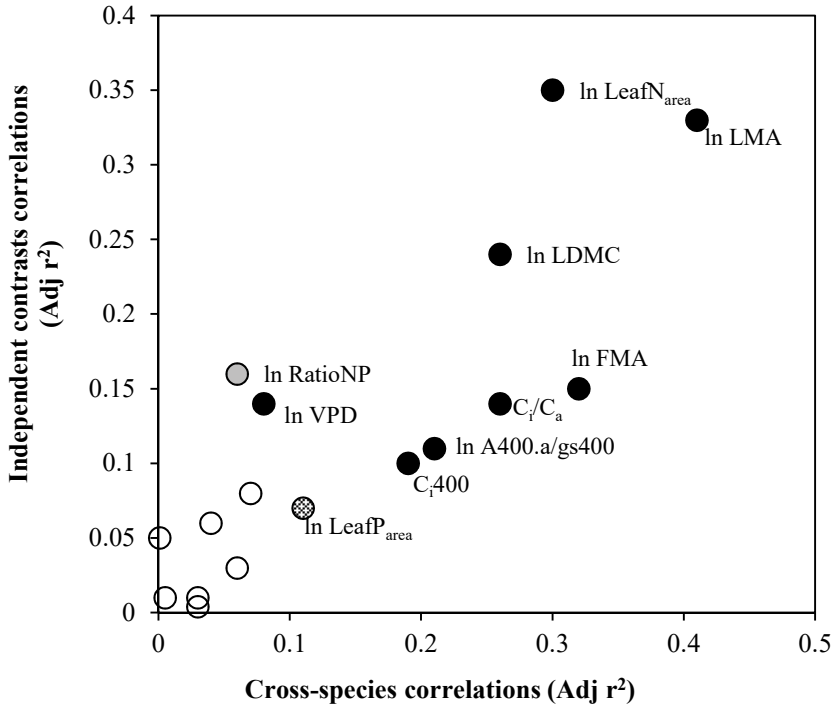

Figure 5.6: Scatterplot of cross-species correlations *versus* independent contrast correlations of $\Delta^{13}C$-trait relationships.

Closed black circles: correlations significant both in non-phylogenetic and PIC analysis; closed grey circles: correlations significant only in PIC analyses, grey circle with patterns: correlations significant only in non-phylogenetic analysis and open white circles: all other non-significant correlations.

Table 5.4: Phylogenetic signal (residuals) and results from GLS, pGLS and PIC analysis of $\Delta^{13}C$-leaf-trait relationships

AIC = Akaike Information Criterion; lower AIC score indicating a better fit. S.E. = standard errors of slopes and intercepts from GLS and pGLS models

Traits correlated with $\Delta^{13}C$	Phylogenetic signal (residuals)		Non-phylogenetic model							Phylogenetic models								
			SMA		GLS					SMA PIC		pGLS (caper)						
	K	λ	slope	Adj r^2	Y-int	SE	Slope	SE	AIC	Slope	Adj r^2	λ	Y-int	SE	Slope	SE	AIC	Adj r^2
A400.a	0.31	0.26	-1.37	0.005	9.86	4.63	-0.11	0.20	251.63	-1.83	0.01	0	9.86	4.63	-0.11	0.20	248.55	-0.02
ln E400.a	0.29	0.29	0.29	0.001	0.03	0.94	0.011	0.04	105.34	0.35	0.05	0	0.03	0.94	0.011	0.04	95.88	-0.02
ln VPD	**0.40•**	0	-0.14	**0.08•**	1.29	0.46	-0.04	0.02	39.98	-0.17	**0.14***	**0.68**	1.29	0.46	-0.04	0.02	27.70	**0.06•**
sqrt g_s400	0.25	0	0.04	0.03	0.16	0.15	0.008	0.01	-62.02	0.058	0.004	0	0.16	0.15	0.008	0.01	-78.13	0.007
ln A400.a/g_s400	0.32	0	-0.13	**0.21****	5.68	0.39	-0.06	0.02	23.68	-0.13	**0.11•**	0	5.68	0.39	-0.06	0.02	10.71	**0.19****
C_i/C_a	**0.37•**	0	0.04	**0.26****	0.21	0.11	0.02	0.01	-91.50	0.034	**0.14****	**0.61**	0.34	0.13	0.014	0.01	-110.7	**0.12***
C_i400	0.32	0	15.57	**0.19****	88.67	48.6	7.36	2.17	467.9	16.04	**0.10•**	**0.56**	152	54.1	4.93	2.31	471.6	**0.07•**
ln LDMC	**0.47***	**0.88•**	-0.09	**0.26*****	0.19	0.25	-0.05	0.01	-17.52	-0.08	**0.24****	**0.91**	-0.03	0.28	-0.04	0.01	-40.24	**0.19****
ln LMA	0.32	0	-0.20	**0.41*****	7.84	0.51	-0.13	0.02	49.29	-0.19	**0.33*****	**0.67**	7.01	0.58	-0.09	0.02	34.07	**0.24****
ln FMA	0.28	0	-0.15	**0.32*****	7.63	0.40	-0.84	0.02	26.34	-0.14	**0.15***	**0.70**	6.98	0.44	-0.06	0.02	9.91	**0.14***
ln $LeafN_{mass}$	0.28	0	0.16	0.03	2.18	0.51	0.03	0.02	49.21	-0.15	0.01	**0.85**	2.86	0.56	-0.01	0.02	28.60	-0.02
ln $LeafP_{mass}$	0.31	0	0.19	0.07	-1.64	0.64	0.06	0.03	69.71	0.18	0.08	**0.63**	-1.21	0.75	0.04	0.03	59.96	0.006
ln Ratio NP	**0.37•**	0.39	-0.09	0.06	4.06	0.45	-0.03	0.02	35.72	-0.15	**0.16***	0	3.71	0.53	-0.02	0.02	41.27	-0.01
ln $LeafN_{area}$	**0.61****	**0.92****	-0.18	**0.30*****	3.11	0.52	-0.10	0.02	50.20	-0.19	**0.35*****	**0.92**	2.85	0.57	-0.10	0.02	29.30	**0.30*****
ln $LeafP_{area}$	0.35	0	-0.16	**0.11***	6.10	0.65	-0.07	0.03	70.98	-0.14	0.07	0	6.08	0.65	-0.07	0.03	60.04	**0.09•**
PNUE	0.31	0.29	0.75	0.06	-0.68	2.48	0.19	0.11	194.2	0.84	0.03	0	-0.68	2.48	0.19	0.11	188.6	0.04
ln PPUE	0.29	0	0.26	0.04	2.83	1.09	0.07	0.05	118.21	0.28	0.06	0	2.84	1.10	0.07	0.05	107.97	0.02

***p<0.0001, **p<0.001, *p<0.01, •p<0.05

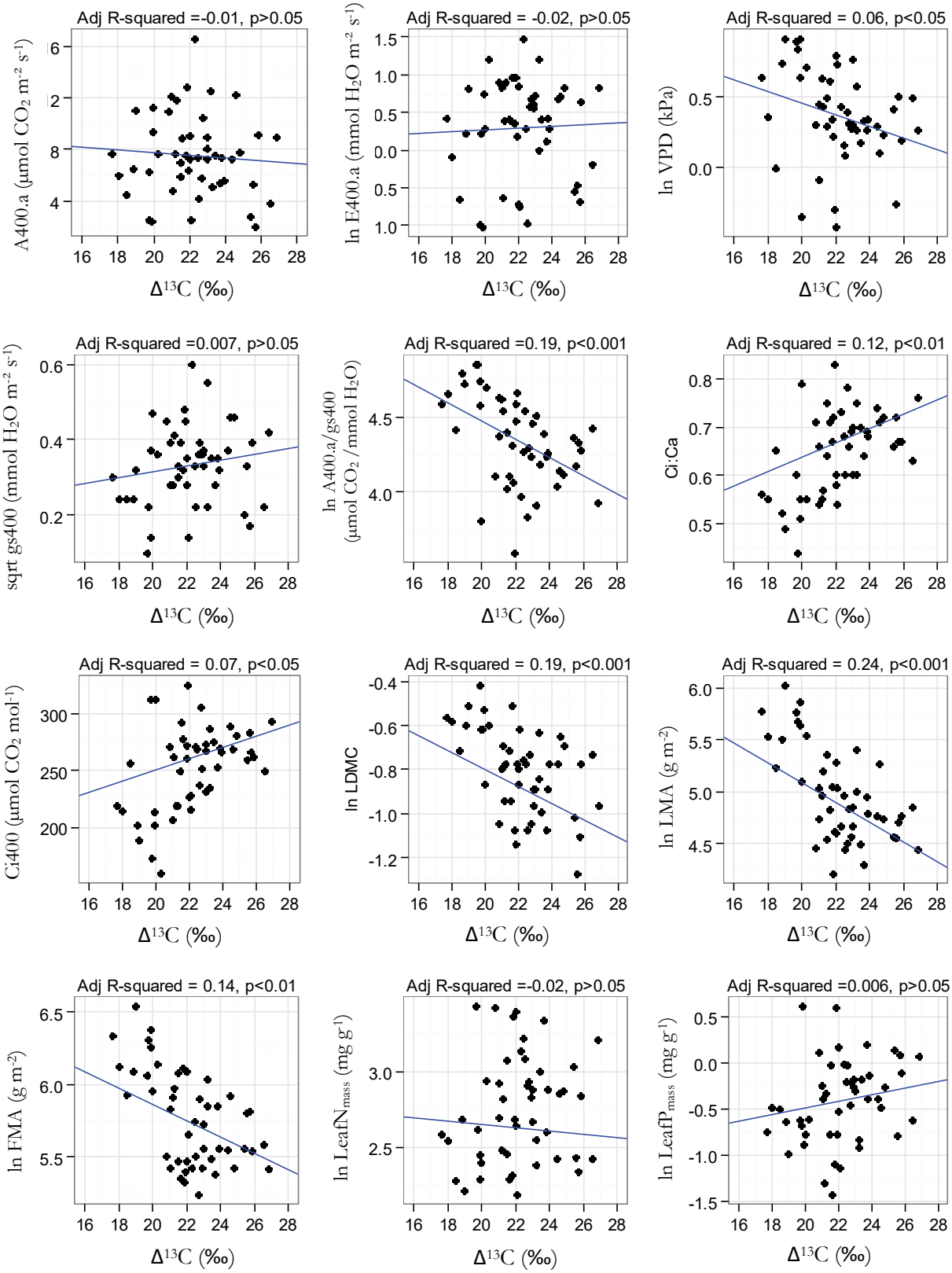
Adj R-squared =-0.01, p>0.05
A400.a (µmol CO2 m-2 s-1)
Δ13C (‰)
Adj R-squared = -0.02, p>0.05
ln E400.a (mmol H2O m-2 s-1)
Δ13C (‰)
Adj R-squared = 0.06, p<0.05
ln VPD (kPa)
Δ13C (‰)
Adj R-squared =0.007, p>0.05
sqrt gs400 (mmol H2O m-2 s-1)
Δ13C (‰)
Adj R-squared =0.19, p<0.001
ln A400.a/gs400 (µmol CO2 /mmol H2O)
Δ13C (‰)
Adj R-squared = 0.12, p<0.01
Ci:Ca
Δ13C (‰)
Adj R-squared = 0.07, p<0.05
Ci400 (µmol CO2 mol-1)
Δ13C (‰)
Adj R-squared = 0.19, p<0.001
ln LDMC
Δ13C (‰)
Adj R-squared = 0.24, p<0.001
ln LMA (g m-2)
Δ13C (‰)
Adj R-squared = 0.14, p<0.01
ln FMA (g m-2)
Δ13C (‰)
Adj R-squared =-0.02, p>0.05
ln LeafNmass (mg g-1)
Δ13C (‰)
Adj R-squared =0.006, p>0.05
ln LeafPmass (mg g-1)
Δ13C (‰)

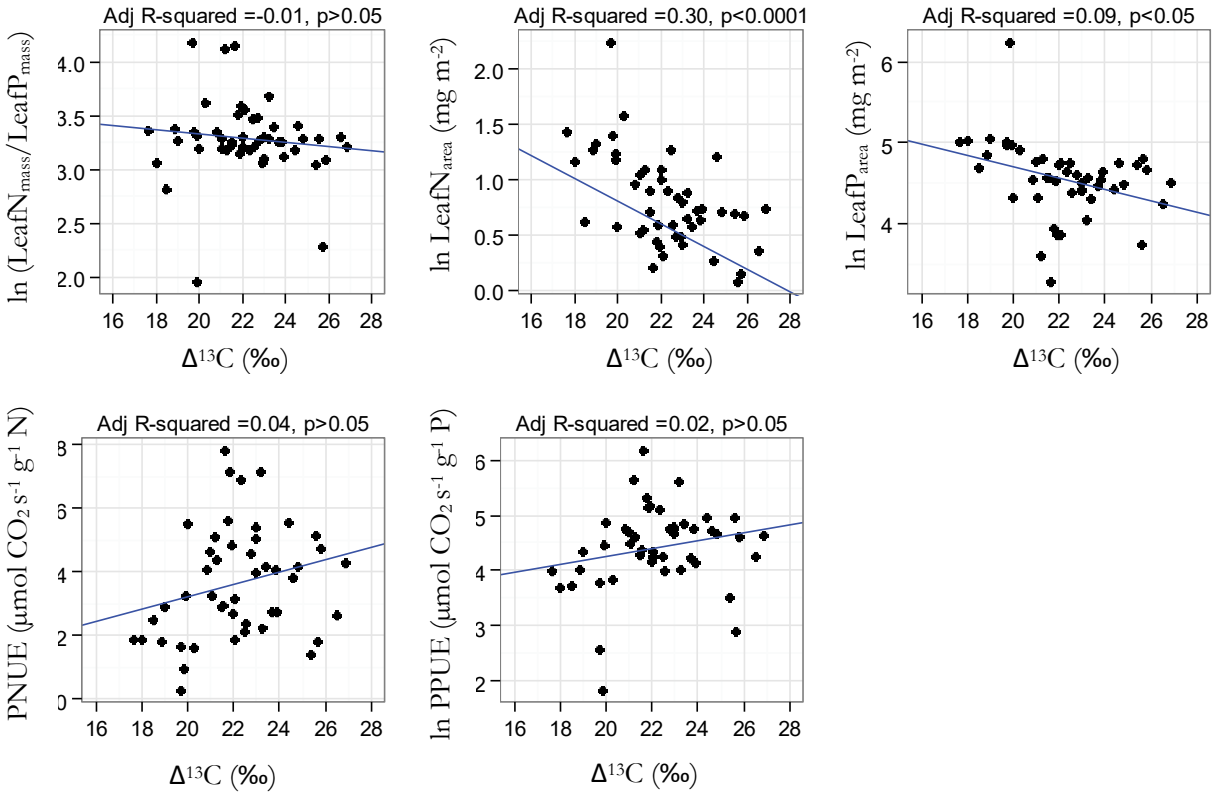

Figure 5.7: Carbon isotope discrimination in leaf dry matter (Δ^{13}C) *versus* leaf structural, nutrient and gas-exchange traits.

The best-fit phylogenetic GLS (blue) lines are displayed for each leaf-trait. Branch lengths scaled by the maximum likelihood of Pagel's λ parameter were used in the phylogenetic models (**Table 5.1**). Adjusted r^2 and associated p-values from the pGLS analysis are also shown.

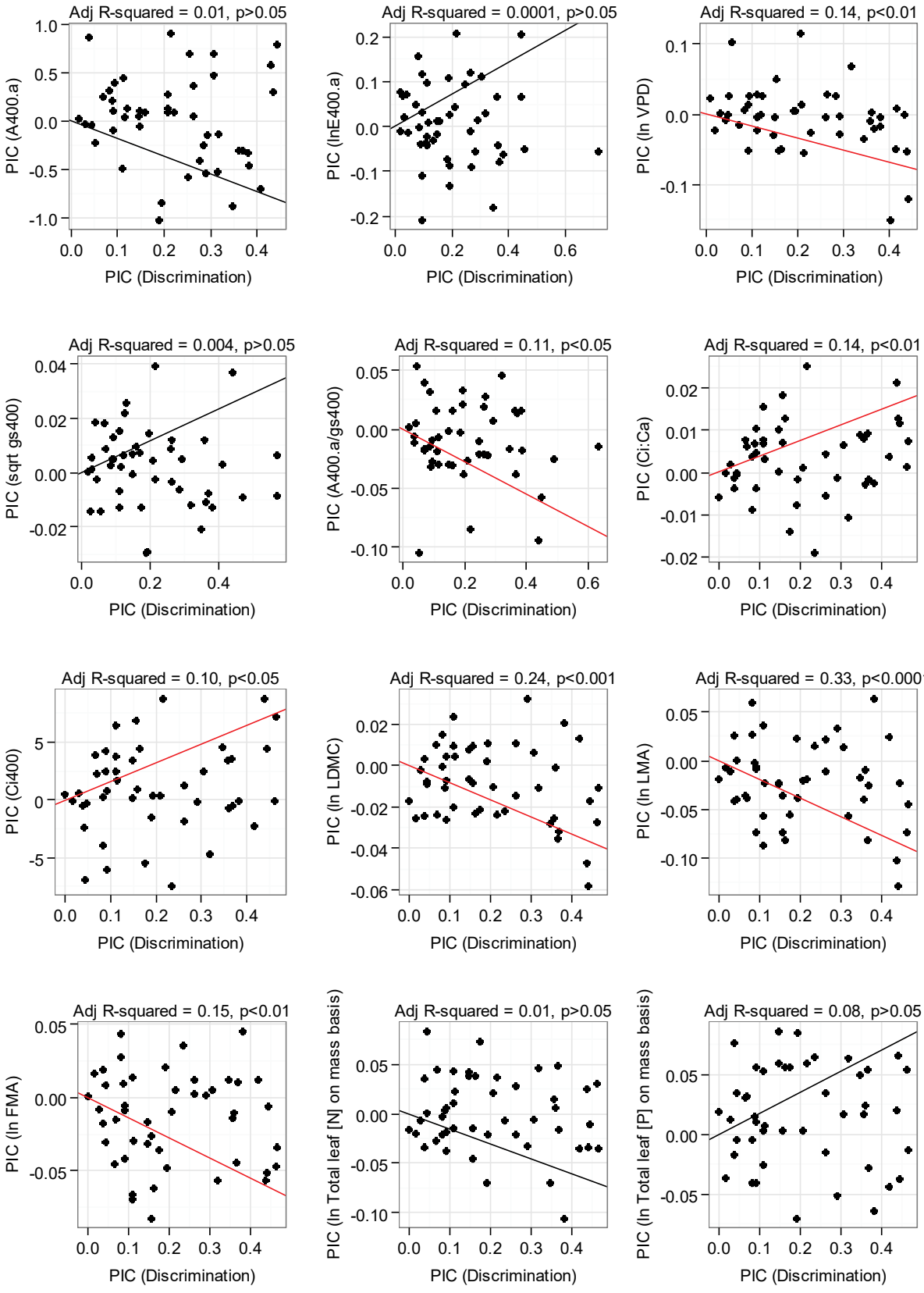
Adj R-squared = 0.01, p>0.05
PIC (A400.a)
PIC (Discrimination)
Adj R-squared = 0.0001, p>0.05
PIC (lnE400.a)
PIC (Discrimination)
Adj R-squared = 0.14, p<0.01
PIC (ln VPD)
PIC (Discrimination)
Adj R-squared = 0.004, p>0.05
PIC (sqrt gs400)
PIC (Discrimination)
Adj R-squared = 0.11, p<0.05
PIC (A400.a/gs400)
PIC (Discrimination)
Adj R-squared = 0.14, p<0.01
PIC (Ci:Ca)
PIC (Discrimination)
Adj R-squared = 0.10, p<0.05
PIC (Ci400)
PIC (Discrimination)
Adj R-squared = 0.24, p<0.001
PIC (ln LDMC)
PIC (Discrimination)
Adj R-squared = 0.33, p<0.0001
PIC (ln LMA)
PIC (Discrimination)
Adj R-squared = 0.15, p<0.01
PIC (ln FMA)
PIC (Discrimination)
Adj R-squared = 0.01, p>0.05
PIC (ln Total leaf [N] on mass basis)
PIC (Discrimination)
Adj R-squared = 0.08, p>0.05
PIC (ln Total leaf [P] on mass basis)
PIC (Discrimination)

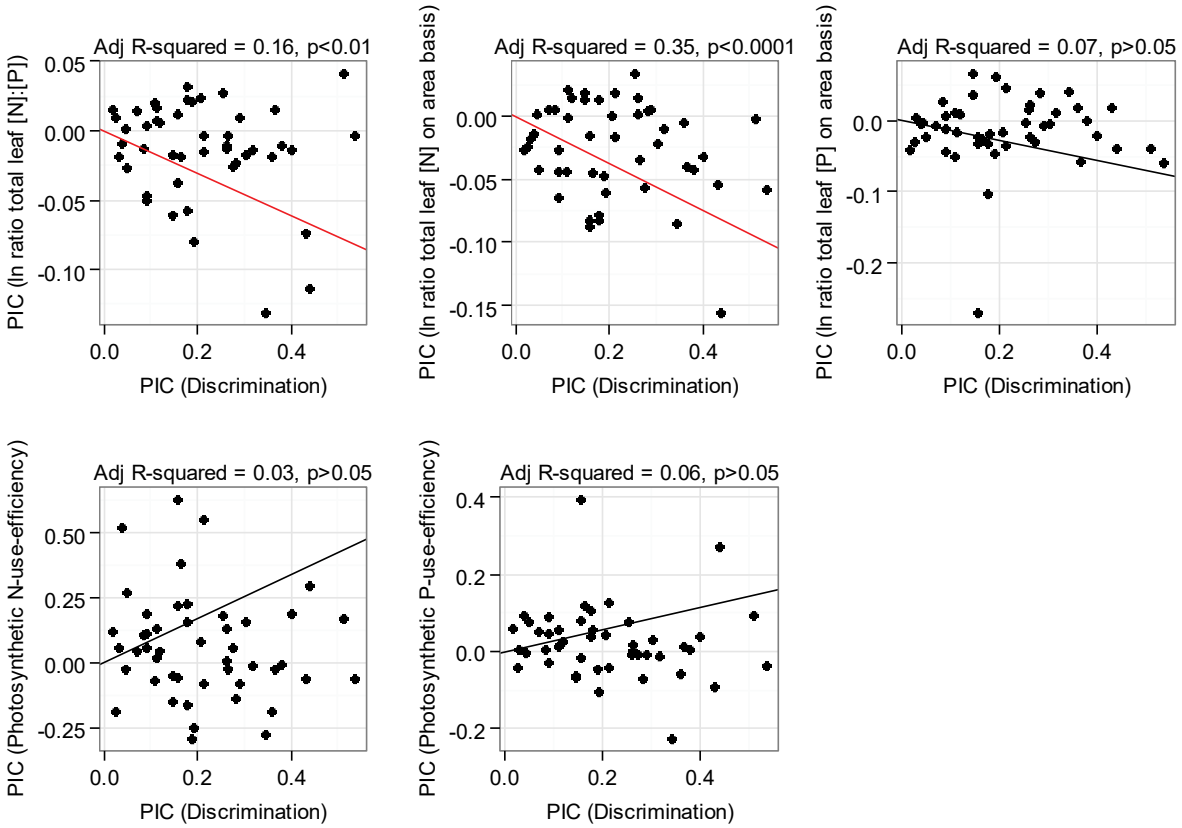

Figure 5.8: Scatterplots of independent contrasts of carbon isotope discrimination ($\Delta^{13}C$) *versus* climate variables.

Correlation analyses using independent contrasts are calculated through the origin. Red-lines: statistically significant best-fit lines for relationships between contrasts of discrimination and climate variables. Black-line: non-significant relationships. Adjusted r^2 and associated p-values are also shown.

Discussion

Similarity of $\Delta^{13}C$ in closely related species

The primary objective of the analyses performed in this chapter was to re-examine the cross-species relationships of $\Delta^{13}C$ with 19 climate variables and 16 other leaf-traits including formally the ancestral history of the plant species. These analyses were undertaken in order to investigate whether there exists significant discrepancies between standard non-phylogenetic and phylogenetic relationships that might have resulted from the potential similarity between the closely related species. To achieve this, first I investigated whether $\Delta^{13}C$ as a leaf-trait itself as well as the climate variables and other leaf-traits involved in the analysis were phylogenetically structured. The results suggest that variation of $\Delta^{13}C$ between species is related, at least to some extent, to their evolutionary trajectories among 55 species across Australia. This is because $\Delta^{13}C$ showed significant moderate phylogenetic signal in terms of both K and λ parameters (K= 0.39, $p<0.05$ and λ=0.67, $p<0.01$ after including intraspecific variations). When species-mean $\Delta^{13}C$ values were plotted by branches of the working phylogeny, closely related species were found to resemble each other more than expected by chance. For example, all species of the genus *Eucalyptus* showed $\Delta^{13}C$-values from the lower end of the spectrum despite their coming from different sites (mostly from the drier end of the rainfall spectrum, **Figure 5.9**). This suggests that even in this phylogenetically diverse set of species there is a pattern of similarity in terms of $\Delta^{13}C$ among closely related species.

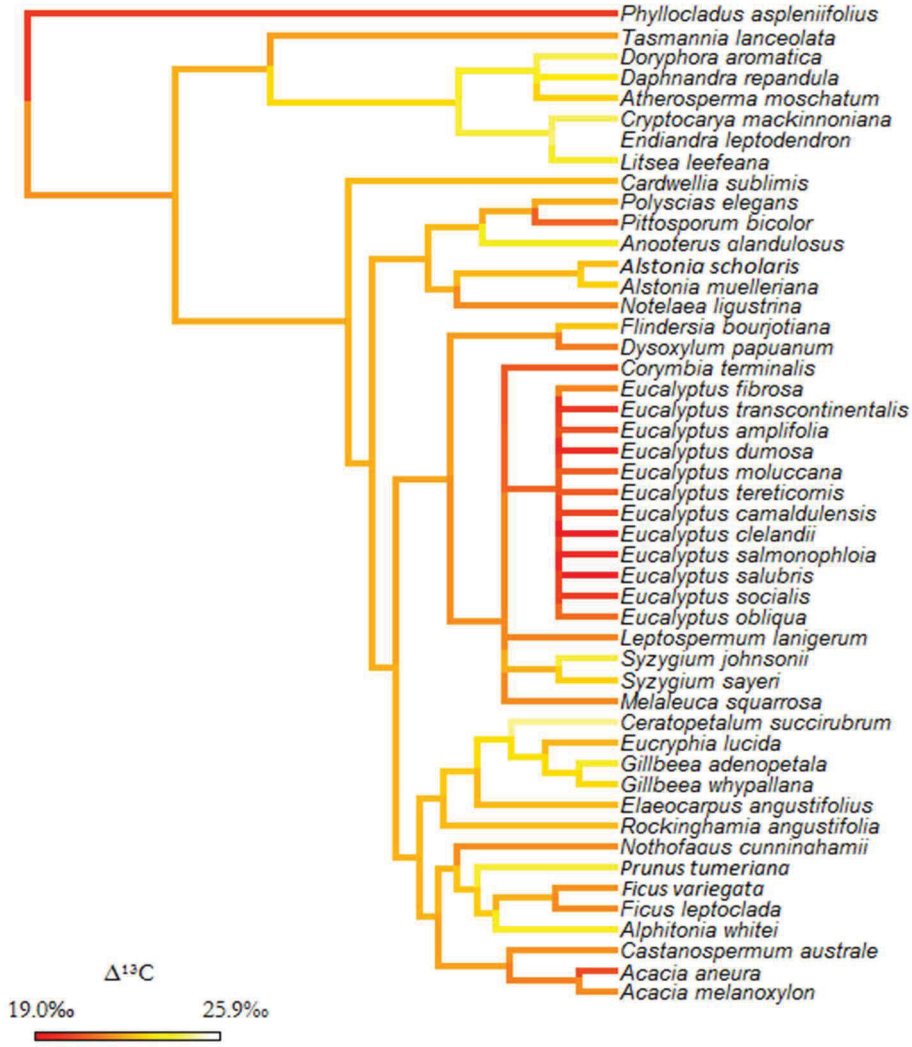

Figure 5.9: Phylogenetic tree depicting $\Delta^{13}C$ values by branches for 55 species considered in this study.

The colour of the branches is indicative of the range of $\Delta^{13}C$ values.

Although a phylogenetic signal gives an extent to which trait values are statistically related to the phylogeny and this has previously been documented for a myriad of morphological, physiological, life-history, behavioural and ecological traits (Blomberg *et al.*, 2003), interpreting evolutionary processes from the phylogenetic signal alone is not straightforward. Revell, (2010) in a simulation study showed that similar evolutionary processes may sometimes show contrasting phylogenetic signal, whereas similar phylogenetic signal may also be observed from completely different evolutionary processes.

This caveat is particularly pertinent to circumstances where phylogenetic signal is weak (Revell, 2010). In the case of $\Delta^{13}C$, Pagel's λ (which is a scaling parameter for correlations relative to the correlation expected under a Brownian motion model of evolution) showed a moderate signal and p-values were statistically significantly smaller ($p < 0.01$) from the likelihood ratio tests simulated from 1000 random phylogenies. Blomberg's *K*-value, however, does not vary linearly with the strength of Brownian motion, and its upper limit depends on the number of species in the phylogeny (Blomberg *et al.*, 2003; Münkemüller *et al.*, 2012). The *K*-value for $\Delta^{13}C$ ($K=0.39$, $p<0.05$) in this present study fell around the inferred upper limit for 55 species involved in this study (from Figure 2 in Münkemüller *et al.*, (2012)). *K*-values for $\Delta^{13}C$ were also found to be significantly larger ($p<0.05$) from randomization tests involving 1000 random phylogenies. When closely related species tend to resemble each other, theoretically, the variances obtained from the independent contrasts are expected to be low. A randomization test using the variance of independent contrasts simulated from 1000 random phylogenies also showed that the variance of $\Delta^{13}C$ was smaller than 95% random variances (see **Appendix B** for figures). All these findings, with due caution, suggests that species-mean values of bulk-leaf $\Delta^{13}C$ were significantly phylogenetically aggregated, although, this does not provide further implications regarding the actual mechanisms that may have caused the resemblance.

Phylogenetic signal in climate variables and leaf-traits

The next objective was to determine whether phylogenetic signals can be detected from the climate variables across seven SuperSites in Australia. In addition to estimating *K* and λ-values for each WorldClim variable, randomization tests for *K*, likelihood ratio tests for λ and separate randomization tests using variances of independent contrasts were performed using 1000 random phylogenies in all tests. Five temperature related variables and five precipitation related variables showed significant non-random phylogenetic signal in all tests; these are: mean diurnal range, isothermality, temperature seasonality, minimum temperature of the coldest month and annual range among the temperature variables and MAP, precipitation of the wettest month and wettest quarter, precipitation seasonality and precipitation of the warmest quarter among the precipitation variables. This result suggests that particular climate conditions were also phylogenetically clustered in the scale of 55 species investigated here. Mean annual precipitation as an example of a phylogenetically clustered climate variable is plotted in the tips of the working phylogeny (see **Figure 5.10**). **Figure 5.10** shows that, wet conditions (MAP > 1000 mm) were located within particular

clades in the phylogeny, while, dry moderate conditions (MAP < 1000) were located within other clades.

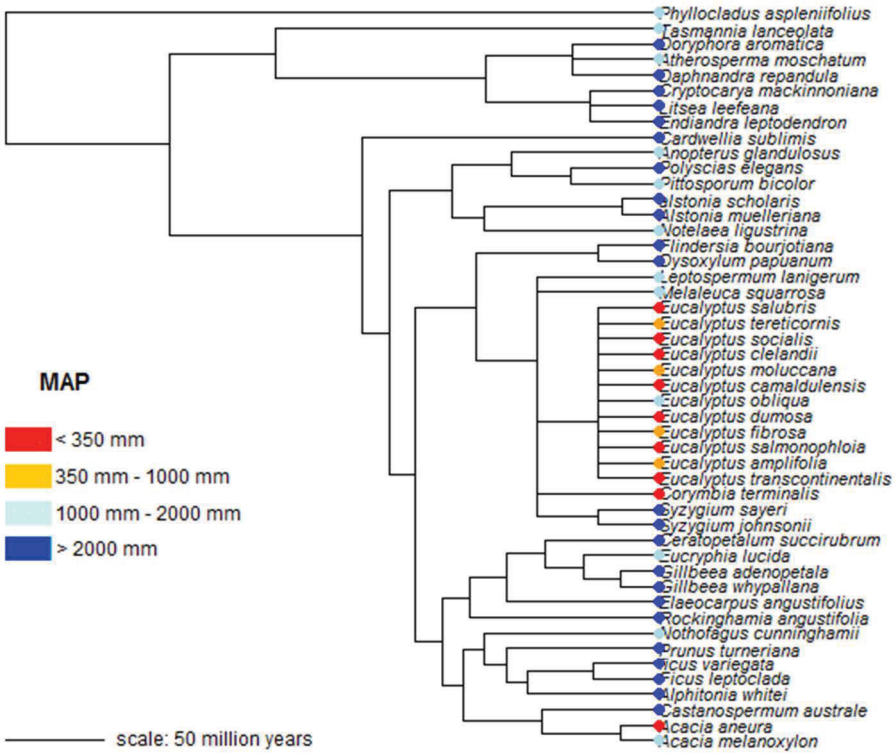

Figure 5.10: Phylogenetic clustering of Mean Annual Precipitation (MAP).

Significant non-random phylogenetic signals in most of the climate variables involved in the analysis imply that more closely related species are found under a given set of climate conditions across the gradient at a large spatial scale in Australia. From an evolutionary perspective, either an ancestor will have been present at a particular location in the past followed by speciation events thereby producing a set of closely related species there and/or closely related species with similar traits have dispersed there and established themselves, producing non-random phylogenetic signals. Strong phylogenetic signals in possible selective forces have previously been used in interpreting the signals in species-

specific traits (Kamilar and Cooper, 2013). If possible selective forces, for example, environmental conditions, play a significant role in shaping aspects of specific traits, there should also be a positive correlation between the environmental similarity of sites and the traits displayed by populations at those sites while controlling for their evolutionary relatedness (Kamilar and Cooper, 2013). In this dataset, all climate variables that showed significant non-random phylogenetic signals in all tests were also the variables that showed the strongest relationships with $\Delta^{13}C$ (both in non-phylogenetic and phylogenetic regressions, **Table 5.2**) among 19 climate variables. This result indicates that the climatic conditions experienced by the species indeed drove the variation in their bulk-leaf $\Delta^{13}C$ signatures. A significant non-random phylogenetic signal for the precipitation-temperature niche space is therefore likely to explain significant phylogenetic signals detected in $\Delta^{13}C$.

Other than $\Delta^{13}C$, a significant phylogenetic signal was detected in all leaf structural traits such as leaf mass per unit area (LMA), fresh mass per unit area (FMA) and ratio of dry to fresh mass (LDMC) in all tests. Among leaf nutrient traits, total leaf [N] was the only trait that showed strong phylogenetic signal in all tests. C_i/C_a and C_i400 among all the gas-exchange traits showed significant phylogenetic signal. Leaf intrinsic water-use-efficiency calculated from the ratio of A400.a to g_s400 as well as calculated from bulk-leaf $\Delta^{13}C$ showed significant non-random phylogenetic signal in all tests. Interestingly, as observed for $\Delta^{13}C$, all of these traits in several previous studies showed strong relationships with climate conditions, more specifically water-availability; for example, low rainfall was associated with higher LMA/FMA (Eamus *et al.*, 2006b; Fonseca *et al.*, 2000; Turner, 1994), high N-concentrations in leaves (Cunningham *et al.*, 1999; Schulze *et al.*, 1998b; Taylor and Eamus, 2008; Wright *et al.*, 2001) and low C_i/C_a (Wright 2001). Significant phylogenetic clustering of these traits in the scale of the species analysed in this chapter might therefore also be associated with climate conditions experienced by these species.

While evidence of phylogenetic clustering in $\Delta^{13}C$, climate variables and leaf-traits provides information on the extent to which trait values/climate variables are statistically related to phylogeny, it does not justify the use of taking genealogical information into account while studying cross-species variations in these traits. This is because the core assumptions of independence and constant variance that are made in the standard statistical models apply to the "residuals" from the models and not to the response or predictor variables *per se* (Hansen, 2014; Revell, 2010). Strong phylogenetic signal in the response variables or both

predictor and response variables does not necessarily invalidate the results from standard non-phylogenetic models. This will be further discussed in the following section.

Phylogenetic and standard non-phylogenetic relationships of ⊿^{13}C

Since closely related species had more similar values of $\Delta^{13}C$ and some other leaf-traits indicative of these traits were phylogenetically aggregated, I investigated how shared phylogenetic history of the species involved in this study affected the standard non-phylogenetic relationships of $\Delta^{13}C$. The parameter λ estimated from the phylogenetic generalized least square analysis from *caper* gives the amount of phylogenetic signal obtained from the residual errors of a particular relationship, not the strength of signal in the response variable or predictor variables, and also accounts for the amount of signal in the data by altering the properties of the variance–covariance matrix (Hansen, 2014). If there is no phylogenetic signal in the data, pGLS returns estimates identical to an ordinary least squares regression analysis, whereas, in the case of intermediate phylogenetic signals, pGLS corrects for phylogeny to the appropriate degree (Hansen, 2014). Interestingly, in this dataset, most of the climate variables that had the strongest relationships with $\Delta^{13}C$ (mean diurnal range, isothermality, temperature seasonality, T annual range, MAP, precipitation of the wettest month and precipitation of the wettest quarter) did not show strong phylogenetic signals in the error structures and consequently results from pGLS and standard non-phylogenetic GLS were virtually identical (**Table 5.2**). The climate variables that showed significant phylogenetic signal in the error structure also, in most cases, did not have strong cross-species relationships with $\Delta^{13}C$. This result indicates that analyses and interpretations of the relationships of $\Delta^{13}C$ with climate variables based on cross-species patterns from this dataset are well supported from a phylogenetic perspective.

Among the gas-exchange traits, only C_i/C_a and C_i400 showed moderate phylogenetic signal in the error structure and the slopes and intercepts of these traits were slightly different in pGLS models than non-phylogenetic GLS models (**Table 5.4**, **Figure 5.7**), although the direction of the slope remained the same even after accounting for ancestral history. This result was expected since $\Delta^{13}C$ was found to be phylogenetically structured and as C_i/C_a ratio of the leaves is what primarily drives bulk-leaf $\Delta^{13}C$ signatures (Cernusak *et al.*, 2011), it should also reflect similar phylogenetic patterns. The C_i/C_a ratio is again controlled by the balance between A400.a and g_s400 (**Chapter 4**) and both of these traits did not show any phylogenetic signal. Evolutionary lability of A400.a and g_s400 indicates that both of

these traits responded to possible selective forces in order to give a relatively stable C_i/C_a ratio of the leaves. All leaf structural traits (LDMC, LMA and FMA) showed moderately strong phylogenetic signals of the residuals but their relationships with $\Delta^{13}C$ still remained significant. Overall, the nature and magnitude of significant relationships of $\Delta^{13}C$ with other leaf-traits generally remained quite similar in both phylogenetic and non-phylogenetic models even after controlling for phylogenetic history.

Correlated evolution of ∠I^{13}C with climate variables and leaf-traits

Correlations across evolutionary divergences (for example, correlations of the PICs of two variables) describe whether divergences in one variable have consistently been associated with divergences in another through evolutionary history. Given that bulk-leaf $\Delta^{13}C$ showed statistically significant relationships with some of the climate variables/leaf-traits in the dataset, the next goal was to investigate whether these relationships are further supported by divergences between closely related species. More specifically, I assessed whether phylogenetically independent divergence events of bulk-leaf $\Delta^{13}C$ were consistently associated with divergences of the climate variables of the habitats occupied by the species and also with divergences of leaf structural, nutrient and gas-exchange traits. Correlated evolution is more commonly assessed in studies using independent contrasts (PICs), however, pGLS also provides equivalent information to PICs though couched in slightly different ways (Blomberg *et al.*, 2012; Garland Jr and Ives, 2000; Grafen, 1989; Rohlf, 2001; Symonds and Blomberg, 2014).

Overall PIC and pGLS analyses produced similar results, with significant association still remaining present between $\Delta^{13}C$ and its main climatic/leaf-trait correlates. The phylogenetic divergences of $\Delta^{13}C$ were correlated with divergences of climate variables and leaf structural, nutrient and gas-exchange traits (from both pGLS and PIC analyses) in a manner that the nature of correlated evolutions of $\Delta^{13}C$ with climate variables/leaf-traits were consistently similar in nature (although weaker) to those obtained from non-phylogenetic regressions of the contemporary species. This confirms that the observed cross-species relationships of $\Delta^{13}C$ were evident at the level of divergences between closely related species as well. This was especially true for the climate variables that did not show significant phylogenetic signal in the error structure obtained from pGLS analysis (**Table 5.2**). For example, among 19 climate variables investigated in the analysis, MAP showed the most significant cross-species relationship with $\Delta^{13}C$ (Adj r^2=0.55, p<0.0001), λ=0 from

pGLS and also the most significant evolutionary correlation with $\Delta^{13}C$ from PIC analysis (Adj r^2=0.46, $p<0.0001$). This result implies that where there was an evolutionary divergence of low $\Delta^{13}C$, there was also an evolutionary divergence of low MAP and *vice versa* throughout most of the working phylogeny, and, divergences occurred in multiple independent branches, thereby providing repeated evidence of correlated evolutionary divergence.

There were, however, climate variables in which the cross-species approach and independent contrast approach were quantitatively different from each other. For example, the relationships of mean T of the wettest quarter, mean T of the coldest quarter and precipitation seasonality with $\Delta^{13}C$ would be considered significant based on cross-species analyses but found to be non-significant based on independent contrasts. This occurred because the observed relationship of $\Delta^{13}C$ with these variables was not present in multiple evolutionary divergences throughout the working phylogeny. For example, there was evidence of multiple correlated evolutionary divergences between $\Delta^{13}C$ and all of the above climate variables in the clade "Rosales", but not in the clade "Myrtaceae"– ultimately resulting in an overall weak relationship between PICs of these variables and $\Delta^{13}C$. All species of the clade Myrtaceae came from the sites with smaller values of mean T of the wettest quarter, mean T the of coldest quarter and precipitation seasonality whereas, species of the clade Rosales came from sites with larger values for all of these variables. Also, the clade Myrtaceae consisted of species mostly coming from the sites at the drier end of the spectrum and species of the clade Rosales came from the sites with MAP>2000 mm. It therefore appears that in the wetter sites with larger values of mean temperature and precipitation seasonality, where there was an evolutionary divergence of smaller values of all these variables there was also an evolutionary divergence of smaller $\Delta^{13}C$ - which did not occur in the drier sites in the particular set of species in this dataset.

Another interesting observation was the phylogenetic relationships of both precipitation of the driest month and quarter with $\Delta^{13}C$ – which were non-significant in cross-species analysis but emerged as significant relationships in the independent contrast analysis (**Table 5.2**). These PIC relationships were significant such that, where there was an evolutionary divergence of smaller values of precipitation of the driest month/quarter, there was also an evolutionary divergence of smaller $\Delta^{13}C$. These relationships of annual mean of $\Delta^{13}C$ with these two variables were non-significant or only marginally significant with low r^2 values from the cross-species analysis. Also, the residuals both of these

relationships showed moderate phylogenetic signal. Precipitation of the wettest month/quarter on the other hand showed strong and significant relationships with $\Delta^{13}C$ in cross-species as well as PIC (and pGLS) analysis. The fact that the relationships of precipitation of the driest month and quarter with $\Delta^{13}C$ emerged as significant only in the PIC analysis highlights the importance of incorporating the phylogenetic information underpinning these variables in the analysis as well as the importance of taking into account the variation of seasonal water availability and how it influences variation in $\Delta^{13}C$.

Evidence of correlated evolution of a suite of leaf-traits with $\Delta^{13}C$ was identified from the PIC and pGLS analyses from these dataset. These traits were VPD, C_i/C_a, C_i400 and intrinsic WUE (calculated from the ratio of A400.a and g_s400), all leaf structural traits and two leaf nutrient traits (ratio of N to P and $LeafN_{area}$) and all of these traits presumably were tightly linked to water availability (**Chapter 4**). These traits also showed significant cross-species relationships and the direction of divergences of all of these traits proved to support the cross-species correlations. Most of these traits, interestingly, also showed moderate to strong phylogenetic signal themselves as well as in the residuals of the relationships, theoretically therefore, have most likely evolved by gradual changes over time (e.g. a Brownian motion model of evolution)(Symonds and Blomberg, 2014).

Patterns in $\Delta^{13}C$ with water availability: an evolutionary perspective

Researches across a broad array of terrestrial plants often reveal correlations among a suite of leaf structural, functional or nutrient traits and results are often interpreted as coordinated leaf-physiological strategies (Wright *et al.*, 2004). Cross-species trait analysis of contemporary species generally supports the idea that leaf-traits are evolutionary labile and adaptable because their observed plasticity in response to possible selective forces (Schwilk and Ackerly, 2001). **Chapter 4** of this thesis documented that, among 19 climate variables, bulk-leaf $\Delta^{13}C$ showed the strongest and the most significant relationship with MAP. Several other global and regional studies have also previously recorded this correlation (this is discussed in detail in **Chapter 4**).

One final aspect of this chapter was to investigate the relationships of bulk-leaf $\Delta^{13}C$ with water availability, observed in the cross-species analysis, from an evolutionary perspective. More specifically, does the relationship of $\Delta^{13}C$ with water availability reflect patterns of evolutionary convergence providing evidence of adaptive radiation? Or, does this

relationship occur due to contrasting characteristics of major seed-plant lineages indicative of phylogenetic niche conservatism? The results showed two lines of evidence suggesting that variation in $\Delta^{13}C$ with water availability primarily resulted from adaptive environmental convergence at least at the scale of species investigated in this present study. First, there was an absence of phylogenetic signal in the error structures of the relationships of $\Delta^{13}C$ and most of the precipitation related climate variables that showed strong cross-species relationships (MAP, precipitation of the wettest month, precipitation of the wettest quarter and precipitation of the warmest quarter). Both the response variable ($\Delta^{13}C$) and the predictor variables (precipitation related variables) of these relationships, however, showed significant non-random phylogenetic signals themselves. Typically this result arises when adaptation is rapid and supports the assumption that the modern day variation of $\Delta^{13}C$ with water availability principally results from adaptive environmental convergence (Hansen, 2014). The signal in the response variable ($\Delta^{13}C$) in this case is expected to occur because of related species occurring in similar environments (i.e., having similar values of their predictor variables) (Hansen, 2014). Second, interspecific relationships among $\Delta^{13}C$ and precipitation related variables reflected significant patterns of correlated evolutionary changes from the PIC analysis. A similar result has previously been observed in *Pereskia* (Cactaceae) species where ^{13}C compositions of leaf dry matter were found to be evolutionary correlated with MAP and moisture index (Edwards, 2006). Correlated evolution among $\Delta^{13}C$ and precipitation related variables (as denoted by significant coefficient of determination (r^2) of the fitted regression through origin between PIC of $\Delta^{13}C$ and PIC precipitation variables) means evolutionary changes in $\Delta^{13}C$ were significantly associated with parallel modifications in water availability - indicative theoretically of greater homoplasy (Ackerly and Donoghue, 1998) and lends further support to the adaptive interpretations of these relationships.

Conclusions

This chapter focused on presenting a comprehensive analysis of phylogenetic patterns in $\Delta^{13}C$, climate variables and leaf structural, nutrient and gas-exchange traits. More specifically, I looked at $\Delta^{13}C$ - climate /$\Delta^{13}C$ - leaf-trait relationships and their residuals and brought together all these patterns to compare and understand the relationships across species (non-phylogenetic) and among evolutionary divergences (phylogenetic). Results of these analyses demonstrated that cross-species relationships of $\Delta^{13}C$ and climate variables/leaf-traits were generally quite robust and well supported from an evolutionary

perspective. Correlated evolution between $\Delta^{13}C$ and climate variables as well as $\Delta^{13}C$ and leaf-traits also provided evidence of cross-species correlations being present at the level of divergence between closely related species. Significant non-random phylogenetic signals in most of the climate variables as well as $\Delta^{13}C$/leaf-traits were identified which indicated that climate played an important role in shaping the distribution of the species at a large spatial scale in Australia. Furthermore, combining phylogenetic and trait-based information supported the hypothesis that climate variables, mainly variables related to precipitation, influenced the evolution of discriminatory traits of leaves of the dominant species by decreasing discrimination against ^{13}C with reduced water availability and with high temperature. The results documented in this chapter highlights that accumulating more phylogenetic and trait-based information can indeed be a powerful approach for a closer evaluation of ecological adaptation of plants across a range of spatial scales.

Chapter 6 General Discussion

The work described in this thesis aimed to provide a detailed understanding of variations in sources of water uptake by vegetation as well as contrasting water use strategies across spatial and temporal scales a range of sites across Australia. In particular, I employed stable hydrogen, oxygen and carbon isotope analyses techniques to investigate variations in sources of water uptake by vegetation, discrimination against ^{13}C and water-use-efficiency across a range of contrasting sites as well as at a continental scale. At smaller spatial scales, analyses were performed along two naturally occurring depth-to-groundwater gradients in two contrasting mesic and arid ecosystems. The first study was undertaken at the Kangaloon bore-field in the Southern Highlands, NSW; the second study was undertaken in the Ti Tree basin, Central Australia (**Chapter 2** and **Chapter 3**). At a continental scale, discrimination against ^{13}C and water-use-efficiency of the dominant overstorey species were investigated across seven sites around Australia representing six contrasting biomes with mean annual temperature ranging from 10°C to ~28°C and mean annual precipitation from 255 to 2,140 mm $year^{-1}$ (**Chapter 4**). In a separate study (**Chapter 5**), the focus moved from ecological communities along moisture/climate gradients to examining 55 species spanning different habitats by incorporating genealogical relationships in order to re-evaluate some of the observed relationships of discrimination against ^{13}C with climate/leaf-trait attributes from an evolutionary perspective. Throughout this final chapter, I will highlight the principal findings from my analyses in association with what I consider are the most pressing avenues for future research that build upon the foundation of work presented in this thesis.

Variation in sources of water uptake and water use strategies along depth-to-groundwater gradients in mesic and arid ecosystems

Identifying the proportional contribution of different water sources (e.g., upper soil profile, deep soil profile or groundwater) in plant water uptake is a question investigated in a number of ecohydrological studies. As a continent with 70% of its land classified as semi-arid (Eamus *et al.*, 2006b; O'Grady *et al.*, 2011; O'Grady *et al.*, 2006c), many of Australia's ecosystems rely on groundwater to varying degrees (**Chapter 2**). A clear challenge to sustainable land and water resources management is to define a safe limit for groundwater draw-down, considering ecosystem requirements, in addition to human needs for groundwater. One of the aims of this research was to identify the proportional contribution of groundwater in water used by dominant overstorey and understorey species in two contrasting (mesic and semi-arid) ecosystems in Australia using stable isotope analyses. A combination of deuterium ($\delta^{2}H$) and oxygen-18 ($\delta^{18}O$) analysis along a naturally occurring depth-to-groundwater gradient in the mesic Kangaloon bore-field site in NSW clearly demonstrated that, even at these sites with consistently large mean annual rainfall of > 1000 mm received over 12 months before the study, increased access to groundwater still exerted some influence on sources of water uptake by the dominant overstorey and understorey species. The proportional contribution of groundwater in plant water uptake did not significantly increase as depth-to-groundwater decreased as I hypothesised. However, there was a clear differentiation between source water-uptake of sites with differential depth-to-groundwater such that, at the shallower sites, plant water uptake was constrained to the shallow unsaturated zone of the soil profile whereas, at the deeper sites, both overstorey and understorey species shifted to recent rain water (represented by the superficial layers of the soil profile) as their principal source of water. Results from stable deuterium and ^{18}O analysis also supported the findings from previous studies that investigated the groundwater dependent ecosystems in this particular area and concluded that the threshold access of groundwater was ~9 to 10 m in this region and beyond this depth there were minimal changes in vegetation structure and function in response to increase in depth of the water table (Zolfaghar *et al.*, 2014; Zolfaghar *et al.*, 2015). These studies in this region have also documented significantly larger aboveground biomass and net primary productivity at the shallower end of the depth-to-groundwater gradient (Zolfaghar *et al.*, 2014; Zolfaghar *et al.*, 2015).

Since putative access to groundwater appeared to influence the structural and functional traits of vegetation in these sites, I further hypothesised that access to a permanent water source (i.e., groundwater) will be manifested in discrimination against ^{13}C and water-use-efficiency calculated from stable ^{13}C isotopes at the leaf-level. Consistent with the findings from stable water isotope analysis that could not identify any significant differences in proportional groundwater uptake along the gradient, ^{13}C analysis at the *leaf-level* also could not identify significant variations in discrimination against ^{13}C and water-use-efficiency along the depth-to-groundwater gradient. I propose that the absence of significant trends in proportional contribution of groundwater and water-use-efficiency of the dominant vegetation in these mesic sites have arisen because of the exceptionally wet summer with 46% and 11% larger rainfall than the long-term mean experienced in the study sites in two consecutive years prior to sampling (also associated with the 2010/2011 global land sink anomaly (Poulter *et al.*, 2014)). Associated with this significantly larger annual rainfall was the lower-than-average vapour pressure deficit (VPD) and temperature, arising from the extensive cloud cover during this period (Zolfaghar, 2014). Reduced VPD, temperature and solar radiation imposed large constraints on the daily, seasonal and annual rates of transpiration and photosynthesis, which may therefore have contributed to the lack of ^{13}C discrimination at the leaf-scale. To examine the influence of recent above average rainfall on water uptake and use by dominant vegetation, ^{13}C-content of stem-wood as a function of depth through tree stems was measured to compare recent sapwood samples with heartwood samples that represent climate conditions experienced by the vegetation in the past. Analysis of ^{13}C-content of the heartwood samples clearly identified that, in drier climatic conditions, trees in shallower sites were able to successfully tap into groundwater and therefore were also less efficient in their water use. In this instance, I ask how/when might we identify significant variation in groundwater uptake by the dominant species at these mesic sites in Kangaloon? The results from carbon isotope analysis of the stem heartwood samples suggest that, groundwater resources in these sites are likely to be more important during the dry-season, as observed in Australian savannas previously, where at least 50% of water used for transpiration in some species came from deeper water sources during dry conditions (Lamontagne *et al.*, 2005). Consequently, future research can focus on how vegetation in this region respond in terms of their water uptake/use strategies in drier conditions when soil water availability is reduced. Another modification of the methodology adopted in the current work that can potentially improve the results of the stable isotope mixing models is to sample soil up to the actual depth to the water table,

especially at the deeper sites, which will enable more accurate identification of the isotopic composition of distinct water pools throughout different depths of the soil profile and therefore a more accurate estimation of proportional contributions of each of these water pools in plant branch (xylem) water.

Australia's climate is highly heterogeneous spatially and temporally and its key features in relation to ecology are the amount and timing of rainfall and seasonal mean maximum and minimum temperatures (Eamus *et al.*, 2006b). Stable isotope analysis of branch water, rain water, soil water and groundwater and ^{13}C-content at the leaf-level was also performed in a semi-arid ecosystem in Ti Tree basin located in 200 km north of Alice Springs in Central Australia. These two selected study sites (described in **Chapter 2** and **Chapter 3** respectively) fell at two opposite ends of the spectrum pertaining to their key climatic features. While the Kangaloon site had received >1000 mm year $^{-1}$ rainfall, especially for the two years immediately prior to sampling, the Ti Tree region received < 350 mm year^{-1} rainfall and experiences a highly monsoonal climate, with prolonged periods of zero rainfall during the dry-season and >60% of mean annual rainfall during the wet-season. Mean maximum temperature in January was 24.3°C and 46.2°C in Kangaloon and Ti Tree respectively. Consequently, the composition, structure and functional attributes of vegetation in these two sites are significantly different. The mesic Kangaloon site was characterised by very dense broad-leaf evergreen *Eucalyptus* woodland of very tall trees (26±0.66 m at the shallowest site) (Zolfaghar *et al.*, 2014), whereas, the Ti Tree basin was characterised by (a) evergreen needle-leaf *Acacia* woodlands of short (3-7 m) stature; (b) discontinuous canopies and *Corymbia* savanna of taller and widely spaced broad-leaf evergreen trees and (c) riparian forest composed principally of *Eucalyptus camaldulensis* (Cleverly *et al.*, 2016). Stable isotope analysis was able to capture some of the key contrasting features in these two different ecosystems. The local meteoric water line of the mesic Kangaloon site ($LMWL_{Kangaloon}$: $\delta^2H = 8.66\ \delta^{18}O + 12.60$) did not vary significantly from the global meteoric water line (GMWL, $\delta^2H = 8.13\ \delta^{18}O + 10$) (Rozanski *et al.*, 1993). In contrast, rain water isotopic composition in Ti Tree showed values typical of water-limited regions and the slope of the LMWL was less steep compared to the GMWL which classically occurs due to "the evaporation effect" ($LMWL_{Ti\ Tree}$: $\delta^2H = 4.53\ \delta^{18}O + 3.03$). Also in contrast to mesic Kangaloon sites, stable isotope analysis of branch water and ^{13}C-content at the leaf-level could reliably and consistently identify access to groundwater by vegetation in the sites of the semi-arid Ti Tree basin. Consistent with several previous

studies in Central Australia and in Ti Tree basin, deuterium and ^{18}O analysis branch water of *Eucalyptus* and *Corymbia spp.* consistently identified that these deep-rooted species relied primarily on groundwater as their source of water uptake in these semi-arid regions especially when groundwater was available within their root-zone (Cook *et al.*, 2008; Howe *et al.*, 2007; O'Grady *et al.*, 2006a; O'Grady *et al.*, 2006c). These trees also did not shift to any other sources despite increased soil water availability during the wet-season. Deep-rooted species in this semi-arid region can therefore be classified as groundwater dependent ecosystems (GDEs) that are *obligate users* of groundwater when groundwater is available within their rooting zone. In contrast, the shallower rooted *Acacia spp.*, dominant in Mulga (*Acacia*) woodland of this region, were dependent primarily on shallow soil water, with some uptake occurring from perched water (hence representing an ephemeral groundwater source) accumulating above the widespread shallow hardpan (Cleverly *et al.*, 2016). Analysis of deuterium and ^{18}O isotopes from branch (xylem) water and soil water could also identify variations in soil water and xylem water isotope composition for both shallow- and deep-rooted species between dry- and wet-season in these semi-arid sites. Furthermore, variability of sources of water between plants spanning across different micro-habitats at a particular site commonly observed in this region was also captured by deuterium-^{18}O analysis. These micro-habitats were identified as "within the *Acacia* patch"; "the transition zone between the *Acacia* and the *Corymbia* savanna" and "within the *Corymbia* savanna". Deuterium-^{18}O analysis could identify access to groundwater by deep-rooted *Corymbia* trees in the *Corymbia* savanna where the roots were not subjected to restricted growth due to the existence of siliceous hardpan. These trees continued to access groundwater even during the wet-season despite increased soil water availability. Variability within micro-habitats was also apparent in the ^{13}C analysis at the leaf-level such that, the *Corymbia* trees identified as accessing groundwater from deuterium-^{18}O analysis also showed largest discrimination against ^{13}C (and smallest WUE_i) from ^{13}C analysis.

Water-use-efficiency is an important attribute of vegetation: almost all terrestrial ecosystems experience some limitation in growth and productivity at some point by reduced water availability and this is especially prevalent in arid/semi-arid regions (Huxman *et al.*, 2004). Vegetation at sites with limited water resources generally exhibit higher water-use-efficiency (Ford *et al.*, 2008) than vegetation growing in mesic sites. One of the potential outcomes identified from my research in semi-arid regions of Central Australia was the fact that discrimination against ^{13}C ($\Delta^{13}C$) and leaf intrinsic water-use-efficiency

(WUE_i) calculated from stable ^{13}C isotopes at the leaf-level could accurately identify water availability, specifically, groundwater use and spatial and/or seasonal patterns of groundwater use in these sites. Consistent with the results of deuterium and ^{18}O from branch water, ^{13}C analysis at the leaf-level did not vary significantly with depth-to-groundwater in shallower rooted *Acacia spp.* However, in the deep-rooted species with plausible access to groundwater, discrimination against ^{13}C declined and water-use-efficiency increased significantly with increasing depth to groundwater up to a threshold value of depth-to-groundwater of 13.9 m and then showed non-significant trends from 13.9 m to 49.5 m. These findings support previous studies performed in Ti Tree basin that recorded the highest rate of daily water use of deep-rooted *Corymbia* trees at depth-to-groundwater <10 m from sapflow measurements, which decreased as depth-to-groundwater increased to 20 m (Howe *et al.*, 2007). Overall, my results indicate that analysis of stable ^{13}C isotopes at the leaf-level for deep-rooted trees accurately mirrored access to groundwater inferred from deuterium-^{18}O analysis at the shallower end of the groundwater gradient in this semi-arid region. Results obtained from ^{13}C analysis of the dominant vegetation in the Ti Tree basin were also replicated in Allungra Creek waterhole, a frequent recharge zone located at the southern boundary of the Ti Tree basin. Trees closest to the creek (including *Acacia* species) discriminated against ^{13}C significantly more (and consequently showed smaller WUE_i) suggesting access to this water source by all species. No significant difference was detected in both *Acacia* and *Corymbia* trees further down the transect as distance from the water source increased. These findings from Ti Tree basin study and Allungra Creek study reinforce my initial hypothesis that analysis of stable isotopes is a powerful tool in determining source of water uptake and water use strategies in vegetation especially when there is a distinct water availability gradient.

While my research has identified that stable ^{13}C analysis is a sufficiently good proxy of leaf-level WUE_i measurements, further investigation on gas-exchange attributes, especially photosynthetic assimilation, stomatal conductance and the ratio of intercellular to atmospheric concentration to CO_2 (C_i/C_a ratio) and their correlations with $\Delta^{13}C$ and WUE_i along depth-to-groundwater gradients will provide valuable insights on the physiological underpinnings of these relationships observed at the scale of this research.

Linking leaf structural and functional traits- can variation in leaf morphological traits explain variations in $\Delta^{13}C$?

This research also reinforced the importance of considering effects of differential access to water between species manifested as changes in morphological traits of plants, particularly at the leaf-level. Inherent leaf structural traits, for example, leaf vein density (LVD) influence the whole-plant performance and has increasingly been gaining attention and have been shown to be influenced by morphological and environmental factors (Uhl and Mosbrugger, 1999). LVDs observed in species from the Ti Tree basin fell close to the higher end of the global spectrum (Figure 4, Sack and Scoffoni, (2013)) consistent with higher LVDs obtained from "semi-desert" species in this present study. Higher LVDs allow more even spatial distribution of water across the phyllode/lamina during water-stress, further contributing to greater consistency of mesophyll hydration (Sommerville *et al.*, 2010). In turn, more consistent mesophyll hydration allows continued photosynthetic carbon assimilation during water-stress (Sommerville *et al.*, 2010). Two interesting relationships pertaining to water availability have been identified in my study with LVD. First, LVD of the deep-rooted *Corymbia* species increased from depth-to-groundwater 4.4 m to 13.9 m with no statistically significant relationships as depth increases beyond 13.9 m. Second, a stronger linear relationship was observed between LVD and bulk-leaf $\Delta^{13}C$ such that, significantly smaller vein-densities were observed in leaves that also showed larger discrimination against ^{13}C. LVD is influenced by a number environmental variables such as temperature, light interception, soil dryness, humidity and nutrient availability (Sack and Scoffoni, 2013; Uhl and Mosbrugger, 1999). However, water availability has been attributed as the most important factor that influence venation density (Uhl and Mosbrugger, 1999). Since leaf veins essentially carry the water that is lost through the stomata during transpiration, the propensity for leaves to lose water should match the capacity of the xylem to deliver the same water (Brodribb and Holbrook, 2007; Meinzer and Grantz, 1990; Sperry, 2000) and consequently creates a plausible relationship of vein density with water availability. I found a statistically significant relationship between LVD and depth-to-groundwater was observed up to a depth of 13.9 m. However, no significant relationship was found beyond this depth (i.e. depth-to-groundwater 13.9 m – 49.5 m) where depth of the water table had presumably exceeded the rooting depth of the plants. Moreover, no significant relationship was observed between the LVDs of shallower rooted *Acacia* species with depth-to-groundwater, lending further support on variation in LVD with water availability through access to groundwater. The most interesting relationship obtained from

this study was that of an inverse linear relationship between $\Delta^{13}C$ and LVD in deep-rooted *Corymbia* species. In this instance, I investigated how we might explain the link between a structural leaf-trait like LVD with a functional trait like $\Delta^{13}C$ (and WUE_i) in these groundwater accessing species. As a consequence of stomatal opening for gas-exchange during photosynthesis (g_s), plants loose a considerable amount of water via transpiration. To gain carbon most economically with respect to water, stomata should function in such a manner that the marginal water cost of carbon assimilation ($\frac{\partial A}{\partial E}$) remains constant (Cowan and Farquhar, 1977; Farquhar and Sharkey, 1982) and this particular aspect of stomatal control effectively couples structural traits involved with water-flow with traits associated with primary production (Brodribb and Holbrook, 2007). Consequently LVD is directly related to leaf hydraulic conductance (K_{leaf}) and also with photosynthetic assimilation (A) as previously observed in several studies (Brodribb *et al.*, 2007; Brodribb *et al.*, 2010; Brodribb *et al.*, 2005; Brodribb and Jordan, 2008; Sack and Holbrook, 2006; Sack and Scoffoni, 2013). A significant relationship of LVD with $\Delta^{13}C$ (which is also modulated by the A/g_s ratio) therefore suggests that supply of water through veins was optimized by these plants with respect to assimilation-related loss of water. However, this relationship was observed only in deep-rooted *Corymbia* species and not in shallower rooted *Acacia* species at the scale of the species studied in this research. Consequently, there are questions, beyond the scope of the current work, regarding factors not addressed as yet such as - whether these relationships are observed in plants of different functional types or between structurally different leaves such as phyllodes/needle leaves.

Hydrological niche separation in arid ecosystems

One of the long-standing ecological questions related to resource partitioning within communities is: How do co-existing plants co-exist? Resource-based competition theory hypothesizes that the basis of stable co-existence between species in species-rich ecosystems is that each species is a superior competitor in its own niche (Williamson, 1957). An ambiguity associated with this theory is that all plants species essentially use and compete for the same resources (e.g., water, CO_2, light etc.) which they acquire in a very limited variety of ways; therefore, there exist significant overlaps between the observed niches of these co-occurring species (Mahdi *et al.*, 1989; Tilman, 1984). In water-limited ecosystems, however, environmental conditions and resource supply rates are highly heterogeneous both spatially and temporally, providing an additional axis of differentiation

for niche separation and species co-existence. Consequently, several ecological studies identified the "differences in access to, and use of, water in space and time" to be a fundamental axis for niche separation (Araya *et al.*, 2011; Silvertown *et al.*, 1999).

Deuterium and ^{18}O analysis in the semi-arid Ti Tree basin described in **Chapter 3** of this thesis has identified that the two dominant co-occurring species in this region, i.e., shallower-rooted *Acacia spp.* and deep-rooted *E. camaldulensis* and *Corymbia opaca* segregated along a continuous depth-to-groundwater gradient and across distinctly different micro-habitats maintained their relative isotopic rankings in two sampling dates with contrasting water availability (i.e., the late dry- and wet-season). When groundwater was beyond the rooting-depth, sources of water uptake of deep-rooted *Eucalyptus* and *Corymbia* species did not vary significantly from that of the shallower-rooted *Acacia* species. When groundwater was within the rooting-depth, however, the deep-rooted species showed continued access to groundwater even during the wet-season despite sufficient soil water availability. Discrimination against ^{13}C and leaf intrinsic WUE_i calculated from stable ^{13}C isotopes at the leaf-level also mirrored contrasting water uptake strategies between the shallow and deep-rooted species inferred from deuterium -^{18}O analysis at the shallower end of the DTGW gradient and across contrasting micro-habitats such that, larger discrimination against ^{13}C and smaller WUE_i was observed from the trees that had access to groundwater. These results from stable isotope analyses is suggestive of the existence of "hydrological isotopic niches" driven by the difference in the rooting-depths of this two co-occurring dominant species leading to spatial and temporal partitioning of limiting water-resources in this semi-arid region. These results also show that screening of plant species deuterium, ^{18}O and ^{13}C isotope ratios can be a powerful tool to characterize the diversity of water uptake/water use strategies and associated niche segregation present in severely arid/semi-arid ecosystems.

Variation in $\Delta^{13}C$ along a continental-scale climate gradient

From an ecohydrological perspective, it is important to understand how leaf-level structural and physiological characteristics vary with large spatial and temporal heterogeneity of Australian climate at a continental-scale in addition to smaller spatial scales. Analysis performed at smaller spatial scales provides opportunities to investigate how leaf-traits like $\Delta^{13}C$ and WUE_i varied with differential access to water while still being under similar climate envelopes. However, analysis performed across sites located in distinctly different

climate biomes provides a comparison of these traits and their variations across a wide range of environmental conditions experienced in different sites, for instance, from strongly water-limited ecosystems with pulsed water-resource availability and high mean daily temperature to extremely wet ecosystems with water surplus and moderate mean daily temperature throughout the year. In principal, $\Delta^{13}C$ and WUE_i is modulated by the ratio of intercellular and atmospheric concentration of CO_2, which is regulated by leaf-level stomatal conductance. The propensity for leaves to impose stomatal regulation on gas-exchange, in turn, is largely dependent on the environmental conditions experienced by the leaves, and therefore, an analysis across contrasting ecosystems provides a novel understanding of how plant species respond to different environmental stresses in different climatic conditions.

Two recent meta-analyses of variation in $\Delta^{13}C$ across contrasting ecosystems at a global scale have documented decreasing $\Delta^{13}C$ (and concomitant increase in WUE_i) with decreasing MAP where MAP explains about half of the variation in $\Delta^{13}C$ across the globe (Diefendorf *et al.*, 2010; Kohn, 2010). At smaller spatial scales in Australia, previous studies have found varying responses of $\Delta^{13}C$ across climate gradients. Stewart *et al.*, (1995) for example, have documented a strong response of averaged bulk-leaf $\delta^{13}C$ (i.e., the natural abundance of ^{13}C in leaves related inversely to $\Delta^{13}C$) to rainfall in eastern Australia. In contrast, a number of studies in northern Australia (Cernusak *et al.*, 2011; Miller *et al.*, 2001; Schulze *et al.*, 1998b) and in south-western Australia (Schulze *et al.*, 2006; Turner *et al.*, 2008) have observed only weak community-level responses of $\Delta^{13}C$ to MAP. This thesis presents the largest spatial analyses across Australia to which correlation of $\Delta^{13}C$ to MAP has been documented taking seasonal availability of water into account as well. Based on - (i) the spatial scale and hence climate zones and types of biomes, (ii) numbers of phylogenetically distant species and (iii) number of leaf-traits (other than $\Delta^{13}C$) analysed together, the scale at which $\Delta^{13}C$ responses have been investigated in this thesis is substantially larger than some of those of previous data compilations (Cernusak *et al.*, 2011; Miller *et al.*, 2001; Schulze *et al.*, 1998b; Stewart *et al.*, 1995). Across an eight-fold increase in MAP through the climate gradient, I found strong positive correlations of bulk-leaf $\Delta^{13}C$ (and a strong negative correlation of WUE_i calculated from $\Delta^{13}C$) of the dominant overstorey species with MAP and moisture index (defined by the ratio of precipitation to potential evaporation) during both dry- and wet-season. Up to 3.7‰ and 4.5‰ differences among biomes during the dry- and wet-season respectively were observed in $\Delta^{13}C$. Among

19 other climate parameters in addition to MAP that were considered in the multiple regression analyses, isothermality (i.e., the day-to-night temperature oscillation relative to the mean summer-to-winter oscillation) as a secondary predictor during the wet-season was the only model with notable explanatory power indicating that less stomatal regulation was imposed on leaves in the sites which had more even day-to-night temperature oscillations over the course of the year, thereby generating an influence of isothermality on $\Delta^{13}C$.

$\Delta^{13}C$ as a proxy of intrinsic water-use-efficiency

Using $\Delta^{13}C$ as a proxy of leaf intrinsic water-use-efficiency, WUE_i (defined by the ratio of net photosynthetic assimilation to stomatal conductance for water) modelled by Farquhar and Richards, (1984) has been the basis for investigating variation in water-use-efficiency *per se* across moisture/climate gradients in this research. This model has also been extensively applied in a number of both early and recent studies (Comstock and Ehleringer, 1992; Ehleringer and Cooper, 1988; Miller *et al.*, 2001; Schulze *et al.*, 1998b; Williams and Ehleringer, 1996). Essentially, WUE_i is estimated based on the modelled relationship between discrimination against ^{13}C *during* photosynthesis (i.e., $\Delta^{13}C$) and the C_i/C_a ratio (the ratio of CO_2 mole fractions in intercellular air spaces and in the atmosphere) (**Chapter 1**). Most of these studies have documented varying degrees of correlations between WUE_i and $\Delta^{13}C$ reinstating its plasticity in response to environmental changes such as water availability, vapour pressure deficit or temperature. Also, estimating WUE_i from $\Delta^{13}C$ of leaf/stem-wood organic matter is less challenging or time-consuming than measuring water-use-efficiency from gas-exchange measurements, which is also subject to a temporal variability and/or measurement uncertainties (Flexas *et al.*, 2007). However, interpretation of $WUE_i/\Delta^{13}C$ is not always straightforward because of processes that lead to discrimination against ^{13}C independent of the C_i/C_a ratio, such as mesophyll conductance or post-photosynthetic discrimination (Evans and Von Caemmerer, 2013; Seibt *et al.*, 2008; Warren *et al.*, 2005). For example, the model of estimating WUE_i from $\Delta^{13}C$ in its simplest form assumes that the mesophyll conductance to CO_2 is infinite (Farquhar and Richards, 1984), whereas, several studies proposed this to be of similar order of magnitude as stomatal conductance (Evans and Von Caemmerer, 1996; Flexas *et al.*, 2007; Warren, 2008). In this instance, I tested the tightness of the relationships between $\Delta^{13}C$ estimated from plant organic matter and gas-exchange traits estimated by instantaneous gas-exchange measurements. At a continental scale, the C_i/C_a ratio was tightly correlated with $\Delta^{13}C$ and stomatal conductance during both dry- and wet-season across an eightfold increase in mean

annual precipitation (MAP). This then explained a strong response of $\Delta^{13}C$ to MAP. $\Delta^{13}C$ and WUE_i (estimated from $\Delta^{13}C$ of leaf-organic matter) also significantly correlated with instantaneous estimates of intrinsic water-use-efficiency (WUE_i) from gas-exchange measurements, albeit with lower adjusted r^2 values (Adj r^2: dry-season=0.26, wet-season=0.17). One possible explanation of this lower than expected correlation between $\Delta^{13}C$ and WUE_i estimated from gas-exchange measurements is that $\Delta^{13}C$ gives a time-integrated estimate of intrinsic water-use-efficiency from the leaf was formed, whereas, gas-exchange measurements gives an instantaneous estimate of WUE. However, it remains unclear to what extent mesophyll conductance or post-photosynthetic discrimination is coordinated with $\Delta^{13}C$ and WUE_i estimated from leaf-organic matter in these species. For example, would including mesophyll conductance and/or post photosynthetic discrimination in the model improve the correlation between bulk-leaf $\Delta^{13}C$ and WUE_i and WUE_i estimated from instantaneous gas-exchange measurements at a continental scale in Australia? Results from my investigation of relationships between bulk-leaf $\Delta^{13}C$ and its correlates (**Chapter 4**) provide an ideal foundation of further investigations on how factors such as mesophyll conductance or post-photosynthetic discrimination coordinate with discrimination against ^{13}C at the leaf-level and also influence its observed relationships with climate and other leaf-trait variables.

Consideration of leaf morphological and nutrient features are also relevant to the current interest in using $\Delta^{13}C$ as a proxy of leaf intrinsic water-use-efficiency (Hanba *et al.*, 1999; Lamont *et al.*, 2002; Schulze *et al.*, 1998b). Leaf morphological and nutrient-status traits such as leaf mass per unit area, leaf life span, leaf nitrogen and phosphorus concentrations etc. scale strongly with a number of climate variables, particularly, rainfall as an index of water availability (Cunningham *et al.*, 1999; Eamus *et al.*, 2006b; Fonseca *et al.*, 2000; Schulze *et al.*, 1998b; Taylor and Eamus, 2008; Turner, 1994; Wright *et al.*, 2001; Wright *et al.*, 2004). The C_i/C_a ratio of leaves can be altered if leaf size and structure adapt in response to water stress (Seibt *et al.*, 2008). Intercellular concentration of CO_2, C_i, is also influenced by nutrient availability through its effect on photosynthetic capacity (Lamont *et al.*, 2002; Radin, 1984). I investigated correlations between bulk-leaf $\Delta^{13}C$ with leaf morphological and nutrient traits at individual species level as well as site-specific species assemblage level (**Chapter 4**). I observed a strong negative correlation between $\Delta^{13}C$ and leaf mass per unit area (LMA) at a continental scale suggesting that these two functional ($\Delta^{13}C$) and structural (LMA) leaf-traits are possibly linked also through the effects of low (soil) water availability

on decreasing C_i. Consequently, further research can focus on the underpinnings of the observed relationship between $\Delta^{13}C$ and LMA to address questions such as, whether- a) greater demand for carbon per unit leaf area, or b) altered mesophyll conductance or c) increased resistance to water flow generated by thicker palisade and denser tissues due to an increase in LMA have influenced the C_i values and consequently $\Delta^{13}C$ of leaves.

$\Delta^{13}C$ (and WUE_i) responses to seasonal water availability

This thesis highlighted the importance of considering seasonal water availability while interpreting the responses of $\Delta^{13}C$ (and WUE_i calculated from $\Delta^{13}C$) and C_i/C_a particularly in studies performed along moisture gradients across large spatial/temporal scales. Bulk-leaf $\Delta^{13}C$ provides a time-integrated measure of WUE_i (Diefendorf *et al.*, 2010), therefore can either provide information about C_i/C_a only during favourable conditions in the wet-season when canopy photosynthesis is the most active, or about year-round variation in C_i/C_a along the precipitation gradient, including during the dry-season when water is the least available (Cernusak *et al.*, 2011). The framework described in **Figure 6.1**, derived from the work described in this thesis summarizes the inter-relationships of $\Delta^{13}C$ (and opposite relationships of WUE_i) with leaf structural, nutrient and gas-exchange traits and MAP taking seasonal differences of water availability into account. Patterns described in this framework are also consistent with global patterns of leaf-trait variation along gradients of moisture availability (Diefendorf *et al.*, 2010; Kohn, 2010; Wright *et al.*, 2004) and provides insights into how and why less water availability (in lower rainfall sites and/or during the dry-season) can be associated with smaller discrimination against ^{13}C and larger intrinsic WUE. MAP is strongly correlated with leaf structural traits (e.g., leaf mass per unit area, LMA), leaf nutrient traits (e.g., total leaf [N] expressed on a leaf area basis, N_{area}) and leaf gas-exchange traits (e.g., A and g_s) especially during the dry-season, all of which influence the C_i/C_a ratio in varying degrees. Bulk-leaf $\Delta^{13}C$ (and WUE_i), modulated by the canopy C_i/C_a ratio at the time when the leaf dry matter was synthesized, therefore showed a strong response to water availability along the gradient. Theoretically, stomatal regulation imposed by plants in response to water stress is primarily what drives the C_i/C_a ratio and this was supported by strong and significant relationships between stomatal conductance (g_s) and C_i/C_a ratio observed during both dry- and wet-season. Another ambiguity associated with interpreting the bulk-leaf $\Delta^{13}C$ is to adequately explain the relative contribution of net photosynthetic assimilation and stomatal conductance in controlling the C_i/C_a ratio. I observed that, during the dry-season, $\Delta^{13}C$ and WUE_i was more strongly regulated by

stomatal conductance than photosynthetic capacity (**Figure 6.1a**). In contrast during the wet-season when canopy photosynthesis is the most active under favourable conditions of water availability, photosynthetic capacity was found to have a stronger relationship with $\Delta^{13}C$ than stomatal conductance at a continental scale (**Figure 6.1b**). These findings highlight the importance of taking seasonal water availability into account while determining the relative contribution assimilation and stomatal conductance to $\Delta^{13}C$ and WUE_i especially while investigating $\Delta^{13}C$ signatures along moisture/climate gradients.

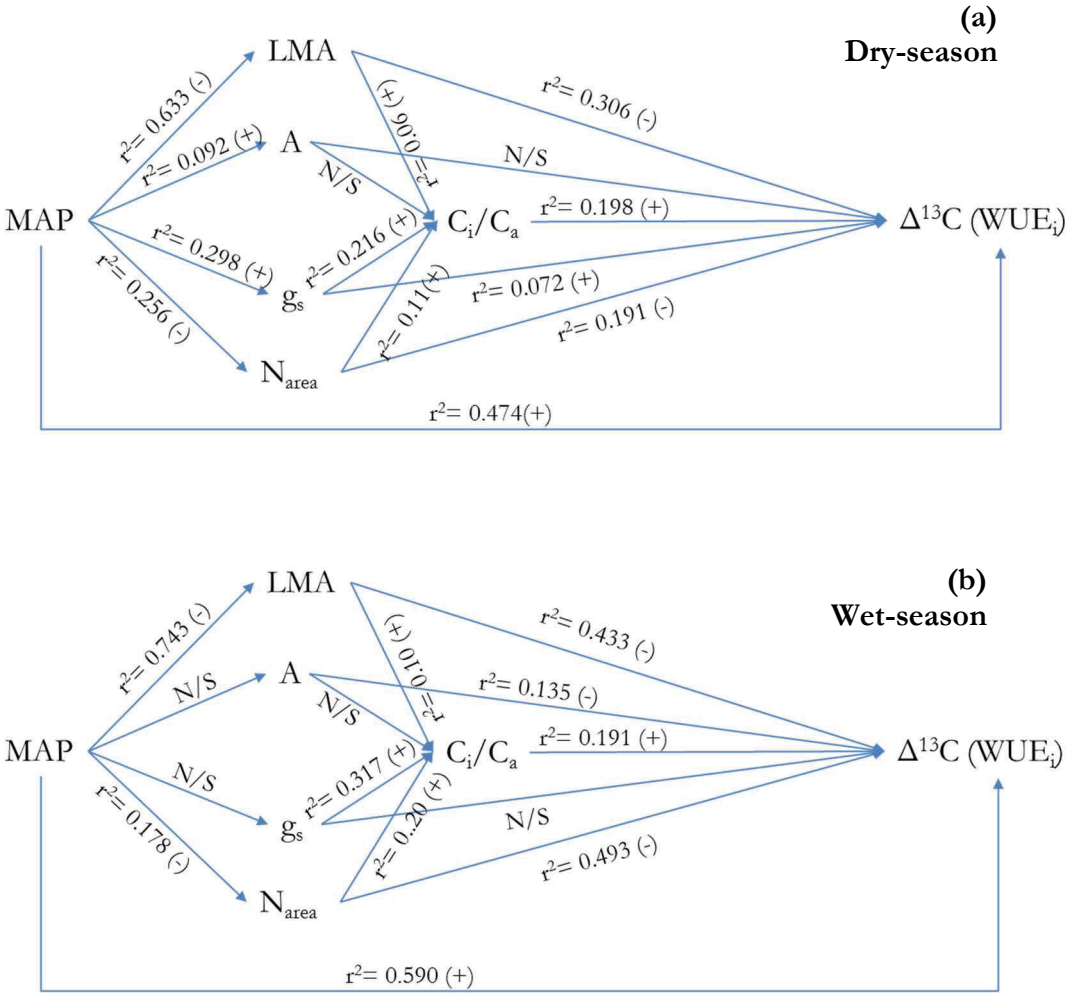

Figure 6.1: Diagram showing the inter-relationships amongst $\Delta^{13}C$ (WUE_i), leaf structural, nutrient and gas-exchange traits and MAP during (a) dry- and (b) wet-season in plant species across seven SuperSites (MAP 255 mm - 2140 mm) in Australia.

Values over the connecting lines represents the (adjusted) r^2 values of the relationship of the two parameters connected by the line. The signs (+) and (-) indicate the directionality of the relationship. N/S = non-significant.

Variation in $\Delta^{13}C$ and its correlates from an evolutionary perspective

One of the more novel aspects of the work described in this thesis has been the opportunity to combine genealogical information with the traditional cross-species data in analysing the relationships of bulk-leaf $\Delta^{13}C$ with climate and leaf-trait variables to look at these relationships from an evolutionary perspective. Coupling phylogenetics with ecological and functional trait data is a powerful way to investigate community/trait assemblage as well as to determine the evolution of plant functions (Araya *et al.*, 2012; Savage and Cavender-Bares, 2012). These analyses provide an understanding of significant discrepancies between standard non-phylogenetic (cross-species) and phylogenetic relationships (if such exist), that might have resulted from the potential similarity between closely related species. In 55 dominant overstorey species spanning across seven SuperSites in Australia, I found that there was a pattern of similarity in terms of species mean value of $\Delta^{13}C$ among closely related species even in this phylogenetically diverse set of species. For example, all species from the genus *Eucalyptus* showed $\Delta^{13}C$-values from the lower end of the spectrum despite their coming from different sites with distinctly different climate conditions (**Chapter 5, Figure 5.10**). Significant phylogenetic signal was also detected in the climate variables across seven SuperSites in Australia. In particular for example, plotting mean annual precipitation (MAP) in the tips of the working phylogeny showed that, wet conditions (MAP > 1000 mm) were located within particular clades in the phylogeny, while, dry to moderate conditions (MAP < 1000) were located within other clades. Comparing both non-phylogenetic and phylogenetic relationships of $\Delta^{13}C$ with climate variables, I found that climate variables that showed significant non-random phylogenetic signals were also the variables that showed the strongest relationships with $\Delta^{13}C$. Based on these findings, I conclude that variation in bulk-leaf $\Delta^{13}C$ signatures, at least at the scale of the species analysed in this work, was driven by the climatic conditions experienced by these species and this remains true even after accounting for the underpinning phylogenetic relationships between these species. Combining phylogenetic information into cross-species regressions also implied that interpretations of these relationships of $\Delta^{13}C$ with climate and leaf-trait variables based on interspecific patterns from this dataset were well supported from a phylogenetic perspective.

Based on the results that showed species mean values of bulk-leaf $\Delta^{13}C$ was significantly phylogenetically structured, I assessed whether phylogenetically independent divergence events of $\Delta^{13}C$ were consistently associated with divergences of the climate variables of the

habitats occupied by the species and also with divergences of leaf structural, nutrient and gas-exchange traits. Results from Phylogenetic Independent Contrast (PIC) analysis provided repeated evidence of correlated evolutionary divergences of $\Delta^{13}C$ with climate and also leaf-trait variables. For example, where there was an evolutionary divergence of low $\Delta^{13}C$, there was also an evolutionary divergence of low MAP and *vice versa* throughout most of the working phylogeny. PIC analysis also identified correlated evolution of $\Delta^{13}C$ with a suite of other leaf-traits such as VPD, C_i/C_a, C_i400 and intrinsic WUE (calculated from the ratio of A400.a and g_s400), all leaf structural traits and two leaf nutrient traits (ratio of N to P and $LeafN_{area}$) and all of these traits presumably were tightly linked to water availability from the cross-species analyses (**Chapter 4**). These results lend further support to the initial hypothesis of a significant relationship between $\Delta^{13}C$ and access to/ availability of water. A final aspect of this work was to investigate whether relationships of bulk-leaf $\Delta^{13}C$ with water availability reflect patterns of adaptive radiation or they occur due mainly to contrasting characteristics of major seed-plant lineages. Results from two phylogenetic comparative methods (PCMs) employed in these analyses (i.e., phylogenetic least square regression and phylogenetic independent contrast analyses) suggest that the modern day variation of $\Delta^{13}C$ with water availability principally results from adaptive environmental convergence (**Chapter 5**).

Overall, this thesis makes a significant and novel contribution to the understanding of water uptake and water use strategies of dominant overstorey species across contrasting ecosystems in Australia. One of the more novel aspects of this work has been the incorporation of ancestral history of the species and the comparison of traditional cross-species (non-phylogenetic) and the phylogenetic relationships of $\Delta^{13}C$ with climate/leaf-trait variables. Cross-disciplinary collaboration, in this case, ecophysiology with phylogenetics (**Chapter 5**) and meteorology can lead to exciting and new understandings of the functioning of plants, especially pertaining to water availability. Future work that integrates knowledge of traditional cross-species patterns of $\Delta^{13}C$ and the phylogenetic information of the species within and among populations at smaller spatial scales as well as a continental scale will continue to develop our understanding of plants' response to water availability and water stress, especially across distinctly different ecosystems around Australia and globally.

Appendix A

Table A1: List of species, their functional types, $\Delta^{13}C$ and calculated intrinsic WUE_i (plant functional type codes: BlT= broad leaf tree, NlT= needle leaf tree and S=shrub).

Species	Site	PFT	$\Delta^{13}C$ (‰)	Calculated WUE_i
Acacia aneura	AMU	NlT	19.71±0.21	78.67
Acacia melanoxylon	WR	BlT	22.46±0.46	49.00
Acmena graveolens	CT	BIT	21.96±0.31	54.37
Alphitonia whitei	RC	BlT	24.81±0.58	23.63
Alstonia muelleriana	RC	BlT	23.42±0.4	38.58
Alstonia scholaris	CT	BlT	22.76±0.36	45.75
Anopterus glandulosus	WR	S	25.58±0.44	15.34
Argyrodendron peralatum	CT	BIT	24.89±0.26	22.75
Atherosperma moschatum	WR	BlT	22.57±0.85	47.80
Cardwellia sublimis	CT	BlT	22.46±0.58	48.92
Castanospermum australe	CT	BlT	22.04±0.4	53.48
Ceratopetalum succirubrum	RC	BlT	26.52±0.13	5.21
Corymbia terminalis	AMU	BlT	19.89±0.29	76.65
Cryptocarya mackinnoniana	CT	BlT	24.59±0.12	26.02
Daphnandra repandula	RC	BlT	23.69±0.57	35.69
Doryphora aromatica	RC	BlT	25.41±0.88	17.19
Dysoxylum papuanum	CT	BlT	20.83±0.44	66.59
Elaeocarpus grandis	CT	BlT	22.34±0.1	50.30
Endiandra leptodendron	CT	BlT	26.86±0.6	1.51
Eucalyptus amplifolia	CP	BlT	21.02±0.31	64.53
Eucalyptus camaldulensis	AMU	BlT	20.28±0.35	72.43
Eucalyptus clelandii	GWW	BlT	17.68±0.17	100.56
Eucalyptus dumosa	CM	BlT	19.01±0.42	86.15
Eucalyptus fibrosa	CP	BlT	23.24±0.32	40.57
Eucalyptus miniata	LF	BlT	21.86±0.07	55.39
Eucalyptus moluccana	CP	BlT	21.48±0.24	59.50
Eucalyptus obliqua	WR	BlT	22.01±0.73	53.79
Eucalyptus salmonophloia	GWW	BlT	18.88±0.09	87.56
Eucalyptus salubris	GWW	BlT	18.02±0.19	96.82
Eucalyptus socialis	CM	BlT	19.94±0.18	76.17
Eucalyptus tereticornis	CP	BlT	21.27±0.26	61.85
Eucalyptus tetrodonta	LF	BlT	19.82±0.34	77.39
Eucalyptus transcontinentalis	GWW	BlT	19.75±0.31	78.24
Eucryphia lucida	WR	BlT	22.07±0.06	53.16
Ficus leptoclada	RC	BlT	21.53±0.49	59.01
Ficus variegata	CT	BlT	21.85±0.29	55.60
Flindersia bourjotiana	RC	BlT	23.8±0.43	34.54
Gillbeea adenopetala	RC	BlT	24.41±0.26	27.94

Species	Site	PFT	$\Delta^{13}C$ (‰)	Calculated WUE_i
Gillbeea whypallana	CT	BIT	23.22±0.42	40.79
Leptospermum lanigerum	WR	BIT	21.61±0.39	58.15
Litsea leefeana	RC	BIT	23.9±0.48	33.38
Melaleuca squarrosa	WR	BIT	21.94±0.25	54.60
Myristica globosa	CT	BIT	24.04±0.53	31.91
Notelaea ligustrina	WR	BIT	21.2±0.51	62.52
Nothofagus cunninghamii	WR	BIT	21.06±0.59	64.02
Phyllocladus aspleniifolius	WR	S	18.48±0.68	91.93
Pittosporum bicolor	WR	BIT	19.99±0.67	75.63
Polyscias elegans	RC	BIT	22.96±0.6	43.60
Pomaderris apetala	WR	S	23.55±0.44	37.21
Prunus turneriana	RC	BIT	25.83±0.74	12.59
Rockinghamia angustifolia	CT	BIT	22.69±0.35	46.49
Synima cordierorum	CT	BIT	22.8±0.39	45.33
Syzygium johnsonii	RC	BIT	25.7±0.07	13.99
Syzygium sayeri	CT	BIT	23.01±0.46	43.04
Tasmannia lanceolata	WR	S	21.8±0.26	56.03
Xanthophyllum octandrum	CT	BIT	22.64±0.6	47.08

Table A2: List of meteorological stations for SILO patched point data

SuperSite	Station No	Station name	Lat °	Long °	Elevation (m)
Calperum Mallee	24024	Loxton research centre	-34.4390	140.5978	30
Great Western Woodlands	12038	Kalgoorlie-boulder airport	-30.7847	121.4533	365
Alice Mulga	15643	Territory grape farm	-22.4518	133.6377	565
Cumberland Plain	30045	Richmond post office	-20.7289	143.1425	211
Warra Tall Eucalypt	95003	Bushy park (bushy park estates)	-42.7097	146.8983	27
Litchfield Savanna	14015	Darwin Airport	-12.4239	130.8925	30
FNQ	31011	Cairns aero	-16.8736	145.7458	2

Appendix B

Results from randomization tests from **Chapter 5**

Figure B1: Randomization tests of phylogenetic signal (Blomberg's *K*) for climate variables.

Dashed lines indicate values of Blomberg's *K* for each climate variable. Histogram bars represent *K*-values based on 1000 randomizations and black dotted lines give the 95% confidence interval. Bold dashed lines outside the intervals indicate *K*-value significantly larger than 95% random *K*-values.

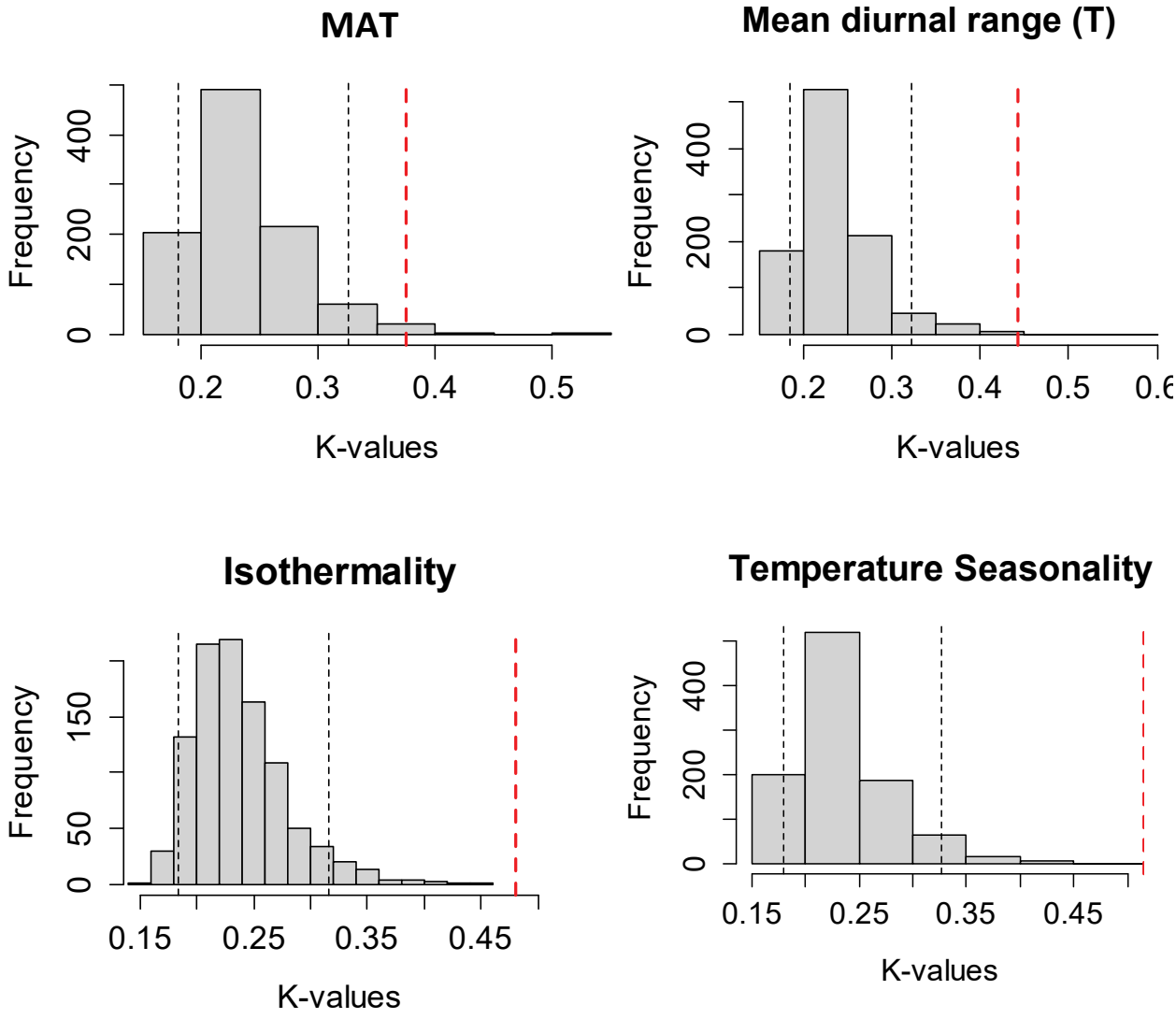

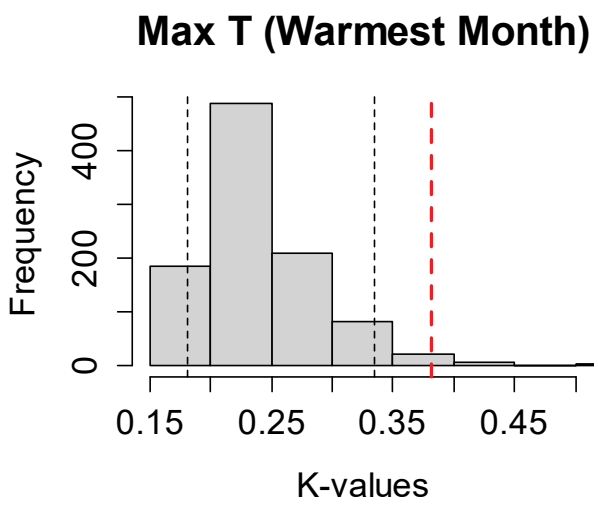
Max T (Warmest Month)
Frequency
0
200
400
0.15
0.25
0.35
0.45
K-values

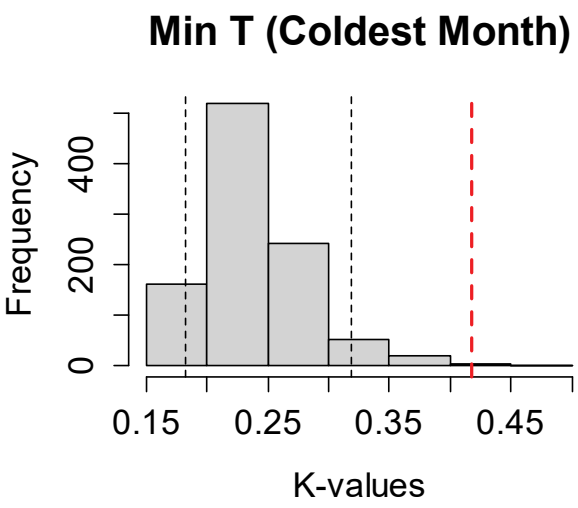
Min T (Coldest Month)
Frequency
0
200
400
0.15
0.25
0.35
0.45
K-values

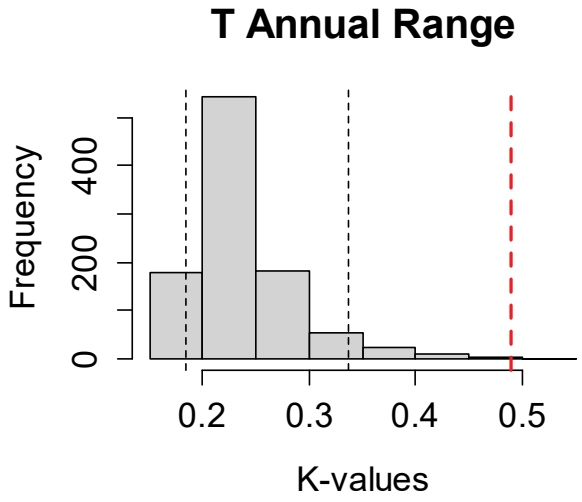
T Annual Range
Frequency
0
200
400
0.2
0.3
0.4
0.5
K-values

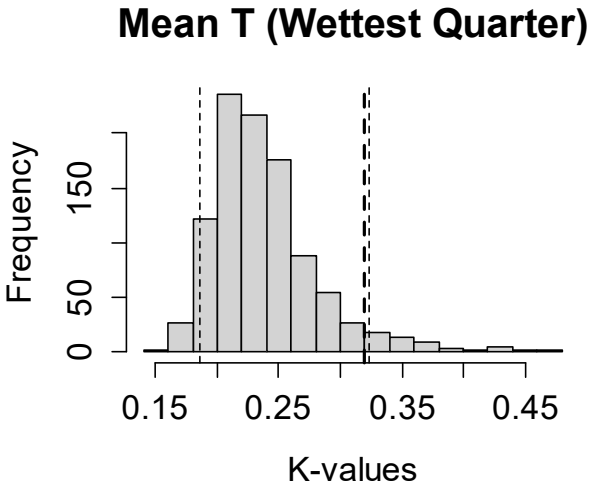
Mean T (Wettest Quarter)
Frequency
0
50
150
0.15
0.25
0.35
0.45
K-values

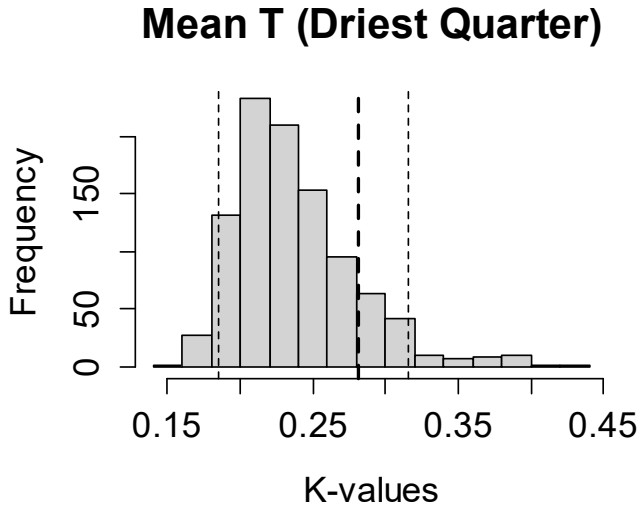
Mean T (Driest Quarter)
Frequency
0
50
150
0.15
0.25
0.35
0.45
K-values

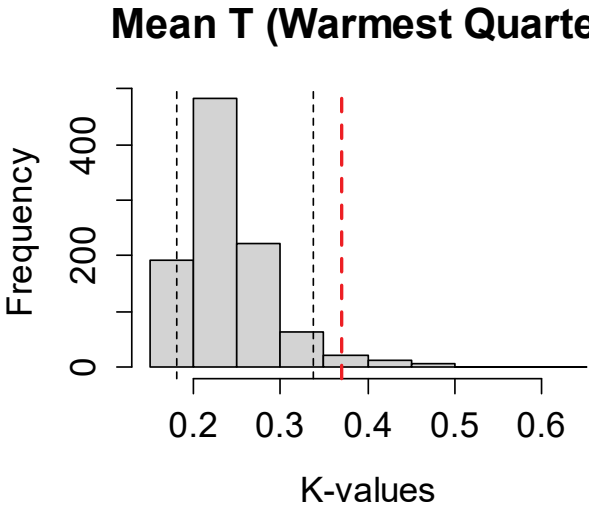
Mean T (Warmest Quarte
Frequency
0
200
400
0.2
0.3
0.4
0.5
0.6
K-values

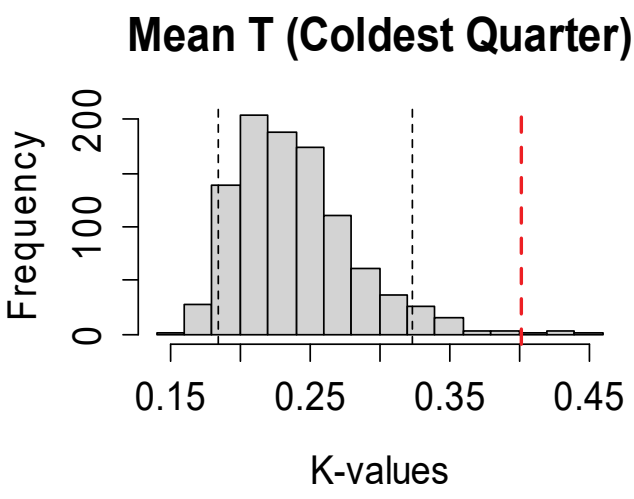
Mean T (Coldest Quarter)
Frequency
0
100
200
0.15
0.25
0.35
0.45
K-values

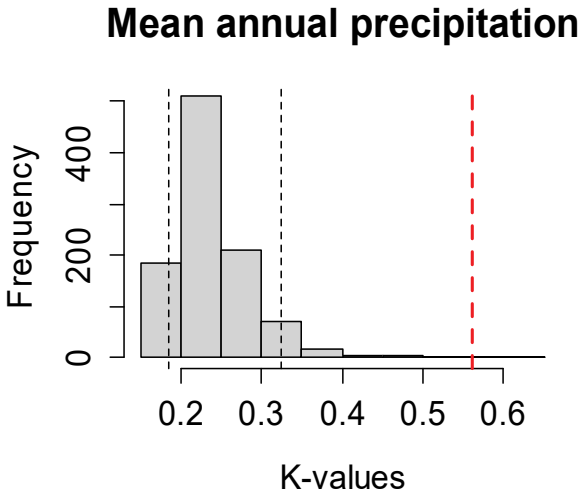
Mean annual precipitation
Frequency
0
200
400
0.2
0.3
0.4
0.5
0.6
K-values

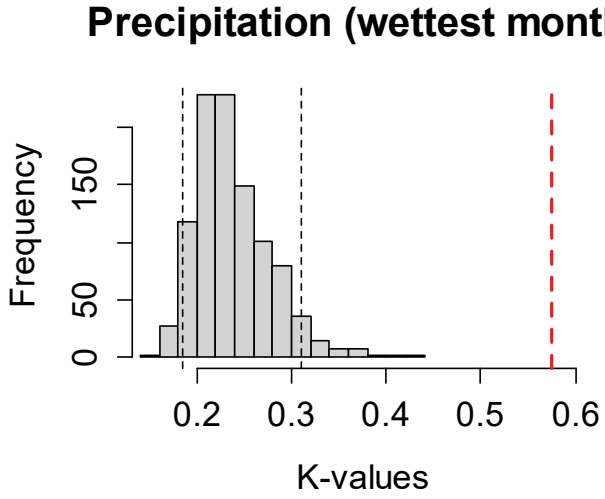
Precipitation (wettest month)
Frequency
0
50
150
0.2
0.3
0.4
0.5
0.6
K-values

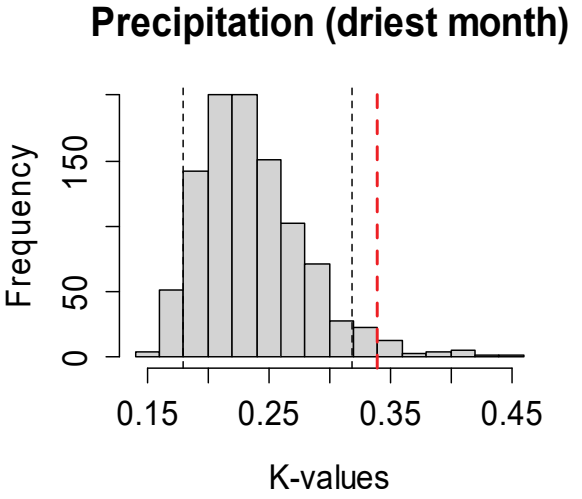
Precipitation (driest month)
Frequency
0
50
150
0.15
0.25
0.35
0.45
K-values

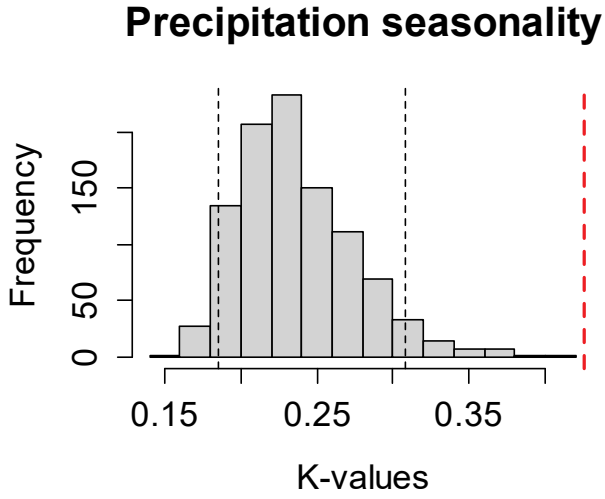
Precipitation seasonality
Frequency
0
50
150
0.15
0.25
0.35
K-values

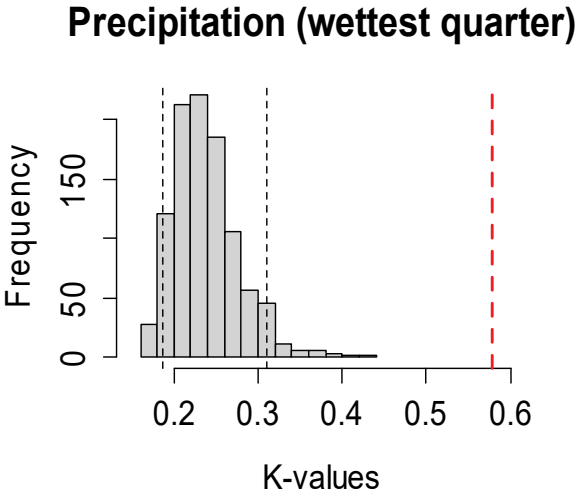
Precipitation (wettest quarter)
Frequency
0
50
150
0.2
0.3
0.4
0.5
0.6
K-values

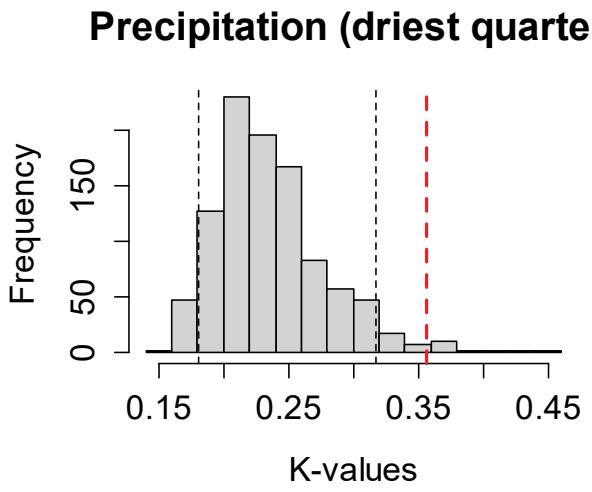
Precipitation (driest quarter)
Frequency
0
50
150
0.15
0.25
0.35
0.45
K-values

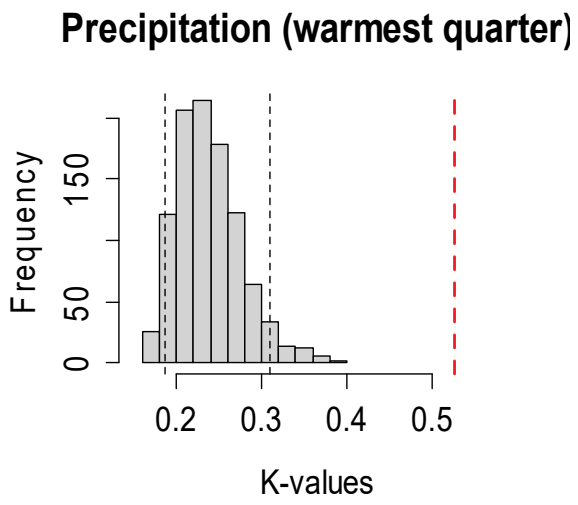
Precipitation (warmest quarter)
Frequency
0
50
150
0.2
0.3
0.4
0.5
K-values

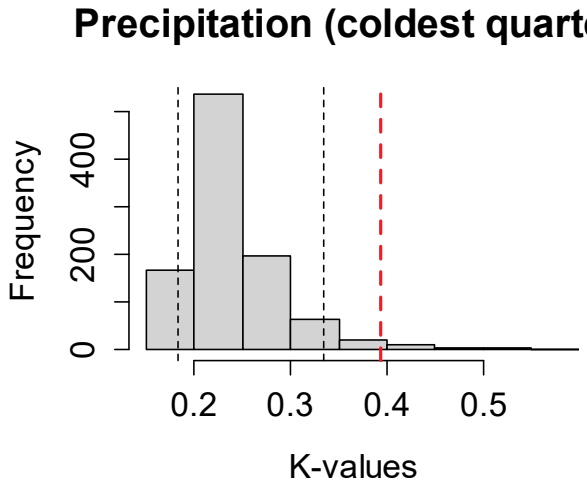
Precipitation (coldest quarter)
Frequency
0
200
400
0.2
0.3
0.4
0.5
K-values

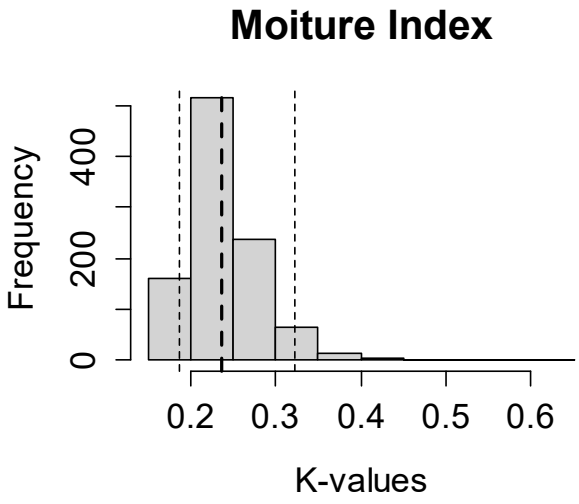
Moiture Index
Frequency
0
200
400
0.2
0.3
0.4
0.5
0.6
K-values

Figure B2: Randomization tests of phylogenetic signal (PIC variance) for climate variables.

Dashed lines indicate PIC variance for each climate variable. Histogram bars represent variances based on 1000 randomizations and black dotted lines give the 95% confidence interval. Bold dashed lines outside the intervals indicate PIC variance significantly smaller than 95% random PIC variances.

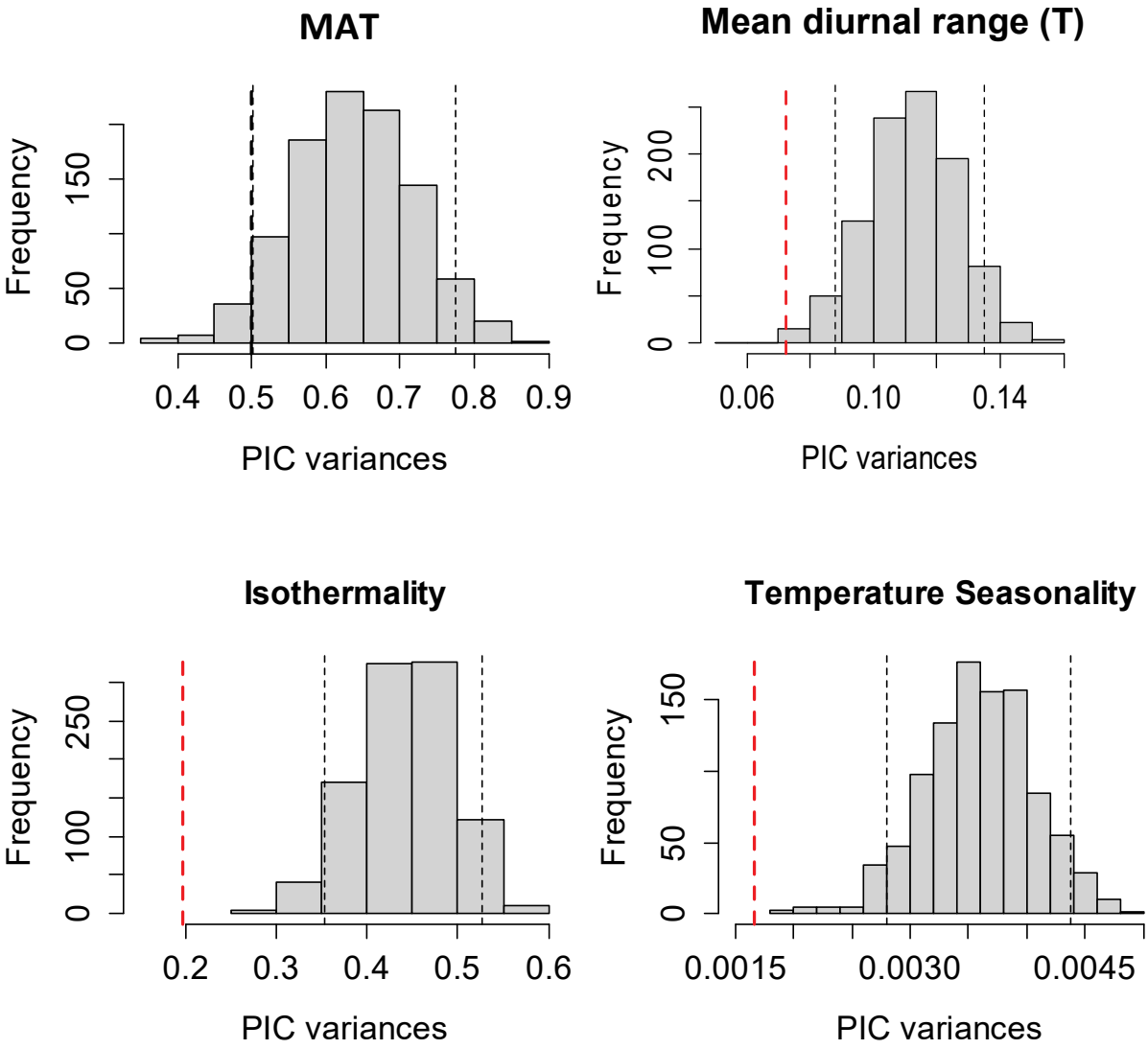

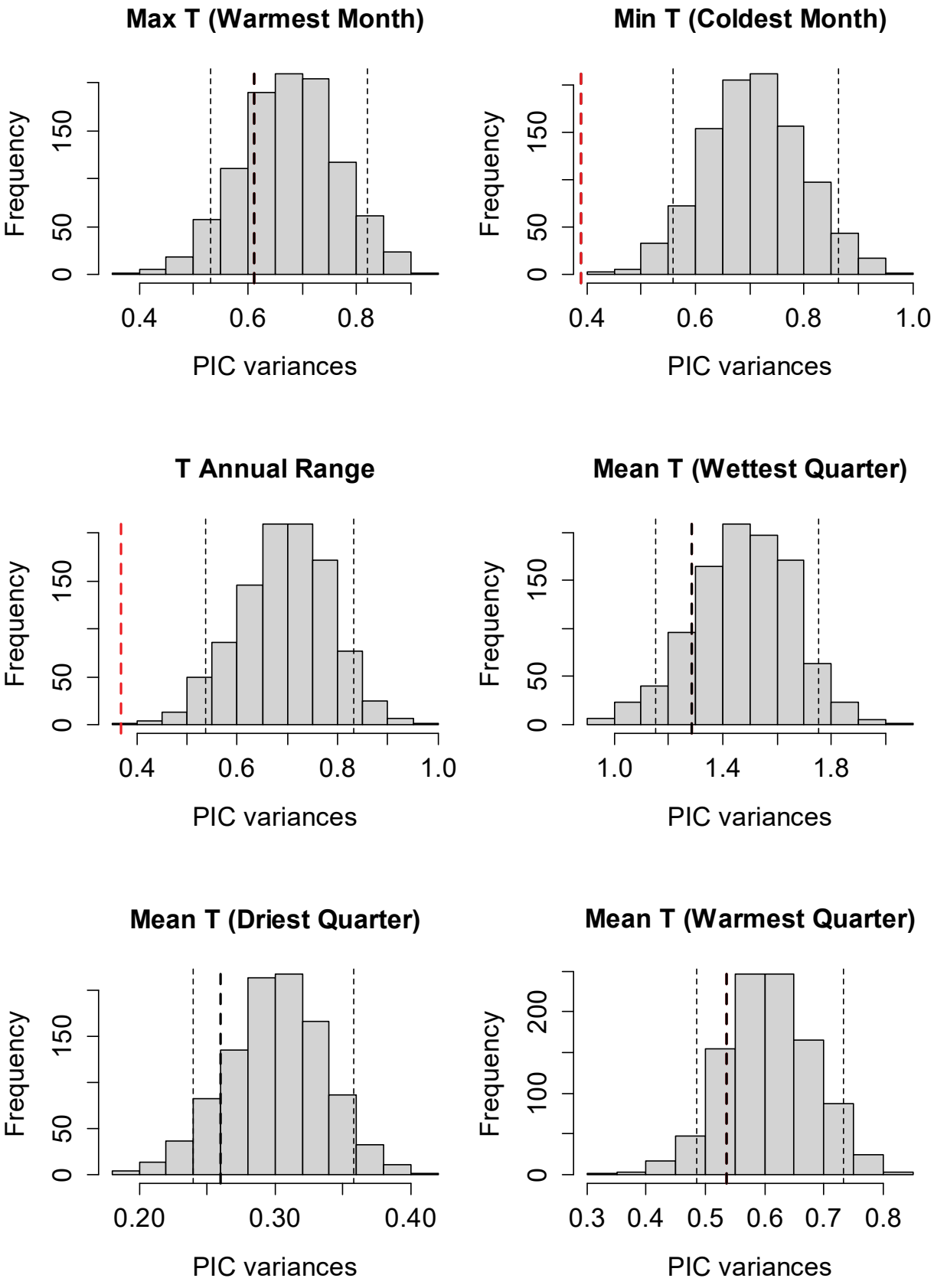
Max T (Warmest Month)
Frequency
0
50
150
0.4
0.6
0.8
PIC variances
Min T (Coldest Month)
Frequency
0
50
150
0.4
0.6
0.8
1.0
PIC variances
T Annual Range
Frequency
0
50
150
0.4
0.6
0.8
1.0
PIC variances
Mean T (Wettest Quarter)
Frequency
0
50
150
1.0
1.4
1.8
PIC variances
Mean T (Driest Quarter)
Frequency
0
50
150
0.20
0.30
0.40
PIC variances
Mean T (Warmest Quarter)
Frequency
0
100
200
0.3
0.4
0.5
0.6
0.7
0.8
PIC variances

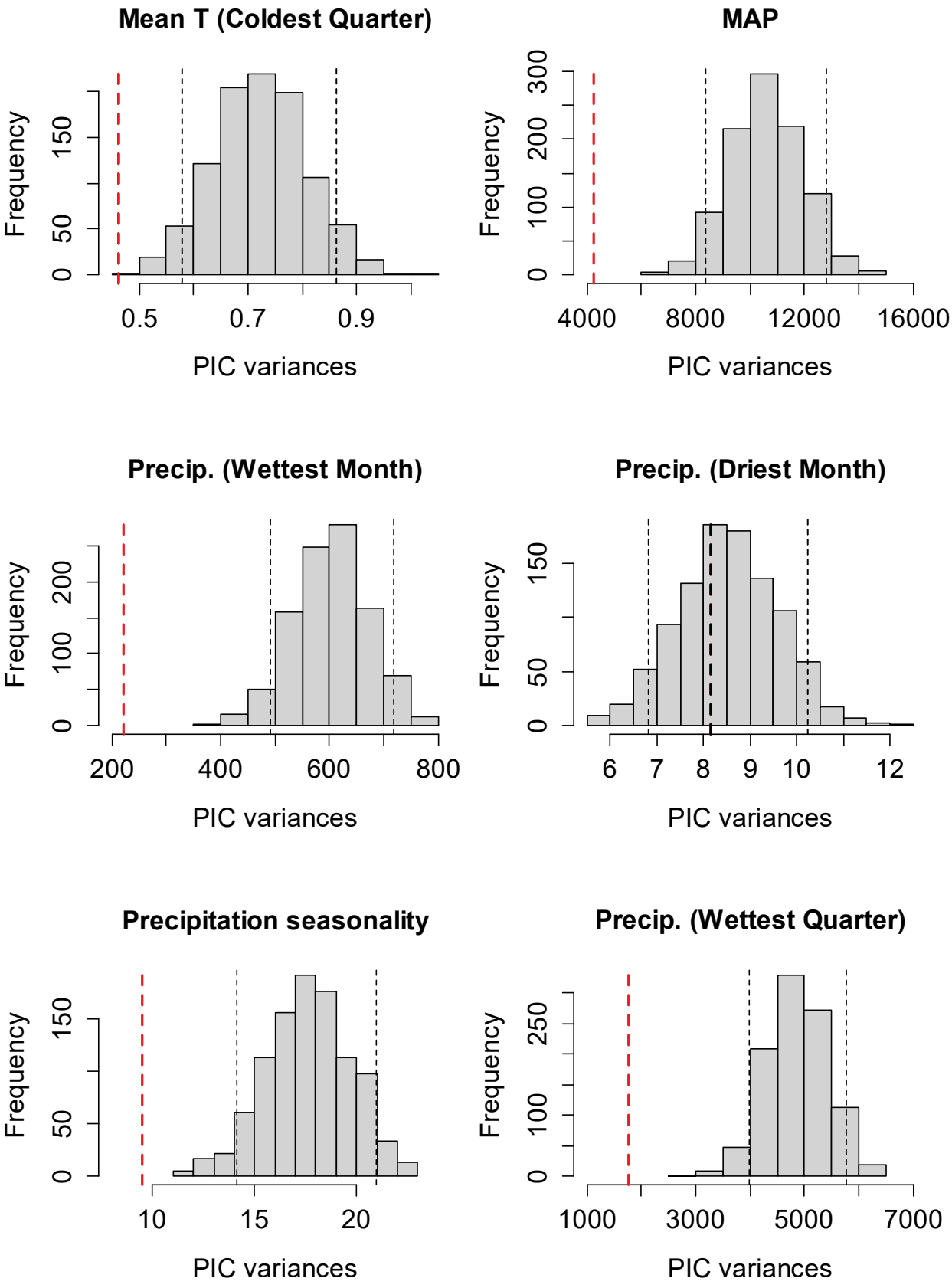
Mean T (Coldest Quarter)
Frequency
0
50
150
0.5
0.7
0.9
PIC variances
MAP
Frequency
0
100
200
300
4000
8000
12000
16000
PIC variances
Precip. (Wettest Month)
Frequency
0
100
200
200
400
600
800
PIC variances
Precip. (Driest Month)
Frequency
0
50
150
6
7
8
9
10
12
PIC variances
Precipitation seasonality
Frequency
0
50
150
10
15
20
PIC variances
Precip. (Wettest Quarter)
Frequency
0
100
250
1000
3000
5000
7000
PIC variances

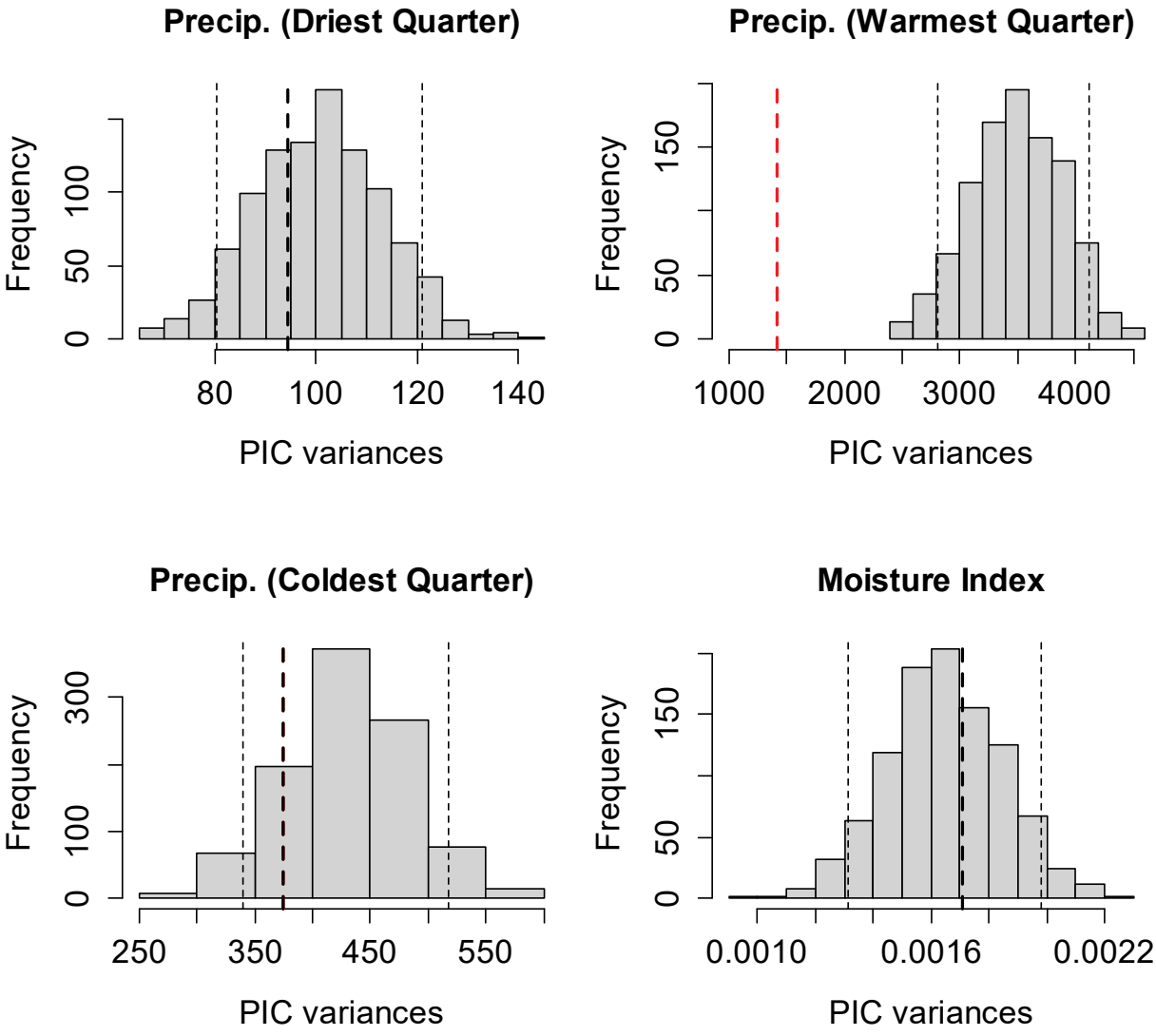
Precip. (Driest Quarter)
Frequency
0
50
100
80
100
120
140
PIC variances
Precip. (Warmest Quarter)
Frequency
0
50
150
1000
2000
3000
4000
PIC variances
Precip. (Coldest Quarter)
Frequency
0
100
300
250
350
450
550
PIC variances
Moisture Index
Frequency
0
50
150
0.0010
0.0016
0.0022
PIC variances

Figure B3: Randomization tests of phylogenetic signal (Blomberg's *K*) for leaf-traits.

Dashed lines indicate values of Blomberg's *K* for each leaf-trait. Histogram bars represent *K*-values based on 1000 randomizations and black dotted lines give the 95% confidence interval. Bold dashed lines outside the intervals indicate *K*-value significantly larger than 95% random *K*-values.

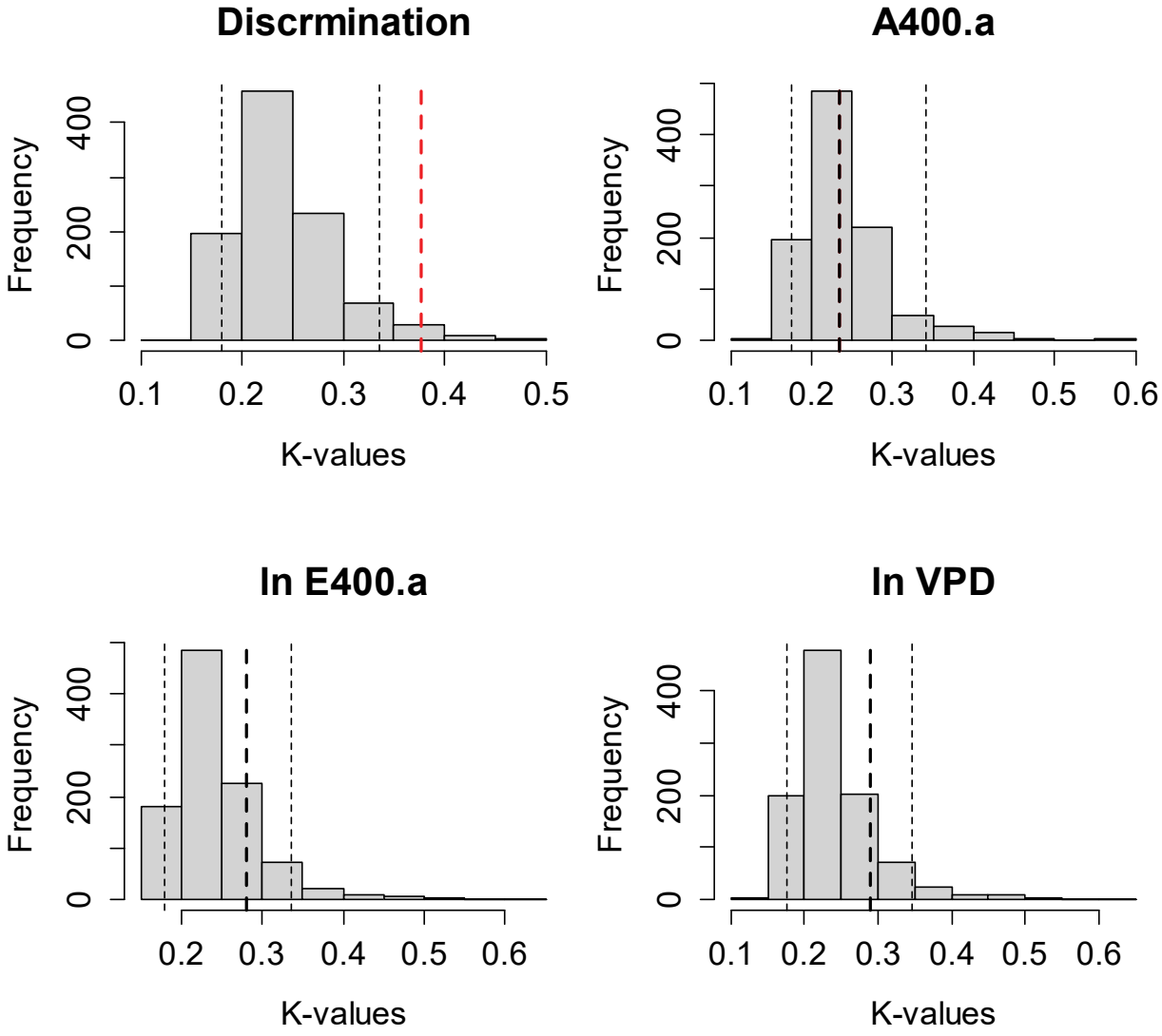

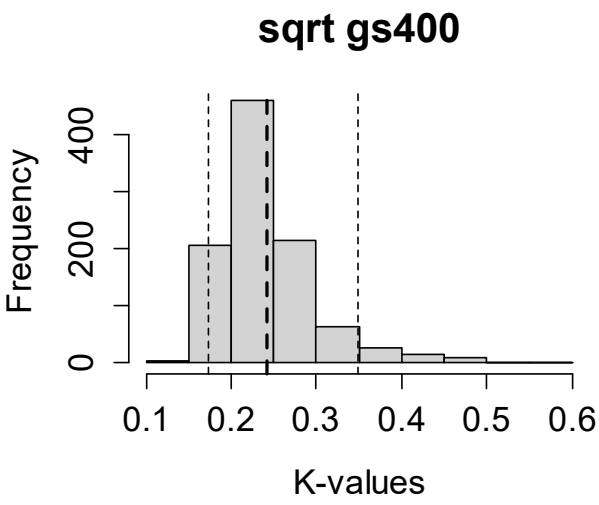
sqrt gs400
Frequency
0
200
400
0.1
0.2
0.3
0.4
0.5
0.6
K-values

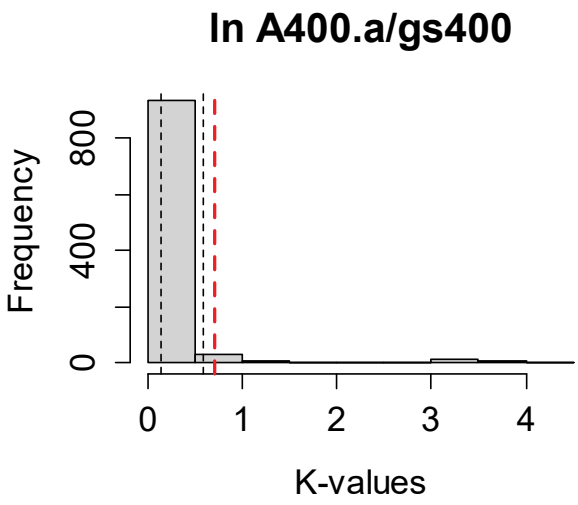
ln A400.a/gs400
Frequency
0
400
800
0
1
2
3
4
K-values

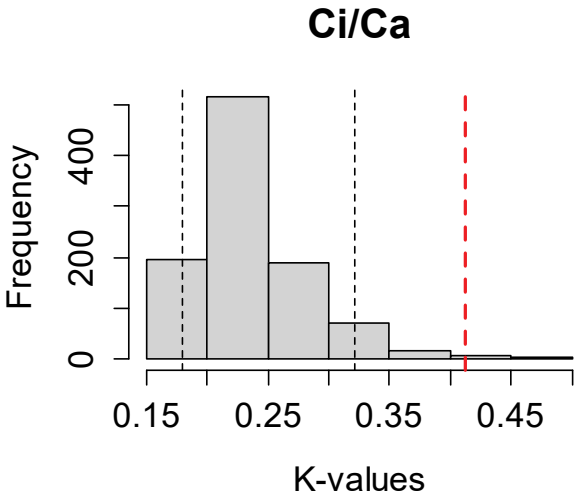
Ci/Ca
Frequency
0
200
400
0.15
0.25
0.35
0.45
K-values

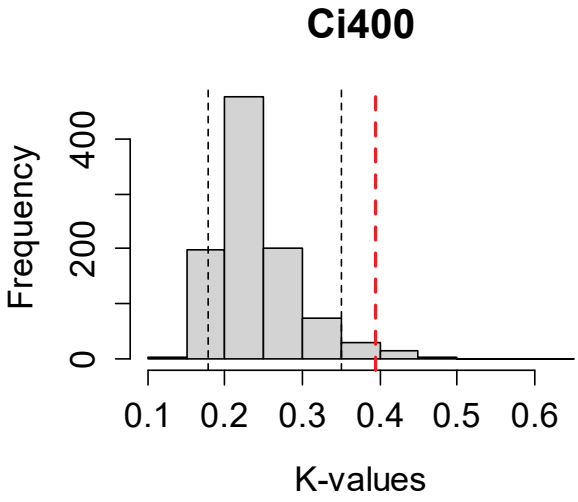
Ci400
Frequency
0
200
400
0.1
0.2
0.3
0.4
0.5
0.6
K-values

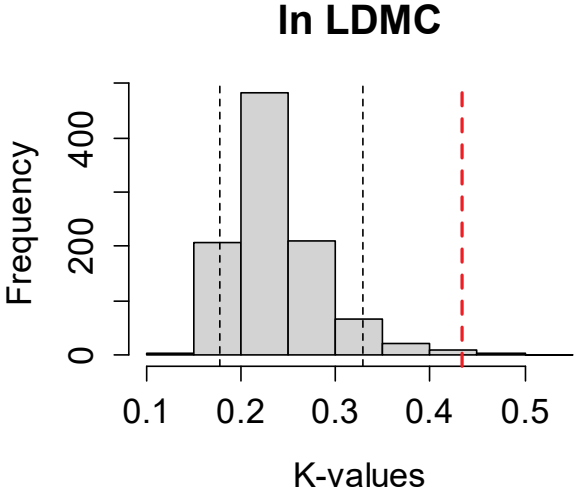
ln LDMC
Frequency
0
200
400
0.1
0.2
0.3
0.4
0.5
K-values

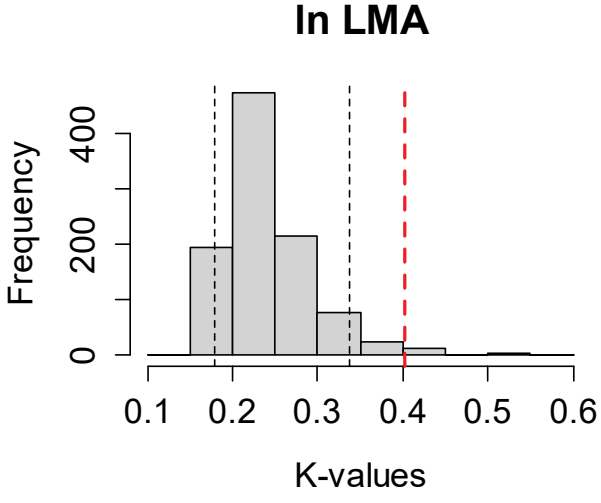
ln LMA
Frequency
0
200
400
0.1
0.2
0.3
0.4
0.5
0.6
K-values

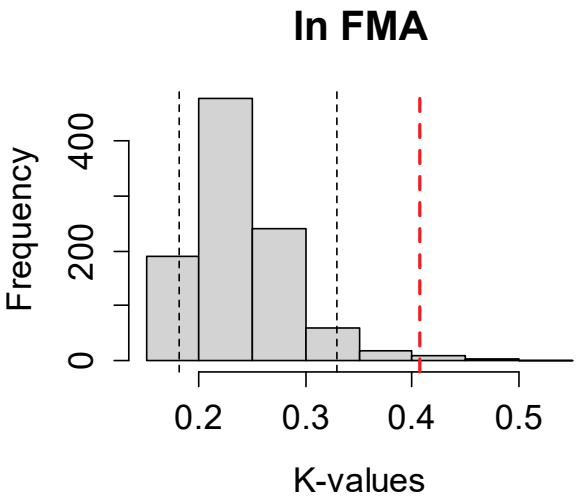
ln FMA
Frequency
0
200
400
0.2
0.3
0.4
0.5
K-values

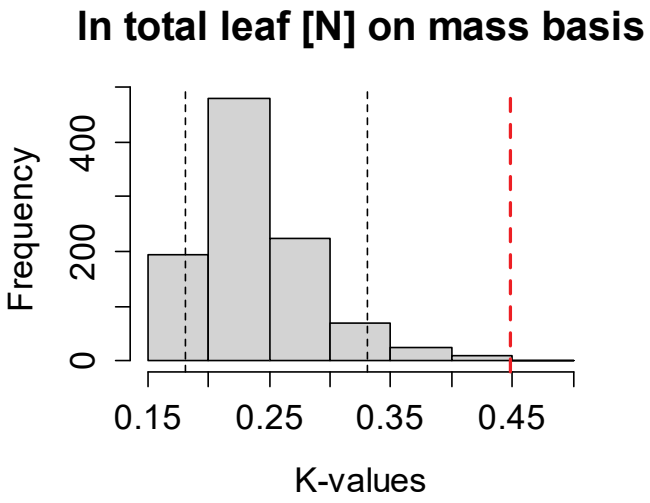
ln total leaf [N] on mass basis
Frequency
0
200
400
0.15
0.25
0.35
0.45
K-values

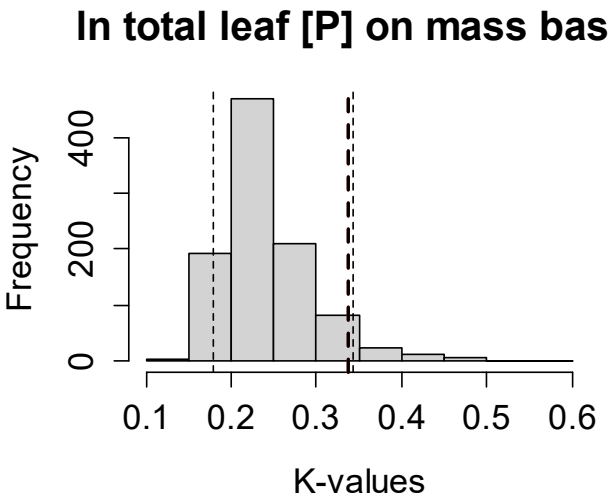
ln total leaf [P] on mass basi
Frequency
0
200
400
0.1
0.2
0.3
0.4
0.5
0.6
K-values

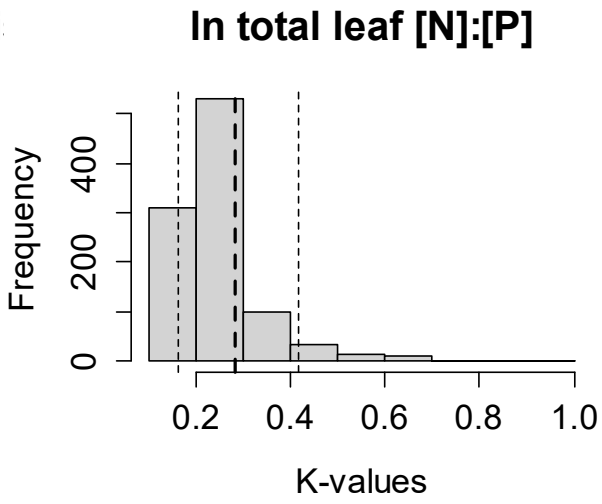
ln total leaf [N]:[P]
Frequency
0
200
400
0.2
0.4
0.6
0.8
1.0
K-values

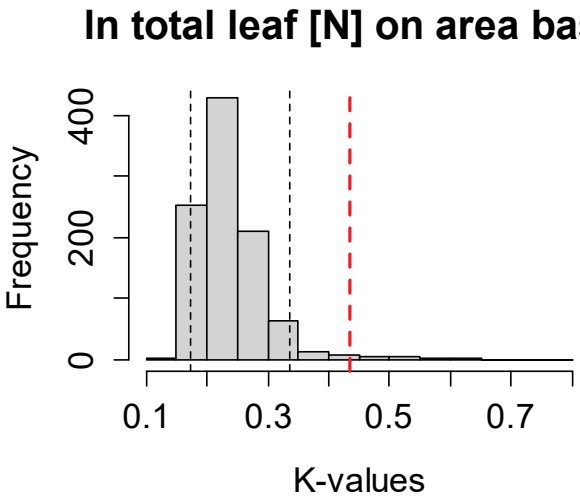
ln total leaf [N] on area basis
Frequency
0
200
400
0.1
0.3
0.5
0.7
K-values

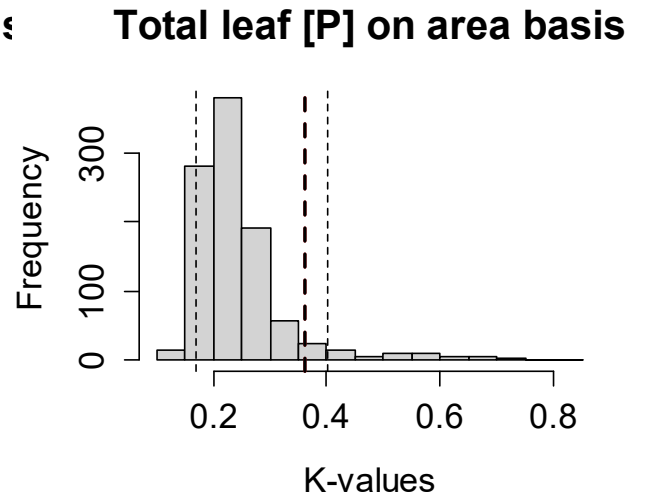
Total leaf [P] on area basis
Frequency
0
100
300
0.2
0.4
0.6
0.8
K-values

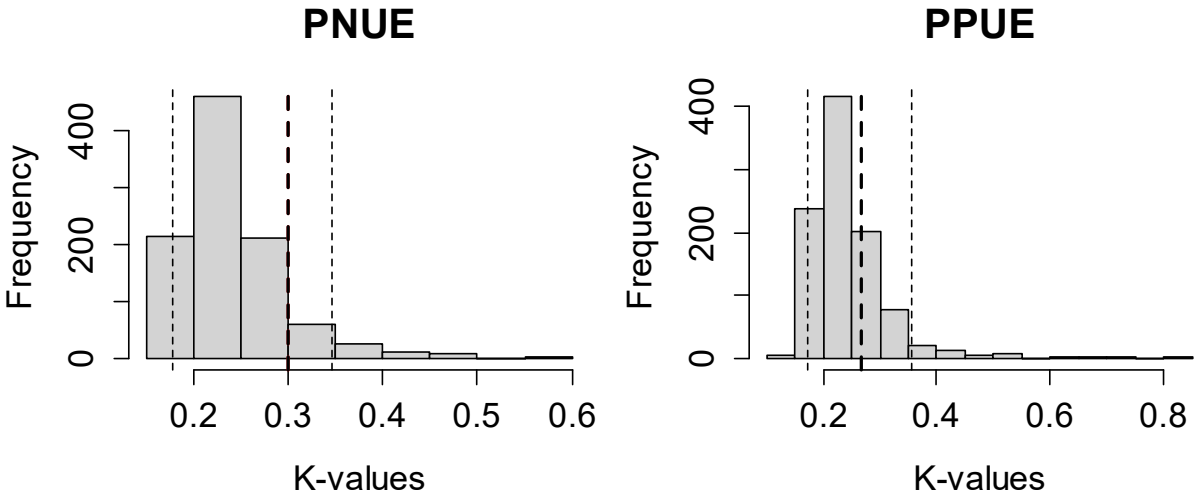
PNUE
Frequency
0
200
400
0.2
0.3
0.4
0.5
0.6
K-values
PPUE
Frequency
0
200
400
0.2
0.4
0.6
0.8
K-values

Figure B4: Randomization tests of phylogenetic signal (PIC variances) for leaf-traits.

Dashed lines indicate PIC variance for each leaf-trait. Histogram bars represent variances based on 1000 randomizations and black dotted lines give the 95% confidence interval. Bold dashed lines outside the intervals indicate PIC variance significantly smaller than 95% random PIC variances.

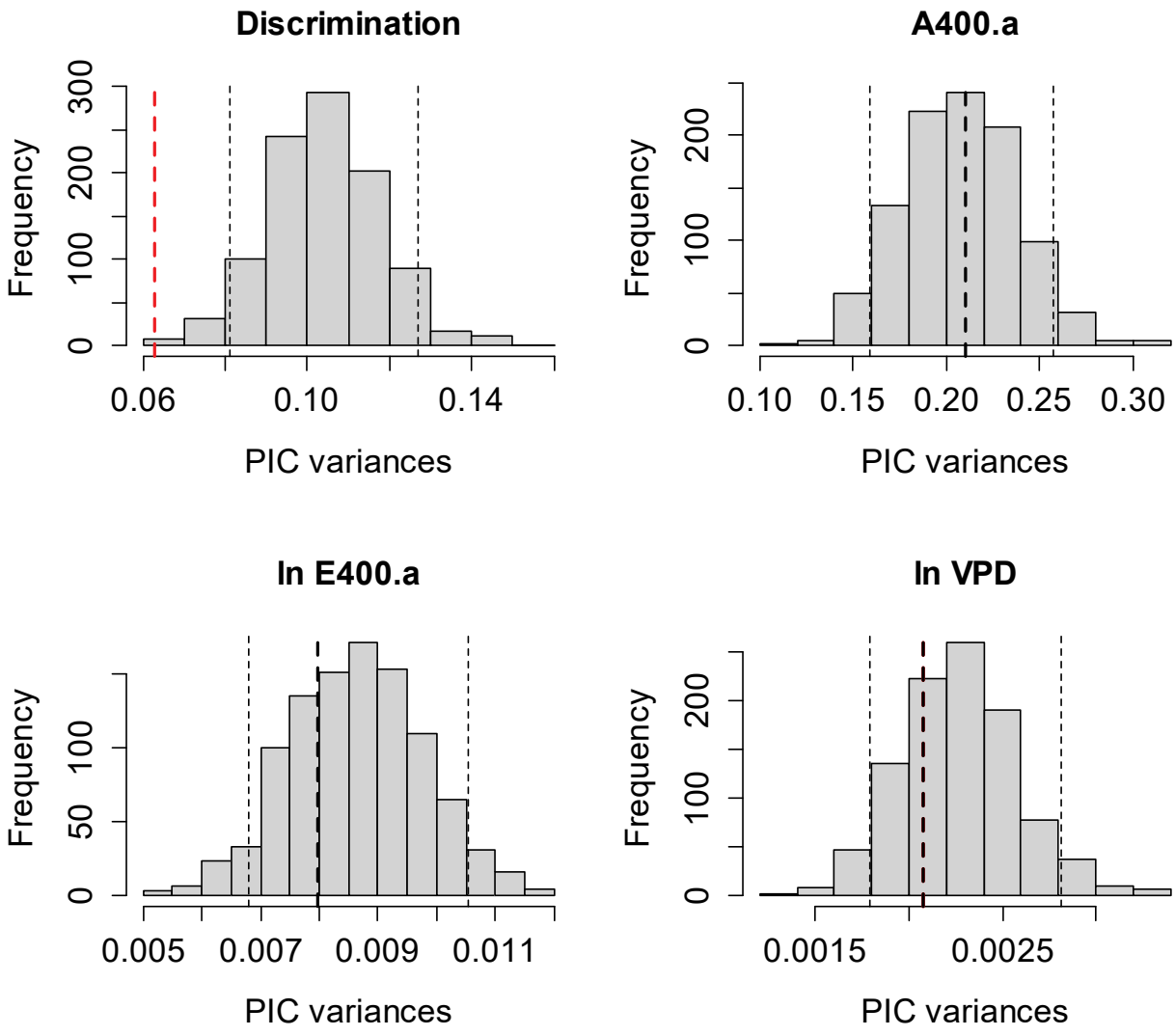

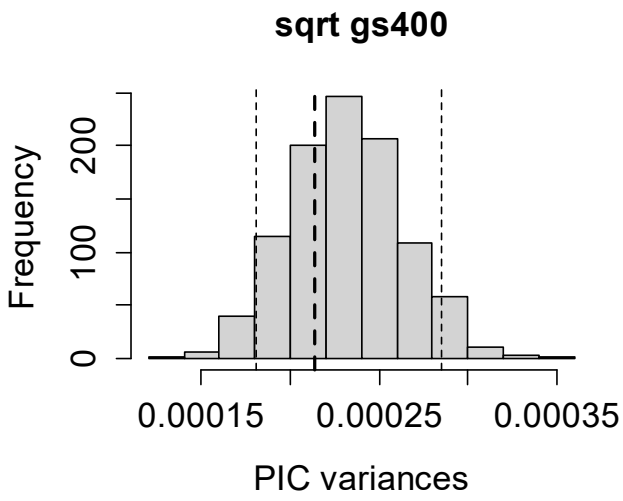
sqrt gs400
Frequency
0
100
200
0.00015
0.00025
0.00035
PIC variances

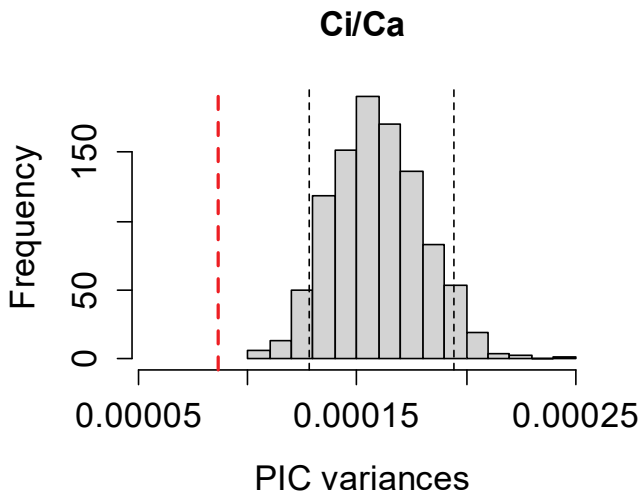
Ci/Ca
Frequency
0
50
150
0.00005
0.00015
0.00025
PIC variances

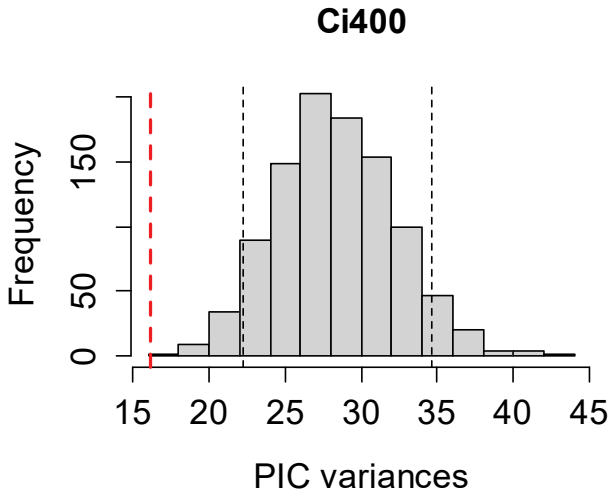
Ci400
Frequency
0
50
150
15
20
25
30
35
40
45
PIC variances

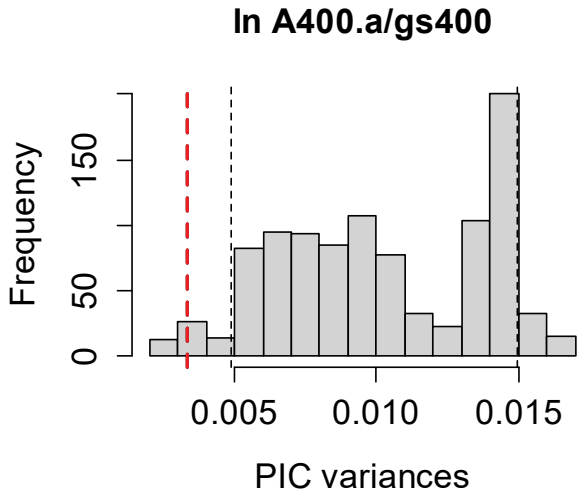
ln A400.a/gs400
Frequency
0
50
150
0.005
0.010
0.015
PIC variances

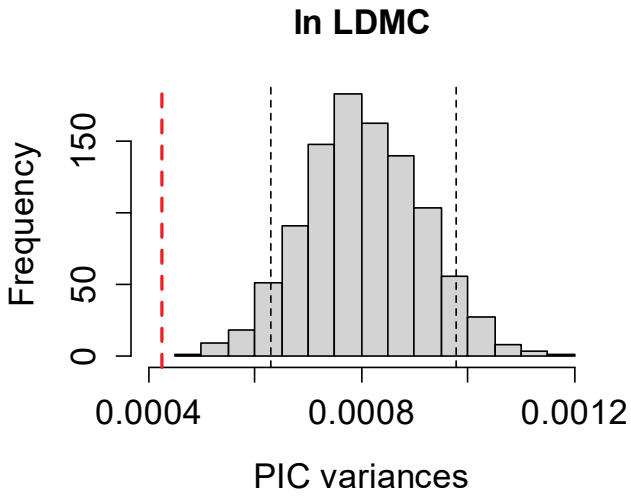
ln LDMC
Frequency
0
50
150
0.0004
0.0008
0.0012
PIC variances

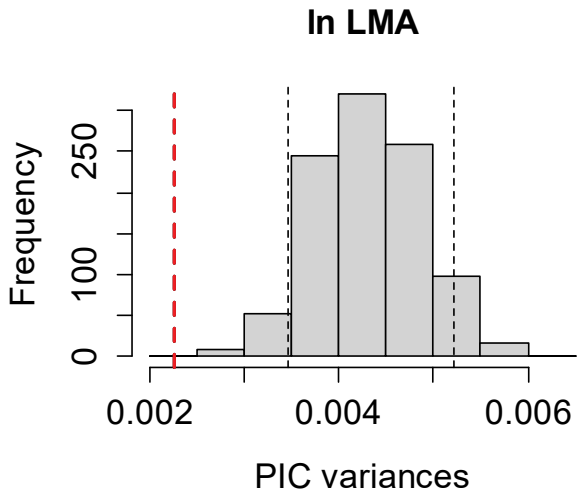
ln LMA
Frequency
0
100
250
0.002
0.004
0.006
PIC variances

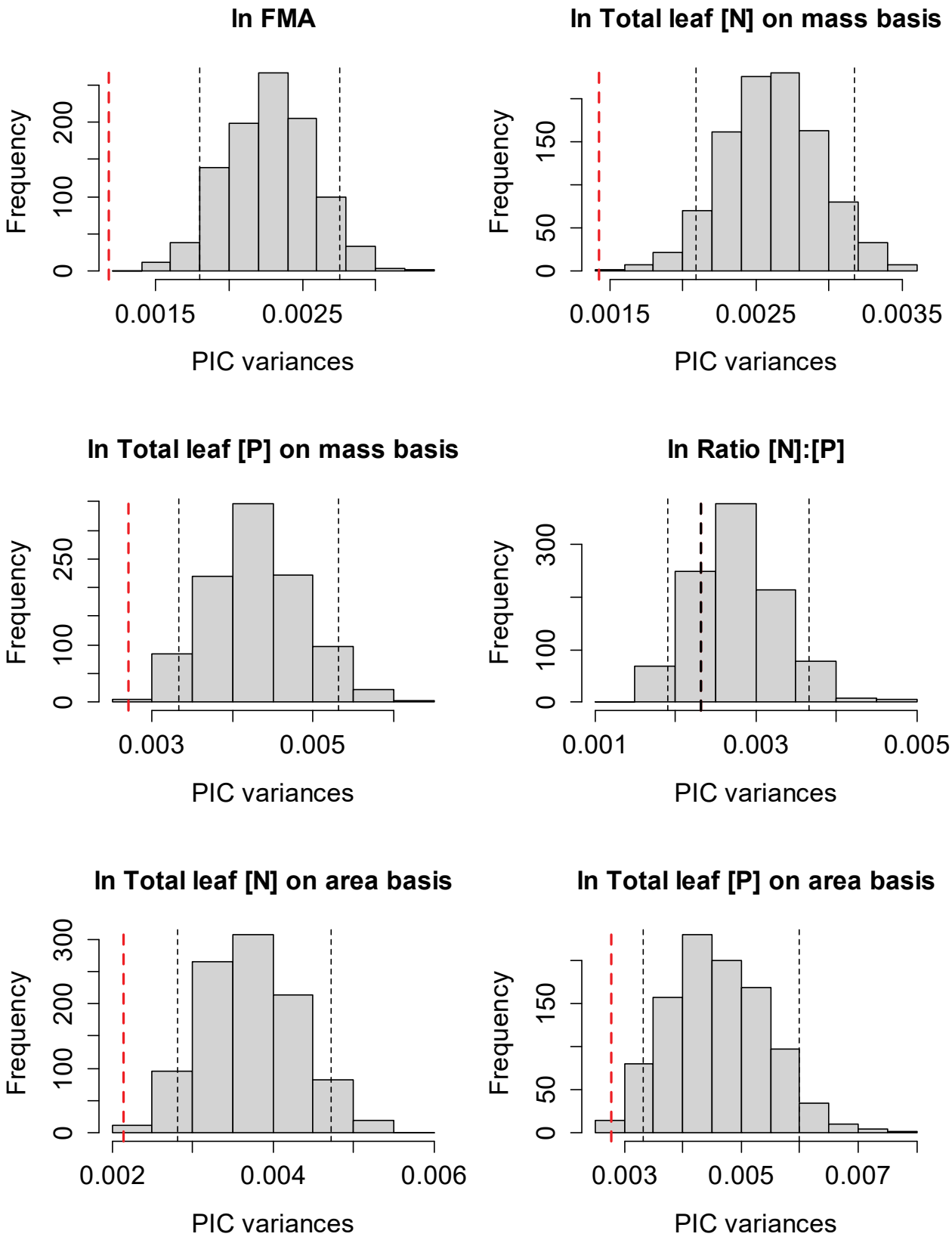
ln FMA
Frequency
0
100
200
0.0015
0.0025
PIC variances
ln Total leaf [N] on mass basis
Frequency
0
50
150
0.0015
0.0025
0.0035
PIC variances
ln Total leaf [P] on mass basis
Frequency
0
100
250
0.003
0.005
PIC variances
ln Ratio [N]:[P]
Frequency
0
100
300
0.001
0.003
0.005
PIC variances
ln Total leaf [N] on area basis
Frequency
0
100
200
300
0.002
0.004
0.006
PIC variances
ln Total leaf [P] on area basis
Frequency
0
50
150
0.003
0.005
0.007
PIC variances

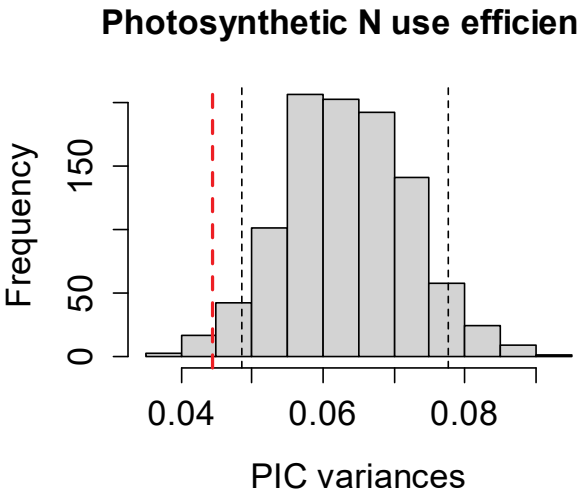
Photosynthetic N use efficiency
Frequency
0
50
150
0.04
0.06
0.08
PIC variances

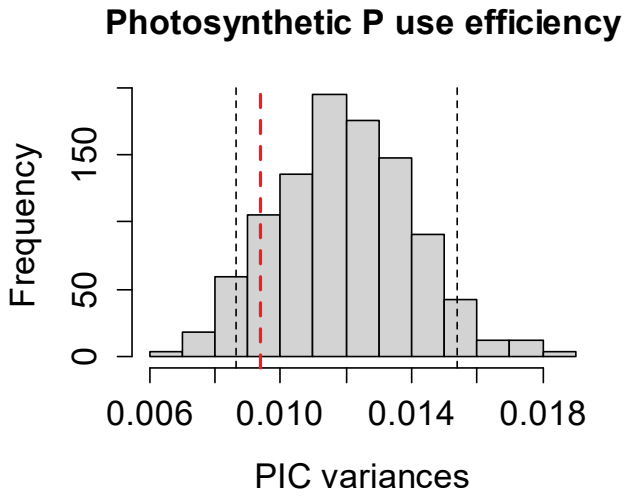
Photosynthetic P use efficiency
Frequency
0
50
150
0.006
0.010
0.014
0.018
PIC variances

References

Abrams, M.D., Kubiske, M.E. and Mostoller, S.A., 1994. Relating wet and dry year ecophysiology to leaf structure in contrasting temperate tree species. *Ecology*, 75(1): 123-133.

Ackerly, D.D. and Donoghue, M., 1998. Leaf size, sapling allometry, and Corner's rules: phylogeny and correlated evolution in maples (*Acer*). *The American Naturalist*, 152(6): 767-791.

Ackerly, D.D. and Reich, P.B., 1999. Convergence and correlations among leaf size and function in seed plants: a comparative test using independent contrasts. *American Journal of Botany*, 86(9): 1272-1281.

Addington, R.N., Donovan, L.A., Mitchell, R.J., Vose, J.M., Pecot, S.D., Jack, S.B., Hacke, U.G., Sperry, J.S. and Oren, R., 2006. Adjustments in hydraulic architecture of *Pinus palustris* maintain similar stomatal conductance in xeric and mesic habitats. *Plant, Cell & Environment*, 29(4): 535-545.

Addo-Bediako, A., Chown, S.L. and Gaston, K.J., 2000. Thermal tolerance, climatic variability and latitude. *Proceedings of the Royal Society of London B: Biological Sciences*, 267(1445): 739-745.

Allen, R.G., Pereira, L. S., Raes, D. and Smith, M., 1998. FAO Irrigation and Drainage Paper – no. 56: Crop Evapotranspiration (Guidelines for Computing Crop Water Requirements), *FAO, Water Resources, Development and Management Service*, Rome, Italy, pp. 300.

Araya, Y.N., Silvertown, J., Gowing, D.J., McConway, K.J., Linder, H.P. and Midgley, G., 2012. Do niche-structured plant communities exhibit phylogenetic conservatism? A test case in an endemic clade. *Journal of Ecology*, 100(6): 1434-1439.

Araya, Y.N., Silvertown, J., Gowing, D.J., McConway, K.J., Linder, H.P. and Midgley, G., 2011. A fundamental, eco-hydrological basis for niche segregation in plant communities. *New Phytologist*, 189(1): 253-258.

Bacon, M., 2009. *Water-use-efficiency in plant biology*. John Wiley & Sons.

Baird, K.J., Stromberg, J.C. and Maddock III, T., 2005. Linking riparian dynamics and groundwater: an ecohydrologic approach to modeling groundwater and riparian vegetation. *Environmental Management*, 36(4): 551-564.

Baldocchi, D.D. and Ryu, Y., 2011. A synthesis of forest evaporation fluxes–from days to years–as measured with eddy covariance, *Forest Hydrology and Biogeochemistry*. Ecological studies. Springer, Netherlands, pp. 101-116.

Baraloto, C., Timothy Paine, C., Poorter, L., Beauchene, J., Bonal, D., Domenach, A.M., Hérault, B., Patino, S., Roggy, J.C. and Chave, J., 2010. Decoupled leaf and stem economics in rain forest trees. *Ecology Letters*, 13(11): 1338-1347.

Barton, C.V.M., Duursma, R.A., Medlyn, B.E., Ellsworth, D.S., Eamus, D., Tissue, D.T., Adams, M.A., Conroy, J., Crous, K.Y. and Liberloo, M., 2012. Effects of elevated atmospheric [CO_2] on instantaneous transpiration efficiency at leaf and canopy scales in Eucalyptus saligna. *Global Change Biology*, 18(2): 585-595.

Beer, C., Ciais, P., Reichstein, M., Baldocchi, D.D., Law, B., Papale, D., Soussana, J.F., Ammann, C., Buchmann, N. and Frank, D., 2009. Temporal and among-site variability of inherent water-use-efficiency at the ecosystem level. *Global Biogeochemical Cycles*, 23(2): GB2018.

Bender, M.M., 1971. Variations in the $^{13}C/^{12}C$ ratios of plants in relation to the pathway of photosynthetic carbon dioxide fixation. *Phytochemistry*, 10(6): 1239-1244.

Benyon, R. and Doody, T.M., 2004. *Water use by tree plantations in south east South Australia*. CSIRO. Forestry and Forest Products.

Benyon, R.G., Theiveyanathan, S. and Doody, T.M., 2006. Impacts of tree plantations on groundwater in south-eastern Australia. *Australian Journal of Botany*, 54(2): 181-192.

Blomberg, S.P. and Garland, T., 2002. Tempo and mode in evolution: phylogenetic inertia, adaptation and comparative methods. *Journal of Evolutionary Biology*, 15(6): 899-910.

Blomberg, S.P., Garland, T. and Ives, A.R., 2003. Testing for phylogenetic signal in comparative data: behavioral traits are more labile. *Evolution*, 57(4): 717-745.

Blomberg, S.P., Lefevre, J.G., Wells, J.A. and Waterhouse, M., 2012. Independent contrasts and PGLS regression estimators are equivalent. *Systematic Biology*, 61(3): 382-391.

Bogino, S.M. and Jobbágy, E.G., 2011. Climate and groundwater effects on the establishment, growth and death of *Prosopis caldenia* trees in the Pampas (Argentina). *Forest Ecology and Management*, 262(9): 1766-1774.

Bowman, D.M., Brown, G., Braby, M., Brown, J., Cook, L.G., Crisp, M., Ford, F., Haberle, S., Hughes, J. and Isagi, Y., 2010. Biogeography of the Australian monsoon tropics. *Journal of Biogeography*, 37(2): 201-216.

Bowman, D.M., Walsh, A. and Milne, D.J., 2001. Forest expansion and grassland contraction within a *Eucalyptus* savanna matrix between 1941 and 1994 at Litchfield National Park in the Australian monsoon tropics. *Global Ecology and Biogeography*, 10(5): 535-548.

Briggs, L.J. and Shantz, H.L., 1913a. The water requirement of plants. II. A review of the literature. *Bureau of Plant Industry, U. S. Department of Agriculture*, 285.

Briggs, L.J. and Shantz, H.L., 1913b. The water requirements of plants. I. Investigation in the Great Plains in 1910 and 1911. *Bureau of Plant Industry, U. S. Department of Agriculture*, 284.

Brodribb, T.J., Feild, T.S. and Jordan, G.J., 2007. Leaf maximum photosynthetic rate and venation are linked by hydraulics. *Plant Physiology*, 144(4): 1890-1898.

Brodribb, T.J., Feild, T.S. and Sack, L., 2010. Viewing leaf structure and evolution from a hydraulic perspective. *Functional Plant Biology*, 37(6): 488-498.

Brodribb, T.J. and Holbrook, N.M., 2003. Changes in leaf hydraulic conductance during leaf shedding in seasonally dry tropical forest. *New Phytologist*, 158(2): 295-303.

Brodribb, T.J. and Holbrook, N.M., 2007. Forced depression of leaf hydraulic conductance in situ: effects on the leaf gas-exchange of forest trees. *Functional Ecology*, 21(4): 705-712.

Brodribb, T.J., Holbrook, N.M., Zwieniecki, M.A. and Palma, B., 2005. Leaf hydraulic capacity in ferns, conifers and angiosperms: impacts on photosynthetic maxima. *New Phytologist*, 165(3): 839-846.

Brodribb, T.J. and Jordan, G.J., 2008. Internal coordination between hydraulics and stomatal control in leaves. *Plant, Cell & Environment*, 31(11): 1557-1564.

Brolsma, R. and Bierkens, M., 2007. Groundwater–soil water–vegetation dynamics in a temperate forest ecosystem along a slope. *Water Resources Research*, 43(1), W01414, doi:10.1029/2005WR004696.

Brookhouse, M., 2006. Eucalypt dendrochronology: past, present and potential. *Australian Journal of Botany*, 54(5): 435-449.

Brugnoli, E. and Farquhar, G.D., 2000. Photosynthetic fractionation of carbon isotopes, *Advances in Photosynthesis and Respiration.* Springer, Neherlands, pp. 399-434.

Bucci, S., Goldstein, G., Meinzer, F., Scholz, F., Franco, A. and Bustamante, M., 2004. Functional convergence in hydraulic architecture and water relations of tropical savanna trees: from leaf to whole plant. *Tree Physiology*, 24(8): 891-899.

Budyko, M.I., 1974. *Climate and Life*. Academic Press, New York, 508 pp.

Burnham, K.P. and Anderson, D.R., 2004. Multimodel inference understanding AIC and BIC in model selection. *Sociological Methods & Research*, 33(2): 261-304.

Busch, D.E., Ingraham, N.L. and Smith, S.D., 1992. Water uptake in woody riparian phreatophytes of the southwestern United States: a stable isotope study. *Ecological Applications*, 2(4): 450-459.

Byrne, M., Yeates, D.K., Joseph, L., Kearney, M., Bowler, J., Williams, M.A.J., Cooper, S., Donnellan, S.C., Keogh, J.S. and Leys, R., 2008. Birth of a biome: insights into the

assembly and maintenance of the Australian arid zone biota. *Molecular Ecology*, 17(20): 4398-4417.

Carter, R. and Klinka, K., 1990. Relationships between growing-season soil water-deficit, mineralizable soil nitrogen and site index of coastal Douglas fir. *Forest Ecology and Management*, 30(1-4): 301-311.

Cerling, T.E., Harris, J.M., MacFadden, B.J., Leakey, M.G., Quade, J., Eisenmann, V. and Ehleringer, J.R., 1997. Global vegetation change through the Miocene/Pliocene boundary. *Nature*, 389(6647): 153-158.

Cernusak, L.A., Hutley, L.B., Beringer, J., Holtum, J.A. and Turner, B.L., 2011. Photosynthetic physiology of *Eucalypts* along a sub-continental rainfall gradient in northern Australia. *Agricultural and Forest Meteorology*, 151(11): 1462-1470.

Cernusak, L.A., Ubierna, N., Winter, K., Holtum, J.A.M., Marshall, J.D. and Farquhar, G.D., 2013. Environmental and physiological determinants of carbon isotope discrimination in terrestrial plants. *New Phytologist*, 200(4): 950-965.

Chiew, F.H. and McMahon, T.A., 1991. The applicability of Morton's and Penman's evapotranspiration estimates in rainfall-runoff modeling. *Journal of the American Water Resources Association*, 27(4): 611-620.

Chimner, R.A. and Cooper, D.J., 2004. Using stable oxygen isotopes to quantify the water source used for transpiration by native shrubs in the San Luis Valley, Colorado USA. *Plant and Soil*, 260(1-2): 225-236.

Clarke, R., 1991. *Water: the international crisis*. Earthscan, London, UK.

Cleverly, J., Boulain, N., Villalobos-Vega, R., Grant, N., Faux, R., Wood, C., Cook, P.G., Yu, Q., Leigh, A. and Eamus, D., 2013. Dynamics of component carbon fluxes in a semi-arid Acacia woodland, central Australia. *Journal of Geophysical Research: Biogeosciences*, 118(3): 1168-1185.

Cleverly, J., Eamus, D., Van Gorsel, E., Chen, C., Rumman, R., Luo, Q., Coupe, N.R., Li, L., Kljun, N. and Faux, R., 2016. Productivity and evapotranspiration of two contrasting semiarid ecosystems following the 2011 global carbon land sink anomaly. *Agricultural and Forest Meteorology*, 220: 151-159.

Cocozza, C., Giovannelli, A., Traversi, M.L., Castro, G., Cherubini, P. and Tognetti, R., 2011. Do tree-ring traits reflect different water deficit responses in young poplar clones? *Trees*, 25(6): 975-985.

Comstock, J. and Ehleringer, J., 1992. Correlating genetic variation in carbon isotopic composition with complex climatic gradients. *Proceedings of the National Academy of Sciences*, 89(16): 7747-7751.

Cook, P.G., O'Grady, A.P., Wischusen, J.D.H., Duguid, A., Fass, T., Eamus, D. and Palmerston, N.T., 2008. Ecohydrology of sandplain woodlands in central Australia. *Department of Natural Resources, Environment and The Arts, Northern Territory Government.*

Cooper, N., Jetz, W. and Freckleton, R.P., 2010. Phylogenetic comparative approaches for studying niche conservatism. *Journal of Evolutionary Biology*, 23(12): 2529-2539.

Cordry, K., 2003. HydraSleeve: A new no-purge groundwater sampler for all contaminants, *ITRC Fall 2003 Conference,* Monterey, California.

Couvreur, V., Vanderborght, J., Draye, X. and Javaux, M., 2014. Dynamic aspects of soil water availability for isohydric plants: focus on root hydraulic resistances. *Water Resources Research*, 50(11): 8891-8906.

Cowan, I.R. and Farquhar, G.D., 1977. Stomatal function in relation to leaf metabolism and environment, *The Society for Experimental Biology Symposium* pp. 471-505.

Craig, H., 1954. Carbon 13 in plants and the relationships between carbon 13 and carbon 14 variations in nature. *The Journal of Geology*: 115-149.

Cramer, V.A., Thorburn, P.J. and Fraser, G.W., 1999. Transpiration and groundwater uptake from farm forest plots of *Casuarina glauca* and *Eucalyptus camaldulensis* in saline areas of southeast Queensland, Australia. *Agricultural water management*, 39(2): 187-204.

Creed, I.F., Spargo, A.T., Jones, J.A., Buttle, J.M., Adams, M.B., Beall, F.D., Booth, E.G., Campbell, J.L., Clow, D. and Elder, K., 2014. Changing forest water yields in response to climate warming: results from long-term experimental watershed sites across North America. *Global Change Biology*, 20(10): 3191-3208.

Cunningham, S.A., Summerhayes, B. and Westoby, M., 1999. Evolutionary divergences in leaf structure and chemistry, comparing rainfall and soil nutrient gradients. *Ecological Monographs*, 69(4): 569-588.

Dansgaard, W., 1964. Stable isotopes in precipitation. *Tellus*, 16(4): 436-468.

Davies, T.J., Barraclough, T.G., Chase, M.W., Soltis, P.S., Soltis, D.E. and Savolainen, V., 2004. Darwin's abominable mystery: insights from a supertree of the angiosperms. *Proceedings of the National Academy of Sciences of the United States of America*, 101(7): 1904-1909.

Dawson, T., 1990. Spatial and physiological overlap of three co-occurring alpine willows. *Functional Ecology*, 4(1): 13-25.

Dawson, T.E. and Brooks, P.D., 2001. Fundamentals of stable isotope chemistry and measurement, *Stable isotope techniques in the study of biological processes and functioning of ecosystems*. Springer, Netherlands, pp. 1-18.

Dawson, T.E. and Ehleringer, J.R., 1991. Streamside trees that do not use stream water. *Nature*, 350(6316): 335-337.

Dawson, T.E. and Ehleringer, J.R., 1993. Gender-specific physiology, carbon isotope discrimination, and habitat distribution in boxelder, *Acer negundo*. *Ecology*, 74: 798-815.

Dawson, T.E., Mambelli, S., Plamboeck, A.H., Templer, P.H. and Tu, K.P., 2002. Stable isotopes in plant ecology. *Annual Review of Ecology and Systematics*, 23: 507-559.

Diefendorf, A.F., Mueller, K.E., Wing, S.L., Koch, P.L. and Freeman, K.H., 2010. Global patterns in leaf ^{13}C discrimination and implications for studies of past and future climate. *Proceedings of the National Academy of Sciences*, 107(13): 5738-5743.

Dodd, M., Lauenroth, W. and Welker, J., 1998. Differential water resource use by herbaceous and woody plant life-forms in a shortgrass steppe community. *Oecologia*, 117(4): 504-512.

Donohue, R., Roderick, M. and McVicar, T., 2007. On the importance of including vegetation dynamics in Budyko's hydrological model. *Hydrology and Earth System Sciences Discussions*, 11(2): 983-995.

Donohue, R., Roderick, M. and McVicar, T.R., 2010. Can dynamic vegetation information improve the accuracy of Budyko's hydrological model? *Journal of Hydrology*, 390(1): 23-34.

Donohue, R.J., McVICAR, T. and Roderick, M.L., 2009. Climate-related trends in Australian vegetation cover as inferred from satellite observations, 1981–2006. *Global Change Biology*, 15(4): 1025-1039.

Dragoni, D., Caylor, K. and Schmid, H., 2009. Decoupling structural and environmental determinants of sap velocity: Part II. Observational application. *Agricultural and Forest Meteorology*, 149(3): 570-581.

Drake, P. and Franks, P., 2003. Water resource partitioning, stem xylem hydraulic properties, and plant water use strategies in a seasonally dry riparian tropical rainforest. *Oecologia*, 137(3): 321-329.

Drew, D.M. and Downes, G.M., 2009. The use of precision dendrometers in research on daily stem size and wood property variation: A review. *Dendrochronologia*, 27: 169-172.

Dupouey, J.L., Leavitt, S., Choisnel, E. and Jourdain, S., 1993. Modelling carbon isotope fractionation in tree rings based on effective evapotranspiration and soil water status. *Plant, Cell & Environment*, 16(8): 939-947.

Eamus, D., 1991. The interaction of rising CO_2 and temperatures with water-use-efficiency. *Plant, Cell & Environment*, 14(8): 843-852.

Eamus, D., 2009. Identifying ground water dependent ecosystems: A guide for land and water managers. Land and Water Australia.

Eamus, D., Cleverly, J., Boulain, N., Grant, N., Faux, R. and Villalobos-Vega, R., 2013. Carbon and water fluxes in an arid-zone Acacia savanna woodland: An analyses of seasonal patterns and responses to rainfall events. *Agricultural and Forest Meteorology*, 182: 225-238.

Eamus, D., Froend, R., Loomes, R., Hose, G. and Murray, B., 2006a. A functional methodology for determining the groundwater regime needed to maintain the health of groundwater-dependent vegetation. *Australian Journal of Botany*, 54(2): 97-114.

Eamus, D., Hatton, T., Cook, P. and Colvin, C., 2006b. *Ecohydrology: vegetation function, water and resource management*. CSIRO Publishing: Melbourne.

Eamus, D., O'Grady, A.P. and Hutley, L., 2000. Dry-season conditions determine wet-season water use in the wet–tropical savannas of northern Australia. *Tree Physiology*, 20(18): 1219-1226.

Edwards, E.J., 2006. Correlated evolution of stem and leaf hydraulic traits in *Pereskia* (*Cactaceae*). *New Phytologist*, 172(3): 479-789.

Ehleringer, J.R. and Cooper, T.A., 1988. Correlations between carbon isotope ratio and microhabitat in desert plants. *Oecologia*, 76: 562–566.

Ehleringer, J.R. and Dawson, T.E., 1992. Water uptake by plants: perspectives from stable isotope composition. *Plant, Cell & Environment*, 15(9): 1073-1082.

Ehleringer, J.R., Phillips, S.L., Schuster, W.S. and Sandquist, D.R., 1991. Differential utilization of summer rains by desert plants. *Oecologia*, 88(3): 430-434.

Evans, J.R. and Von Caemmerer, S., 1996. Carbon dioxide diffusion inside leaves. *Plant Physiology*, 110(2): 339.

Evans, J.R. and Von Caemmerer, S., 2013. Temperature response of carbon isotope discrimination and mesophyll conductance in tobacco. *Plant, Cell & Environment*, 36(4): 745-756.

Evans, R. and Hatton, T.J., 1998. *Dependence of ecosystems on groundwater and its significance to Australia*. Land & Water Resources Research & Development Corporation.

Farquhar, G.D., 1991. Use of stable isotopes in evaluating plant water-use-efficiency, *Stable isotopes in plant nutrition, soil fertility and environmental studies*, Proceedings of a symposium Vienna, pp. 475-488.

Farquhar, G.D. and Cernusak, L.A., 2012. Ternary effects on the gas-exchange of isotopologues of carbon dioxide. *Plant, Cell & Environment*, 35(7): 1221-1231.

Farquhar, G.D., Ehleringer, J.R. and Hubick, K.T., 1989. Carbon isotope discrimination and photosynthesis. *Plant Physiology and Plant Molecular Biology*, 40: 503-537.

Farquhar, G.D., O'Leary, M.H. and Berry, J.A., 1982. On the relationship between carbon isotope discrimination and the intercellular carbon dioxide concentration in leaves. *Functional Plant Biology*, 9(2): 121-137.

Farquhar, G.D. and Richards, R.A., 1984. Isotopic composition of plant carbon correlates with water-use-efficiency of wheat genotypes. *Australian Journal of Plant Physiology*, 11(6): 539-552.

Farquhar, G.D. and Sharkey, T.D., 1982. Stomatal conductance and photosynthesis. *Annual Review of Plant Physiology*, 33(1): 317-345.

Felsenstein, J., 1985. Confidence limits on phylogenies: an approach using the bootstrap. *Evolution*: 783-791.

Flexas, J., Díaz-Espejo, A., Berry, J., Cifre, J., Galmés, J., Kaldenhoff, R., Medrano, H. and Ribas-Carbó, M., 2007. Analysis of leakage in IRGA's leaf chambers of open gas-exchange systems: quantification and its effects in photosynthesis parameterization. *Journal of Experimental Botany*, 58(6): 1533-1543.

Fonseca, C.R., Overton, J.M., Collins, B. and Westoby, M., 2000. Shifts in trait-combinations along rainfall and phosphorus gradients. *Journal of Ecology*, 88(6): 964-977.

Ford, C.R., Mitchell, R.J. and Teskey, R.O., 2008. Water table depth affects productivity, water use, and the response to nitrogen addition in a savanna system. *Canadian Journal of Forest Research*, 38(2118-2127).

Freckleton, R.P., Harvey, P.H. and Pagel, M., 2002. Phylogenetic analysis and comparative data: a test and review of evidence. *The American Naturalist*, 160(6): 712-726.

Fu, P.L., Jiang, Y.J., Wang, A.Y., Brodribb, T.J., Zhang, J.L., Zhu, S.D. and Cao, K.F., 2012. Stem hydraulic traits and leaf water-stress tolerance are co-ordinated with the leaf phenology of angiosperm trees in an Asian tropical dry karst forest. *Annals of Botany*, 110 (1): 189-199.

Gardner, R.O., 1975. An overview of botanical clearing technique. *Stain Technology*, 50(2): 99-105.

Garland Jr, T. and Ives, A.R., 2000. Using the past to predict the present: confidence intervals for regression equations in phylogenetic comparative methods. *The American Naturalist*, 155(3): 346-364.

Garland, T., Harvey, P.H. and Ives, A.R., 1992. Procedures for the analysis of comparative data using phylogenetically independent contrasts. *Systematic Biology*, 41(1): 18-32.

Gates, D.M., 1968. Transpiration and leaf temperature. *Annual Review of Plant Physiology*, 19(1): 211-238.

Gentine, P., D'Odorico, P., Lintner, B.R., Sivandran, G. and Salvucci, G., 2012. Interdependence of climate, soil, and vegetation as constrained by the Budyko curve. *Geophysical Research Letters*, 39(19), doi: 10.1029/2012GL053492.

Gerrits, A.M.J., Savenije, H.H.G., Veling, E.J.M. and Pfister, L., 2009. Analytical derivation of the Budyko curve based on rainfall characteristics and a simple evaporation model. *Water Resources Research*, 45(4) , doi: 10.1029/2008WR007308.

Giles, D.G., Black, T.A. and Spittlehouse, D.L., 1985. Determination of growing season soil water deficits on a forested slope using water balance analysis. *Canadian Journal of Forest Research*, 15(1): 107-114.

Givnish, T.J., 1988. Adaptation to sun and shade: a whole-plant perspective. *Functional Plant Biology*, 15(2): 63-92.

Goldsmith, G.R., Muñoz-Villers, L.E., Holwerda, F., McDonnell, J.J., Asbjornsen, H. and Dawson, T.E., 2012. Stable isotopes reveal linkages among ecohydrological processes in a seasonally dry tropical montane cloud forest. *Ecohydrology*, 5(6): 779-790.

Goldstein, G., Meinzer, F.C., Bucci, S.J., Scholz, F.G., Franco, A.C. and Hoffmann, W.A., 2008. Water economy of Neotropical savanna trees: six paradigms revisited. *Tree Physiology*, 28(3): 395-404.

Gonfiantini, R., Gratziu, S. and Tongiorgi, E., 1965. Oxygen isotopic composition of water in leaves. *Isotopes and Radiation in Soil-Plant Nutrition Studies*, IAEA, Vienna, pp. 405-410.

Gosper, C.R., Prober, S.M., Yates, C.J. and Wiehl, G., 2013. Estimating the time since fire of long-unburnt *Eucalyptus salubris* (Myrtaceae) stands in the Great Western Woodlands. *Australian Journal of Botany*, 61(1): 11-21.

Grafen, A., 1989. The phylogenetic regression. *Philosophical Transactions of the Royal Society of London. Series B, Biological Sciences*, 326(1233): 119-157.

Granger, R.J. and Gray, D.M., 1990. Examination of Morton's CRAE model for estimating daily evaporation from field-sized areas. *Journal of Hydrology*, 120(1): 309-325.

Grigg, A.M., Lambers, H. and Veneklaas, E.J., 2010. Changes in water relations for *Acacia ancistrocarpa* on natural and mine-rehabilitation sites in response to an experimental wetting pulse in the Great Sandy Desert. *Plant and Soil*, 326(1-2): 75-96.

Groom, B.P.K., Froend, R.H. and Mattiske, E.M., 2000. Impact of groundwater abstraction on a *Banksia* woodland, Swan Coastal Plain, Western Australia. *Ecological Management & Restoration*, 1(2): 117-124.

Groom, P. and Lamont, B.B., 1997. Xerophytic implications of increased sclerophylly: interactions with water and light in *Hakea psilorrhyncha* seedlings. *New Phytologist*, 136(2): 231-237.

Groom, P.K. and Lamont, B.B., 1999. Which common indices of sclerophylly best reflect differences in leaf structure? *Ecoscience*, 6(3): 471-474.

Hacke, U.G., Sperry, J.S., Ewers, B.E., Ellsworth, D.S., Schäfer, K.V.R. and Oren, R., 2000. Influence of soil porosity on water use in *Pinus taeda. Oecologia*, 124(4): 495-505.

Hanba, Y.T., Miyazawa, S.I. and Terashima, I., 1999. The influence of leaf thickness on the CO_2 transfer conductance and leaf stable carbon isotope ratio for some evergreen tree species in Japanese warm-temperate forests. *Functional Ecology*, 13(5): 632-639.

Hansen, T.F., 2014. Use and misuse of comparative methods in the study of adaptation, *Modern phylogenetic comparative methods and their application in evolutionary biology*. Springer, Berlin Heidelberg, pp. 351-379.

Harrington, G.A., Cook, P.G. and Herczeg, A.L., 2002. Spatial and temporal variability of ground water recharge in central Australia: a tracer approach. *Ground Water*, 40(5): 518-528.

Harvey, P.H. and Pagel, M.D., 1991. *The comparative method in evolutionary biology*, 239. Oxford University Press, Oxford.

Harvey, P.H., Read, A.F. and Nee, S., 1995. Why ecologists need to be phylogenetically challenged. *Journal of Ecology*, 83(3): 535-536.

Helmuth, B., Kingsolver, J.G. and Carrington, E., 2005. Biophysics, physiological ecology, and climate change: does mechanism matter? *Annual Review of Physiology*, 67: 177-201.

Hernández, E., Pausas, J.G. and Vilagrosa, A., 2011. Leaf physiological traits in relation to resprouter ability in the Mediterranean Basin. *Plant Ecology*, 212(12): 1959-1966.

Hesterberg, R. and Siegenthaler, U., 1991. Production and stable isotopic composition of CO2 in a soil near Bern, Switzerland. *Tellus B*, 43(2): 197-205.

Hickey, J.E., Su, W., Rowe, P., Brown, M.J. and Edwards, L., 1999. Fire history of the tall wet *Eucalypt* forests of the Warra ecological research site, Tasmania. *Australian Forestry*, 62(1): 66-71.

Hijmans, R.J., Cameron, S.E., Parra, J.L., Jones, P.G. and Jarvis, A., 2005. Very high resolution interpolated climate surfaces for global land areas. *International Journal of Climatology*, 25(15): 1965-1978.

Hopkins III, J.B. and Ferguson, J.M., 2012. Estimating the diets of animals using stable isotopes and a comprehensive Bayesian mixing model. *PloS one*, 7(1): e28478.

Horton, J.L., Kolb, T.E. and Hart, S.C., 2001. Responses of riparian trees to interannual variation in ground water depth in a semi-arid river basin. *Plant, Cell & Environment*, 24(3): 293-304.

Howe, P., O'Grady, A.P., Cook, P.G. and Fas, T., 2007. Project REM1 – A framework for assessing environmental water requirements for Groundwater Dependent Ecosystems Report-2 Field Studies. Land and Water Australia.

Hughes, L., 2003. Climate change and Australia: trends, projections and impacts. *Austral Ecology*, 28(4): 423-443.

Hultine, K.R., Bush, S.E. and Ehleringer, J.R., 2010. Ecophysiology of riparian cottonwood and willow before, during, and after two years of soil water removal. *Ecological Applications*, 20(2): 347-361.

Hutley, L.B. and Beringer, J., 2010. Disturbance and climatic drivers of carbon dynamics of a north Australian tropical savanna, *Ecosystem function in savannas: measurement and modeling at landscape to global scales*. CRC Press, Boca Raton, pp. 57-75.

Hutley, L.B., Beringer, J., Isaac, P.R., Hacker, J.M. and Cernusak, L.A., 2011. A sub-continental scale living laboratory: Spatial patterns of savanna vegetation over a rainfall gradient in northern Australia. *Agricultural and Forest Meteorology*, 151(11): 1417-1428.

Huxman, T.E., Smith, M.D., Fay, P.A., Knapp, A.K., Shaw, M.R., Loik, M.E., Smith, S.D., Tissue, D.T., Zak, J.C. and Weltzin, J.F., 2004. Convergence across biomes to a common rain-use efficiency. *Nature*, 429: 651-654.

IAEA, 2009. Reference Sheet for VSMOW2 and SLAP2 international measurement standards. International Atomic Energy Agency, Vienna.

Inger, R., Jackson, A., Parnell, A. and Bearhop, S., 2010. SIAR v4 (Stable Isotope Analysis in R): an ecologist's guide. Zostera.

Ingraham, N.L. and Shadel, C., 1992. A comparison of the toluene distillation and vacuum/heat methods for extracting soil water for stable isotopic analysis. *Journal of Hydrology*, 140(1): 371-387.

Ives, A.R., Midford, P.E. and Garland, T., 2007. Within-species variation and measurement error in phylogenetic comparative methods. *Systematic Biology*, 56(2): 252-270.

Jackson, P.C., Meinzer, F.C., Bustamante, M., Goldstein, G., Franco, A., Rundel, P.W., Caldas, L., Igler, E. and Causin, F., 1999. Partitioning of soil water among tree species in a Brazilian *Cerrado* ecosystem. *Tree Physiology*, 19(11): 717-724.

Jobbágy, E., Nosetto, M., Villagra, P. and Jackson, R., 2011. Water subsidies from mountains to deserts: their role in sustaining groundwater-fed oases in a sandy landscape. *Ecological Applications*, 21(3): 678-694.

Johnson, M.T. and Stinchcombe, J.R., 2007. An emerging synthesis between community ecology and evolutionary biology. *Trends in Ecology & Evolution*, 22(5): 250-257.

Jones, J.A., Creed, I.F., Hatcher, K.L., Warren, R.J., Adams, M.B., Benson, M.H., Boose, E., Brown, W.A., Campbell, J.L. and Covich, A., 2012. Ecosystem processes and human influences regulate streamflow response to climate change at long-term ecological research sites. *Bioscience*, 62(4): 390-404.

Jongen, M., Hellmann, C. and Unger, S., 2015. Species-specific adaptations explain resilience of herbaceous understorey to increased precipitation variability in a Mediterranean oak woodland. *Ecology and Evolution*, 5(19): 4246-4262.

Kamilar, J.M. and Cooper, N., 2013. Phylogenetic signal in primate behaviour, ecology and life history, *Philosophical Transactions of the Royal Society of London B: Biological Sciences*, 368(1618), 20120341.

Kamilar, J.M. and Muldoon, K.M., 2010. The climatic niche diversity of Malagasy primates: a phylogenetic perspective. *PloS one*, 5(6): e11073.

Kellermann, V., Loeschcke, V., Hoffmann, A.A., Kristensen, T.N., Fløjgaard, C., David, J.R., Svenning, J.C. and Overgaard, J., 2012. Phylogenetic constraints in key functional traits behind species' climate niches: patterns of desiccation and cold resistance across 95 *Drosophila* species. *Evolution*, 66(11): 3377-3389.

Kelley, G., O'Grady, A.P., Hutley, L.B. and Eamus, D., 2007. A comparison of tree water use in two contiguous vegetation communities of the seasonally dry tropics of northern Australia: the importance of site water budget to tree hydraulics. *Australian Journal of Botany*, 55(7): 700-708.

Kembel, S.W., Cowan, P.D., Helmus, M.R., Cornwell, W.K., Morlon, H., Ackerly, D.D., Blomberg, S.P. and Webb, C.O., 2010. Picante: R tools for integrating phylogenies and ecology. *Bioinformatics*, 26(11): 1463-1464.

Kendall, C. and Caldwell, E.A., 1998. Fundamentals of isotope geochemistry. *Isotope tracers in catchment hydrology*, Elsevier Science B.V., Amsterdam, pp. 51-86.

Kendall, C. and McDonnell, J.J., 2012. *Isotope tracers in catchment hydrology*. Elsevier Science B.V., Amsterdam.

Koch, G.W., Vitousek, P.M., Steffen, W.L. and Walker, B.H., 1995. Terrestrial transects for global change research. *Vegetatio*, 121(1-2): 53-65.

Kohn, M.J., 2010. Carbon isotope compositions of terrestrial C3 plants as indicators of (paleo) ecology and (paleo) climate. *Proceedings of the National Academy of Sciences*, 107(46): 19691-19695.

Koricheva, J., Gurevitch, J. and Mengersen, K., 2013. *Handbook of meta-analysis in ecology and evolution*. Princeton University Press.

Kray, J.A., Cooper, D.J. and Sanderson, J.S., 2012. Groundwater use by native plants in response to changes in precipitation in an intermountain basin. *Journal of Arid Environments*, 83: 25-34.

Lageard, J.G. and Drew, I.B., 2008. Hydrogeomorphic control on tree growth responses in the Elton area of the Cheshire Saltfield, UK. *Geomorphology*, 95(3): 158-171.

Lambers, H. and Poorter, H., 1992. Inherent variation in growth rate between higher plants: a search for physiological causes and ecological consequences. *Advances in Ecological Research*, 23: 187-261.

Lamont, B.B., Groom, P.K. and Cowling, R., 2002. High leaf mass per area of related species assemblages may reflect low rainfall and carbon isotope discrimination rather than low phosphorus and nitrogen concentrations. *Functional Ecology*, 16(3): 403-412.

Lamontagne, S., Cook, P.G., O'Grady, A.P. and Eamus, D., 2005. Groundwater use by vegetation in a tropical savanna riparian zone (Daly River, Australia). *Journal of Hydrology*, 310(1): 280-293.

Leavitt, S.W., 1993. Seasonal $^{13}C/^{12}C$ changes in tree rings: species and site coherence, and a possible drought influence. *Canadian Journal of Forest Research*, 23(2): 210-218.

Leffler, A.J. and Evans, A.S., 1999. Variation in carbon isotope composition among years in the riparian tree *Populus fremontii*. *Oecologia*, 119(3): 311-319.

Legendre, P. and Legendre, L., 1998. *Numerical Ecology*. The Netherlands, Elsevier: Amsterdam.

Leng, X., Cui, J., Zhang, S., Zhang, W., Liu, Y., Liu, S. and An, S., 2013. Differential water uptake among plant species in humid alpine meadows. *Journal of Vegetation Science*, 24(1): 138-147.

Little, S.A., Kembel, S.W. and Wilf, P., 2010. Paleotemperature proxies from leaf fossils reinterpreted in light of evolutionary history. *PloS one*, 5(12): e15161.

Liu, J., Fu, G., Song, X., Charles, S.P., Zhang, Y., Han, D. and Wang, S., 2010. Stable isotopic compositions in Australian precipitation. *Journal of Geophysical Research: Atmospheres*, 115(D23).

Livingston, N.J. and Spittlehouse, D.L., 1996. Carbon isotope fractionation in tree ring early and late wood in relation to intra-growing season water balance. *Plant Cell and Environment*, 19(6): 768-774.

Losos, J.B., 2008. Phylogenetic niche conservatism, phylogenetic signal and the relationship between phylogenetic relatedness and ecological similarity among species. *Ecology Letters*, 11(10): 995-1003.

Macfarlane, C., 2013. Great Western Woodlands OzFlux: Australian and New Zealand Flux Research and Monitoring. hdl: 102.100.100/14226.

Macfarlane, C., Adams, M.A. and White, D.A., 2004. Productivity, carbon isotope discrimination and leaf-traits of trees of *Eucalyptus globulus* Labill. in relation to water availability. *Plant, Cell & Environment*, 27(12): 1515-1524.

Máguas, C., Rascher, K., Martins-Loucao, A., Carvalho, P., Pinho, P., Ramos, M., Correia, O. and Werner, C., 2011. Responses of woody species to spatial and temporal ground water changes in coastal sand dune systems. *Biogeosciences*, 8(12): 3823-3832.

Mahdi, A., Law, R. and Willis, A.J., 1989. Large niche overlaps among coexisting plant species in a limestone grassland community. *The Journal of Ecology*: 386-400.

McAinsh, M.R., Clayton, H., Mansfield, T.A. and Hetherington, A.M., 1996. Changes in stomatal behavior and guard cell cytosolic free calcium in response to oxidative stress. *Plant Physiology*, 111(4): 1031-1042.

McCarroll, D. and Loader, N.J., 2004. Stable isotopes in tree rings. *Quaternary Science Reviews*, 23: 771-801.

Medlyn, B.E., Duursma, R.A., Eamus, D., Ellsworth, D.S., Prentice, I.C., Barton, C.V.M., Crous, K.Y., De Angelis, P., Freeman, M. and Wingate, L., 2011. Reconciling the optical and empirical approaches to modelling stomatal conductance. *Global Change Biology*, 17: 2134-2144.

Meinzer, F.C., 2003. Functional convergence in plant responses to the environment. *Oecologia*, 134(1): 1-11.

Meinzer, F.C. and Grantz, D.A., 1990. Stomatal and hydraulic conductance in growing sugarcane: stomatal adjustment to water transport capacity. *Plant, Cell & Environment*, 13(4): 383-388.

Meyer, W.S., Kondrlovà, E. and Koerber, G.R., 2015. Evaporation of perennial semi-arid woodland in southeastern Australia is adapted for irregular but common dry periods. *Hydrological Processes*, 29(17): 3714-3726.

Michener, R. and Lajtha, K., 2008. *Stable isotopes in ecology and environmental science*. John Wiley & Sons.

Midgley, G.F., Aranibar, J.N., Mantlana, K.B. and Macko, S., 2004. Photosynthetic and gas-exchange characteristics of dominant woody plants on a moisture gradient in an African savanna. *Global Change Biology*, 10(3): 309-317.

Miller, J.M., Williams, R.J. and Farquhar, G.D., 2001. Carbon isotope discrimination by a sequence of *Eucalyptus* species along a subcontinental rainfall gradient in Australia. *Functional Ecology*, 15(2): 222-232.

Moreno-Gutiérrez, C., Dawson, T.E., Nicolás, E. and Querejeta, J.I., 2012. Isotopes reveal contrasting water use strategies among coexisting plant species in a Mediterranean ecosystem. *New Phytologist*, 196(2): 489-496.

Morton, F.I., 1983. Operational estimates of areal evapotranspiration and their significance to the science and practice of hydrology. *Journal of Hydrology*, 66(1): 1-76.

Morton, S., Smith, D.S., Dickman, C.R., Dunkerley, D., Friedel, M., McAllister, R., Reid, J., Roshier, D., Smith, M. and Walsh, F., 2011. A fresh framework for the ecology of arid Australia. *Journal of Arid Environments*, 75(4): 313-329.

Mudd, G., 2000. Mound springs of the Great Artesian Basin in South Australia: a case study from Olympic Dam. *Environmental Geology*, 39(5): 463-476.

Münkemüller, T., Lavergne, S., Bzeznik, B., Dray, S., Jombart, T., Schiffers, K. and Thuiller, W., 2012. How to measure and test phylogenetic signal. *Methods in Ecology and Evolution*, 3(4): 743-756.

Murphy, B.P., Russel-Smith, J. and Prior, L.D., 2010. Frequent fires reduce tree growth in northern Australian savannas: implications for tree demography and carbon sequestration. *Global Change Biology*, 16(1): 331-343.

Niinemets, Ü., 2001. Global-scale climatic controls of leaf dry mass per area, density, and thickness in trees and shrubs. *Ecology*, 82(2): 453-469.

Niinemets, Ü. and Kull, O., 1999. Biomass investment in leaf lamina versus lamina support in relation to growth irradiance and leaf size in temperate deciduous trees. *Tree Physiology*, 19(6): 349-358.

Niinemets, Ü., Portsmuth, A., Tena, D., Tobias, M., Matesanz, S. and Valladares, F., 2007. Do we underestimate the importance of leaf size in plant economics? Disproportional scaling of support costs within the spectrum of leaf physiognomy. *Annals of Botany*, 100(2): 283-303.

Niinemets, Ü., Portsmuth, A. and Tobias, M., 2006. Leaf size modifies support biomass distribution among stems, petioles and mid-ribs in temperate plants. *New Phytologist*, 171(1): 91-104.

Niklas, K.J., 1999. A mechanical perspective on foliage leaf form and function. *New Phytologist*, 143(1): 19-31.

Niklas, K.J., Cobb, E.D., Niinemets, Ü., Reich, P.B., Sellin, A., Shipley, B. and Wright, I.J., 2007. "Diminishing returns" in the scaling of functional leaf-traits across and within species groups. *Proceedings of the National Academy of Sciences*, 104(21): 8891-8896.

Nilson, S.E. and Assmann, S.M., 2007. The control of transpiration. Insights from Arabidopsis. *Plant Physiology*, 143(1): 19-27.

NRETAS, 2009. Ti Tree Basin Water Resource Report *Department of Natural Resources, Environment, the Arts and Sport; Water Branch.*

O'Connor, M.P., Agosta, S.J., Hansen, F., Kemp, S.J., Sieg, A.E., McNair, J.N. and Dunham, A.E., 2007. Phylogeny, regression, and the allometry of physiological traits. *The American Naturalist*, 170(3): 431-442.

O'Grady, A.P., Carter, J.L. and Bruce, J., 2011. Can we predict groundwater discharge from terrestrial ecosystems using existing eco-hydrological concepts? *Hydrology and Earth System Sciences*, 15(12): 3731-3739.

O'Grady, A.P., Cook, P.G., Eamus, D., Duguid, A., Wischusen, J.D.H., Fass, T. and Worldege, D., 2009. Convergence of tree water use within an arid-zone woodland. *Oecologia*, 160(4): 643-655.

O'Grady, A.P., Cook, P.G., Howe, P. and Werren, G., 2006a. Groundwater use by dominant tree species in tropical remnant vegetation communities. *Australian Journal of Botany*, 54: 155-171.

O'Grady, A.P., Eamus, D., Cook, P.G. and Lamontagne, S., 2006b. Comparative water use by the riparian trees *Melaleuca argentea* and *Corymbia bella* in the wet–dry tropics of northern Australia. *Tree Physiology*, 26(2): 219-228.

O'Grady, A.P., Eamus, D., Cook, P.G. and Lamontagne, S., 2006c. Groundwater use by riparian vegetation in the wet–dry tropics of northern Australia. *Australian Journal of Botany*, 54(2): 145-154.

O'Grady, A.P., Eamus, D., Cook, P.G., Lamontagne, S., Kelley, G. and Hutley, L.B., 2002. *Tree water use and sources of transpired water in riparian vegetation along the Daly River, Northern Territory*. Department of the Environment, Water, Heritage and the Arts, Northern Territory Government.

O'Grady, A.P., Eamus, D. and Hutley, L.B., 1999. Transpiration increases during the dry-season: patterns of tree water use in *Eucalypt* open-forests of northern Australia. *Tree Physiology*, 19(9): 591-597.

O'Grady, A.P. and Holland, K., 2010. *Review of Australian groundwater discharge studies of terrestrial systems*. CSIRO National Water Commission.

O'Leary, M.H., 1981. Carbon isotope fractionation in plants. *Phytochemistry*, 20(4): 553-567.

O'Leary, M.H., 1984. Measurement of the isotope fractionation associated with diffusion of carbon dioxide in aqueous solution. *The Journal of Physical Chemistry*, 88(4): 823-825.

O'Leary, M.H., 1988. Carbon isotopes in photosynthesis. *Bioscience*, 38(5): 328-336.

O'Leary, M.H., 1993. Biochemical basis of carbon isotope fractionation. *Stable isotopes and plant carbon-water relations*: 19-28.

O'Meara, B.C., Ané, C., Sanderson, M.J. and Wainwright, P.C., 2006. Testing for different rates of continuous trait evolution using likelihood. *Evolution*, 60(5): 922-933.

Oberhuber, W., Stumboeck, M. and Kofler, W., 1998. Climate-tree-growth relationships of Scots pine stands (*Pinus sylvestris* L.) exposed to soil dryness. *Trees*, 13(1): 19-27.

Orchard, K.A., Cernusak, L.A. and Hutley, L.B., 2010. Photosynthesis and water-use-efficiency of seedlings from northern Australian monsoon forest, savanna, and swamp habitats grown in a common garden. *Functional Plant Biology*, 37: 1050-1060.

Orians, G.H. and Solbrig, O.T., 1977. A cost-income model of leaves and roots with special reference to arid and semiarid areas. *American Naturalist,* 111(980): 677-690.

Orlowski, N., 2010. *Construction and specification of a cryogenic vacuum extraction device for application in stable water isotope analysis*, Gießen, Justus-Liebig-Universität, Masterarbeit.

Orme, D., 2013. The caper package: comparative analysis of phylogenetics and evolution in R. R package version, 5(2).

Osmond, C.B., Björkman, O. and Anderson, D.J., 2012. *Physiological processes in plant ecology: toward a synthesis with Atriplex*. Vol 36. Springer, Berlin Heidelberg, pp. 468.

Pagel, M.D., 1992. A method for the analysis of comparative data. *Journal of Theoretical Biology*, 156(4): 431-442.

Pagel, M.D., 1997. Inferring evolutionary processes from phylogenies. *Zoologica Scripta*, 26(4): 331-348.

Pagel, M.D., 1999. Inferring the historical patterns of biological evolution. *Nature*, 401(6756): 877-884.

Pagel, M.D., 2002. Modelling the evolution of continuously varying characters on phylogenetic trees. *Morphology, shape and phylogeny*: 269-286.

Paradis, E., 2011. *Analysis of Phylogenetics and Evolution with R*. Springer, Jakarta, pp.387.

Parnell, A.C., Inger, R., Bearhop, S. and Jackson, A.L., 2010. Source partitioning using stable isotopes: coping with too much variation. *PloS one*, 5(3): e9672.

Pate, J.S., 2001. Carbon isotope discrimination and plant water-use-efficiency. *Stable isotope techniques in the study of biological processes and functioning of ecosystems*, Springer, Netherlands, pp. 19-36.

Peñuelas, J., Terradas, J. and Lloret, F., 2011. Solving the conundrum of plant species coexistence: water in space and time matters most. *New Phytologist*, 189(1): 5-8.

Perez-Valdivia, C. and Sauchyn, D., 2011. Tree-ring reconstruction of groundwater levels in Alberta, Canada: Long term hydroclimatic variability. *Dendrochronologia*, 29(1): 41-47.

Phillips, D.L. and Gregg, J.W., 2001. Uncertainty in source partitioning using stable isotopes. *Oecologia*, 127(2): 171-179.

Phillips, D.L. and Gregg, J.W., 2003. Source partitioning using stable isotopes: coping with too many sources. *Oecologia*, 136(2): 261-269.

Pinheiro, J., Bates, D., DebRoy, S. and Sarkar, D., 2007. Linear and nonlinear mixed effects models. R package version. 3: 57, *R Foundation for Statistical Computing, Vienna, Austria*.

Poorter, L. and Rozendaal, D.M., 2008. Leaf size and leaf display of thirty-eight tropical tree species. *Oecologia*, 158(1): 35-46.

Pörtner, H.-O. and Farrell, A.P., 2008. Physiology and climate change. *Science*, 322(5902): 690-692.

Poulter, B., Frank, D., Ciais, P., Myneni, R.B., Andela, N., Bi, J., Broquet, G., Canadell, J.G., Chevallier, F., Liu, Y.Y., Running, S.W., Sitch, S. and van der Werf, G.R., 2014. Contribution of semi-arid ecosystems to interannual variability of the global carbon cycle. *Nature*, 509: 600-603.

Pressland, A.J., 1975. Productivity and management of mulga in south-western Queensland in relation to tree structure and density. *Australian Journal of Botany*, 23(6): 965-976.

Preston, K.A. and Ackerly, D.D., 2003. Hydraulic architecture and the evolution of shoot allometry in contrasting climates. *American Journal of Botany*, 90(10): 1502-1512.

Prior, L.D., Eamus, D. and Duff, G.A., 1997. Seasonal and diurnal patterns of carbon assimilation, stomatal conductance and leaf water potential in *Eucalyptus tetrodonta* saplings in a wet–dry savanna in northern Australia. *Australian Journal of Botany*, 45(2): 241-258.

R Development CORE Team, 2009. R: A Language and Environment for Statistical Computing, Vienna, Austria.

Radin, J.W., 1984. Stomatal responses to water stress and to abscisic acid in phosphorus-deficient cotton plants. *Plant Physiology*, 76(2): 392-394.

Reich, P., Walters, M. and Ellsworth, D., 1992. Leaf life-span in relation to leaf, plant, and stand characteristics among diverse ecosystems. *Ecological Monographs*, 62(3): 365-392.

Reich, P.B., Ellsworth, D.S., Walters, M.B., Vose, J.M., Gresham, C., Volin, J.C. and Bowman, W.D., 1999. Generality of leaf-trait relationships: a test across six biomes. *Ecology*, 80(6): 1955-1969.

Revell, L.J., 2010. Phylogenetic signal and linear regression on species data. *Methods in Ecology and Evolution*, 1(4): 319-329.

Revell, L.J., 2012. phytools: an R package for phylogenetic comparative biology (and other things). *Methods in Ecology and Evolution*, 3(2): 217-223.

Reynolds, J.F., Smith, D.M.S., Lambin, E.F., Turner, B., Mortimore, M., Batterbury, S.P., Downing, T.E., Dowlatabadi, H., Fernández, R.J. and Herrick, J.E., 2007. Global desertification: building a science for dryland development. *Science*, 316(5826): 847-851.

Ritchie, J., 1972. Model for predicting evaporation from a row crop with incomplete cover. *Water Resources Research*, 8(5): 1204-1213.

Robertson, E., Jozsa, L. and Spittlehouse, D., 1990. Estimating Douglas-fir wood production from soil and climate data. *Canadian Journal of Forest Research*, 20(3): 357-364.

Rodriguez-Iturbe, I., D'Odorico, P., Laio, F., Ridolfi, L. and Tamea, S., 2007. Challenges in humid land ecohydrology: Interactions of water table and unsaturated zone with climate, soil, and vegetation. *Water Resources Research*, 43(9): W09301.

Roeske, C. and O'Leary, M.H., 1984. Carbon isotope effects on enzyme-catalyzed carboxylation of ribulose bisphosphate. *Biochemistry*, 23(25): 6275-6284.

Rohlf, F.J., 2001. Comparative methods for the analysis of continuous variables: geometric interpretations. *Evolution*, 55(11): 2143-2160.

Rossatto, D.R., Silva, L.d.C.R., Villalobos-Vega, R., Sternberg, L.d.S.L. and Franco, A.C., 2012. Depth of water uptake in woody plants relates to groundwater level and vegetation structure along a topographic gradient in a neotropical savanna. *Environmental and Experimental Botany*, 77: 259-266.

Roussel, M., Dreyer, E., Montpied, P., Le-Provost, G.g., Guehl, J.-M. and Brendel, O., 2009. The diversity of ^{13}C isotope discrimination in a *Quercus robur* full-sib family is associated with differences in intrinsic water-use-efficiency, transpiration efficiency and stomatal conductance. *Journal of Experimental Botany*, 60(8): 2419-2430.

Rozanski, K., Araguás-Araguás, L. and Gonfiantini, R., 1993. Isotopic patterns in modern global precipitation, *Climate change in continental isotopic records*, American Geophysical Union, pp. 1-36.

Sack, L., Cowan, P., Jaikumar, N. and Holbrook, N., 2003. The 'hydrology'of leaves: co-ordination of structure and function in temperate woody species. *Plant, Cell & Environment*, 26(8): 1343-1356.

Sack, L. and Frole, K., 2006. Leaf structural diversity is related to hydraulic capacity in tropical rain forest trees. *Ecology*, 87(2): 483-491.

Sack, L. and Holbrook, N.M., 2006. Leaf hydraulics. *Annual Review of Plant Biology,* 57: 361-381.

Sack, L. and Scoffoni, C., 2013. Leaf venation: structure, function, development, evolution, ecology and applications in the past, present and future. *New Phytologist*, 198(4): 983-1000.

Saugier, B., Ehleringer, J.R., Hall, A.E. and Farquhar, G.D., 2012. *Stable isotopes and plant carbon-water relations*. Elsevier.

Savage, J.A. and Cavender-Bares, J., 2012. Habitat specialization and the role of trait lability in structuring diverse willow (genus Salix) communities. *Ecology*, 93(sp8): S138–S150.

SCA, 2009. *Surface water-groundwater interaction in the sandstone aquifers of the Upper Nepean Catchment*. Sydney Catchment Authority.

Scartazza, A., Vaccari, F.P., Bertolini, T., Di Tommasi, P., Lauteri, M., Miglietta, F. and Brugnoli, E., 2014. Comparing integrated stable isotope and eddy covariance estimates of water-use-efficiency on a Mediterranean successional sequence. *Oecologia*, 176(2): 581-594.

Schmidt, H.L., Winkler, F., Latzko, E. and Wirth, E., 1978. ^{13}C-kinetic isotope effects in photosynthetic carboxylation reactions and δ^{13}C-values of plant material. *Israel Journal of Chemistry*, 17(3): 223-224.

Schmidt, S., Lamble, R.E., Fensham, R.J. and Siddique, I., 2010. Effect of woody vegetation clearing on nutrient and carbon relations of semi-arid dystrophic savanna. *Plant and Soil*, 331(1-2): 79-90.

Schulze, E.D., Caldwell, M.M., Canadell, J., Mooney, H.A., Jackson, R.B., Parson, D., Scholes, R., Sala, O.E. and Trimborn, P., 1998a. Downward flux of water through roots (i.e. inverse hydraulic lift) in dry Kalahari sands. *Oecologia*, 115(4): 460-462.

Schulze, E.D., Kelliher, F.M., Korner, C., Lloyd, J. and Leuning, R., 1994. Relationships among maximum stomatal conductance, ecosystem surface conductance, carbon assimilation rate, and plant nitrogen nutrition: a global ecology scaling exercise. *Annual Review of Ecology and Systematics*, 25: 629-660.

Schulze, E.D., Mooney, H.A., Sala, O.E., Jobbagy, E.l., Buchmann, N., Bauer, G., Canadell, J., Jackson, R.B., Loreti, J. and Oesterheld, M., 1996. Rooting depth, water availability, and vegetation cover along an aridity gradient in Patagonia. *Oecologia*, 108(3): 503-511.

Schulze, E.D., Turner, N.C., Nicolle, D. and Schumacher, J., 2006. Leaf and wood carbon isotope ratios, specific leaf areas and wood growth of *Eucalyptus* species across a rainfall gradient in Australia. *Tree Physiology*, 26(4): 479-492.

Schulze, E.D., Williams, R.J., Farquhar, G.D., Schulze, W., Langridge, J., Miller, J.M. and Walker, B.H., 1998b. Carbon and nitrogen isotope discrimination and nitrogen nutrition of trees along a rainfall gradient in northern Australia. *Functional Plant Biology*, 25(4): 413-425.

Schuur, E.A. and Matson, P.A., 2001. Net primary productivity and nutrient cycling across a mesic to wet precipitation gradient in Hawaiian montane forest. *Oecologia*, 128(3): 431-442.

Schwarcz, H.P., 1991. Some theoretical aspects of isotope paleodiet studies. *Journal of Archaeological Science*, 18(3): 261-275.

Schwilk, D.W. and Ackerly, D.D., 2001. Flammability and serotiny as strategies: correlated evolution in pines. *Oikos*, 94(2): 326-336.

Schwinning, S. and Ehleringer, J.R., 2001. Water use trade-offs and optimal adaptations to pulse-driven arid ecosystems. *Journal of Ecology*, 89(3): 464-480.

Scoffoni, C., Rawls, M., McKown, A., Cochard, H. and Sack, L., 2011. Decline of leaf hydraulic conductance with dehydration: relationship to leaf size and venation architecture. *Plant Physiology*, 156(2): 832-843.

Seibt, U., Rajabi, A., Griffiths, H. and Berry, J.A., 2008. Carbon isotopes and water-use-efficiency: sense and sensitivity. *Oecologia*, 155(3): 441-454.

Shiklomanov, I.A., 1998. *World water resources: a new appraisal and assessment for the 21st century*. United Nations Educational, Scientific and Cultural Organization.

Silvertown, J., 2004. Plant coexistence and the niche. *Trends in Ecology & Evolution*, 19(11): 605-611.

Silvertown, J., Dodd, M.E., Gowing, D.J. and Mountford, J.O., 1999. Hydrologically defined niches reveal a basis for species richness in plant communities. *Nature*, 400(6739): 61-63.

Smith, B.N. and Epstein, S., 1971. Two categories of $^{13}C/^{12}C$ ratios for higher plants. *Plant Physiology*, 47(3): 380-384.

Smith, S.D., Devitt, D.A., Sala, A., Cleverly, J.R. and Busch, D.E., 1998. Water relations of riparian plants from warm desert regions. *Wetlands*, 18(4): 687-696.

Sokal, R.R. and Rohlf, F.J., 1995. *Biometry: the principles and practice of statistics in biological research*. W.H. Freeman & Co., San Francisco.

Somero, G.N., 2010. The physiology of climate change: how potentials for acclimatization and genetic adaptation will determine 'winners' and 'losers'. *The Journal of Experimental Biology*, 213(6): 912-920.

Sommerville, K.E., Gimeno, T.E. and Ball, M.C., 2010. Primary nerve (vein) density influences spatial heterogeneity of photosynthetic response to drought in two Acacia species. *Functional Plant Biology*, 37(9): 840-848.

Sommerville, K.E., Sack, L. and Ball, M.C., 2012. Hydraulic conductance of *Acacia* phyllodes (foliage) is driven by primary nerve (vein) conductance and density. *Plant, Cell & Environment*, 35(1): 158-168.

Sperry, J.S., 2000. Hydraulic constraints on plant gas-exchange. *Agricultural and Forest Meteorology*, 104(1): 13-23.

Spittlehouse, D.L., 1985. Determination of the year-to-year variation in growing season water use of a Douglas-fir stand. In: B.A. Hutchison and B.B. Hicks (Editors), *The Forest-Atmosphere Interaction*. Springer, Netherlands, pp. 235-254.

Stanhill, G., 1986. Water-use-efficiency. *Advances in Agronomy*, 39: 53-85.

Stevens, P., 2001 onwards. Angiosperm Phylogeny Website. Version 12, July 2012 [and more or less continuously updated since], URL (accessed on April 2017): http://www.mobot.org/MOBOT/research/APweb/.

Stewart, G.R., Turnbull, M., Schmidt, S. and Erskine, P., 1995. ^{13}C natural abundance in plant communities along a rainfall gradient: a biological integrator of water availability. *Functional Plant Biology*, 22(1): 51-55.

Stratton, L.C., Goldstein, G. and Meinzer, F.C., 2000. Temporal and spatial partitioning of water resources among eight woody species in a Hawaiian dry forest. *Oecologia*, 124(3): 309-317.

Sun, Q., Meyer, W.S., Koerber, G.R. and Marschner, P., 2015. Response of respiration and nutrient availability to drying and rewetting in soil from a semi-arid woodland depends on vegetation patch and a recent wildfire. *Biogeosciences*, 12(16): 5093-5101.

Swaffer, B.A., Holland, K.L., Doody, T.M., Li, C. and Hutson, J., 2014. Water use strategies of two co-occurring tree species in a semi-arid karst environment. *Hydrological Processes*, 28(4): 2003-2017.

Swenson, N.G., Enquist, B.J., Thompson, J. and Zimmerman, J.K., 2007. The influence of spatial and size scale on phylogenetic relatedness in tropical forest communities. *Ecology*, 88(7): 1770-1780.

Symonds, M.R. and Blomberg, S.P., 2014. A primer on phylogenetic generalised least squares, *Modern phylogenetic comparative methods and their application in evolutionary biology*. Springer, Berlin Heidelberg, pp. 105-130.

Taylor, D. 2008. *Tree leaf and branch trait coordination along an aridity gradient*. A thesis submitted *in* Department of Environmental science. University of Technology Sydney, Sydney, pp 185.

Taylor, D. and Eamus, D., 2008. Coordinating leaf functional traits with branch hydraulic conductivity: resource substitution and implications for carbon gain. *Tree Physiology*, 28(8): 1169-1177.

Tcherkez, G., Mauve, C., Lamothe, M., Le Bras, C. and Grapin, A., 2011. The $^{13}C/^{12}C$ isotopic signal of day-respired CO_2 in variegated leaves of Pelargonium× hortorum. *Plant, Cell & Environment*, 34(2): 270-283.

Thomas, D.S. and Eamus, D., 1999. The influence of predawn leaf water potential on stomatal responses to atmospheric water content at constant Ci and on stem hydraulic conductance and foliar ABA concentrations. *Journal of Experimental Botany*, 50(331): 243-251.

Thorburn, P.J., Hatton, T.J. and Walker, G.R., 1993. Combining measurements of transpiration and stable isotopes of water to determine groundwater discharge from forests. *Journal of Hydrology*, 150(2): 563-587.

Thorburn, P.J., Mensforth, L.J. and Walker, G.R., 1994. Reliance of creek-side river red gums on creek water. *Marine and Freshwater Research*, 45(8): 1439-1443.

Tilman, G.D., 1984. Plant dominance along an experimental nutrient gradient. *Ecology*, 65(5): 1445-1453.

Togashi, H.F., Prentice, I.C., Evans, B.J., Forrester, D.I., Drake, P., Feikema, P., Brooksbank, K., Eamus, D. and Taylor, D., 2015. Morphological and moisture availability controls of the leaf area-to-sapwood area ratio: analysis of measurements on Australian trees. *Ecology and Evolution*, 5(6): 1263-1270.

Troch, P.A., Carrillo, G., Sivapalan, M., Wagener, T. and Sawicz, K., 2013. Climate-vegetation-soil interactions and long-term hydrologic partitioning: signatures of catchment co-evolution. *Hydrology and Earth System Sciences*, 17(6): 2209-2217.

Turner, I.M., 1994. A quantitative analysis of leaf form in woody plants from the world's major broadleaved forest types. *Journal of Biogeography*, 21(4): 413-419.

Turner, N.C., Schulze, E.-D., Nicolle, D. and Kuhlmann, I., 2010. Growth in two common gardens reveals species by environment interaction in carbon isotope discrimination of Eucalyptus. *Tree Physiology*, 30(6): 741-747.

Turner, N.C., Schulze, E.D., Nicolle, D., Schumacher, J. and Kuhlmann, I., 2008. Annual rainfall does not directly determine the carbon isotope ratio of leaves of *Eucalyptus* species. *Physiologia Plantarum*, 132(4): 440-445.

Uhl, D. and Mosbrugger, V., 1999. Leaf venation density as a climate and environmental proxy: a critical review and new data. *Palaeogeography, Palaeoclimatology, Palaeoecology*, 149(1): 15-26.

Unkovich, M.J., Pate, J.S., McNeill, A. and Gibbs, J., 2013. *Stable isotope techniques in the study of biological processes and functioning of ecosystems*. Kluwer Academic Publishers, Netherlands, pp 293.

Vandermeer, J.H., 1972. Niche theory. *Annual Review of Ecology and Systematics*, 3: 107-132.

Vendramini, P.F. and Sternberg, L.d.S., 2007. A faster plant stem-water extraction method. *Rapid Communications in Mass Spectrometry*, 21(2): 164-168.

Verweij, R.J., Higgins, S.I., Bond, W.J. and February, E.C., 2011. Water sourcing by trees in a mesic savanna: responses to severing deep and shallow roots. *Environmental and Experimental Botany*, 74: 229-236.

Wang, D. and Hejazi, M., 2011. Quantifying the relative contribution of the climate and direct human impacts on mean annual streamflow in the contiguous United States. *Water Resources Research*, 47(10).

Warner, T.T., 2004. *Desert Meteorology*. Cambridge University Press, Cambridge, UK, pp 595.

Warren, C.R., 2008. Stand aside stomata, another actor deserves centre stage: the forgotten role of the internal conductance to CO_2 transfer. *Journal of Experimental Botany*, 59(7): 1475-1487.

Warren, C.R., Tausz, M. and Adams, M.A., 2005. Does rainfall explain variation in leaf morphology and physiology among populations of red ironbark (*Eucalyptus sideroxylon subsp. tricarpa*) grown in a common garden? *Tree Physiology*, 25(11): 1369-1378.

Warton, D.I., Duursma, R.A., Falster, D.S. and Taskinen, S., 2012. smatr 3–an R package for estimation and inference about allometric lines. *Methods in Ecology and Evolution*, 3(2): 257-259.

Warton, D.I., Wright, I.J., Falster, D.S. and Westoby, M., 2006. Bivariate line-fitting methods for allometry. *Biological Reviews*, 81(02): 259-291.

Webb, C.O., Ackerly, D.D. and Kembel, S.W., 2007. Phylocom: software for the analysis of community phylogenetic structure and trait evolution. Version 3.41. *Bioinformatics*, 24: 2098-2100.

Weerasinghe, L.K., Creek, D., Crous, K.Y., Xiang, S., Liddell, M.J., Turnbull, M.H. and Atkin, O.K., 2014. Canopy position affects the relationships between leaf respiration and associated traits in a tropical rainforest in Far North Queensland. *Tree Physiology*, 34(6): 564-584.

Weltzin, J.F. and McPherson, G.R., 1997. Spatial and temporal soil moisture resource partitioning by trees and grasses in a temperate savanna, Arizona, USA. *Oecologia*, 112(2): 156-164.

Werner, C. and Máguas, K., 2010. Carbon isotope discrimination as a tracer of functional traits in a mediterranean macchia plant community. *Functional Plant Biology*, 37(5): 467-477.

Werner, C., Schnyder, H., Cuntz, M., Keitel, C., Zeeman, M., Dawson, T., Badeck, F.-W., Brugnoli, E., Ghashghaie, J. and Grams, T., 2012. Progress and challenges in using stable isotopes to trace plant carbon and water relations across scales. *Biogeosciences*, 9: 3083-3111.

Wershaw, R.L., Friedman, I., Heller, S.J. and Frank, P.A., 1966. Hydrogen isotopic fractionation of water passing through trees. *Advances in organic geochemistry*: 55.

West, A.G., Patrickson, S.J. and Ehleringer, J.R., 2006. Water extraction times for plant and soil materials used in stable isotope analysis. *Rapid Communications in Mass Spectrometry*, 20(8): 1317-1321.

Westoby, M. and Wright, I.J., 2003. The leaf size–twig size spectrum and its relationship to other important spectra of variation among species. *Oecologia*, 135(4): 621-628.

Whelan, T., Sackett, W. and Benedict, C.R., 1973. Enzymatic fractionation of carbon isotopes by phosphoenolpyruvate carboxylase from C4 plants. *Plant Physiology*, 51(6): 1051-1054.

White, J.W., Cook, E.R., Lawrence, J.R. and Wallace S, B., 1985. The DH ratios of sap in trees: Implications for water sources and tree ring DH ratios. *Geochimica et Cosmochimica Acta*, 49(1): 237-246.

Whitley, R., Taylor, D., Macinnis-Ng, C., Zeppel, M., Yunusa, I., O'Grady, A.P., Froend, R., Medlyn, B. and Eamus, D., 2013. Developing an empirical model of canopy water flux describing the common response of transpiration to solar radiation and VPD across five contrasting woodlands and forests. *Hydrological Processes*, 27(8): 1133-1146.

Whittaker, R.H., 1975. *Communities and ecosystems, 2nd edition.* Macmillan Publishing Company, New York.

Wiens, J.J. and Graham, C.H., 2005. Niche conservatism: integrating evolution, ecology, and conservation biology. *Annual review of ecology, evolution, and systematics*: 519-539.

Wikström, N., Savolainen, V. and Chase, M.W., 2001. Evolution of the angiosperms: calibrating the family tree. *Proceedings of the Royal Society of London B: Biological Sciences*, 268(1482): 2211-2220.

Williams, C.A., Reichstein, M., Buchmann, N., Baldocchi, D., Beer, C., Schwalm, C., Wohlfahrt, G., Hasler, N., Bernhofer, C. and Foken, T., 2012. Climate and vegetation controls on the surface water balance: Synthesis of evapotranspiration measured across a global network of flux towers. *Water Resources Research*, 48(6).

Williams, D.G. and Ehleringer, J.R., 1996. Carbon isotope discrimination in three semi-arid woodland species along a monsoon gradient. *Oecologia*, 106(4): 455-460.

Williams, R.J., Myers, B.A., Muller, W.J., Duff, G.A. and Eamus, D., 1997. Leaf phenology of woody species in a north Australian tropical savanna. *Ecology*, 78(8): 2542-2558.

Williamson, M.H., 1957. An elementary theory of interspecific competition. *Nature*, 180: 422-425.

Winkler, F.J., Schmidt, H.L., Wirth, E., Latzko, E., Lenhart, B. and Ziegler, H., 1983. Temperature, pH and enzyme-source dependence of the HCO_3^-carbon isotope effect on the phosphoenolpyruvate carboxylase reaction. *Physiologie Végétale*, 21(5): 889-895.

Winkworth, R.E., 1973. Eco-physiology of mulga (*Acacia aneura*). *Tropical Grasslands*, 7(1): 43-48.

Witkowski, E., Lamont, B., Walton, C. and Radford, S., 1992. Leaf demography, sclerophylly and ecophysiology of two Banksias with contrasting leaf life spans. *Australian Journal of Botany*, 40(6): 849-862.

Wright, I.J., Falster, D.S., Pickup, M. and Westoby, M., 2006. Cross-species patterns in the coordination between leaf and stem traits, and their implications for plant hydraulics. *Physiologia Plantarum*, 127(3): 445-456.

Wright, I.J., Reich, P.B. and Westoby, M., 2001. Strategy shifts in leaf physiology, structure and nutrient content between species of high-and low-rainfall and high-and low-nutrient habitats. *Functional Ecology*, 15(4): 423-434.

Wright, I.J., Reich, P.B., Westoby, M., Ackerly, D.D., Baruch, Z., Bongers, F., Cavender-Bares, J., Chapin, T., Cornelissen, J.H. and Diemer, M., 2004. The worldwide leaf economics spectrum. *Nature*, 428(6985): 821-827.

Xiao, S., Xiao, H., Peng, X. and Tian, Q., 2014. Intra-annual stem diameter growth of *Tamarix ramosissima* and association with hydroclimatic factors in the lower reaches of China's Heihe River. *Journal of Arid Land*, 6(4): 498-510.

Yakir, D. and Sternberg, L.d.S., 2000. The use of stable isotopes to study ecosystem gas-exchange. *Oecologia*, 123(3): 297-311.

Zalenski, W.v., 1902. Ueber die Ausbildung der Nervation bei verschiedenen Pflanzen. *Berichte Deutsche Botanicshe Gesellschaft*, 20: 433-440.

Zegada-Lizarazu, W. and Iijima, M., 2005. Deep root water uptake ability and water-use-efficiency of pearl millet in comparison to other millet species. *Plant Production Science*, 8(4): 454-460.

Zencich, S.J., Froend, R.H., Turner, J.V. and Gailitis, V., 2002. Influence of groundwater depth on the seasonal sources of water accessed by *Banksia* tree species on a shallow, sandy coastal aquifer. *Oecologia*, 131(1): 8-19.

Zeppel, M., Macinnis-Ng, C., Palmer, A., Taylor, D., Whitley, R., Fuentes, S., Yunusa, I., Williams, M. and Eamus, D., 2008. An analysis of the sensitivity of sap flux to soil and plant variables assessed for an Australian woodland using a soil–plant–atmosphere model. *Functional Plant Biology*, 35(6): 509-520.

Zhang, L., Potter, N., Hickel, K., Zhang, Y. and Shao, Q., 2008. Water balance modeling over variable time scales based on the Budyko framework – model development and testing. *Journal of Hydrology*, 360(1): 117-131.

Zolfaghar, S., 2014. *Comparative ecophysiology of Eucalyptus woodlands along a depth-to-groundwater gradient*. A thesis submitted *in* Department of Environmental science. University of Technology Sydney, Sydney, pp 228.

Zolfaghar, S., Villalobos-Vega, R., Cleverly, J., Zeppel, M., Rumman, R. and Eamus, D., 2014. The influence of depth-to-groundwater on structure and productivity of *Eucalyptus* woodlands. *Australian Journal of Botany*, 62(5): 428-437.

Zolfaghar, S., Villalobos-Vega, R., Zeppel, M. and Eamus, D., 2015. The hydraulic architecture of *Eucalyptus* trees growing across a gradient of depth-to-groundwater. *Functional Plant Biology*, 42(9): 888-898.